

Università degli Studi di Pavia

---

Dipartimento di Fisica Generale 'Alessandro Volta'

Dottorato di Ricerca in Fisica – XI Ciclo

Parametric Amplification of Light  
in Quantum Communication  
and Measurement

Ph. D. Thesis of

Massimiliano Federico Sacchi

Tutore: **Prof. Giacomo Mauro D'Ariano**

Coordinatore: **Prof. Sergio P. Ratti**

Anno Accademico 1997/1998

---



# Acknowledgments

Primary acknowledgments are due to my thesis supervisor, Prof. Giacomo Mauro D'Ariano. Over the course of my PhD, he has always been approachable and helpful. I am grateful for the general advice and encouragement he gave me. I give thanks for stimulating intellectual and social interactions to my colleagues in the Theoretical Quantum Optics Group of Pavia: Chiara Macchiavello, Lorenzo Maccone, Marco Paini and Matteo Paris.

Many friends deserve to be thanked for their affection and closeness. I am obliged to Annalisa, Antonio, Dorino, Gianni, Leonardo, Marcella, Marco, Moreno and Roberto. I also express my gratitude to my mother and my father for their confidence and support. Finally I thank Valeria for bearing with me throughout the years of my PhD and feeding me on clear and encouraging words.



# List of publications

This thesis is based on the following chronological list of refereed publications.

1. G. M. D'Ariano and M. F. Sacchi, “*Two-mode phase heterodyne detection*”, Phys. Rev. A **52**, R4309 (1995).
2. G. M. D'Ariano and M. F. Sacchi, “*Repeatable two-mode phase measurement*”, in *Quantum Interferometry*, F. De Martini, G. Denardo and Y. Shih Eds. (VCH Publishers, Weinheim, 1996), pp. 307-313.
3. G. M. D'Ariano and M. F. Sacchi, “*Trace forms for the generalized Wigner functions*”, Nuovo Cimento B **112**, 881 (1997).
4. G. M. D'Ariano and M. F. Sacchi “*Optical von Neumann measurement*”, Phys. Lett. A **231**, 325 (1997).
5. G. M. D'Ariano and M. F. Sacchi, “*Communication with nonclassical states in the presence of loss*”, in ‘5<sup>th</sup> Int. Conf. on Squeezed States and Uncertainty Relations’ (NASA Conf. Publ., Washington DC, 1997), pp. 467-472.
6. G. M. D'Ariano and M. F. Sacchi, “*Equivalence between squeezed-state and twin-beam communication channels*”, Mod. Phys. Lett. B. **11**, 1263 (1997).
7. G. M. D'Ariano and M. F. Sacchi, “*Optimized quantum-optical communications in the presence of loss*”, Opt. Comm. **149**, 152 (1998).
8. G. M. D'Ariano, M. G. A. Paris and M. F. Sacchi, “*Generation of phase-coherent states*”, Phys. Rev. A **57**, 4894 (1998).
9. G. M. D'Ariano, C. Macchiavello and M. F. Sacchi, “*On the general problem of quantum phase estimation*”, Phys. Lett. A **248**, 103 (1998).
10. G. M. D'Ariano, P. Kumar and M. F. Sacchi, “*Tomographic measurements of nonclassical radiation states*”, Phys. Rev. A **59**, 826 (1999).

11. G. M. D'Ariano, M. G. A. Paris and M. F. Sacchi, "*On the parametric approximation in quantum optics*", Nuovo Cimento B, 1998, in press.
12. G. M. D'Ariano, L. Maccone, M. F. Sacchi and A. Garuccio: "*Homodyning Bell's inequality*", in '4<sup>th</sup> Int. Conf. on Quantum Communication, Measurement, and Computing' (Plenum, 1998), in press.
13. G. M. D'Ariano, L. Maccone, M. F. Sacchi and A. Garuccio: "*Tomographic test of Bell's inequality*", 1998, submitted to Europ. Phys. J. D.
14. G. M. D'Ariano, M. F. Sacchi and R. Seno: "*Feedback-assisted measurement of the free mass position under the Standard Quantum Limit*", 1998, submitted to Nuovo Cimento B.
15. G. M. D'Ariano, L. Maccone, M. G. A. Paris and M. F. Sacchi: "*Optical Fock-state synthesizer*", 1999, submitted to Phys. Rev. Lett.
16. G. M. D'Ariano, M. F. Sacchi and H. P. Yuen, "*Correspondence between classical and quantum measurements*", 1999, submitted to Phys. Rev. A.

# Contents

<b>Acknowledgments</b>	<b>i</b>
<b>List of publications</b>	<b>iii</b>
<b>Introduction</b>	<b>1</b>
<b>1 Parametric processes of light in nonlinear media</b>	<b>5</b>
1.1 Introduction . . . . .	5
1.2 Effective Hamiltonians . . . . .	5
1.3 On the validity of the parametric approximation . . . . .	11
1.3.1 Displacer . . . . .	13
1.3.2 Squeezer . . . . .	16
1.3.3 Two-mode squeezer . . . . .	22
1.4 Conclusion . . . . .	24
<b>2 Generation of radiation states with enhanced phase properties</b>	<b>27</b>
2.1 Introduction . . . . .	27
2.2 Generation of phase-coherent states . . . . .	28
2.2.1 Twin-beam up conversion . . . . .	31
2.3 Two-mode heterodyne phase detection . . . . .	33
2.3.1 The heterodyne eigenvectors $ z\rangle\rangle$ . . . . .	33
2.3.2 The detection of the two-mode phase . . . . .	35
2.4 A repeatable two-mode phase measurement . . . . .	38
2.4.1 General framework for repeatable measurements . . . . .	39
2.4.2 The interaction Hamiltonian . . . . .	40
2.5 On the general problem of quantum phase estimation . . . . .	43
2.5.1 Optimal POM for the phase-shift estimation . . . . .	44
2.5.2 Optimal POM for multipath interferometer . . . . .	48
2.5.3 Phase-difference of two-mode fields . . . . .	49
2.6 Conclusion . . . . .	52

<b>3</b>	<b>Quantum-optical communication channels</b>	<b>53</b>
3.1	Introduction . . . . .	53
3.2	Optimized channels in the presence of loss . . . . .	54
3.2.1	Heterodyne channel . . . . .	54
3.2.2	Homodyne channel . . . . .	57
3.2.3	Direct-detected channel . . . . .	63
3.2.4	Summary of the results . . . . .	66
3.3	Equivalence between squeezed-state and twin-beam communication channels . . . . .	67
3.3.1	The twin-beam communication scheme . . . . .	68
3.3.2	Equivalence with the squeezed-state channel . . . . .	71
3.4	Optical Fock-state synthesizer . . . . .	73
3.4.1	The experimental set-up . . . . .	74
3.4.2	The output state reduction . . . . .	76
3.5	Conclusion . . . . .	77
<b>4</b>	<b>Testing Quantum Mechanics</b>	<b>85</b>
4.1	Introduction . . . . .	85
4.2	Optical von Neumann measurement . . . . .	86
4.2.1	A feasible interaction Hamiltonian . . . . .	86
4.3	Amplification of entanglement . . . . .	91
4.3.1	Generation of the seed state . . . . .	92
4.3.2	From path indistinguishability to mesoscopic entanglement . . . . .	94
4.3.3	Dynamics of the stimulated down-conversion process . . . . .	97
4.4	Tomographic test of Bell's inequality . . . . .	101
4.4.1	The experimental set-up . . . . .	102
4.4.2	Homodyning Bell's inequality . . . . .	104
4.4.3	Numerical results . . . . .	106
4.5	Tomographic measurement of the nonclassicality of radiation states . . . . .	108
4.5.1	Single-mode nonclassicality . . . . .	109
4.5.2	Two-mode nonclassicality . . . . .	112
4.6	Conclusion . . . . .	115
	<b>Conclusions</b>	<b>119</b>
<b>A</b>	<b>Trace formula for generalized Wigner functions</b>	<b>121</b>
A.1	Introduction . . . . .	121
A.2	Three equivalent trace forms . . . . .	123
A.3	Differential Wigner representations . . . . .	125

---

<b>B On the correspondence between classical and quantum measurements</b>	<b>129</b>
B.1 Introduction . . . . .	129
B.2 Heterodyne detection . . . . .	130
B.3 Ideal amplification of quantum observables . . . . .	132
B.4 Approaching ideal quantum measurements by preamplified heterodyning	134
B.5 Two examples . . . . .	135
B.5.1 Measurement of the quadrature . . . . .	135
B.5.2 Measurement of the photon number . . . . .	136
B.6 A counterexample . . . . .	139
B.7 Conclusions . . . . .	142
<b>Bibliography</b>	<b>145</b>



# Introduction

The invention of the laser allowed the observations of nonlinear optical phenomena such as harmonic generation, parametric amplification and oscillation, stimulated Raman scattering, transient coherent phenomena, optical bistability, phase conjugation, optical solitons, self-focusing, etc. Further efforts in experimental nonlinear optics followed the advent of telecommunications using optical fibers. In the last decades, the nonclassical behavior of light such as antibunching, subpoissonian statistics, squeezing, spontaneous parametric downconversion, entanglement could be observed. Such kind of phenomena have no classical analogue and require the quantum treatment of the radiation field.

The central topic of this thesis concerns the generation of nonclassical states of light by parametric interaction with nonlinear media. On one hand, some practical applications of these kind of states in quantum interferometry and in quantum-optical information channels are suggested. On the other, some original experimental proposals in testing quantum measurement theory and measuring the nonclassicality of radiation states are presented. On this last subject, particular attention will be devoted to experimental set-ups based on the recent technique of quantum homodyne tomography.

With regard to the theoretical approximations used in this thesis, the main point is the single-mode treatment. This approximation is justified by the use of nearly-monochromatic coherent sources and narrow-band photodetectors in all the proposed experimental set-ups. The second point is the thorough assumption of the parametric approximation, namely one of the modes involved in the nonlinear interaction Hamiltonians is treated as a classical undepleted pump. Such kind of approximation is widely discussed in Chapter 1. In all the sections of the thesis a constant attention is addressed to the detrimental effect of losses and to the consequences of nonunit quantum efficiency of photodetectors, in order to give a realistic description of the proposed experimental set-ups.

## Structure of the Thesis

In Chapter 1 the effective interaction Hamiltonians that describe the parametric processes of light in nonlinear media are introduced. Such Hamiltonians write in terms

of different modes of the quantized electromagnetic field, and the role of the phase-matching conditions is discussed. A detailed section of the chapter discuss the validity of the parametric approximation, by comparing some exact numerical results with the approximate ones. The numerical diagonalization of the Hamiltonians that describe both degenerate and non degenerate parametric amplifiers is performed, by exploiting the conservation laws pertaining each device. The conditions under which the parametric approximation holds are shown to be the coherence of the pump after the interaction, rather than its undepletion. The section also introduces some fundamental unitary operators in quantum optics that are experimentally realized by parametric processes.

Chapter 2 presents two novel methods to generate quantum states of radiation with enhanced phase properties through nonlinear parametric interactions. Such states are of interest both in high-sensitivity interferometry and in phase-based communication channels. The first proposed experimental set-up generates the phase-coherent states by a couple of nonlinear  $\chi^{(2)}$  crystals. The phase-coherent states are well-known to approximate the (unnormalizable) Susskind-Glogower states—the optimal states for single-mode phase detection—thus being the privileged states for single-mode phase-based communication channels. The involved nonlinear interactions have been analyzed by means of the numerical diagonalization presented in Chapter 1. The second proposal is an experimental scheme for the generation of two-mode states that approach the (infinite-energy) eigenstates of the heterodyne detector. These states are essentially generated by parametric downconversion of coherent sources, and are shown to achieve the ideal phase sensitivity (inversely proportional to the mean photon number). Finally, an interaction Hamiltonian for a repeatable two-mode phase measurement is also presented. In the last section of the chapter the problem of the phase measurement is addressed with great generality in the realm of estimation theory, along with the derivation of the optimal positive operator-valued measure and the optimal input state. Two relevant examples are analyzed: i) a multi-mode phase shift operator for multipath interferometry; ii) the two mode heterodyne phase detection.

The quantum-optical communication channels are the subject of chapter 3. The customary channels based on heterodyne detection of coherent states, on homodyne detection of squeezed states, and on direct detection of number states are optimized to achieve the maximum information capacity in the presence of loss. The most surprising result is found for the number-state channel, for which the *a priori* probability distribution of the input characters is strongly modified for increasing losses, with improvement of the capacity up to 70 % at low power and for attenuation  $\eta = .15$ . The problem of generating the number eigenstates is crucial not only in quantum information but also in quantum interferometry. In this chapter a scheme for the generation of number states (and superposition of number states) is presented. The scheme is base on the

cross-phase modulation achievable in a  $\chi^{(3)}$  media between a traveling mode and a cavity field. The squeezed-state channel also offers best performances with respect to the classical channel based on coherent states. However, this channel is affected by strong experimental difficulties. The equivalence between the squeezed-state channel and a twin-beam channel (based on the two-mode states presented in Chapter 2) is proved. The experimental advantages in using the latter scheme are emphasized.

Chapter 4 is entirely devoted to some proposed experimental tests of Quantum Mechanics. The following tests are presented. i) An optical scheme that realizes the standard von Neumann measurement model, providing an indirect measurement of a quadrature of the field with controllable Gaussian state-reduction. The scheme represents an optical version of the measurement scheme for the position of a particle formulated in the last chapter of von Neumann's book. ii) A novel method to generate mesoscopic quantum superpositions by *stimulated* down conversion in nonlinear  $\chi^{(2)}$  media. The scheme relies on feeding a nondegenerate parametric amplifier by a single-photon state, in a way that makes signal and idler paths indistinguishable. The amplification process is analyzed realistically by taking into account the effects of cavity losses, and the appearance of mesoscopic quantum superpositions at the output is shown. The last two proposals are based on quantum homodyne tomography. iii) A homodyne detection scheme to verify Bell's inequality on correlated optical beams at the output of a nondegenerate parametric amplifier. The approach is based on tomographic measurement of the joint detection probabilities, which allows using high quantum-efficient detectors and does not need supplementary hypotheses. iv) A more general test to check the nonclassicality of radiation states, even for rather low quantum efficiency. For single-mode states violations of inequalities involving photon-number probability are checked. For two-mode states the nonclassicality test reconstructs some suitable number-operator functions. The proposed test discriminates classical states from states that invalidate the Mandel's semiclassical formula of photon counting.



# Chapter 1

## Parametric processes of light in nonlinear media

### 1.1 Introduction

Optical processes taking place in nonlinear media yield to a considerably rich variety of nonlinear phenomena, both in the semi-classical [1] and in the quantum domain [2]. The quantum statistical properties of the radiation coming out from such interactions have attracted much attention (see, for example, Refs. [3, 4]). Squeezing, anti-bunching and entanglement have been predicted and subsequently observed in a series of fascinating experiments [5, 6]. Most of the theoretical approaches to a quantum theory of nonlinear optical devices have been carried out using the so-called parametric approximation [7]. In this framework one of the field modes is in a strong semi-classical coherent state, so that its depletion as well as its quantum fluctuations can be neglected.

In this chapter the effective interaction Hamiltonians that describe the parametric processes of light in nonlinear media are introduced. Such Hamiltonians write in terms of different modes of the quantized electromagnetic field, and the parametric processes turn out to be effective when the phase-matching conditions are satisfied. The chapter presents a detailed discussion about the validity of the parametric approximation, by comparing some exact numerical results with the approximate ones. The conditions under which the parametric approximation holds are shown to be the coherence of the pump after the interaction, rather than its undepletion.

### 1.2 Effective Hamiltonians

A small part of the energy of a beam of light passing through a transparent homogeneous material is scattered in all directions by the atomic structure of the material. The thermal motion of the atoms modulates the scattered light, changing not only the

direction but also the frequency of light (inelastic scattering). Such kind of phenomena is attributable to the decay of one photon with wave-vector  $\mathbf{k}_3$  and frequency  $\omega_3$  into a pair of photons with wave-vectors  $\mathbf{k}_1$  and  $\mathbf{k}_2$  and frequency  $\omega_1$  and  $\omega_2$ , such that the conservation of energy and momentum is satisfied, namely

$$\mathbf{k}_1 + \mathbf{k}_2 = \mathbf{k}_3 , \quad (1.1)$$

$$\omega_1 + \omega_2 = \omega_3 . \quad (1.2)$$

Let us consider more closely this process in a simple model of a molecular crystal of  $N$  noninteracting molecules regularly arranged in a lattice. We also assume that the system is sufficiently dilute that each of the molecules experiences the same electric field. In the dipole approximation (quite good for light wavelength much longer than the size of the molecules in the crystals) one can estimate the transition rate of the parametric process by using the Fermi's golden rule. Let the field initially contain  $n_1, n_2, n_3$  photons in modes  $a_{\mathbf{k}_1}, a_{\mathbf{k}_2}$  and  $a_{\mathbf{k}_3}$  and all the molecules be in the ground state  $|g\rangle$ . The parametric interaction subtracts one photon in mode  $a_{\mathbf{k}_3}$  and creates two photons, one in mode  $a_{\mathbf{k}_1}$  and the other in mode  $a_{\mathbf{k}_2}$ . At the end of the parametric process the matter returns to its initial state, only the field undergoing a change. The third order of perturbation theory is the lowest in which the transition amplitudes for the three-photon process is nonzero. Hence, the transition rate can be written as follows

$$W_{fi} = \frac{2\pi}{\hbar} |T_{fi}|^2 \delta(E_f - E_i) , \quad (1.3)$$

with

$$T_{fi} = \sum_{v_1, v_2} \frac{\langle f | \hat{V} | v_2 \rangle \langle v_2 | \hat{V} | v_1 \rangle \langle v_1 | \hat{V} | i \rangle}{(E_i - E_{v_2})(E_i - E_{v_1})} . \quad (1.4)$$

We do not take into account intermediate resonances, so that the denominator in Eq. (1.4) are real. The sum over  $v_1, v_2$  include all possible intermediate states, whereas the state in the Dirac notation  $|i\rangle, |f\rangle$  denotes the field+matter states

$$|i\rangle = |g, n_1, n_2, n_3\rangle \equiv |g\rangle |i'\rangle , \quad (1.5)$$

$$|f\rangle = |g, n_1 + 1, n_2 + 1, n_3 - 1\rangle \equiv |g\rangle |f'\rangle , \quad (1.6)$$

and  $\hat{V}$  represents the dipole interaction Hamiltonian

$$\hat{V} = -\mathbf{d} \cdot (\hat{\mathbf{E}}^{(+)} + \hat{\mathbf{E}}^{(-)}) , \quad (1.7)$$

$\hat{\mathbf{E}}^{(+)}$  ( $\hat{\mathbf{E}}^{(-)}$ ) being the positive- (negative-) frequency part of the free electromagnetic quantized field, in SI units

$$\hat{\mathbf{E}}^{(+)}(\mathbf{r}, t) = i \sum_{\mathbf{k}, \lambda} \left( \frac{\hbar \omega_{\mathbf{k}, \lambda}}{2\epsilon_0 V} \right)^{1/2} a_{\mathbf{k}, \lambda} \epsilon_{\mathbf{k}, \lambda} e^{i(\mathbf{k} \cdot \mathbf{r} - \omega_{\mathbf{k}, \lambda} t)} , \quad \hat{\mathbf{E}}^{(-)}(\mathbf{r}, t) = [\hat{\mathbf{E}}^{(+)}(\mathbf{r}, t)]^\dagger . \quad (1.8)$$

In Eq. (1.8)  $V$  represents the quantization volume,  $\varepsilon_{\mathbf{k},\lambda}$  the versor for wave-vector  $\mathbf{k}$  and polarization  $\lambda$ ,  $\omega_{\mathbf{k},\lambda} = c|\mathbf{k}|/n_{\mathbf{k},\lambda}$  the angular frequency in the medium ( $n_{\mathbf{k},\lambda}$  being the index of refraction), and  $a_{\mathbf{k},\lambda}$  the corresponding boson annihilation operator. For the sake of notation, in the following we absorb the polarization index  $\lambda$  in  $\mathbf{k}$  and define

$$\mathcal{E}_{\mathbf{k}} = \sqrt{\hbar\omega_{\mathbf{k}}/(2\varepsilon_0V)}. \quad (1.9)$$

By summing the  $3! = 6$  possible sequences of photon emission and absorption for the  $j^{\text{th}}$  molecule one has the scattering amplitude

$$T^{(j)} = -\langle f' | (\beta_j | \hat{\mathbf{E}}_j^{(+)} \hat{\mathbf{E}}_j^{(-)} \hat{\mathbf{E}}_j^{(-)} | i' \rangle), \quad (1.10)$$

where  $\hat{\mathbf{E}}_j$  is the electric field at the  $j^{\text{th}}$ -molecule position  $\mathbf{r}_j$  and  $\beta_j$  is the tensor of the quadratic hyperpolarizability of the molecule

$$\beta = \beta_{\mu\alpha\beta}(-\omega_3; \omega_1, \omega_2) \equiv S_T \sum_{b,c} \frac{d_{ac}^\mu d_{cb}^\alpha d_{ba}^\beta}{\hbar^2(\omega_{ac} - \omega_3)(\omega_{ab} - \omega_1)}, \quad (1.11)$$

$S_T$  denoting the total symmetrized sum over the  $3!$  permutations of the pairs  $(-\omega_3, \mu)$ ,  $(\omega_1, \alpha)$ ,  $(\omega_2, \beta)$ , and  $\mathbf{d}_{ba} = \langle b | \mathbf{d}_j | a \rangle$  representing the dipole matrix elements. The effect of a coherent optical field on the medium is to induce an assembly of electric dipoles which oscillates coherently. Then, in the case of coherent scattering, one has  $W_{12} \sim |\sum_j T^{(j)}|^2$ . By introducing the macroscopic second-order nonlinear susceptibility  $\chi^{(2)} = \beta N / (2\varepsilon_0 V)$ , for slowly-varying fields one has

$$\sum_j \beta_j \mathbf{f}(\mathbf{r}_j) \sim 2\varepsilon_0 \chi^{(2)} \int_V d^3r \mathbf{f}(\mathbf{r}). \quad (1.12)$$

The transition rate then rewrites

$$W_{12} = \frac{2\pi}{\hbar^2} |\langle f' | \hat{V}_{eff} | i' \rangle|^2 \delta(\omega_1 + \omega_2 - \omega_3), \quad (1.13)$$

with the effective interaction Hamiltonian

$$\begin{aligned} \hat{V}_{eff} &= 2i\varepsilon_0 \sum_{\mathbf{k}_1} \sum_{\mathbf{k}_2} \sum_{\mathbf{k}_3} \mathcal{E}_{\mathbf{k}_1} \mathcal{E}_{\mathbf{k}_2} \mathcal{E}_{\mathbf{k}_3} \\ &\times \left[ \chi^{(2)}(-\omega_3; \omega_1, \omega_2) |\varepsilon_{\mathbf{k}_1}^* \varepsilon_{\mathbf{k}_2}^* \varepsilon_{\mathbf{k}_3} a_{\mathbf{k}_1}^\dagger a_{\mathbf{k}_2}^\dagger a_{\mathbf{k}_3} \int_V d^3r e^{i(\mathbf{k}_3 - \mathbf{k}_1 - \mathbf{k}_2) \cdot \mathbf{r}} - \text{h. c.} \right], \end{aligned} \quad (1.14)$$

where the added term  $\hat{\mathbf{E}}^{(+)} \hat{\mathbf{E}}^{(+)} \hat{\mathbf{E}}^{(-)}$  describes the inverse parametric process  $|f\rangle \rightarrow |i\rangle$  and guarantees the hermiticity of the interaction. Notice that in Eqs. (1.13,1.14) we have excluded the molecular variables. This simple model shows that the three-photon process can be described not only in the third, but also in the first order of perturbation theory by taking the effective energy density to be of the form

$$\hat{V}_{eff} \propto \chi^{(2)} |\hat{\mathbf{E}}|^3 \quad (1.15)$$

and by retaining only the terms that provide a time-independent Hamiltonian. Moreover, the integral on the volume in Eq. (1.14) depends strongly on the phase mis-match  $\Delta\mathbf{k} = \mathbf{k}_1 + \mathbf{k}_2 - \mathbf{k}_3$ , and rapidly falls for  $\Delta\mathbf{k} \neq 0$ . Thus, the rate of three-photon processes is effective only when the conservation of momentum (the so-called phase-matching condition) is satisfied. Thus, the conservation of momentum is a consequence of the quantum interference of the transition amplitudes  $T^{(j)}$ .

The assumptions in our model for the description of the nonlinear interactions are very sweep, and the transition between monomolecular and many-molecular formulae are thus oversimplified. Moreover, the local field instead of the macroscopic field should appear in Eq. (1.10). For a detailed treatment of the relation between the microscopic polarizability and the macroscopic susceptibility the reader is referred to Ref. [8]. Notwithstanding its simplicity, the model suggests the main result for the description of parametric processes in nonlinear media, namely the form of the interaction Hamiltonian

$$\hat{H}_I \propto \chi^{(n)} \hat{\mathbf{E}}^{n+1}, \quad (1.16)$$

for nonlinearity of order  $n$ .

The result in Eq. (1.16) can be derived by considering the electric contribution to the electromagnetic energy within the nonlinear medium

$$H = \int_V d^3r \int_0^{\mathbf{D}(\mathbf{r},t)} \mathbf{E}(\mathbf{r},t) \cdot d\mathbf{D}(\mathbf{r},t), \quad (1.17)$$

where  $\mathbf{E}(\mathbf{r},t)$  and  $\mathbf{D}(\mathbf{r},t)$  denote the electric field and the electric displacement vector, and the SI units have been used. In terms of the polarization  $\mathbf{P}(\mathbf{r},t)$ , one has the constitutive relation

$$\mathbf{D}(\mathbf{r},t) = \varepsilon_0 \mathbf{E}(\mathbf{r},t) + \mathbf{P}(\mathbf{r},t). \quad (1.18)$$

Let us introduce the Fourier components of the field and of the  $n^{\text{th}}$ -order polarization, namely

$$\mathbf{E}(\omega) = \frac{1}{2\pi} \int dt \mathbf{E}(\mathbf{r},t) e^{i\omega t} \quad (1.19)$$

$$\mathbf{P}^{(n)}(\omega) = \frac{1}{2\pi} \int dt \mathbf{P}^{(n)}(\mathbf{r},t) e^{i\omega t} \quad (1.20)$$

$$= \varepsilon_0 \int d\omega_1 \cdots d\omega_n \chi^{(n)}(-\omega_\sigma; \omega_1, \dots, \omega_n) |\mathbf{E}(\omega_1) \cdots \mathbf{E}(\omega_n) \delta(\omega - \omega_\sigma),$$

where  $\chi^{(n)}$  denotes the  $n^{\text{th}}$ -order susceptibility tensor,  $\omega_\sigma = \sum_{i=1,n} \omega_i$ , and  $\mathbf{P}(\mathbf{r},t) = \sum_n \mathbf{P}^{(n)}(\mathbf{r},t)$ . Through Eqs. (1.19,1.20), Eq. (1.17) rewrites

$$H = \int_V d^3r \left[ \frac{1}{2} \varepsilon_0 \mathbf{E}^2(\mathbf{r},t) + \sum_{n=1} X_n(\mathbf{r}) \right], \quad (1.21)$$

where

$$\begin{aligned} X_n(\mathbf{r}) &= \frac{\varepsilon_0 n}{n+1} \int d\omega d\omega_1 \cdots d\omega_n e^{-i(\omega+\omega_\sigma)t} \\ &\times \chi^{(n)}(-\omega_\sigma; \omega_1, \dots, \omega_n) |\mathbf{E}(\omega) \mathbf{E}(\omega_1) \cdots \mathbf{E}(\omega_n)|. \end{aligned} \quad (1.22)$$

For small nonlinearities, the canonical quantization of the macroscopic field in the medium can be achieved by replacing the classical field  $\mathbf{E}(\mathbf{r}, t)$  with the corresponding free-field Hilbert space operator  $\hat{\mathbf{E}}^{(+)}(\mathbf{r}, t) + \hat{\mathbf{E}}^{(-)}(\mathbf{r}, t)$ . From Eqs. (1.8) and (1.9) the Fourier components of the quantum field write as follows

$$\hat{\mathbf{E}}(\omega) = i \sum_{\mathbf{k}} \mathcal{E}_{\mathbf{k}} \left[ a_{\mathbf{k}} \varepsilon_{\mathbf{k}} e^{i\mathbf{k}\cdot\mathbf{r}} \delta(\omega - \omega_{\mathbf{k}}) - a_{\mathbf{k}}^\dagger \varepsilon_{\mathbf{k}}^* e^{-i\mathbf{k}\cdot\mathbf{r}} \delta(\omega + \omega_{\mathbf{k}}) \right]. \quad (1.23)$$

Thus, the contribution of the  $n^{\text{th}}$ -order nonlinearity to the quantum Hamiltonian can be obtained by replacing the Fourier components of the quantum field (1.23) in Eq. (1.22). Owing to the phase factors  $e^{i\omega t}$ , many of the terms coming from the product in the last line of Eq. (1.22) are rapidly oscillating and hence average to zero. The surviving terms correspond to sets of frequencies that satisfy the relation

$$\sum_{i=1}^r \omega_{\mathbf{k}_i} = \sum_{i=r+1}^{n+1} \omega_{\mathbf{k}_i} \quad (1.24)$$

and involve product of boson operators of the kind

$$a_{\mathbf{k}_1} a_{\mathbf{k}_2} \cdots a_{\mathbf{k}_r} a_{\mathbf{k}_{r+1}}^\dagger \cdots a_{\mathbf{k}_{n+1}}^\dagger \quad (1.25)$$

and their hermitian conjugates. Let us consider now, for example, the  $\hat{X}_2$  contribution in Eq. (1.21), and fix the frequencies  $\omega_{\mathbf{k}}, \omega_{\mathbf{k}_1}, \omega_{\mathbf{k}_2}$  such that  $\omega_{\mathbf{k}} = \omega_{\mathbf{k}_1} + \omega_{\mathbf{k}_2}$ . By ignoring the oscillating terms (the so-called rotating wave approximation), one obtains

$$\begin{aligned} \int_V d^3r \hat{X}_2(\mathbf{r}) &\simeq 2i\varepsilon_0 \sum_{\mathbf{k}_1} \sum_{\mathbf{k}_2} \sum_{\mathbf{k}_3} \mathcal{E}_{\mathbf{k}_1} \mathcal{E}_{\mathbf{k}_2} \mathcal{E}_{\mathbf{k}_3} \\ &\times \left[ \chi^{(2)}(-\omega_3; \omega_1, \omega_2) |\varepsilon_{\mathbf{k}_1} \varepsilon_{\mathbf{k}_2} \varepsilon_{\mathbf{k}_3}^* a_{\mathbf{k}_1} a_{\mathbf{k}_2} a_{\mathbf{k}_3}^\dagger \int_V d^3r e^{i(\mathbf{k}_1 + \mathbf{k}_2 - \mathbf{k}_3)\cdot\mathbf{r}} - \text{h. c.} \right], \end{aligned} \quad (1.26)$$

which is equivalent to Eq. (1.14).

With regard to the approximations in deriving Eq. (1.22), we notice the following.

- i) The electric dipole approximation is implicitly assumed by considering  $\chi^{(n)}(\omega)$  independent on the wave-vector  $\mathbf{k}$ .
- ii) In the electromagnetic energy of the medium, terms of order  $\omega \partial \chi^{(n)} / \partial \omega$  have been ignored. Such approximation holds for small dispersive media, for which  $\omega \partial \chi^{(n)} / \partial \omega \ll \chi^{(n)}$ , and far away from resonances.
- iii) The canonical quantization of the field should be performed in the nonlinear medium. Thus, small nonlinearities have been assumed.

Again we find that the phase-matching condition  $\Delta\mathbf{k} = \mathbf{k}_1 + \mathbf{k}_2 - \mathbf{k}_3 = 0$  turns out to be the crucial requirement for the effectiveness of the parametric process. In classical terms the phase-matching condition guarantees the synchronism of the phase velocity of the electric field and the polarization waves. For normal dispersion usually one has  $\Delta\mathbf{k} \neq 0$ . Hence anomalous dispersion, optical activity and more conveniently birefringence must be employed for achieving phase-matching conditions. For a detailed discussion on phase-matching techniques in crystals, see [9].

The relevant modes of the radiation involved in a nonlinear parametric process can be easily determined by the condition (1.24) and the corresponding phase-matching condition

$$\sum_{i=1}^r \mathbf{k}_i = \sum_{i=r+1}^{n+1} \mathbf{k}_i . \quad (1.27)$$

The effective Hamiltonians so derived can describe a number of nonlinear parametric processes, according to which excited modes impinge onto the crystal. For example, let us take into account the three-wave interaction

$$\hat{H} \propto \chi^{(2)} abc^\dagger + \text{h. c.} , \quad (1.28)$$

where  $a, b, c$  are three different modes at frequency  $\omega_a, \omega_b, \omega_c$ , respectively. Hamiltonian (1.28) can describe

- a) sum-frequency mixing for input  $a$  and  $b$  and  $\omega_c = \omega_a + \omega_b$ ,
- b) difference-frequency mixing for input  $a$  and  $c$  and  $\omega_b = \omega_a - \omega_c$ ,
- c) nondegenerate parametric amplification for input  $c$ , and  $\omega_c = \omega_a + \omega_b$ .

It is possible that some of the modes in Hamiltonian (1.28) degenerate in the same mode (i.e. at the same frequency, wave vector and polarization), thus leading to a so-called degenerate parametric process as

- d) second harmonic generation for input  $a \equiv b$  and  $\omega_c = 2\omega_a$ ,
- e) degenerate parametric amplification for input  $c$ , and  $\omega_c = 2\omega_a$ , with  $a \equiv b$ ,
- f) other effects as optical rectification and Pockels effect involving d.c. fields.

The interaction Hamiltonians  $\hat{H}_I$  derived in the rotating wave approximation are time-independent. Thus, the unitary operators  $\hat{U}(t)$  that describe the evolution of the radiation field through parametric processes are given by

$$\hat{U}(t) = \exp\left(-i\hat{H}_I t/\hbar\right) , \quad (1.29)$$

the effective gain being proportional to the susceptibility tensor and to the optical path of the field inside the crystal.

The interactions of different radiation modes through nonlinear crystals allow the generation of interesting states of light, which exhibit a rich variety of phenomena. Most of the theoretical analyses and the experimental configurations usually refer to situations where at least one mode—the so-called “pump” mode—is placed in a high-amplitude coherent state (the state at the output of a well-stabilized laser). In this case the parametric approximation is widely used to compute the dynamical evolution [7]. In such approximation the pump mode is classically treated as a  $c$ -number, thus neglecting both the depletion mechanism and the quantum fluctuations. As a result, bilinear and trilinear Hamiltonians as those derived in Eq. (1.28) are reduced to linear and quadratic forms in the field operators, respectively, and hence some useful mathematical tools—typically decomposition formulas for Lie algebras—can be exploited for calculations [10, 11, 12]. The validity regime of the parametric approximation is discussed in the next section, with particular attention to the parametric processes that allow to realize experimentally some fundamental unitary operators in quantum optics.

### 1.3 On the validity of the parametric approximation

In the validity regime of the parametric approximation different optical devices experimentally realize different unitary operators in quantum optics. For example, a beam splitter, by suitably mixing the signal state with a strong local oscillator at the same frequency, realizes the displacement operator

$$\hat{D}(\alpha) = \exp\left(\alpha a^\dagger - \bar{\alpha} a\right), \quad (1.30)$$

which generates the coherent state  $|\alpha\rangle$  from the vacuum. Similarly, a degenerate parametric amplifier realizes the squeezing operator

$$\hat{S}(\xi) = \exp\left[\frac{1}{2}\left(\xi a^{\dagger 2} - \bar{\xi} a^2\right)\right], \quad (1.31)$$

which is the generator of the squeezed vacuum. Finally, a nondegenerate parametric amplifier realizes the two-mode squeezing operator

$$\hat{S}_2(\chi) = \exp\left(\chi a^\dagger b^\dagger - \bar{\chi} ab\right), \quad (1.32)$$

i.e. the generator of twin beam.

The conditions under which the parametric approximation holds have been considered by a number of authors [13, 14, 15, 16], however without giving a general validity criterion, which is the main concern of this section. Quantum effects in two-mode optical amplifiers have been extensively analyzed [14, 15, 17, 18, 19, 20, 21, 22, 23, 24].

Frequency couplers with intensity dependent coupling have been studied [19, 20, 25], whereas the case of degenerate parametric amplifier has been considered by many authors [14, 15, 18, 21, 22, 23, 24]. Phase correlations [22] and the signal-pump degree of entanglement [23] have been examined. The effect of pump squeezing has been also considered [24]. On the other hand, though trilinear processes have been thoroughly analyzed in Refs. [26, 18, 28], only little attention has been devoted to the parametric approximation in nondegenerate amplifiers [16].

The most explicit conditions for the validity of the parametric approximation have been derived in Refs. [13] and [14], for the beam splitter and the degenerate parametric amplifier, respectively. In both references sufficient conditions have been derived, which however can be widely breached in relevant cases of interest, as we will show in the following.

In this section we perform the exact numerical diagonalization of the full Hamiltonians pertaining the three above-mentioned devices [27]. As it was already noted by other authors [17, 18, 28] such a numerical treatment is made amenable by the presence of constants of motion that characterizes each Hamiltonian. In fact, the Hilbert space can be decomposed into the direct sum of subspaces that are invariant under the action of the unitary evolution. Therefore, one needs to diagonalize the Hamiltonian just inside each invariant subspace, thus considerably reducing the dimension of the diagonalization space [17, 18, 28].

We analyze in different subsections the cases of the beam splitter, the degenerate parametric amplifier and the nondegenerate parametric amplifier. The case of the beam splitter can be treated analytically, but we also present some numerical results in order to introduce the general approach that will be used for the parametric amplifiers. For each device, we look for the conditions under which the parametric approximation holds, for both vacuum and non-vacuum input signal states. The comparison between the exact evolution and the theoretical predictions from the parametric approximation is made in terms of the overlap  $\mathcal{O} = \sqrt{\text{Tr}(\hat{\rho}_{\text{out}} \hat{\rho}_{\text{th}})}$  between the state  $\hat{\rho}_{\text{out}}$  that exits the device and the theoretical state  $\hat{\rho}_{\text{th}}$  obtained within the approximation. An explicit comparison in terms of photon number distributions and Wigner functions is also given for some interesting and representative cases.

The main result of the section is to show that the usual requirements for the validity of the parametric approximation, namely short interaction time and strong classical undepleted pump, are too strict. Indeed, we show that the only relevant requirement is the coherence of the pump after the interaction, rather than its undepletion. In fact, we will show typical examples in which the pump at the input is weak (one photon in average), after the interaction it is highly depleted, and notwithstanding the parametric approximation still holds. On the other hand, there are cases in which the pump after the interaction is only slightly depleted, however is no longer coherent,

and the approximation fails. Finally, we show some interesting features such as pump squeezing and Schrödinger-cat-like state generation that arise when the parametric approximation breaks down.

### 1.3.1 Displacer

The beam splitter is a passive device that couples two different modes of radiation at the same frequency through a first-order susceptibility-tensor  $\chi^{(1)}$  medium. Such device is widely used in quantum optics [2, 29], from homodyne/heterodyne detection [30], to directional couplers [31] and cavity QED [32]. In the rotating wave approximation and under phase-matching conditions, the beam splitter Hamiltonian writes in terms of the two mode operators  $a$  and  $b$  as follows

$$\hat{H}_{BS} = \kappa \left( ab^\dagger + a^\dagger b \right) , \quad (1.33)$$

where  $\kappa$  is the coupling constant proportional to the  $\chi^{(1)}$  of the medium. The unitary evolution operator of the device in the interaction picture writes

$$\hat{U}_{BS} = \exp \left[ -i\tau \left( ab^\dagger + a^\dagger b \right) \right] = e^{-i \tan \tau ab^\dagger} | \cos \tau |^{a^\dagger a - b^\dagger b} e^{-i \tan \tau a^\dagger b} , \quad (1.34)$$

where  $\tau$  is the interaction time rescaled by the coupling  $\kappa$ . The factorization of the operator  $\hat{U}_{BS}$  in Eq. (1.34) has been derived by applying the Baker-Campbell-Hausdorff formula for the SU(2) algebra [10, 11, 12]. The Heisenberg evolution of the field modes reads

$$\hat{U}_{BS}^\dagger \begin{pmatrix} a \\ b \end{pmatrix} \hat{U}_{BS} = \begin{pmatrix} a \cos \tau - ib \sin \tau \\ -ia \sin \tau + b \cos \tau \end{pmatrix} . \quad (1.35)$$

From Eq. (1.35) it turns out that the transmissivity  $\theta$  at the beam splitter is given by the relation  $\theta = \cos^2 \tau$ .

The parametric approximation refers to situations in which one mode—say mode  $b$ —is excited in a strong coherent state. In this case in the first line of Eq. (1.34) the operator  $b$  might be replaced by a  $c$ -number, namely the complex amplitude  $\beta$  of the coherent state. Under this assumption, the evolution operator (1.34) would rewrite as the displacement operator  $\hat{D}(-i\beta\tau)$  of Eq. (1.30). A more refined approximation can take into account the  $2\pi$ -periodicity in the exact Heisenberg equations (1.35), thus leading to the operator  $\hat{D}(-i\beta \sin \tau)$ . Indeed, this more precise result can be obtained by recasting the factorized expression in Eq. (1.34) in normal order with respect to mode  $a$ , after taking the expectation over mode  $b$  [33, 34]. The simple form of the bilinear Hamiltonian in Eq. (1.33) allows to clarify the conditions under which the parametric approximation (1.30) holds [13]. A set of sufficient requirements are given by

$$\begin{aligned} |\beta| &\rightarrow \infty , & \sin \tau &\rightarrow 0 \\ |\beta| \sin \tau &= \text{constant} , \end{aligned} \quad (1.36)$$

without any assumption on the “signal” state for mode  $a$ . Hence, by combining a signal input state  $\hat{\rho}_{\text{in}}$  with a strong coherent local oscillator  $|\beta\rangle$  in a beam splitter with very high transmissivity, one can achieve the displacement operator in Eq. (1.30). The theoretically expected state  $\hat{\rho}_{\text{th}}$  then writes

$$\hat{\rho}_{\text{th}} = \hat{D}(-i\beta \sin \tau) \hat{\rho}_{\text{in}} \hat{D}^\dagger(-i\beta \sin \tau) . \quad (1.37)$$

Here we present some numerical results concerning the exact unitary evolution of Eq. (1.34). The dynamics generated by the Hamiltonian (1.33) preserves the total number of photons involved in the process, in agreement with the following commutation relation

$$\left[ \hat{H}_{BS}, a^\dagger a + b^\dagger b \right] = 0 . \quad (1.38)$$

Therefore, it is convenient to decompose the Hilbert space  $\mathcal{H}_a \otimes \mathcal{H}_b$  as a direct sum of subspaces with a fixed number  $N$  of photons, since these are invariant under the action of the unitary evolution operator (1.34). Such a decomposition can be written as follows

$$\mathcal{H}_a \otimes \mathcal{H}_b = \bigoplus_{N=0}^{+\infty} \mathcal{H}_N \quad (1.39)$$

where

$$\mathcal{H}_N = \text{Span} \{ |m\rangle \otimes |N-m\rangle , m \in [0, N] \} , \quad (1.40)$$

$\text{Span}\{\cdot\}$  denoting the Hilbert subspace linearly spanned by the orthogonal vectors within the brackets, and  $|n\rangle \otimes |m\rangle \equiv |n, m\rangle$  representing the common eigenvector of the number operator of the two modes. The decomposition in Eq. (1.39) makes the Hamiltonian (1.33) block-diagonal, namely

$$\hat{H}_{BS} = \sum_{N=0}^{+\infty} \hat{h}_N , \quad (1.41)$$

where  $\hat{h}_N$  acts just inside the subspace  $\mathcal{H}_N$ . Correspondingly, a generic two-mode state  $|\psi_0\rangle$  can be written in the orthogonal basis (1.40) as follows

$$|\psi_0\rangle = \sum_{N=0}^{+\infty} \sum_{m=0}^N c_{m, N-m} |m, N-m\rangle . \quad (1.42)$$

The diagonalization is performed inside each invariant subspace, and the truncation of the series in Eqs. (1.41) and (1.42) corresponds to fix the maximum eigenvalue of the constant of motion  $a^\dagger a + b^\dagger b$ .

The state  $\hat{\rho}_{\text{out}}$  evaluated by the exact evolution operator (1.34) is given by

$$\hat{\rho}_{\text{out}} = \text{Tr}_b[\hat{U}_{BS}(\hat{\rho}_{\text{in}} \otimes |\beta\rangle\langle\beta|)\hat{U}_{BS}^\dagger] , \quad (1.43)$$

where  $\text{Tr}_b$  denotes the partial trace on  $\mathcal{H}_b$ . The comparison between the theoretical state  $\hat{\rho}_{\text{th}}$  of Eq. (1.37) within the parametric approximation and the actual state  $\hat{\rho}_{\text{out}}$  is made in terms of the relative overlap

$$\mathcal{O} \equiv \sqrt{\text{Tr}[\hat{\rho}_{\text{th}}\hat{\rho}_{\text{out}}]} . \quad (1.44)$$

In the case of coherent input signal the overlap is evaluated analytically. One has

$$\hat{U}_{BS}|\alpha\rangle \otimes |\beta\rangle = |\alpha \cos \tau - i\beta \sin \tau\rangle \otimes |\beta \cos \tau - i\alpha \sin \tau\rangle , \quad (1.45)$$

and thus

$$\mathcal{O} = |\langle \alpha - i\beta \sin \tau | \alpha \cos \tau - i\beta \sin \tau \rangle| = \exp\left(-4|\alpha|^2 \sin^4 \frac{\tau}{2}\right) . \quad (1.46)$$

From Eq. (1.46) it is apparent that the parametric approximation gives always exact results for vacuum input state ( $\alpha \equiv 0$ ), whereas it is justified for coherent state as long as  $4|\alpha|^2 \sin^4(\tau/2) \ll 1$ , independently on the pump intensity.

We introduce the quantity  $\tau^*$  which represents, for a fixed value of the pump amplitude  $|\beta|$ , the maximum interaction time leading to an overlap larger than 99%. The value of  $\tau^*$  clearly depends on the input signal: in agreement with Eq. (1.46) it is not defined for the vacuum (parametric approximation is exact), whereas for a coherent input signal  $|\alpha\rangle$  it is given by

$$\tau^* = 2 \arcsin \sqrt{\frac{C}{|\alpha|}} \quad C = \frac{1}{2} (-\ln 0.99)^{1/2} \simeq 0.05 . \quad (1.47)$$

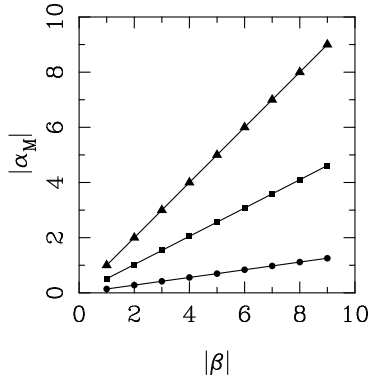


Figure 1.1: Performances of a beam splitter in achieving the displacement operator. We report the maximum displacing amplitude  $|z_M|$  achievable by a beam splitter as a function of the pump amplitude  $|\beta|$ . In the picture triangles refers to vacuum input, squares to coherent state input  $|\alpha \equiv 1\rangle$ , and circles to number state input  $|n \equiv 1\rangle$ .

The quantity  $\tau^*$  also determines the maximum displacing amplitude  $|\alpha_M| \equiv |\beta| \sin \tau^*$  that can be achieved by a beam splitter with a coherent pump  $|\beta\rangle$ . In Fig. 1.1 we have

reported  $|\alpha_M|$  for the vacuum, a coherent state and a number state as a function of the pump amplitude  $|\beta|$ . The linear behavior of the plots indicates that  $\tau^*$  is independent on the pump intensity. In the case of vacuum input we have complete energy transfer from the pump to the signal (slope of  $|\alpha_M|$  vs  $|\beta|$  equal to unit). Although they have the same energy, the coherent and number input states show different slopes, the coherent being more similar to the vacuum. Actually the set of coherent states is closed under the action of the displacement operator, so that the parametric approximation can fail only in predicting the exact amplitude of the output coherent state.

We conclude that the first of requirements (1.36) is too tight. At least for coherent and number states, as long as the signal average photon number is less than the pump one, the beam splitter can “displace” the signal also for very weak pump.

In the next sections we will deal with the problem of parametric approximation in nonlinear amplifiers.

### 1.3.2 Squeezer

The degenerate parametric amplifier couples a signal mode  $a$  at frequency  $\omega_a$  with a pump mode  $c$  at double frequency  $\omega_c = 2\omega_a$ . The interaction is mediated by the second-order susceptibility tensor  $\chi^{(2)}$  of the medium. Each photon in the pump mode produces a photon pair in the signal mode, giving rise to light with a number of interesting properties, such as phase-sensitive amplification, squeezing and antibunching [3, 4, 5, 6, 26]. In the rotating wave approximation and under phase-matching conditions the Hamiltonian writes

$$\hat{H}_{DP} = \kappa \left( a^2 c^\dagger + a^{\dagger 2} c \right), \quad (1.48)$$

with  $\kappa \propto \chi^{(2)}$ . The corresponding unitary evolution operator in the interaction picture reads

$$\hat{U}_{DP} = \exp \left[ -i\tau \left( a^2 c^\dagger + a^{\dagger 2} c \right) \right], \quad (1.49)$$

where  $\tau$  represents a rescaled interaction time. The parametric approximation replaces the pump mode  $c$  by the complex amplitude  $\beta$  of the corresponding coherent state, such that the operator (1.49) rewrites

$$\hat{S}(-2i\tau\beta) \equiv \exp \left[ -i\tau \left( \beta a^{\dagger 2} + \bar{\beta} a^2 \right) \right], \quad (1.50)$$

$\hat{S}(\zeta)$  being the squeezing operator [3]. In the case of coherent input signal  $|\alpha\rangle$ , the predicted state at the output is the squeezed state

$$\hat{S}(-2i\tau\beta)|\alpha\rangle = \hat{S}(-2i\tau\beta)\hat{D}(\alpha)|0\rangle = \hat{D}(\tilde{\alpha})\hat{S}(-2i\tau\beta)|0\rangle \equiv |\tilde{\alpha}, -2i\tau\beta\rangle, \quad (1.51)$$

with  $\tilde{\alpha} = \alpha \cosh(-2i\tau\beta) + \bar{\alpha} \sinh(-2i\tau\beta)$ . Notice that, differently from the beam splitter operator of Eq. (1.34), we have no method available to order Eq. (1.49) normally with

respect to mode  $c$  [as in Eq. (1.34) for  $b$ ] and then replace such mode by the  $c$ -number  $|\beta|$ . Hence, we have no analogous nonperturbative method to estimate the validity of the parametric approximation. Hillery and Zubairy have been approached the question [14] in terms of a perturbation series for the propagator of the Hamiltonian (1.48). For initial vacuum state at mode  $a$ , they write the following conditions

$$\begin{aligned} 1/|\beta| &\ll 1, & \tau &\ll 1, \\ \tau e^{4|\beta|\tau} &\ll 1, & e^{4|\beta|\tau} &\ll |\beta|. \end{aligned} \quad (1.52)$$

Here we evaluate the exact evolution generated by the operator (1.49) through numerical diagonalization of the Hamiltonian (1.48), using the method based on the constant of motion. In this case one has

$$\left[ \hat{H}_{DP}, a^\dagger a + 2c^\dagger c \right] = 0, \quad (1.53)$$

and the Hilbert space  $\mathcal{H}_a \otimes \mathcal{H}_c$  is decomposed in terms of invariant subspaces corresponding to the eigenvalues of the constant of motion  $a^\dagger a + 2c^\dagger c$ , namely

$$\mathcal{H}_a \otimes \mathcal{H}_c = \bigoplus_{N=0}^{+\infty} \mathcal{H}_N, \quad (1.54)$$

with

$$\mathcal{H}_N = \text{Span} \{ |N - 2m\rangle \otimes |m\rangle, m \in [0, \lfloor N/2 \rfloor] \}, \quad (1.55)$$

$\lfloor \cdot \rfloor$  denoting the integer part of  $x$ . Hence the Hamiltonian in Eq. (1.48) rewrites in the same fashion as in Eq. (1.41) and the block-diagonalization is performed for each  $\hat{h}_N$ , with  $N$  from 0 to the maximum allowed value of the constant of motion. Similarly to Eq. (1.42), a generic two-mode state  $|\psi_0\rangle$  is written as follows

$$|\psi_0\rangle = \sum_{N=0}^{+\infty} \sum_{m=0}^{\lfloor N/2 \rfloor} c_{N-2m,m} |N - 2m, m\rangle. \quad (1.56)$$

The performances of a degenerate parametric amplifier in realizing the squeezing operator  $\hat{S}(\zeta) = \exp[(\zeta a^{\dagger 2} - \bar{\zeta} a^2)/2]$  of Eq. (1.50) are depicted in Fig. 1.2. In Fig. 1.2a we have reported the maximum interaction time  $\tau^*$  that leads to an output signal whose overlap with the theoretical squeezed state is larger than 99%, as a function of the pump intensity  $|\beta|^2$ . In 1.2b we have shown the maximum squeezing parameter  $|\zeta_M|$  achievable by the amplifier, as a function of the pump amplitude  $|\beta|$ . According to Eq. (1.50) one has  $|\zeta_M| = 2|\beta|\tau^*$ . In both pictures we have considered the vacuum, a coherent state and two different number states at the input of the amplifier. For the same set of input states, we have also shown in Fig. 1.3 the average signal photon number as a function of the interaction time  $\tau$ , for five different values of the pump amplitude.

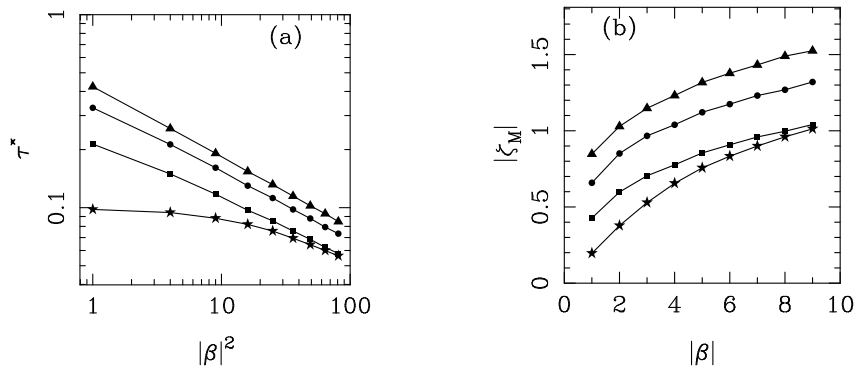


Figure 1.2: Performances of a degenerate parametric amplifier in providing the squeezing operator  $\hat{S}(\zeta)$ . In both pictures triangles refers to vacuum input, squares to coherent state input  $|\alpha \equiv 1\rangle$ , circles to number state input  $|n \equiv 1\rangle$ , and stars to number state input  $|n \equiv 2\rangle$ . In (a) we report the quantity  $\tau^*$ , namely the maximum interaction time that leads to an output signal whose overlap with the theoretical squeezed state is larger than 99%, as a function of the pump intensity  $|\beta|^2$ . In (b) we show the maximum squeezing parameter  $|\zeta_M|$  achievable by the degenerate parametric amplifier, as a function of the pump amplitude  $|\beta|$ .

From Fig. 1.2 it turns out that the requirements for vacuum input signal in Eq. (1.52) are too strict. In particular, the two conditions in the second line are not satisfied for  $1 < |\beta| < 9$  [see the line with triangles in Fig 1.2(a)]. Moreover, Fig. 1.2 shows that one can realize a squeezing operator even through a weak pump with just one photon.

By definition the validity of the parametric approximation is guaranteed for  $\tau < \tau^*$ ,  $\tau^*$  depending on  $|\beta|$  and on the input state. However, we want to provide a general criterion that can be easily checked experimentally. As we will show in the following, the undepletion of the pump is not a valid criterion. We argue that the relevant parameter, in order to confirm whether the parametric approximation is justified or not, is the degree of coherence of the pump *after* the nonlinear interaction. These statements are supported by the following numerical results.

Let us consider the case of a number input state  $|n = 1\rangle$  with pump amplitude  $|\beta| = 9$ . From Fig. 1.2 one can extract the maximum interaction time  $\tau^* \simeq 0.073$  for the validity of the parametric approximation, and the corresponding maximum squeezing parameter  $|\zeta_M| \simeq 1.314$ . The average photon number of the output state can be drawn from Fig. 1.3c as  $\langle n \rangle_{\text{out}} \simeq 9.68$ , corresponding to a pump depletion of about 5.4%. One might consider such a small depletion as the sign of the goodness of the parametric approximation. On the other hand, from Fig. 1.3c one recognizes the region  $0.33 \lesssim \tau \lesssim 0.44$ , in which the output signal is even less excited than that in the above example, and consequently the pump is less depleted. Nevertheless the parametric approximation does not hold in such range of interaction time, since  $\tau$  is larger than  $\tau^*$ . Let us now consider the Fano factor  $F = \langle \Delta \hat{n}^2 \rangle / \langle \hat{n} \rangle$  of the pump at the

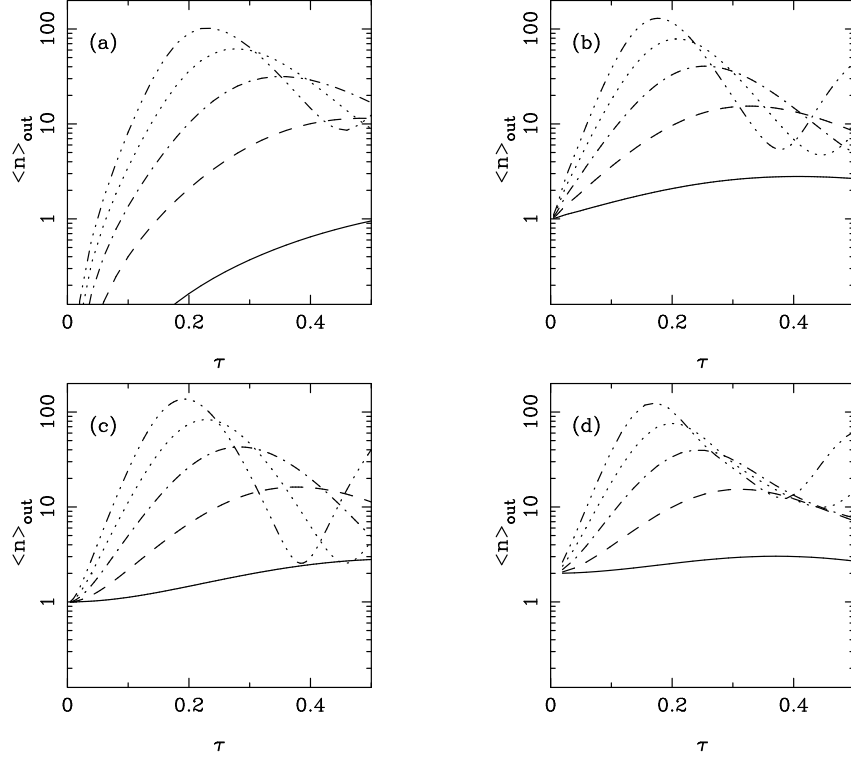


Figure 1.3: Average photon number  $\langle \hat{n} \rangle_{\text{out}}$  of the signal at the output of a degenerate parametric amplifier, as a function of the interaction time  $\tau$ . In (a) the case of vacuum input, in (b) coherent input  $|\alpha \equiv 1\rangle$ , in (c) number input  $|n \equiv 1\rangle$ , and in (d) number input  $|n \equiv 2\rangle$ . Different line-styles refer to different pump amplitudes:  $\beta = 9$  (dot-dot-dashed),  $\beta = 7$  (dotted),  $\beta = 5$  (dot-dashed),  $\beta = 3$  (dashed),  $\beta = 1$  (solid).

output. One finds that in the region  $0.33 \lesssim \tau \lesssim 0.44$  the Fano factor is always larger than  $F = 1.13$ , whereas for  $\tau < \tau^*$  it never exceeds  $F = 1.10$ .

More generally, in all situations in which the parametric approximation is satisfied we found that the Fano factor of the pump at the output never exceeds  $F = 1.10$ . This holds also when the pump is weak ( $|\beta|^2 = 1 \div 10$ ). Indeed, in this case the depletion of the pump can be strong, nevertheless the parametric approximation does not break down. In Fig. 1.4 we show the Fano factor of the output pump as a function of the interaction time  $\tau$ , for different values of the pump amplitude. Plots refer to vacuum input and to coherent state input  $|\alpha \equiv 1\rangle$ : similar plots can be obtained for other input states.

As the condition of pump undepletion does not guarantee the validity of the parametric approximation, so pump depletion by itself does not sign its failure: rather we have to consider the Fano factor of the pump. In order to stress this point, let us consider the extreme case of a pump with only one photon, and the input signal in the

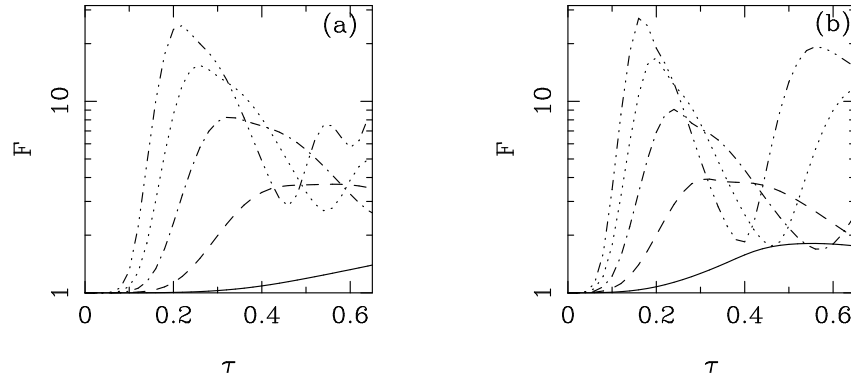


Figure 1.4: Fano factor  $F$  of the pump at the output of a degenerate parametric amplifier, as a function of the interaction time  $\tau$ . In (a) the case of vacuum input; in (b) of coherent input  $|\alpha \equiv 1\rangle$ . Different line-styles refer to different pump amplitude:  $\beta = 9$  (dot-dot-dashed),  $\beta = 7$  (dotted),  $\beta = 5$  (dot-dashed),  $\beta = 3$  (dashed),  $\beta = 1$  (solid).

vacuum. The exact numerical solution indicates that the parametric approximation holds for interaction time up to  $\tau^* \simeq 0.42$ , the squeezing parameter and the output signal photon number increasing up to  $|\zeta_M| \simeq 0.84$  and  $\langle n \rangle_{\text{out}} \simeq 0.74$ , respectively [see Figs. 1.2 and 1.3a]. Correspondingly, the pump depletion grows up to 37% at  $\tau = \tau^*$ . In spite of the strong depletion, the pump preserves a good degree of coherence: the Fano factor achieves at most the value  $F = 1.10$  at  $\tau = \tau^*$ .

In summary, the validity regime  $\tau < \tau^*$  for the parametric approximation does not identify with the condition of pump undepletion, rather it corresponds to a Fano factor not exceeding the initial coherent level more than 10%.

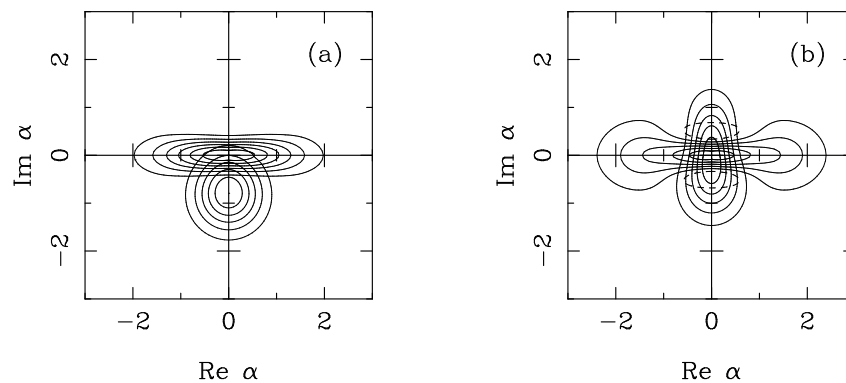


Figure 1.5: Contour plot Wigner functions of both the signal and the pump modes at the output of a degenerate parametric amplifier. The input signal is the vacuum, whereas the pump is initially in a coherent state  $\beta = -i$ . The time interaction is equal to  $\tau = \tau^* = 0.42$  in (a) and to  $\tau = 2\tau^* = 0.84$  in (b). Dotted lines in (b) denote negative values in the Wigner function of the signal.

What happens beyond the parametric regime? For interaction time larger than  $\tau^*$  new quantum effects arise at the output. In Fig. 1.5 we show the Wigner functions of both the signal and the pump modes at the output of the amplifier for  $\tau = \tau^*$  and  $\tau = 2\tau^*$ , with vacuum input and weak pump  $|\beta| = 1$ . In Fig. 1.6 the case of a stronger pump is given. As  $\tau$  increases, the pump first empties, then it starts refilling, preferably for even photon numbers, leading to oscillations in the photon number distribution. Remarkably, the corresponding Wigner functions of the pump and the signal exhibit interference in the phase space [35], the signal resembling a Schrödinger-cat.

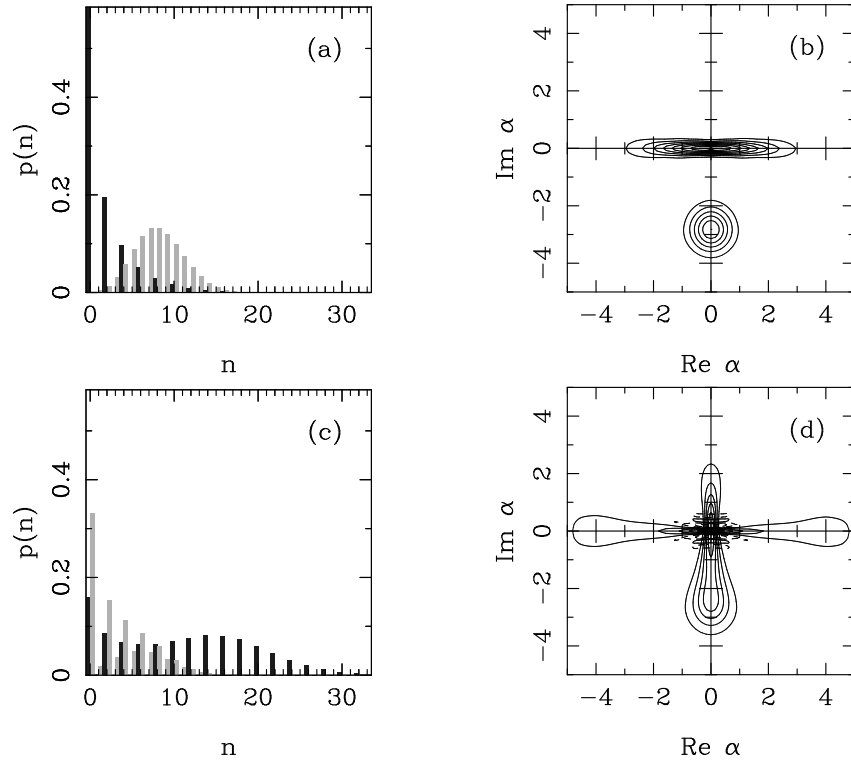


Figure 1.6: Photon number probability and contour plot Wigner function for both the signal and the pump mode at the output of a degenerate parametric amplifier. The plots refer to a situation in which the signal mode is initially in the vacuum and the pump mode is excited to a coherent state with amplitude  $\beta = -3i$ . In (a) and (b) the interaction time is equal to  $\tau \equiv \tau^* = 0.19$ , whereas (c) and (d) refer to an interaction time  $\tau = 0.43 > 2\tau^*$ . In the first case the parametric approximation well describes the real interaction, which produces a squeezed vacuum state with squeezing parameter  $r = 1.146$  corresponding to about 2 squeezing photons. On the other hand, parametric approximation does not hold in the second case. Notice that the break-down of parametric approximation is connected with the appearance of negative values in the Wigner function, which is a signature of quantum interference in the phase space.

### 1.3.3 Two-mode squeezer

The nondegenerate parametric amplifier involves three different modes of the radiation field—say the signal  $a$ , the idler  $b$  and the pump  $c$ —which are coupled by a  $\chi^{(2)}$  nonlinear medium. The relation between the frequencies of the field modes is given by  $\omega_c = \omega_a + \omega_b$ . The Hamiltonian of the amplifier under phase-matched conditions can be written in the rotating wave approximation as follows

$$\hat{H}_{NP} = \kappa \left( abc^\dagger + a^\dagger b^\dagger c \right), \quad (1.57)$$

with  $\kappa \propto \chi^{(2)}$ . The Hamiltonian in Eq. (1.57) describes also the case in which the frequencies pertaining modes  $a$  and  $b$  are the same, provided that the respective wave vectors and/or polarizations are different. The dynamics induced by the Hamiltonian (1.57) leads to a considerably rich variety of phenomena, such as generation of strongly correlated photon pairs by parametric downconversion [36, 37, 38], phase insensitive amplification [10, 7], generation of heterodyne eigenstates that are suitable for optimal phase detection [39, 40], polarization entanglement [41] and realization of Bell states [38, 41, 42, 43]. The unitary evolution operator in the interaction picture reads

$$\hat{U}_{NP} = \exp \left[ -i\tau \left( abc^\dagger + a^\dagger b^\dagger c \right) \right], \quad (1.58)$$

where  $\tau$  represents a rescaled interaction time. In the parametric approximation the pump mode  $c$  is replaced with the complex amplitude  $\beta$  of the corresponding coherent state, thus achieving the two-mode squeezing operator

$$\hat{S}_2(-i\tau\beta) \equiv \exp \left[ -i\tau \left( \beta a^\dagger b^\dagger + \bar{\beta} ab \right) \right]. \quad (1.59)$$

The two-mode squeezing operator yields a suppression of the quantum fluctuations in one quadrature of the sum and difference of modes  $a \pm b$  [44]. When applied to vacuum input, the unitary operator in Eq. (1.59) generates the so-called twin beam

$$\hat{S}_2(\chi)|0,0\rangle = (1 - |\lambda|^2)^{1/2} \sum_{n=0}^{\infty} \lambda^n |n,n\rangle, \quad (1.60)$$

where  $\lambda = \arg(\chi) \tanh |\chi|$ . The expression in Eq. (1.60) can be easily derived by factorizing the  $\hat{S}_2$  operator through the decomposition formulas for the SU(1,1) Lie algebra [10, 11, 12].

The dynamics of the nondegenerate parametric amplifier admits two independent constants of motion. We choose them as follows

$$\hat{N} = \frac{1}{2} \left[ a^\dagger a + b^\dagger b + 2c^\dagger c \right], \quad \hat{K} = a^\dagger a + c^\dagger c. \quad (1.61)$$

Correspondingly, we decompose the Hilbert space  $\mathcal{H}_a \otimes \mathcal{H}_b \otimes \mathcal{H}_c$  in the direct sum

$$\mathcal{H}_a \otimes \mathcal{H}_b \otimes \mathcal{H}_c = \bigoplus_{N=0}^{\infty} \bigoplus_{K=0}^N \mathcal{H}_{NK}, \quad (1.62)$$

where the invariant subspaces  $\mathcal{H}_{NK}$  are given by

$$\mathcal{H}_{NK} = \text{Span} \{ |K - m\rangle \otimes |N - K - m\rangle \otimes |m\rangle, m \in [0, \min(K, N - K)] \}. \quad (1.63)$$

The Hamiltonian  $\hat{H}_{NP}$  and a generic three-mode state  $|\psi_0\rangle$  will be consistently written as follows

$$\hat{H}_{NP} = \sum_{N=0}^{+\infty} \sum_{K=0}^N \hat{h}_{NK}, \quad (1.64)$$

$$|\psi_0\rangle = \sum_{N=0}^{+\infty} \sum_{K=0}^N \sum_{m=0}^{\min(K, N-K)} c_{K-m, N-K-m, m} |K - m, N - K - m, m\rangle. \quad (1.65)$$

To compute the exact dynamical evolution, one then diagonalizes each block  $\hat{h}_{NK}$  in Eq. (1.64) up to a fixed maximum value of  $N$  and makes the input state evolve in the representation of Eq. (1.65).

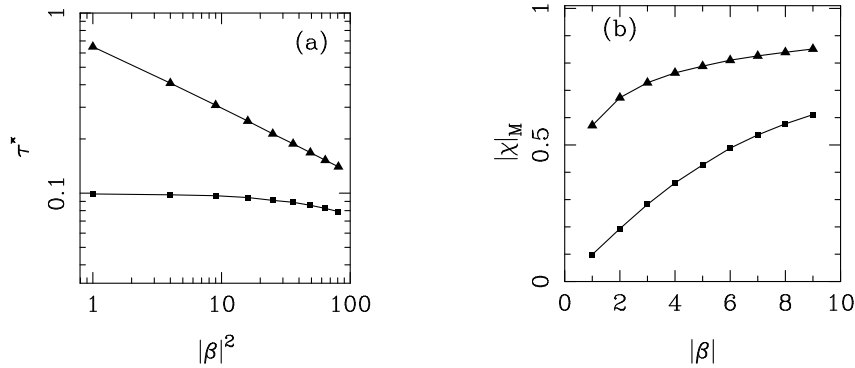


Figure 1.7: Performances of a nondegenerate parametric amplifier in achieving the two-mode squeezing operator (1.60). In both pictures triangles refers to vacuum input and circles to photon number state  $|1, 1\rangle$  input. In (a) we report the quantity  $\tau^*$ , namely the maximum interaction time that leads to an output signal whose overlap with the theoretical state is larger than 99%, as a function of the pump intensity  $|\beta|^2$ . In (b) we show the corresponding maximum two-mode squeezing parameter  $|\chi_M|$  achievable by the nondegenerate parametric amplifier, as a function of the pump amplitude  $|\beta|$ .

As in Sec. 1.3.2, we have evaluated the maximum interaction time  $\tau^*$  that provides an output state—in the signal and idler modes—whose overlap with the state predicted by the parametric approximation is larger than 99%. The time  $\tau^*$  for vacuum input and number input  $|n \equiv 1, n \equiv 1\rangle$  is plotted as a function of the pump intensity in Fig. 1.7a. The corresponding achievable two-mode squeezing parameter—the maximum argument  $|\chi_M|$  in the operator (1.60)—is represented in Fig. 1.7b. In Fig. 1.8 we show the average photon number  $\langle n \rangle_{\text{out}}$  of the output signal mode as a function of the interaction time, and for different values of the pump amplitude. Notice that the

quantity  $a^\dagger a - b^\dagger b$  is conserved, so that, for the considered input states, the idler mode has the same average photon number as the signal one.

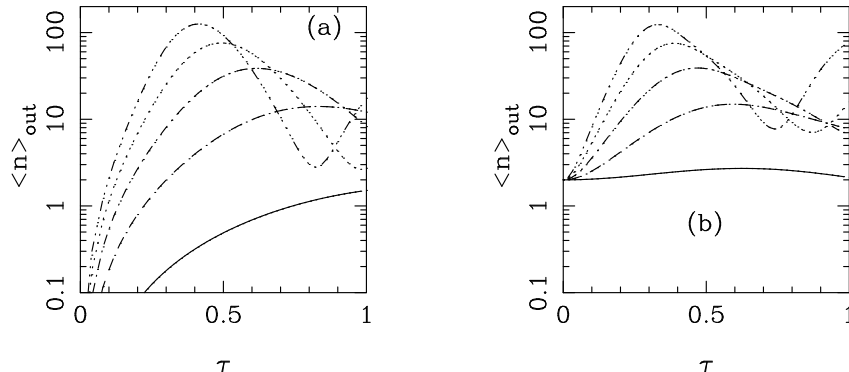


Figure 1.8: Average photon number  $\langle \hat{n} \rangle_{\text{out}}$  of the signal at the output of a nondegenerate parametric amplifier, as a function of the interaction time  $\tau$ . In (a) the case of vacuum input, and in (b) the case of photon number input  $|1, 1)$ . Different line-styles refer to different pump amplitudes:  $\beta = 9$  (dot-dot-dashed),  $\beta = 7$  (dotted),  $\beta = 5$  (dot-dashed),  $\beta = 3$  (dashed),  $\beta = 1$  (solid).

As shown for the degenerate case, here also the requirement of a strong pump is not peremptory, whereas the undepletion of the pump does not guarantee the validity of the parametric approximation. Again, it is the Fano factor  $F$  of the pump after the interaction that well discriminates the working regimes of the amplifier. As long as  $F \leq 1.10$ , the overlap between the states at the output and those predicted by the parametric approximation is larger than 99%. For interaction time longer than  $\tau^*$ , the pump mode reveals its quantum character, by showing oscillations in the number probability. This is illustrated in Fig. 1.9, where we report the photon number probabilities for both the signal and the pump modes in the case of vacuum input and pump amplitude equal to  $|\beta| = 5$ , for different values of the interaction time.

## 1.4 Conclusion

The quantum description of many optical devices is based on interaction Hamiltonians that couple different modes of radiation through the susceptibility tensor of the medium that supports the interaction. When the frequency of the radiation modes are far away from the resonances of the medium, a parametric process due to the coherence of the dipoles excited inside the crystal is effective, provided that the phase-matching conditions are satisfied. The theoretical predictions about such interactions are usually drawn in the so-called parametric approximation, i.e. by treating the pump mode classically as a fixed  $c$ -number. Owing to such approximation, an analytical treatment is possible with the help of the factorization formulas for Lie algebras.

We have investigated the conditions under which the parametric approximation holds in the treatment of  $\chi^{(2)}$  nonlinear amplifiers, by resorting to the exact diagonalization of their full Hamiltonians. We have explicitly compared the states evaluated by the exact evolution with those predicted by the parametric approximation, in terms of the overlap between such states. On one hand, we have shown that the regime of validity of the parametric approximation is very large, including also the case of weak pump with  $1 \div 10$  mean photon number. On the other, we have found that neither the condition of pump undepletion guarantees the goodness of the approximation, nor the condition of pump depletion signs its failure. We found that the degree of coherence of the pump *after* the interaction is a univocal parameter that discriminates the working regimes of the amplifiers. In terms of the pump Fano factor we found that a deviation from the coherent level smaller than 10% guarantees an overlap larger than 99% between the states predicted within the parametric approximation and those evaluated by the exact Hamiltonian.

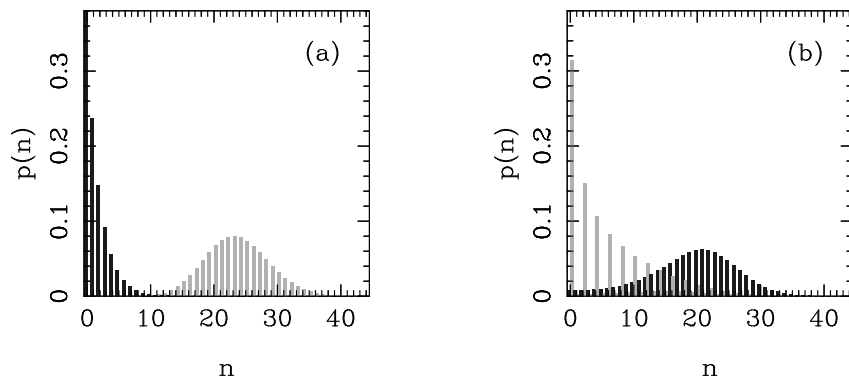


Figure 1.9: Photon number probabilities for both the signal and the pump modes at the output of a nondegenerate parametric amplifier. The plots refer to a situation in which the signal mode is initially in the (two-mode) vacuum and the pump mode is excited to a coherent state with amplitude  $\beta = -5i$ . The interaction time is equal to  $\tau \equiv \tau^* = 0.214$  in (a), and to  $\tau = 3\tau^*$  in (b). In the first case the parametric approximation well describes the real interaction, which produces a twin-beam state with two-mode squeezing parameter  $\chi = 0.789$  corresponding to about 3.3 output photons. On the other hand, parametric approximation does not hold in the second case, as it can be easily recognized from the pump squeezing. The pump Fano factor in (b) is about  $F = 7.4$ .

For long interaction times the approximation breaks down, and the quantum character of the pump mode is revealed. Oscillations in the pump number probability appear and, correspondingly, the Wigner function of the signal mode assumes negative values and resembles a Schrödinger-cat state.



## Chapter 2

# Generation of radiation states with enhanced phase properties

### 2.1 Introduction

The quantum-mechanical measurement of the phase of the radiation field is the essential problem of high sensitive interferometry, and has received much attention in quantum optics [45, 46]. Most of the work has been devoted to measurements on a single-mode electromagnetic field, where the measurement cannot be achieved exactly, even in principle, due to the lack of a unique self-adjoint operator. Quantum estimation theory provides a more general description of quantum statistics in terms of positive operator-valued measures (POM) and gives the theoretical definition of an optimized phase measurement [47]. However, no feasible scheme has been devised yet, which can even approach such optimal measurement.

Among the single-mode radiation states, the phase-coherent states introduced in Ref. [48] are particularly interesting because they are optimal phase states for both the Süssmann and the reciprocal peak likelihood measure of phase uncertainty [48, 49, 50]. Moreover, the phase-coherent states maintain phase coherence under phase amplification <sup>1</sup>, such that they are privileged states for phase-based communication channels. The first proposed experimental set-up in the present chapter is an interaction scheme involving nonlinear  $\chi^{(2)}$  media for the generation of phase-coherent states. The scheme is based on spontaneous parametric downconversion followed by upconversion of the resulting twin beam.

The absence of a proper self-adjoint operator in the single-mode phase measurement is mainly due to the semiboundedness of the spectrum of the number operator [48, 53], which is canonically conjugated to the phase in the sense of a Fourier-transform

---

<sup>1</sup>The concept of quantum phase amplification can be given a precise meaning in the context of the quantum estimation theory. For more details see Refs. [47, 51, 52]

pair [54]. This observation discloses the route toward an exact phase measurement in terms of two-mode fields, where a phase-difference operator becomes conjugated to an unbounded number-difference operator [55]. The second proposal of the chapter is an experimental scheme that achieves ideal phase detection on a two-mode field. The field is obtained by means of a twin-beam state followed by a high-transmissivity beam-splitters with strong local oscillators, or alternatively by nondegenerate parametric amplification of coherent states. The ideal detection is achieved through an unconventional use of the heterodyne detector. Finally, the scheme for a repeatable two-mode phase measurement is also presented. The property of repeatability allows to check the evolution of the signal under successive measurements, and possibly also to drive the evolution itself through the state reduction.

The general problem of phase estimation is solved in the last section of the chapter, by means of a generalization of the Holevo method [52].

## 2.2 Generation of phase-coherent states

In the following we propose an experimental set-up for the generation of phase-coherent states (PCS) based on parametric amplification of vacuum followed by up-conversion of the resulting twin beam. The three-wave dynamics is evaluated without approximation resorting to the numerical block-diagonalization of the Hamiltonian in invariant subspaces of the constants of motion, along similar lines as in Chapter 1. We will show that there is an experimentally achievable working regime to approximate PCS with high conversion rate [56].

In the rotating wave approximation, according to Sec. 1.2, the nondegenerate three-wave interactions are described by the Hamiltonian

$$\hat{H} \propto \chi^{(2)} \left[ abc^\dagger + a^\dagger b^\dagger c \right], \quad (2.1)$$

where  $a$ ,  $b$  and  $c$  are the annihilation operators of the three relevant modes, whose frequencies satisfy the relation  $\omega_c = \omega_a + \omega_b$ . Depending on the input state of the field, the Hamiltonian (2.1) describes phase-insensitive amplification or frequency up- or down-conversion. The first kind of process occurs in situations with small  $a$  and  $b$  and large coherent  $c$ , so that the parametric approximation can be applied. On the other hand, when all the three modes participates to the quantum dynamics we are in the presence of frequency up- and down-conversion processes.

In the present section we are interested in the situation depicted in Fig. 2.1, where the interaction Hamiltonian (2.1) is applied twice: in the first step as a parametric (spontaneous) down-conversion of the vacuum state, generating a twin beam on modes  $a$  and  $b$ , and in the second step as the up-conversion of twin beam into mode  $c$ .

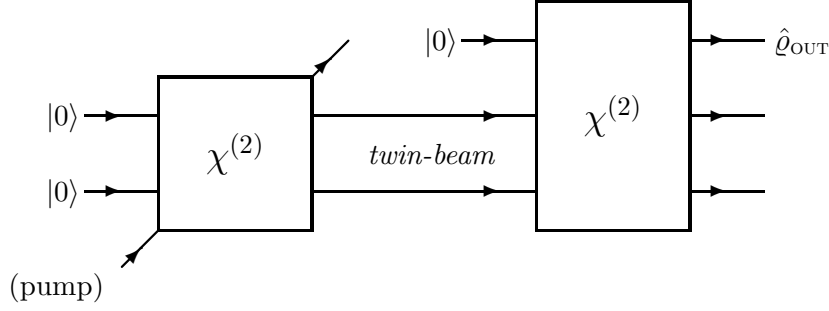


Figure 2.1: Scheme of generation of phase-coherent states.

The outgoing quantum state of radiation will be shown to resemble closely the phase-coherent state (PCS)

$$|\lambda\rangle = \sqrt{1 - |\lambda|^2} \sum_{n=0}^{\infty} \lambda^n |n\rangle, \quad (2.2)$$

which has been introduced by Shapiro *et al.* in Ref. [48]. The phase-coherent states are interesting because they are optimal phase states for both the Süssmann and the reciprocal peak likelihood [48] measure of phase uncertainty [49, 50]. On the other hand, they also could serve as *seed* states [57, 58, 59] in sampling canonical phase distribution by unconventional heterodyne detection [39]. Moreover, one should mention that the PCS maintain phase coherence under phase amplification [51], such that they are privileged states for phase-based communication channels.

In suggesting the present scheme we have been inspired by Ref. [10], where an ideal scheme using a photon number duplicator was suggested for PCS synthesis from twin beam. As a matter of fact, in such recombination process the photon number duplicator is well approximated by the up-conversion from Hamiltonian (2.1) with mode  $c$  initially in the vacuum [60, 61]. What we are showing now is that the interaction scheme sketched in Fig. 2.1 is indeed effective for the generation of PCS. We analyze the performances of the twin-beam up-conversion in producing phase-coherent states in the second stage of the scheme of Fig. 2.1.

According to Sec. 1.3.3, within the parametric approximation the dynamics of the nondegenerate parametric amplifier is governed by the evolution operator

$$\hat{U} = \exp\left(\zeta a^\dagger b^\dagger - \bar{\zeta} ab\right), \quad (2.3)$$

where  $\zeta = -i\kappa t\alpha$ ,  $t, \kappa, \alpha$  being the interaction time, the coupling constant containing the nonlinear susceptibility, and the pump amplitude, respectively. For vacuum input, the corresponding output state is given by the twin-beam state

$$|\chi\rangle = \sqrt{1 - |\chi|^2} \sum_{n=0}^{\infty} \chi^n |n, n\rangle, \quad (2.4)$$

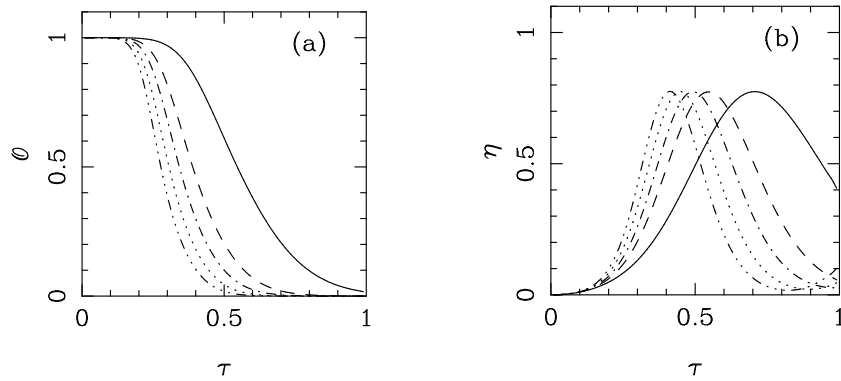


Figure 2.2: In (a): overlap  $\mathcal{O} = \sqrt{\langle \chi | \hat{\rho}' | \chi \rangle}$  between the state  $\hat{\rho}'$  coming from the exact evolution and the twin beam  $|\chi\rangle$  expected within the parametric approximation, as a function of the scaled time  $\tau = \kappa t$  for different values of the pump input photon number. In (b): energy conversion rate  $\eta$  as a function of the scaled time for different values of the pump input photon number. In both plots different line styles denotes different values of pump intensity:  $\langle \hat{n}_c \rangle = 81$  (dot-dot-dashed),  $\langle \hat{n}_c \rangle = 64$  (dotted),  $\langle \hat{n}_c \rangle = 49$  (dot-dashed),  $\langle \hat{n}_c \rangle = 36$  (dashed),  $\langle \hat{n}_c \rangle = 16$  (solid). The interaction time leading to maximum conversion rate follows the relation  $\tau_{opt} \propto \langle \hat{n}_c \rangle^{-1/3}$ .

where

$$\chi = -i \tanh(\kappa t |\alpha|) e^{i \arg \alpha}. \quad (2.5)$$

We have used the numerical diagonalization of Sec. 1.3.3 to evaluate the overlap

$$\mathcal{O} = \sqrt{\langle \chi | \hat{\rho}' | \chi \rangle} \quad (2.6)$$

between the state  $\hat{\rho}'$  coming from the exact evolution and the expected twin beam  $|\chi\rangle$ . In Fig. 2.2(a) we show the behavior of the overlap as a function of the scaled interaction time  $\tau = \kappa t$  for different values of the pump input power. In order to evaluate the efficiency of the process we have also considered the energy conversion rate  $\eta$ , which is defined as

$$\eta = \frac{1}{2} \frac{\text{Tr} [\hat{\rho}' (\hat{n}_a + \hat{n}_b)]}{\text{Tr} [|\psi_0\rangle\langle\psi_0| \hat{n}_c]}, \quad (2.7)$$

where  $|\psi_0\rangle = |0, 0, \alpha\rangle$ . In Eq. (2.7)  $\eta$  runs between zero and one, the factor 1/2 coming from frequency conversion. In Fig. 2.2(b) we show the behavior of  $\eta$  as a function of the scaled interaction time  $\tau$  for different values of the input power, as in Fig. 2.2(a). It is apparent that parametric approximation is valid also for moderate input power, and that one has a considerably wide range of values of the interaction time leading to an overlap very close to unit, the weaker is the pump, the larger is this range. On the

other hand, these values of the interaction time correspond to a low conversion rate. By the way, we note that the interaction time leading to maximum conversion rate follows the relation  $\tau_{opt} \propto \langle \hat{n}_c \rangle^{-1/3}$ .

### 2.2.1 Twin-beam up conversion

In this section we analyze the second step of the PCS generation set-up reported in Fig. 2.1, namely the three-wave interaction starting from the twin-beam input state

$$|\chi\rangle = \sqrt{1 - |\chi|^2} \sum_{n=0}^{\infty} \chi^n |n, n, 0\rangle. \quad (2.8)$$

The complex amplitude  $\chi$  is confined in the unit circle, and the mean photon number pertaining the state (2.8) is given by

$$\langle \chi | \hat{n}_a + \hat{n}_b + \hat{n}_c | \chi \rangle = 2|\chi|^2 / (1 - |\chi|^2). \quad (2.9)$$

The synthesis of the PCS (2.2) starting from  $|\chi\rangle$  would be easily achieved by having at disposal a device that performs the photon number recombination

$$|n, n, 0\rangle \longrightarrow |0, 0, n\rangle. \quad (2.10)$$

Such kind of transformation has been analyzed in Ref. [10], and has been shown to correspond to the interaction Hamiltonian

$$\hat{H}_r = a^\dagger b^\dagger (b^\dagger b + 1)^{-\frac{1}{2}} c + c^\dagger (b^\dagger b + 1)^{-\frac{1}{2}} ab. \quad (2.11)$$

Unfortunately, the Hamiltonian (2.11) cannot be realized by known optical devices. However, one may notice that the perfect number recombination  $|1, 1, 0\rangle \rightarrow |0, 0, 1\rangle$  is performed by the Hamiltonian (2.1), and this suggests to substitute the intensity dependent factor in Eq. (2.11) by its expectation value. In spite of this rather crude approximation, the trilinear interaction (2.1) has been shown [60, 61] to provide a good approximation of the photon recombination in the case of a single photon number state at the input. Further details on the technique of quantum frequency conversion can be found in Refs. [62, 63]. Here, we analyze the case of the input twin-beam state (2.8). Our aim is to demonstrate that the scheme of Fig. 2.1 is indeed effective in synthesizing a PCS. As a parameter to evaluate the effectiveness of PCS synthesis we use the overlap  $\mathcal{O} = \sqrt{\langle \lambda | \hat{\rho}^{out} | \lambda \rangle}$  between the state

$$\hat{\rho}^{out} = \text{Tr}_{ab} \left[ \exp(-it\hat{H}) |\chi\rangle\langle\chi| \exp(it\hat{H}) \right], \quad (2.12)$$

exiting the  $\chi^{(2)}$  crystal in the mode  $c$  and a theoretical PCS  $|\lambda\rangle$  corresponding to the same mean photon number. In order to evaluate the efficiency of the process we also consider the conversion rate  $\eta$ , defined as follows

$$\eta = 2 \frac{\text{Tr}(\hat{\rho}^{out} \hat{n}_c)}{\langle \chi | (\hat{n}_a + \hat{n}_b) | \chi \rangle}. \quad (2.13)$$

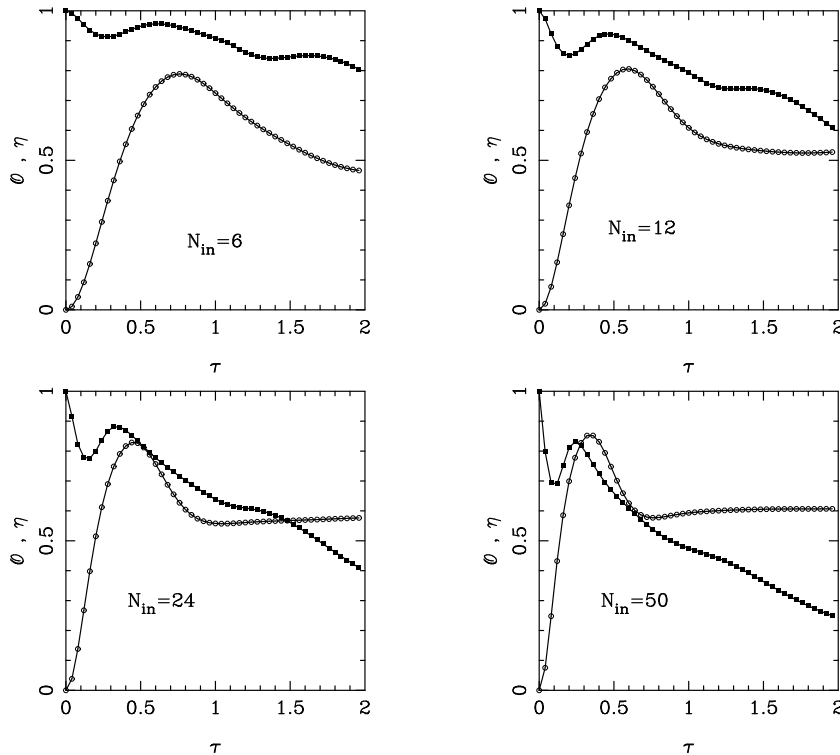


Figure 2.3: Behavior of the overlap  $\mathcal{O}$  (circles) and the conversion rate  $\eta$  (squares) as a function of the scaled interaction time for different intensity  $N_{in}$  of the incoming twin beam.

In Fig. 2.3 we show the behavior of the overlap  $\mathcal{O}$  and the conversion rate  $\eta$  as a function of the scaled interaction time for different intensity of the incoming twin beam. A remarkable fact is apparent: interaction times corresponding to high conversion rate also optimize the overlap between the outgoing state and the theoretical PCS. This means that the up-conversion, although only approximated, produces a recombination process which is at the same time efficient and quite precise. One should also mention that for the same interaction times one has a small degree of mixing, indicating that the outgoing states are quite pure, and minimum reciprocal peak likelihood, thus confirming good phase-coherence properties.

In Fig. 2.4 we report the maximum overlap, along with the corresponding interaction time and conversion rate, as a function of the twin-beam input energy  $N_{in} = \langle \hat{n}_a + \hat{n}_b \rangle$ . The overlap  $\mathcal{O}$  slowly decreases versus the input energy  $N_{in}$ , whereas the conversion rate  $\eta$  is almost independent on this quantity, saturating to a value close to 80%. This results in a reliable generation of PCS with overlap between 80% and 100%, for outgoing states with energy  $N_{out} = \langle \hat{n}_c \rangle$  up to  $N_{out} = 20$  mean photon number. The corresponding reciprocal peak likelihood  $\delta\phi$  shows the scaling  $\delta\phi \propto N_{out}^{-3/4}$  which, though it is worse than the ideal PCS performances  $\delta\phi \propto N_{out}^{-1}$ , it is far superior to the

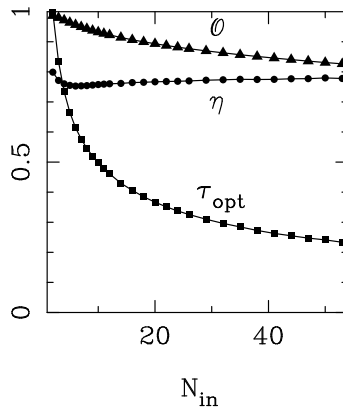


Figure 2.4: The optimized overlap along with the corresponding interaction time and conversion rate as a function of the twin-beam input photons.

coherent state level  $\delta\phi \propto N_{out}^{-1/2}$ .

The interaction time  $\tau_{opt}$ , which corresponds to the maximum overlap, decreases with the input energy  $N_{in}$ . By a best fit on data in Fig. 2.4 we obtained the scaling power-law  $\tau_{opt} \simeq 1.4N_{in}^{-0.45}$ . Remarkably, the same scaling is observed as a function of the output energy  $N_{out}$ , with only a slight change in the proportionality constant  $\tau_{opt} \simeq 0.9N_{out}^{-0.45}$ .

## 2.3 Two-mode heterodyne phase detection

A two-mode field corresponds to a complex photocurrent  $\hat{Z}$  such that  $[\hat{Z}, \hat{Z}^\dagger] = 0$ , with a self-adjoint phase operator  $\hat{\phi} = \arg(\hat{Z})$  that can concretely be measured. Despite its promising possibilities, not much work has been devoted to the two-mode phase detection, and attention has been focused mostly on the algebraic structure of the photocurrents (see Refs. [53, 54, 55] and references therein). Only in Ref. [64] a concrete experimental set-up has been devised, based on unconventional field heterodyning with the signal and image-band modes both nonvacuum. Following the route opened by Ref. [64], we study the eigenstates of the heterodyne photocurrent  $\hat{Z}$  and provide an experimental scheme that approaches them. We then analyze the measurement of the two-mode phase  $\hat{\phi} = \arg(\hat{Z})$  showing that the ideal sensitivity limit  $\delta\phi = 1/\bar{n}$  can be achieved for large mean number of photons  $\bar{n}$  [65].

### 2.3.1 The heterodyne eigenvectors $|z\rangle\rangle$

It has been proved by Yuen and Shapiro [66] that the output photocurrent  $\hat{Z}$  of a heterodyne detector (for unit quantum efficiency, and in the limit of strong local oscillator

and vanishing beam splitter reflectivity) is just the operator  $\hat{Z} = a + b^\dagger$ , where  $a$  and  $b$  denote (the annihilator of) the signal and the image-band mode, respectively. In ordinary heterodyning the image-band mode  $b$  is vacuum, and is responsible for the 3dB additional noise. Here, similarly to Ref. [64], we use the heterodyne detector in an unconventional way, namely with a nonvacuum  $b$  mode, and look for field states which are eigenvectors of the current  $\hat{Z}$ . Indeed, the heterodyne detector jointly measures the real and the imaginary part of  $\hat{Z}$ , which are expressed as a function of the quadratures  $\hat{c}_\phi = \frac{1}{2}(c^\dagger e^{i\phi} + \text{h.c.})$  of the single modes  $c = a, b$  as follows

$$\hat{Z}_1 = \text{Re}\hat{Z} = \hat{a}_0 + \hat{b}_0 \quad \hat{Z}_2 = \text{Im}\hat{Z} = \hat{a}_{\pi/2} - \hat{b}_{\pi/2} . \quad (2.14)$$

$\hat{Z}_1$  and  $\hat{Z}_2$  are self-adjoint commuting operators, so that they can be jointly measured without the additional 3dB noise suffered by joint measurement of conjugated quadratures.

It is easy to check that the following vector [64]

$$\begin{aligned} |z\rangle\rangle &= \int_{-\infty}^{+\infty} \frac{dx}{\sqrt{\pi}} e^{2ix\text{Im}z} |x\rangle_0 \otimes |\text{Re}z - x\rangle_0 \\ &= \int_{-\infty}^{+\infty} \frac{dy}{\sqrt{\pi}} e^{-2iy\text{Re}z} |y + \text{Im}z\rangle_{\pi/2} \otimes |y\rangle_{\pi/2} \end{aligned} \quad (2.15)$$

is eigenvector of  $\hat{Z}$  with complex eigenvalue  $z$ . In Eq. (2.15)  $|\psi\rangle \otimes |\varphi\rangle$  denotes a vector in the two-mode Hilbert space  $\mathcal{H} = \mathcal{H}_a \otimes \mathcal{H}_b$ , and  $|x\rangle_\phi$  represents an eigenvector of the quadrature  $\hat{c}_\phi$  of the pertaining mode  $c = a, b$ . The notation  $|\rangle\rangle$  remembers that the state is a two-mode one. It is also convenient to write the eigenstate of  $\hat{Z}$  corresponding to complex eigenvalue  $z$  as follows

$$|z\rangle\rangle = \frac{e^{-\frac{|z|^2}{2}}}{\sqrt{\pi}} \exp(-a^\dagger b^\dagger) |z\rangle \otimes |\bar{z}\rangle , \quad (2.16)$$

where  $|z\rangle$  denotes a customary coherent state.

The set  $\{|z\rangle\rangle\}$  is complete orthonormal for  $\mathcal{H}$ , with scalar product:

$$\langle\langle z|z'\rangle\rangle = \delta^{(2)}(z - z') \equiv \delta(\text{Re}z - \text{Re}z') \delta(\text{Im}z - \text{Im}z') . \quad (2.17)$$

In the number representation the vector (2.15) reads as follows

$$|z\rangle\rangle = e^{i\text{Re}z\text{Im}z} \sum_{n,m=0}^{\infty} c_{n,m}(z, \bar{z}) |n\rangle \otimes |m\rangle , \quad (2.18)$$

with

$$c_{n,n+\lambda}(z, \bar{z}) = \bar{c}_{n+\lambda,n}(z, \bar{z}) = \frac{(-)^n}{\sqrt{\pi}} \sqrt{\frac{n!}{(n+\lambda)!}} \bar{z}^\lambda L_n^\lambda(|z|^2) \exp\left(-\frac{1}{2}|z|^2\right) . \quad (2.19)$$

Eq. (2.19) is obtained from Eq. (2.15) using the number representation of the quadrature

$$\phi\langle x|n\rangle = \left(\frac{2}{\pi}\right)^{1/4} \frac{e^{in\phi}}{\sqrt{2^n n!}} e^{-x^2} H_n(\sqrt{2}x), \quad (2.20)$$

along with the following identity between Hermite and Laguerre polynomials

$$\int_{-\infty}^{+\infty} \frac{dx}{\sqrt{\pi}} e^{-x^2} H_n(x+y) H_{n+\lambda}(x+t) = 2^{n+\lambda} n! L_n^\lambda(-2yt) t^\lambda. \quad (2.21)$$

### 2.3.2 The detection of the two-mode phase

The Dirac-normalized states  $|z\rangle\rangle$  have infinite total number of photons, and we seek physically realizable states approaching  $|z\rangle\rangle$  for infinite photon numbers. The eigenstate corresponding to zero eigenvalue is given by:

$$|0\rangle\rangle = \frac{1}{\sqrt{\pi}} \sum_{n=0}^{\infty} (-)^n |n\rangle \otimes |n\rangle. \quad (2.22)$$

This is just the twin beam of Eq. (1.60) at the output of a nondegenerate parametric amplifier, in the limit of infinite gain [10], namely

$$|0\rangle\rangle = \lim_{\lambda \rightarrow 1^-} |0\rangle\rangle_\lambda, \quad (2.23)$$

with

$$|0\rangle\rangle_\lambda = (1 - \lambda^2)^{1/2} \sum_{n=0}^{\infty} (-\lambda)^n |n\rangle \otimes |n\rangle = \exp[\tanh^{-1} \lambda (ab - a^\dagger b^\dagger)] |0\rangle \otimes |0\rangle. \quad (2.24)$$

In the parametric approximation modes  $a$  and  $b$  are identified with a couple of signal and idler modes of the amplifier with gain  $(1 - \lambda^2)^{-1}$ . All the other states with  $z \neq 0$  can be approached by suitably displacing either mode  $a$  or  $b$ , or both of them, as follows

$$|z\rangle\rangle_\lambda = D_a(u) D_b(\bar{v}) e^{\tanh^{-1} \lambda (ab - a^\dagger b^\dagger)} |0\rangle \otimes |0\rangle \quad (z = u + v), \quad (2.25)$$

where  $D_c(u) = e^{uc^\dagger - \bar{u}c}$  denotes the displacement operator of the mode  $c = a, b$ . According to Sec. 1.3.1, the physical realization of the states  $|z\rangle\rangle_\lambda$  can be achieved by combining the twin beam  $|0\rangle\rangle_\lambda$  with strong coherent local oscillators with amplitude  $\beta$  and  $\gamma$  in beam splitters with transmissivity  $\theta, \theta' \rightarrow 1$ , such that  $|\beta|\sqrt{1-\theta} = |u|$  and  $|\gamma|\sqrt{1-\theta'} = |v|$ .

Using the identity

$$e^{-\xi(ab - a^\dagger b^\dagger)} D_a(u) D_b(\bar{v}) e^{\xi(ab - a^\dagger b^\dagger)} = D_a(u \operatorname{ch} \xi + v \operatorname{sh} \xi) D_b(\bar{u} \operatorname{sh} \xi + \bar{v} \operatorname{ch} \xi) \quad (2.26)$$

Eq. (2.25) rewrites as follows

$$|z\rangle\rangle_\lambda = e^{\tanh^{-1} \lambda (ab - a^\dagger b^\dagger)} \left| \frac{u + \lambda v}{\sqrt{1 - \lambda^2}} \right\rangle \otimes \left| \frac{\lambda \bar{u} + \bar{v}}{\sqrt{1 - \lambda^2}} \right\rangle \quad (z = u + v). \quad (2.27)$$

Hence, the state  $|z\rangle_\lambda$  can also be obtained through phase-insensitive amplification of input signal and idler which have the precise amplitude relation in Eq. (2.27). In the next chapter we will show that such kind of state is effective for the realization of a quantum communication channel with the same performances of the squeezed-state channel.

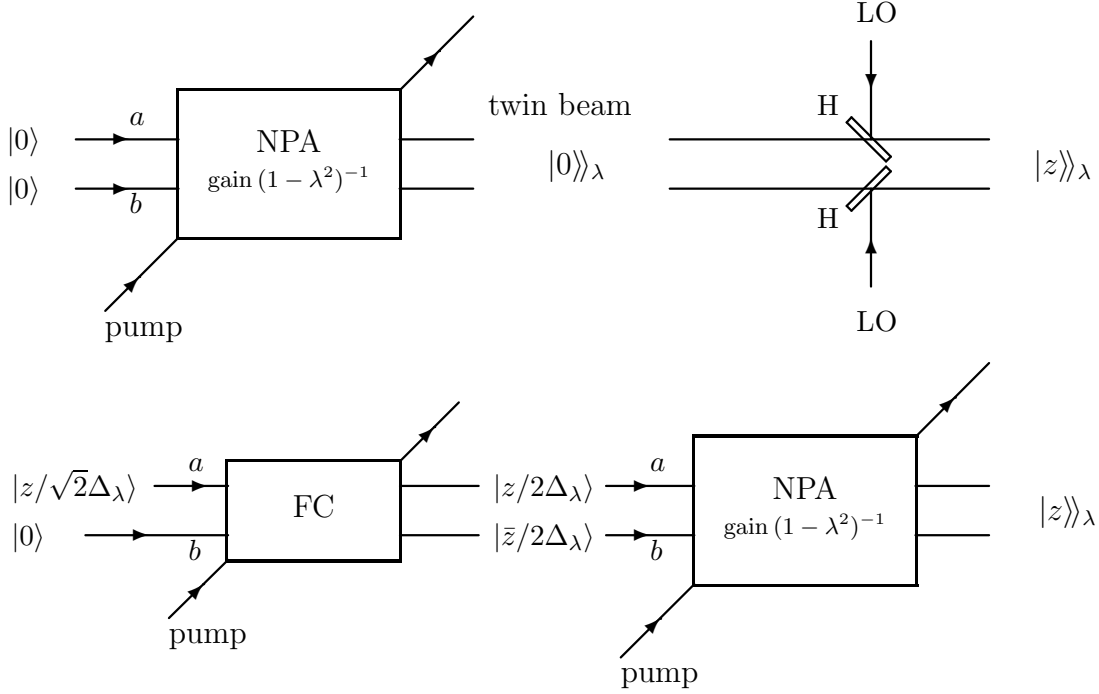


Figure 2.5: Outline of the two alternative experimental set-ups to generate the two-mode states  $|z\rangle_\lambda$  of Eq. (2.34). The labels H and LO denote high-transmissivity beam splitters and local oscillators respectively, which realize the displacement operators in Eq. (2.25). The input states at the nondegenerate parametric amplifier (NPA) are the vacuum state in the upper scheme, and two independent coherent states in the lower one. In the last case the couple of coherent states is generated by a single coherent state through frequency conversion (FC).

The average number of photons of (2.25) is given by

$$\bar{n} = {}_\lambda \langle\langle z | a^\dagger a + b^\dagger b | z \rangle\rangle_\lambda = |u|^2 + |v|^2 + \frac{2\lambda^2}{1 - \lambda^2}. \quad (2.28)$$

The state (2.25) is now impinged into a heterodyne detector with signal mode  $a$  and image-band mode  $b$ . The probability density of getting the value  $z$  for the output photocurrent  $\hat{Z}$  with the field in the state  $|w\rangle_\lambda$  is given by

$$|\langle\langle z | w \rangle\rangle_\lambda|^2 = (1 - \lambda^2) \left| \sum_{n=0}^{\infty} (-\lambda)^n c_{n,n}(z - w, \overline{z - w}) \right|^2$$

$$\begin{aligned}
&= \frac{1-\lambda^2}{\pi} \exp(-|z-w|^2) \left| \sum_{n=0}^{\infty} \lambda^n L_n(|z-w|^2) \right|^2 \\
&= \frac{1}{\pi \Delta_\lambda^2} \exp\left(-\frac{|z-w|^2}{\Delta_\lambda^2}\right)
\end{aligned} \tag{2.29}$$

where

$$\Delta_\lambda^2 = \frac{1-\lambda}{1+\lambda}. \tag{2.30}$$

In the limit  $\lambda \rightarrow 1^-$  one has that  $|\langle z|w \rangle_\lambda|^2 \rightarrow \delta^{(2)}(z-w)$ , confirming that the state  $|w \rangle_\lambda$  approaches the eigenstate  $|w \rangle$  of the current  $\hat{Z}$ .

The detection of the phase  $\hat{\phi} = \arg(\hat{Z})$  is described by the marginal probability density of (2.29), namely

$$\begin{aligned}
p(\phi) &= \frac{1}{\pi \Delta_\lambda^2} \int_0^{+\infty} dr r \exp\left(-\frac{|r e^{i\phi} - |w| e^{i\theta}|^2}{\Delta_\lambda^2}\right) \\
&= \frac{1}{2\pi} e^{-\frac{|w|^2}{\Delta_\lambda^2}} + \frac{|w|}{\pi \Delta_\lambda} \cos(\phi - \theta) \frac{\sqrt{\pi}}{2} \left[ 1 + \operatorname{erf}\left(\frac{|w| \cos(\phi - \theta)}{\Delta_\lambda}\right) \right] e^{-\frac{|w|^2}{\Delta_\lambda^2} \sin^2(\phi - \theta)},
\end{aligned} \tag{2.31}$$

where  $\theta = \arg(w)$ , and  $\operatorname{erf}(x)$  denotes the error function  $\operatorname{erf}(x) = \frac{2}{\sqrt{\pi}} \int_0^x dt e^{-t^2}$ . Notice that the probability density (2.31) is just the Born rule for the self-adjoint operator  $\hat{\phi} = \arg(\hat{Z}) = -\frac{i}{2} \log(\hat{Z}/\hat{Z}^\dagger)$ : this is well defined on the Hilbert space  $\mathcal{H}_0^\perp$ , orthogonal complement in  $\mathcal{H}$  of the space  $\mathcal{H}_0$  spanned by vector  $|0 \rangle$  in Eq. (2.22). The integral over  $r$  in Eq. (2.31) just sums up degeneracies of eigenvectors (2.18): the zero-eigenvalue vector is not degenerate, and gives a zero-measure contribution to the integral. The first Gaussian term in the last side of Eq. (2.31) gives a uniform phase probability distribution for the twin-beam input state  $|0 \rangle_\lambda$ .

For  $\Delta_\lambda \ll |w|$  Eq. (2.31) approaches the Gaussian form

$$p(\phi) \simeq \frac{|w|}{\sqrt{\pi} \Delta_\lambda} \exp\left[-\frac{|w|^2}{\Delta_\lambda^2} (\phi - \theta)^2\right]. \tag{2.32}$$

For Gaussian distributions the average maximizes the likelihood and is an asymptotically efficient estimate of the phase shift  $\theta$  with efficiency equal to the variance (see Ref. [67]). Hence the r.m.s. phase sensitivity corresponding to Eq. (2.32) is given by

$$\delta\phi = \langle \Delta\phi^2 \rangle^{1/2} = \frac{1}{\sqrt{2}} \frac{\Delta_\lambda}{|w|}. \tag{2.33}$$

In the limit of infinite gain at the amplifier ( $\lambda \rightarrow 1^-$ ) one has  $\Delta_\lambda^2 \simeq \frac{1}{2}(1-\lambda)$  and  $\bar{n} \simeq |w|^2 + (1-\lambda)^{-1}$ . Notice that the probability density (2.29) does not depend explicitly on  $u$  and  $v$  (the share of displacement of the two modes), while the mean number of photons does. The constraint  $u+v=w$  over states (2.25) and (2.27) implies

that for each  $z$  there is a family of states approaching the eigenstate  $|z\rangle\rangle$  according to Eq. (2.29). For  $u = v = z/2$ , the most symmetrical state

$$|z\rangle\rangle_\lambda = e^{\tanh^{-1}\lambda(ab - a^\dagger b^\dagger)} |z/2\Delta_\lambda\rangle \otimes |\bar{z}/2\Delta_\lambda\rangle \quad (2.34)$$

achieves the best phase sensitivity. In fact, by optimizing  $\delta\phi$  versus  $|w| = |u + v|$  at fixed  $\bar{n}$  one obtains

$$\delta\phi \simeq \frac{1}{\sqrt{2\bar{n}}} \quad (2.35)$$

for  $|u|^2 = |v|^2 = 1/[2(1-\lambda)]$ , namely for signal photons equal to the twin-beam photons. The sensitivity (2.35) obeys the same power-law as the ideal sensitivity for one-mode phase detection (actually it is improved by a constant factor equal to 1.92: see Ref. [45]).

The couple of coherent states on the right of Eq. (2.34) can be generated by means of a single coherent state and a frequency conversion device with suitable pump strength and phase. In fact, for any complex  $\alpha$ , one has

$$\exp\left[\frac{\pi}{4}\left(e^{i\arg\alpha}a^\dagger b - e^{-i\arg\alpha}ab^\dagger\right)\right] |\sqrt{2}\alpha\rangle \otimes |0\rangle = |\alpha\rangle \otimes |\bar{\alpha}\rangle, \quad (2.36)$$

where the unitary operator on the left side of Eq. (2.36) describes a frequency conversion device. In the parametric approximation this can be realized through a three-wave (or degenerate four-wave) mixing in a nonlinear  $\chi^{(2)}$  ( $\chi^{(3)}$ ) medium. For the technique of quantum frequency conversion, see Refs. [62, 63]. The two alternative experimental set-ups to generate the state (2.25) are sketched in Fig. 2.5.

The ideal phase sensitivity (2.35) has been derived with the hypothesis of unit efficiency at the heterodyne photodetector. It is easy to show that for non-unit quantum efficiency (independent on frequency in the range between signal and image-band modes) Eq. (2.30) becomes

$$\Delta_\lambda^2 \rightarrow \Delta_\lambda^2(\eta) = \Delta_\lambda^2 + \frac{1-\eta}{\eta}. \quad (2.37)$$

Then, it is clear that the result (2.35) holds only in the limit  $1-\eta \ll |w|^{-2}$ , whereas in the opposite situation  $1-\eta \gg |w|^{-2}$  one obtains the usual shot noise  $\delta\phi = \sqrt{(1-\eta)/2\bar{n}}$ . Hence, the two-mode phase detection can be experimentally achieved, but the technical requirements are strict: linear amplification for high gains, with the pump still undepleted and very good quantum efficiency. This shows how technical difficulties can rise when going from one-mode to two-mode phase detection.

## 2.4 A repeatable two-mode phase measurement

A measurement scheme to perform a repeatable phase detection on a two-mode field is presented in this section. We will give also some hints for its experimental realization

[68]. Since we want to perform a phase measurement on a generic two-mode field without destroying it, we need a general theoretical framework for describing repeatable measurements.

### 2.4.1 General framework for repeatable measurements

In order to have a measurement that does not completely destroy the state that the system had before the measurement, the scheme must involve a probe that interacts with the system and later is “measured” to yield information on the original state of the system [69]. This *indirect* measurement scheme is completely specified once the following ingredients are given: i) the unitary operator  $\hat{U}$  that describes the system-probe interaction; ii) the state  $|\varphi\rangle$  of the probe before the interaction; iii) the observable  $\hat{X}$  which is measured on the probe. At the end of the system-probe interaction, one can consider another measurement on the system, say the ideal measurement of an observable  $\hat{Y}$  (both  $\hat{X}$  and  $\hat{Y}$  have continuous spectrum, with eigenvectors  $|x\rangle$  and  $|y\rangle$ , respectively). Then the conditional probability density  $p(y|x)$  of getting a result  $y$  from the second measurement given the result of the first one being  $x$  can be written in terms of the Born’s rule  $p(y|x)dy = \langle y|\hat{\rho}_x|y\rangle$  upon defining a “reduced state”  $\hat{\rho}_x$  as follows

$$\hat{\rho}_x = \frac{\hat{\Omega}(x)\hat{\rho}\hat{\Omega}^\dagger(x)}{\text{Tr}[\hat{\rho}\hat{\Omega}^\dagger(x)\hat{\Omega}(x)]}, \quad (2.38)$$

where the system operator  $\hat{\Omega}(x)$  is given by

$$\hat{\Omega}(x) = \langle x|\hat{U}|\varphi\rangle. \quad (2.39)$$

The “probability operator-valued measure” (POM) of the apparatus [69]

$$d\hat{\mu}(x) = \hat{\Omega}^\dagger(x)\hat{\Omega}(x)dx \quad (2.40)$$

provides the Born’s rule for the measurement as follows

$$p(x)dx = \text{Tr}[\hat{\rho}d\hat{\mu}(x)]. \quad (2.41)$$

Equations (2.38-2.41) are the most general form of the state reduction and of the Born’s rule for a “pure” or “quasi-complete” measurement, namely a measurement that leaves pure states as pure (due to the pure state preparation of the probe). Apart from an irrelevant phase factor, the non-unitary *reduction operator*  $\hat{\Omega}(x)$  uniquely characterizes the quantum measurement, and two measurements that have the same operator  $\hat{\Omega}(x)$  will be considered as identical, both having the same probability density (2.41) and the same state-reduction (2.38). On the other hand, the fact that many measurements can share the same POM  $d\hat{\mu}(x)$ —while having different state reduction—is immediately apparent from the fact that a unitary transformation of the reduction operator

$$\hat{\Omega}(x) \rightarrow \hat{\Omega}'(x) = \hat{V}(x)\hat{\Omega}(x) \quad (2.42)$$

changes only the state-reduction, but leaves the POM (2.40) invariant. A unitary transformation  $\hat{V}(x)$  that depends on the result  $x$  of a measurement is the quantum mechanical description of a feedback mechanism, which in turn represents the easiest way of engineering a prescribed (admissible) state reduction.

### 2.4.2 The interaction Hamiltonian

The repeatable phase measurement we propose is obtained through unconventional heterodyne detection performed on a probe field after a suitable interaction with the system. The property of repeatability allows to check the evolution of the signal under successive measurements, and possibly also to drive the evolution itself by state reduction (i.e. by selecting the state after the measurement). Finally—more interesting for foundations—a repeatable phase measurement is a good candidate for detecting Schrödinger-cat states (see, for example, Ref. [70]). In the following we compute the probability distribution and the reduced state depending on the outcome of the measurement.

The interaction Hamiltonian between the system and the probe is bilinear in the four field modes  $a, b$  (for the system) and  $c, d$  (for the probe) and is given by

$$\hat{H} = -K \frac{i}{2} \left[ (a^\dagger c + bc + ad + b^\dagger d) - \text{h.c.} \right], \quad (2.43)$$

where  $K$  is a coupling constant. From definitions (2.14), and introducing the complex current for the probe field

$$\hat{A} \equiv c + d^\dagger = \hat{A}_1 + i\hat{A}_2, \quad (2.44)$$

the Hamiltonian (2.43) rewrites

$$\hat{H} = K \left[ \hat{Z}_1(\hat{c}_{\pi/2} + \hat{d}_{\pi/2}) - \hat{Z}_2(\hat{c}_0 - \hat{d}_0) \right]. \quad (2.45)$$

The Heisenberg evolution of a probe operator of the form  $f(\hat{A})$  for an interaction time  $\tau = \hbar/K$  is

$$\hat{U}^\dagger f(\hat{A}) \hat{U} = f(\hat{A} + \hat{Z}), \quad (2.46)$$

where

$$\hat{U} = \exp(-i\hat{H}\tau) = \exp \left\{ -i \left[ \hat{Z}_1(c_{\pi/2} + d_{\pi/2}) - \hat{Z}_2(c_0 - d_0) \right] \right\} \quad (2.47)$$

is the unitary evolution operator. After the interaction, the probe modes  $c$  and  $d$  are heterodyne measured, with  $c$  as the signal mode and  $d$  as the image-band mode. As explained in the previous section, this corresponds to measure the photocurrent  $\hat{A}$ . This indirect measurement provides information about the probability density of the

complex eigenvalue  $z$  pertaining the system operator  $\hat{Z}$ . The probability density is computed through the relation

$$\text{Tr}_S[\hat{F}(z)\hat{\rho}_S] = \text{Tr}_{S,P}[|z\rangle\langle z|\hat{U}(\hat{\rho}_S \otimes \hat{\rho}_P)\hat{U}^\dagger], \quad (2.48)$$

where  $\hat{F}(z)$  is a probability operator-valued measure (POM) and  $|z\rangle\langle z|$  represents an orthogonal projector on the eigenspace of the two-mode probe Hilbert space  $\mathcal{H}_c \otimes \mathcal{H}_d$  relative to the eigenvalue  $z$  of  $\hat{A}$ . The tensor product  $\hat{\rho}_S \otimes \hat{\rho}_P$  denotes the (disentangled) state of system and probe before the interaction. We now specify the probe preparation as the twin-beam state (2.24). The corresponding POM  $\hat{F}(z)$  writes

$$\hat{F}(z) = {}_\lambda \langle\langle 0|\hat{U}^\dagger|z\rangle\rangle \langle\langle z|\hat{U}|0\rangle\rangle_\lambda \doteq \hat{\Omega}^\dagger(z) \hat{\Omega}(z). \quad (2.49)$$

From the Eqs. (2.15), (2.47) and (2.29) with  $w=0$ , taking into account the additional phase  ${}_\lambda \langle\langle 0|z\rangle\rangle = e^{iz_1z_2} |{}_\lambda \langle\langle 0|z\rangle\rangle|^2$  the reduction operator  $\hat{\Omega}^\dagger(z)$  is evaluated as follows

$$\begin{aligned} \hat{\Omega}^\dagger(z) &= \exp \left\{ i\hat{Z}_1 \left( i\frac{\partial}{\partial z_1} + z_2 \right) + i\hat{Z}_2 \left( i\frac{\partial}{\partial z_2} + z_1 \right) \right\} {}_\lambda \langle\langle 0|z\rangle\rangle \\ &= \frac{e^{iz_1z_2}}{\sqrt{\pi}\Delta_\lambda} \exp \left( -\frac{|\hat{Z} - z|^2}{2\Delta_\lambda^2} \right), \end{aligned} \quad (2.50)$$

where  $\Delta_\lambda$  is given by Eq. (2.30). As a consequence, one gets the expression for the POM

$$\hat{F}(z) = \frac{1}{\pi\Delta_\lambda^2} \exp \left( -\frac{|\hat{Z} - z|^2}{\Delta_\lambda^2} \right), \quad (2.51)$$

which provides the probability density

$$P(z|\hat{\rho}_S) = \text{Tr}[\hat{F}(z)\hat{\rho}_S] = \frac{1}{\pi\Delta_\lambda^2} \int_C d^2z' {}_S \langle\langle z'|\hat{\rho}_S|z'\rangle\rangle_S \exp \left( -\frac{|z' - z|^2}{\Delta_\lambda^2} \right). \quad (2.52)$$

Here  $\{|z'\rangle_S\}$  are the eigenstates of the system operator  $\hat{Z}$  and the integral is over the complex plane. Eq. (2.52) is a convolution of the ideal probability with a Gaussian that narrows for increasing gain of the parametric amplifier. Notice that the result (2.51) can be derived more easily through Eqs. (2.49) and (2.46), upon defining formally the projector for  $\hat{A}$  as a Dirac delta on the complex plane, namely

$$|z\rangle\langle z| = \delta^{(2)}(\hat{A} - z), \quad (2.53)$$

then obtaining from Eq. (2.49)

$$\hat{F}(z) = {}_\lambda \langle\langle 0|\delta^{(2)}(\hat{A} + \hat{Z} - z)|0\rangle\rangle_\lambda; \quad (2.54)$$

---

<sup>2</sup>This phase relation can be derived from the number representation of vectors  $\{|z\rangle\rangle$  given in Eq. (2.18).

hence, using Eq. (2.29), one gets the result. Notice that with respect to the scheme of Fig. 2.5, here we no longer need a beam splitter for displacing the state, because the interaction Hamiltonian itself transfers signal to the twin beam before heterodyne detection.

The operator  $\hat{\Omega}(z)$  has been explicitly computed because its adjoint action on the system state  $\hat{\rho}_S$  provides the reduced state  $\hat{\rho}_z$  after the measurement with outcome  $z$ . According to Eq. (2.38) one has

$$\hat{\rho}_z = \frac{\hat{\Omega}(z) \hat{\rho}_S \hat{\Omega}^\dagger(z)}{\text{Tr}[\hat{F}(z) \hat{\rho}_S]} = \frac{1}{\pi \Delta_\lambda^2} \frac{\exp\left(-\frac{|\hat{Z}-z|^2}{2\Delta_\lambda^2}\right) \hat{\rho}_S \exp\left(-\frac{|\hat{Z}-z|^2}{2\Delta_\lambda^2}\right)}{\text{Tr}[\hat{F}(z) \hat{\rho}_S]}. \quad (2.55)$$

The POM that provides the probability density for the phase is the marginal one of  $\hat{F}(z)$  in Eq. (2.51), namely

$$\begin{aligned} d\hat{\mu}(\phi) &= \int_0^{+\infty} d|z| |z| \hat{F}(z) \\ &= \frac{1}{2\pi} \exp\left(-\frac{|\hat{Z}|^2}{\Delta_\lambda^2}\right) + \frac{1}{\pi \Delta_\lambda} \text{Re}\left(\hat{Z} e^{-i\phi}\right) \exp\left\{-\frac{1}{\Delta_\lambda^2} \left[\text{Im}\left(\hat{Z} e^{-i\phi}\right)\right]^2\right\} \\ &\times \frac{\sqrt{\pi}}{2} \left\{ 1 + \text{erf}\left[\frac{\text{Re}\left(\hat{Z} e^{-i\phi}\right)}{\Delta_\lambda}\right] \right\}, \end{aligned} \quad (2.56)$$

with  $\phi = \arg(z)$ . In the limit of infinite average number of photons at the twin beam ( $\Delta_\lambda \rightarrow 0$ ), Eq. (2.56) approaches the ideal POM

$$d\hat{\mu}(\phi) = \delta\left(\hat{\Phi} - \phi\right) \quad (2.57)$$

where  $\hat{\Phi} = \arg(\hat{Z})$ . With regard to the case of a heterodyne detection with quantum efficiency  $\eta < 1$ , the projector in the right side of Eq. (2.48) needs to be replaced by the POM [34]

$$\hat{A}_\eta(z) = \frac{\eta}{\pi(1-\eta)} \exp\left(-\frac{\eta}{1-\eta} |\hat{A} - z|^2\right). \quad (2.58)$$

This increases the variance (2.30) of the POM (2.51), according to Eq. (2.37). The corresponding reduced state  $\hat{\rho}_z^{(\eta)}$  becomes

$$\hat{\rho}_z^{(\eta)} = \text{Tr}[\hat{F}_\eta(z) \hat{\rho}_S]^{-1} \int_C d^2 z' \frac{\eta}{\pi(1-\eta)} e^{-\frac{\eta}{1-\eta} |z'-z|^2} \hat{\Omega}(z') \hat{\rho}_S \hat{\Omega}^\dagger(z'), \quad (2.59)$$

where  $\hat{\Omega}(z')$  is the same as in Eq. (2.50) and  $\hat{F}_\eta(z)$  is the new POM after the substitution (2.37).

Eq. (2.59) displays a conceptually noteworthy difference from Eq. (2.55): the ideal measurement reduces a pure initial state into a pure state (it is a quasi-complete measurement, according to Ozawa's definition [71]), whereas a non-unit quantum efficiency leads to mixing.

Regarding the experimental feasibility of the repeatable measurement scheme here presented, we notice that Hamiltonian (2.43) can be achieved in the parametric approximation by means of two classical undepleted pumps. The interaction Hamiltonian in the Dirac picture is obtained in the rotating wave approximation from a nonlinear susceptibility  $\chi^{(2)}$  (*three-wave mixing*). Indeed, the following frequency arrangement of the probe mode  $d$  and the pump modes  $\gamma, \xi$  in comparison with the probe mode  $c$  and the system modes  $a, b$  ( $\omega_a < \omega_b$ )

$$\begin{cases} \omega_d = \omega_c + \omega_b - \omega_a \\ \omega_\xi = \omega_c - \omega_a \\ \omega_\gamma = \omega_c + \omega_b \end{cases} \quad (2.60)$$

with the restrictions

$$\begin{aligned} \omega_b &\neq 2\omega_a; & \omega_c &> \omega_b \\ \omega_c &\neq \frac{3}{2}\omega_a, 2\omega_a, \omega_a + \frac{\omega_b}{2}, \omega_a + \omega_b, 2\omega_a + \omega_b \end{aligned} \quad (2.61)$$

insures that the only surviving terms in the rotating wave approximation are represented by the Hamiltonian

$$\hat{H} \propto \left[ \left( a^\dagger c \xi^\dagger + b^\dagger d \xi^\dagger + a d \gamma^\dagger + b c \gamma^\dagger \right) + \text{h.c.} \right]. \quad (2.62)$$

The Hamiltonian (2.62) coincides with the Hamiltonian in Eq. (2.43) in the parametric approximation of undepleted pumps. It is clear that for a suitable frequency arrangement, one could also use a *four-wave mixing*  $\chi^{(3)}$  medium.

## 2.5 On the general problem of quantum phase estimation

The problem of estimating the phase shift experienced by a radiation beam has been the object of hundreds of studies in the last forty years [46]. We already noticed that the problem arises because for a single mode of the electromagnetic field there is no selfadjoint operator for the phase, owing to the semiboundedness of the spectrum of the number operator. The most general and, at the same time, concrete approach to the problem of the phase measurement is quantum estimation theory [47], a framework that has become popular only in the last ten years in the field of quantum information. The most powerful method for deriving the optimal phase measurement was given by Holevo [52] in the covariant case. In this way the optimal positive operator-valued measure (POM) for phase estimation has been derived for a single-mode field. Regarding the multi-mode case, only little theoretical effort has been spent [53], mostly devoting attention to the Lie algebraic structure for two modes [53, 72, 55]. For two modes one can adopt the difference between their photon numbers as the phase shift operator, which thus is no longer bounded from below. This opens the route toward an exact

phase measurement based on a selfadjoint operator with a concrete experimental setup using unconventional heterodyne detection, as shown in Sec. 2.3. The problem is however complicated by the (infinite) degeneracy of the shift operator, and for this reason the optimal states for this case have never been derived.

In this section, the general problem of estimating the phase shift  $\phi$  is addressed for any degenerate shift operator with discrete spectrum, either  $S = \mathbb{Z}$  (unbounded), or  $S = \mathbb{N}$  (bounded from below), or  $S = \mathbb{Z}_q$  (bounded), generalizing the Holevo method for the covariant estimation problem. We find the optimal POM for estimating the phase shift of a state  $|\psi_0\rangle$ , and then we optimize the state itself [73]. The degeneracy of the shifting operator is removed through a simple projection technique. The case of mixed input state, which is generally very difficult, is considered in some special situations. Sections 2.5.2 and 2.5.3 are devoted to the analysis of two relevant examples: one concerning a multi-mode phase estimation problem that arises in multi-path interferometry; the other involving a shift operator that is the difference between the number of photons of two modes, corresponding to unconventional heterodyne detection of the phase.

### 2.5.1 Optimal POM for the phase-shift estimation

We address the problem of estimating the phase-shift  $\phi$  pertaining to the unitary transformation

$$\hat{\varrho}_\phi = e^{-i\phi\hat{H}} \hat{\varrho}_0 e^{i\phi\hat{H}} \quad (2.63)$$

where  $\hat{H}$  is a self-adjoint operator degenerate on the Hilbert space  $\mathcal{H}$  with discrete (un)bounded spectrum  $S = \mathbb{Z}$ , or  $S = \mathbb{N}$ , or  $S = \mathbb{Z}_q$ ,  $q > 0$ , and  $\hat{\varrho}_0$  is a generic initial state (actually in the following we will mostly restrict to the pure state case). The estimation problem is posed in the most general framework of quantum estimation theory [47] on the basis of a cost function  $C(\phi_*, \phi)$  which weights the errors for the estimate  $\phi_*$  given the true value  $\phi$ . For a given *a priori* probability density  $p_0(\phi)$  for the true value  $\phi$  the estimation problem consists in minimizing the average cost

$$\bar{C} = \int_0^{2\pi} d\phi p_0(\phi) \int_0^{2\pi} d\phi_* C(\phi_*, \phi) p(\phi_*|\phi), \quad (2.64)$$

where  $p(\phi_*|\phi)$  is the conditional probability of estimating  $\phi_*$  given the true value  $\phi$ . The average cost is minimized by optimizing the POM  $d\hat{\mu}(\phi_*)$  which gives the conditional probability by the Born rule

$$p(\phi_*|\phi)d\phi_* = \text{Tr}[d\hat{\mu}(\phi_*)e^{-i\phi\hat{H}} \hat{\varrho}_0 e^{i\phi\hat{H}}]. \quad (2.65)$$

We consider the general situation in which  $\phi$  is *a priori* uniformly distributed, i.e. with probability density  $p_0(\phi) = 1/2\pi$ . Moreover, we want to weight errors independently on the value  $\phi$  of the phase, but only versus the size of the error  $\phi_* - \phi$ , so that the

cost function becomes an even function of only one variable, i.e.  $C(\phi_*, \phi) \equiv C(\phi_* - \phi)$ . It follows that also the optimal conditional probability will depend only on  $\phi_* - \phi$ , and the optimal POM can be obtained restricting attention only to phase-covariant POM's, i.e. of the form

$$d\hat{\mu}(\phi_*) = e^{-i\hat{H}\phi_*} \hat{\xi} e^{i\hat{H}\phi_*} \frac{d\phi_*}{2\pi}, \quad (2.66)$$

where  $\hat{\xi}$  is a positive operator satisfying the completeness constraints needed for the normalization of the POM  $\int_0^{2\pi} d\hat{\mu}(\phi) = 1$ . In fact, using Eq. (2.65) and the invariance of the trace under cyclic permutations one can easily recognize that  $p(\phi_*|\phi) \equiv p(\phi_* - \phi)$  if and only if  $d\hat{\mu}(\phi_*)$  is covariant. Hence the optimization problem resorts to finding the best positive operator  $\hat{\xi}$  for a given cost function  $C(\phi)$  and a generic given state  $\hat{\rho}_0$ . As we will see, the POM obtained in this way is optimal for a whole class of cost functions and initial states  $\hat{\rho}_0$ . Once the best POM is obtained, one further optimizes the state  $\hat{\rho}_0$ . This resorts to solving a linear eigenvalue problem. In fact, the average cost can be written as the expectation value of the cost operator  $\hat{C}$ , i.e.

$$\bar{C} = \text{Tr}[\hat{C}\hat{\rho}_0] \quad (2.67)$$

where

$$\hat{C} = \int d\hat{\mu}(\phi) C(\phi). \quad (2.68)$$

Using the Lagrange multipliers method to account for normalization one has to minimize the function

$$\mathcal{L}[\hat{\rho}_0] = \text{Tr}[\hat{C}\hat{\rho}_0] - \lambda \text{Tr}[\hat{\rho}_0] \quad (2.69)$$

which for a pure state  $|\psi_0\rangle\langle\psi_0|$  is a quadratic form whose minimum is given by the eigenvalue equation

$$\hat{C}|\psi_0\rangle = \lambda|\psi_0\rangle \quad (2.70)$$

with the Lagrange parameter  $\lambda$  playing the role of an eigenvalue. The linear problem can be easily extended to account also for finite mean-energy constraint.

In summary, our problem is to minimize the cost  $\bar{C}$  for a given cost function  $C(\phi)$  in Eq. (2.64). This is done in two steps: i) by optimizing the positive operator  $\hat{\xi}$  for given generic fixed state  $\hat{\rho}_0$ , thus obtaining a POM which is optimal for an equivalence class of states  $\mathcal{E}(\hat{\rho}_0)$ ; ii) by further optimizing the state in the equivalence class  $\mathcal{E}(\hat{\rho}_0)$ . Since the original state was arbitrarily chosen, this will give the absolute minimum cost and the corresponding set of optimal states and POM's.

The solution of the optimization problem is conveniently posed in the representation where  $\hat{H}$  is diagonal. The operator  $\hat{H}$  is generally degenerate, and we will denote by

$|n\rangle_\nu$  a choice of (normalized) eigenvectors corresponding to eigenvalue  $n$ ,  $\nu$  being a degeneracy index, and by  $\Pi_n$  the projector onto the corresponding degenerate eigenspace. The problem for an input generally mixed state  $\hat{\rho}_0$  is too difficult to address: therefore, we focus our attention on the case of pure state  $\hat{\rho}_0 = |\psi_0\rangle\langle\psi_0|$ , and we will leave some general assertions on the mixed state case for the following. The problem is restricted to the Hilbert space  $\mathcal{H}_\parallel$  spanned by the (normalized) vectors

$$|n\rangle \propto \Pi_n |\psi_0\rangle \neq 0 \quad (2.71)$$

with the choice of the arbitrary phases such that  $\langle n|\psi_0\rangle > 0$ . Hence the POM can be chosen of the block diagonal form on  $\mathcal{H} = \mathcal{H}_\parallel \otimes \mathcal{H}_\perp$ , namely

$$d\hat{\mu}(\phi) = d\hat{\mu}_\parallel(\phi) \oplus d\hat{\mu}_\perp(\phi) , \quad (2.72)$$

with  $d\hat{\mu}_\perp(\phi)$  any arbitrary POM on  $\mathcal{H}_\perp$ . For the optimization of the POM we consider  $\Pi_n |\psi_0\rangle \neq 0 \forall n \in S$ , as it is clear that the resulting POM will be optimal also for states having zero projection for some  $n \in S$ . In this fashion the problem is reduced to the “canonical” phase estimation problem restricted to  $\mathcal{H}_\parallel$  with the replacement

$$|\psi_0\rangle \rightarrow \exp(i\hat{H}_\parallel\phi)|\psi_0\rangle \quad (2.73)$$

where

$$\hat{H}_\parallel = \sum_{n \in S} n |n\rangle\langle n| \quad (2.74)$$

and

$$|\psi_0\rangle = \sum_{n \in S} w_n |n\rangle . \quad (2.75)$$

Now the problem is to find the positive operator  $\hat{\xi}_\parallel$  that minimizes the cost  $\bar{C}$  in Eq. (2.64). On the  $|n\rangle$  basis the operator  $\hat{\xi}_\parallel$  is written as

$$\hat{\xi}_\parallel = \sum_{n,m \in S} \xi_{nm} |n\rangle\langle m| . \quad (2.76)$$

For a generic even  $2\pi$ -periodic function  $C(\phi) = -\sum_{l=0}^{\infty} c_l \cos l\phi$  the average cost is given by

$$\bar{C} = -c_0 - \frac{1}{2} \sum_{l=1}^{\infty} c_l \sum_{|n-m|=l} \langle \psi_0|n\rangle\langle m|\psi_0\rangle \xi_{nm} . \quad (2.77)$$

Positivity of  $\hat{\xi}$  implies the generalized Schwartz inequalities

$$|\xi_{nm}| \leq \sqrt{\xi_{nn}\xi_{mm}} = 1 , \quad (2.78)$$

where the last equality comes from the POM completeness  $\int d\hat{\mu}_{\parallel}(\phi) = 1_{\parallel}$ . One can write

$$\text{sign}(c_l) \sum_{|n-m|=l} \langle \psi_0 | n \rangle \langle m | \psi_0 \rangle \xi_{nm} \leq \sum_{|n-m|=l} |\langle \psi_0 | n \rangle| |\langle m | \psi_0 \rangle|, \quad (2.79)$$

and the equality is obtained only for  $\xi_{nm} = \text{sign}(c_{|n-m|})$  (notice that we chose  $\langle \psi_0 | n \rangle > 0 \forall n \in S$ ). The minimum cost is

$$\bar{C} = -c_0 - \frac{1}{2} \sum_{l=1}^{\infty} |c_l| \sum_{|n-m|=l} |\langle \psi_0 | n \rangle| |\langle m | \psi_0 \rangle| \quad (2.80)$$

where we put  $\text{sign}(c_0) = 1$ , since the cost  $\bar{C}$  is independent of  $\xi_{nm}$  for  $c_{|n-m|} = 0$ . Notice that positivity of  $\hat{\xi}_{\parallel}$  is not generally guaranteed for any set of  $\text{sign}(c_l)$ . However, one can easily check that  $\hat{\xi}_{\parallel} > 0$  if  $\text{sign}(c_{|n-m|}) = \exp[i\pi(\epsilon_n - \epsilon_m)]$ ,  $\epsilon_n$  being any integer valued function of  $n$ . In fact, this choice corresponds to a unitary transformation of the operator  $\hat{\xi}_{\parallel}$  optimized with all  $c_l \geq 0 \forall l \geq 1$  (the parameter  $c_0$  is irrelevant). The particular choice  $c_l \geq 0 \forall l \geq 1$  has been considered by Holevo [52], and includes a large class of cost functions corresponding to the most popular optimization criteria, as

- i) the likelihood criterion for  $C(\phi) = -\delta_{2\pi}(\phi)$ ;
- ii) the  $2\pi$ -periodic ‘‘variance’’ for  $C(\phi) = 4 \sin^2(\phi/2)$ ;
- iii) the fidelity optimization for  $C(\phi) = 1 - |\langle \psi_0 | e^{i\hat{H}\phi} | \psi_0 \rangle|^2$  (here  $c_l = 2 \sum_{|n-m|=l} |w_n|^2 |w_m|^2$ ).

For the Holevo class of cost functions the optimal POM becomes

$$d\hat{\mu}_{\parallel}(\phi) = \frac{d\phi}{2\pi} |e(\phi)\rangle \langle e(\phi)|, \quad (2.81)$$

where the (Dirac) normalizable vectors  $|e(\phi)\rangle$  are given by

$$|e(\phi)\rangle = \sum_{n \in S} e^{in\phi} |n\rangle. \quad (2.82)$$

The vectors  $|e(\phi)\rangle$  generalize the Susskind-Glogower states  $|e^{i\phi}\rangle = \sum_{n=0}^{\infty} e^{in\phi} |n\rangle$  for generic integer spectrum. Therefore, the optimal POM  $d\hat{\mu}(\phi)$  is the projector on the state  $|e(\phi)\rangle$  in the Hilbert space  $\mathcal{H}_{\parallel}$ , and it is orthogonal for either  $S = \mathbb{Z}$ , or  $S = \mathbb{Z}_q$ , whereas it is not for  $S = \mathbb{N}$ . Notice that the POM (2.81) is also optimal for a density matrix  $\hat{\rho}_0$  which is a mixture of states in  $\mathcal{H}_{\parallel}$ , with the additional constraint of having constant phase along the diagonals. This can be easily proved by re-phasing the basis  $|n\rangle$  in such a way that all matrix elements of  $\hat{\rho}_0$  become positive. Then the assertion easily follows in a way similar to the derivation from Eq. (2.77) to Eq. (2.80). Moreover, it is easy to see that the pure state case minimizes the cost, which for the optimal

POM is given by  $\bar{C} = -\sum_{l=1}^{\infty} c_l \sum_{n \in S} \langle n | \hat{\rho}_0 | n+l \rangle$  (remember that  $\hat{\rho}_0 > 0$  implies that  $|\langle n | \hat{\rho}_0 | m \rangle|^2 \leq \langle n | \hat{\rho}_0 | n \rangle \langle m | \hat{\rho}_0 | m \rangle$ , and the bound is achieved by the pure state case  $\langle n | \hat{\rho}_0 | m \rangle = w_n^* w_m$ ). Finally we want to emphasize that for the bounded spectrum  $S = \mathbb{Z}_q$  there is no need for considering a continuous phase  $d\hat{\mu}(\phi)$ . In fact, it is easy to show [74] that the same average cost is achieved by restricting  $\phi$  to the set of discrete values  $\{\phi_s = \frac{2\pi s}{q}, s \in \mathbb{Z}_q\}$ , ( $q \equiv \dim(\mathcal{H}_{||})$ ), and using as the optimal POM the orthogonal projector-valued operator  $|e(\phi_s)\rangle\langle e(\phi_s)|$ .

Once the form of the optimal POM is fixed, one can optimize the state  $|\psi_0\rangle$  solving the linear problem in Eq. (2.70). In the following we show two examples of estimation of the phase shift pertaining to highly degenerate integer operators (finite dimensional cases are considered in Ref. [74]). In the first example we consider the operator  $\hat{H} = \sum_{l=1}^M l a_l^\dagger a_l$  that describes a multipath interferometer, involving  $M$  different modes of radiation. In the second, we focus our attention on the two-mode phase estimation using unconventional heterodyne detection, where the phase shift operator  $\hat{H} = a^\dagger a - b^\dagger b$  is given by the difference of photon numbers of the two modes.

### 2.5.2 Optimal POM for multipath interferometer

We consider the operator

$$\hat{H} = \sum_{l=1}^M l a_l^\dagger a_l \quad (2.83)$$

as the generator of the phase shift in Eq. (2.63). Such phase shift affects a  $M$ -mode state of radiation in a multipath interferometer, where contiguous paths suffer a fixed relative phase shift  $\phi$  [75] (this is also a schematic representation of the phase shift accumulated by successive reflections in a Fabry-Perot cavity). The operator  $\hat{H}$  in Eq. (2.83) has integer degenerate spectrum  $S = \mathbb{N}$ . We can take into account the degeneracy by renaming the number of photons of different modes as follows

$$\hat{H}|n\rangle_\nu = n|n\rangle_\nu, \quad (2.84)$$

with  $\nu = (\nu_2, \nu_3, \dots, \nu_M)$ , and

$$|n\rangle_\nu \doteq \left| n - \sum_{l=2}^M l\nu_l \right\rangle \otimes |\nu_2\rangle \otimes |\nu_3\rangle \otimes \dots \otimes |\nu_M\rangle. \quad (2.85)$$

The allowed values of  $\nu$  are restricted to the set  $\mathcal{E}_k$  given by

$$\mathcal{E}_k \doteq \left\{ \nu_2 = 0, 1, \dots, \left\lfloor \frac{k}{2} \right\rfloor, \nu_3 = 0, 1, \dots, \left\lfloor \frac{k - 2\nu_2}{3} \right\rfloor, \dots, \nu_M = \left\lfloor \frac{k - \sum_{l=2}^{M-1} l\nu_l}{M} \right\rfloor \right\} \quad (2.86)$$

where  $\lfloor x \rfloor$  denotes the integer part of  $x$ .

For the unshifted initial state  $|\psi_0\rangle$  we choose a linear symmetrized superposition of eigenvectors in Eq. (2.84), namely

$$|\psi_0\rangle = \sum_{n=0}^{\infty} w_n |n\rangle_{\text{sym}} , \quad (2.87)$$

where

$$|n\rangle_{\text{sym}} = \frac{1}{\sqrt{N_n}} \sum_{\{\nu_l\}} \delta \left( \sum_{l=1}^M l\nu_l - n \right) |\nu_1\rangle \otimes |\nu_2\rangle \otimes \dots \otimes |\nu_M\rangle , \quad (2.88)$$

$N_n$  being the number of elements  $\nu \in \mathcal{E}_n$ . Without loss of generality, the basis  $|n\rangle_{\text{sym}}$  has been chosen such that the coefficients  $w_n$  in Eq. (2.87) are real and positive. According to Eqs. (2.81) and (2.82) the optimal POM readily writes as follows

$$d\hat{\mu}(\phi) = \frac{d\phi}{2\pi} \sum_{n,m=0}^{\infty} e^{i(n-m)\phi} |n\rangle_{\text{sym}} \langle m| . \quad (2.89)$$

One can now choose a cost function and then minimize the average cost for the POM (2.89) upon varying the coefficients  $w_n$  of the state (2.87). By choosing the cost function  $C(\phi) = 4 \sin^2(\phi/2)$  and by imposing the normalization constraint through the Lagrange multiplier  $\lambda$ , the eigenvalue equation (2.70) gives the recursion for the coefficients  $w_n$  of the form

$$w_n + w_{n+2} - 2\lambda w_{n+1} = 0 . \quad (2.90)$$

The solutions of Eq. (2.90) can be found in terms of the Chebyshev's polynomials, and the corresponding optimal state writes as follows

$$|\psi\rangle = \left( \frac{2}{\pi} \right)^{1/2} \sum_{n=0}^{\infty} \sin[(n+1)\theta] |n\rangle_{\text{sym}} , \quad \theta = \arccos \lambda . \quad (2.91)$$

The state in Eq. (2.91) is Dirac-normalizable. It is formally equivalent to the eigenstate of the cosine operator  $\hat{C}$  of the phase of a single mode [76]. The Dirac normalizability comes from the nonexistence of normalizable states that minimize the uncertainty relation for cosine and sine operators

$$\Delta \hat{C} \Delta \hat{S} \geq \frac{1}{2} \left| \langle [\hat{C}, \hat{S}] \rangle \right| = \frac{1}{4} \langle |0\rangle \langle 0| \rangle , \quad (2.92)$$

as proved in Ref. [77].

### 2.5.3 Phase-difference of two-mode fields

In the previous example  $\hat{H}$  was bounded from below and  $S \equiv \mathbb{N}$ , such that the degenerate case is reduced to the standard Holevo's problem. For the difference operator

$\hat{H} = a^\dagger a - b^\dagger b$  one has  $S \equiv \mathbb{Z}$ , and the set of eigenvectors  $|d\rangle_\nu$  can be written in terms of the joint eigenvector  $|n\rangle|m\rangle$  for the number operators  $a^\dagger a$  and  $b^\dagger b$  with eigenvalues  $n$  and  $m$  as follows

$$|d\rangle_\nu = |d + \nu\rangle|\nu\rangle, \quad d \in \mathbb{Z}; \quad \nu \in [\max(0, -d), +\infty). \quad (2.93)$$

We consider an initial state  $|\psi_0\rangle$  of the form

$$|\psi_0\rangle = h_0|0\rangle|0\rangle + \sum_{n=1}^{+\infty} (h_n|n\rangle|0\rangle + h_{-n}|0\rangle|n\rangle), \quad (2.94)$$

where the basis has been chosen to have  $h_n \geq 0, \forall n$ . The optimal POM writes in the form of Eq. (2.81) in terms of the vectors  $|\lambda_n\rangle, n \in \mathbb{Z}$ , where

$$|\lambda_n\rangle = \begin{cases} |n\rangle_0 \equiv |n\rangle|0\rangle, & n \geq 0, \\ |n\rangle_{|n|} \equiv |0\rangle|n\rangle, & n \leq 0. \end{cases} \quad (2.95)$$

Here, the generalized Susskind-Glogower vector  $|e(\phi)\rangle$  is given by

$$|e(\phi)\rangle = \sum_{n \in \mathbb{Z}} e^{in\phi} |\lambda_n\rangle \equiv |0\rangle|0\rangle + \sum_{d=1}^{+\infty} \left( e^{id\phi} |d\rangle|0\rangle + e^{-id\phi} |0\rangle|d\rangle \right). \quad (2.96)$$

Notice that, differently from the usual case of spectrum  $S = \mathbb{N}$ , now the POM is orthogonal (in the Dirac sense):

$$\langle e(\phi) | e(\phi') \rangle = \sum_{n=-\infty}^{+\infty} e^{in(\phi-\phi')} = \delta_{2\pi}(\phi - \phi'), \quad (2.97)$$

where  $\delta_{2\pi}(\phi)$  is the Dirac comb. This means that in this case it is possible to define a selfadjoint phase operator

$$\hat{\phi} = \int_{-\pi}^{+\pi} d\phi |e(\phi)\rangle \langle e(\phi)| \phi, \quad (2.98)$$

as already noticed by Shapiro [64].

We now address the problem of finding the normalized state of the form (2.94) with finite mean photon number that minimizes the average cost evaluated through the ideal POM (2.81). As a cost function we choose again  $C(\phi) = 4 \sin^2(\phi/2)$  (periodicized-variance criterion), corresponding to the cost operator

$$\hat{C} = 2 - e^+ - e^-, \quad (2.99)$$

where

$$e^+ = \sum_{n \in \mathbb{Z}} |\lambda_{n+1}\rangle \langle \lambda_n|, \quad e^- = (e^+)^\dagger. \quad (2.100)$$

Introducing the energy operator  $\hat{E} = a^\dagger a + b^\dagger b$  and an additional Lagrange parameter accounting for finite mean energy  $\langle \hat{E} \rangle$ , the eigenvalue problem in Eq. (2.70) rewrites as follows

$$[\hat{C} - \lambda' - \mu'(a^\dagger a + b^\dagger b)]|\psi_0\rangle = 0, \quad (2.101)$$

where  $\lambda'$  and  $\mu'$  are the Lagrange multipliers for normalization and mean energy, respectively. The following recursion relations for the coefficients  $h_n$  is obtained

$$h_{n+1} + h_{n-1} - \mu(\lambda + |n|)h_n = 0, \quad (2.102)$$

with  $\lambda = (\lambda' - 2)/\mu'$  and  $\mu = -\mu'$ . The solution of Eq. (2.102) is given in terms of Bessel functions of the first kind in the following form

$$h_n = k(\lambda, \mu) J_{\lambda+|n|}(2/\mu), \quad (2.103)$$

$k(\lambda, \mu)$  being the constant of normalization

$$k(\lambda, \mu) = \left[ \sum_{n=-\infty}^{+\infty} J_{\lambda+|n|}^2(2/\mu) \right]^{-1/2}. \quad (2.104)$$

The matching of the recursion for positive and negative indices leads to the condition

$$\lambda J_\lambda(2/\mu) - (2/\mu) J_{\lambda+1}(2/\mu) = (2/\mu) \frac{d}{d(2/\mu)} J_\lambda(2/\mu) = 0. \quad (2.105)$$

Eq. (2.105) has infinitely many solutions  $\mu = \mu(\lambda)$ , and one needs to further minimize the average cost in Eq. (2.64) versus the average photon number  $N$  parameterized by  $\lambda$  and  $\mu = \mu(\lambda)$

$$N = 2k(\lambda, \mu)^2 \left[ \sum_{n=0}^{+\infty} n J_{\lambda+n}^2(2/\mu) \right]. \quad (2.106)$$

In this way one can find the normalized and finite-energy states that achieve the minimum cost for the optimal POM.

The solution (2.103) of the recursive relation (2.102) has some similarity with the solution for the minimum phase-uncertainty states of a single-mode field [76, 77]. The proof of convergence of the series in Eq. (2.104) can be found in Ref. [77]. However, the matching condition (2.105) (instead of the vanishing condition for  $h_n$  with  $n < 0$  for one mode) makes the two-mode phase estimation problem more difficult, since one cannot exploit the properties of the zeros of the Bessel functions in an asymptotic approximation, as done in Ref. [78] for the single-mode case.

## 2.6 Conclusion

In this chapter we have suggested a scheme to generate the phase-coherent states introduced in Ref. [48]. The set-up involves two  $\chi^{(2)}$  nonlinear crystals and it is based on parametric amplification of the vacuum followed by up-conversion of the resulting twin beam, the up-conversion playing the role of an approximate photon number recombination.

We found that the up-conversion process is both power-efficient and quite precise in the generation of PCS. It is a remarkable fact that the range of interaction times leading to high conversion rate also optimize the overlap between the outgoing state and the theoretical PCS. We have explored the case of twin-beam input photon number ranging from 0 to 54, and we have observed a conversion rate about 80%, with an overlap with ideal PCS between 80% and 100%. This corresponds to a reliable generation of PCS up to  $N_{out} = 20$  photons at the output.

The second proposed experimental set-up concerns the generation of two-mode radiation states that approach the heterodyne eigenvectors, thus leading to a detection scheme with optimal sensitivity  $\delta\phi \propto 1/\bar{n}$ ,  $\bar{n}$  being the total number of photons. The ideal r.m.s. sensitivity is achieved for large photon numbers  $\bar{n} \gg 1$  and for signal photons  $|w|^2/2 = \bar{n}/2$ . The gain of the amplifier is tuned to the value  $g = \bar{n}/4$ , and the quantum efficiency at the photodetector must be very good, namely  $1 - \eta \ll 2/\bar{n}$ .

Finally, we have settled the general theoretical framework for describing repeatable measurements and have shown a repeatable scheme for the two-mode phase measurement.

The problem of estimating a generic phase-shift experienced by a quantum state has been addressed for a generally degenerate phase shift operator in the last part of the chapter. The optimal positive operator-valued measure has been derived along with the optimal input state through quantum estimation theory. Two relevant examples have been analyzed: i) a multi-mode phase shift operator for multipath interferometry; ii) the two-mode heterodyne phase detection.

## Chapter 3

# Quantum-optical communication channels

### 3.1 Introduction

The detrimental effect of loss is a serious problem for optical communications based on transmission of nonclassical states of radiation. The results for the lossless case rapidly do not hold anymore for increasing losses [79, 80, 81]. The “nonclassical” channels based on direct detection of number states and homodyning of squeezed states—channels that have been originally proposed in order to improve the capacity of the “classical” channel based on heterodyning of coherent states—both are much more sensitive to loss than the classical channel. Hence, for long haul communications the great advantage of using nonclassical states is completely lost, since a minimum loss of 0.3dB/km is unavoidable with the current optical-fiber technology. In the above scenario the optimization of the quantum channels in the presence of loss is the most relevant issue for achieving reliable communication schemes in practical situations.

Through a systematic approach, in this chapter we evaluate the optimal *a priori* probability in the presence of loss, for both the squeezed-state and the number-state channels, and compare the relative effectiveness in terms of mutual information. As we will show in the following, the improvement due to the optimization is quite dramatic at low power regime and for very strong attenuation, giving rise to unexpected results.

With regard to the generation of the squeezed states and the number states involved in the nonclassical channels, this chapter also suggests a solution. On one hand, we show the equivalence between a couple of customary squeezed-state channels and a more easily achievable communication channel based on the two-mode heterodyne states we introduced in Sect. 2.3. On the other hand, we present an experimental scheme to synthesize optical number states (and also superpositions of number states) from coherent sources. The scheme involves a ring cavity coupled to a traveling wave by a

cross-Kerr medium and a triggering photodetection. It is noteworthy that low quantum efficiency at the photodetector does not reduce the effectiveness of the process. The number states, of course, are of particular interest not only for quantum communication channels, but also for fundamental tests of Quantum Mechanics [6] as well as for relevant applications like interferometry [82].

## 3.2 Optimized channels in the presence of loss

The communication channels based on nonclassical states of radiation are much more sensitive to the effect of losses than the classical channel based on the customary coherent states. They also have been shown [81] to be easily degraded by additive Gaussian noise, which models any kind of environmental effect due to linear interactions with random fields. In this section we evaluate the optimal *a priori* probability in the presence of loss, for both the squeezed-state and the number-state channels, and compare the relative effectiveness in terms of mutual information. We will show that for sufficiently high average transmitted power the optimized nonclassical channels are anyway beaten by the classical one. At low power levels, however, the enhancement of the mutual information from optimization makes both nonclassical channels more effective than the heterodyne one [83, 84]. This section is accompanied by many optimality capacity diagrams (Figs. 3.2, 3.3, 3.6, 3.8 and 3.9), which compare the different communication channels, giving the regions in the loss-power plane where each channel is optimal with respect to the others.

### 3.2.1 Heterodyne channel

The communication channel based on heterodyne detection encodes a complex variable on a coherent state with Gaussian *a priori* distribution. The heterodyne 3dB detection noise is itself Gaussian additive, and the Gaussian form of the *a priori* probability density that achieves the channel capacity is dictated by the Shannon's theorem [79, 85] for Gaussian channels subjected to the quadratic constraint of fixed average power. Under such constraint the variance of the optimal Gaussian distribution equals the value of the mean photon number  $N$ . In the following we briefly redraw the analytical derivation of this result, in order to show how the optimal *a priori* probability remains unchanged in the presence of loss.

The effect of loss on a single-mode communication channel is determined by the master equation

$$\partial_t \hat{\rho} = \mathcal{L}_\Gamma \hat{\rho} \doteq \Gamma(n_a + 1)L[a]\hat{\rho} + \Gamma n_a L[a^\dagger]\hat{\rho} \simeq \Gamma L[a]\hat{\rho}, \quad (3.1)$$

where the superoperator  $\mathcal{L}_\Gamma$  gives the time derivative of the density matrix  $\hat{\rho}$  of the radiation state (in the interaction picture) through the action of the Lindblad super-

operators [86]

$$L[c]\hat{\rho} = c\hat{\rho}c^\dagger - \frac{1}{2}(c^\dagger c\hat{\rho} + \hat{\rho}c^\dagger c) \quad (3.2)$$

The coefficient  $\Gamma$  represents the damping rate, whereas  $n_a$  denotes the mean number of thermal photons at the frequency of mode  $a$ , and can be neglected at optical frequencies.

We introduce the energy attenuation factor, or “loss”, defined as follows

$$\eta \doteq \exp(-\Gamma t), \quad (3.3)$$

according to the evolution of the average power

$$\langle a^\dagger a(t) \rangle \equiv \text{Tr}[a^\dagger a \hat{\rho}(t)] = \text{Tr}[a^\dagger a e^{\mathcal{L}_\Gamma t} \hat{\rho}(0)] = \eta \langle a^\dagger a(0) \rangle. \quad (3.4)$$

More generally,  $\eta$  gives the scaling factor of any normal-ordered operator function, namely

$$e^{\mathcal{L}_\Gamma^\vee t} :f(a^\dagger, a): = :f(\eta^{1/2} a^\dagger, \eta^{1/2} a):, \quad (3.5)$$

where  $\mathcal{L}_\Gamma^\vee$  denotes the dual Liouvillian, which is defined through the identity

$$\text{Tr} \left[ (e^{\mathcal{L}_\Gamma^\vee t} \hat{O}) \hat{\rho} \right] = \text{Tr} \left[ \hat{O} (e^{\mathcal{L}_\Gamma t} \hat{\rho}) \right] \quad (3.6)$$

valid for any operator  $\hat{O}$ . The mutual information transmitted throughout the channel for *a priori* distribution  $p(\alpha)$  of the encoded complex variable  $\alpha$ , and for input-output conditional probability density  $Q(\beta|\alpha)$ , is given by [90, 91, 79, 85]

$$I = \int d^2\alpha p(\alpha) \int d^2\beta Q(\beta|\alpha) \ln \frac{Q(\beta|\alpha)}{\int d^2\alpha' p(\alpha') Q(\beta|\alpha')}, \quad (3.7)$$

where the integrations are performed on the complex plane with measure  $d^2\alpha = d\text{Re}\alpha d\text{Im}\alpha$ . For heterodyning of a coherent state  $|\alpha\rangle$ , the conditional probability density is given by

$$Q(\beta|\alpha) = |\langle \beta|\alpha \rangle|^2 = \frac{1}{\pi} \exp(-|\beta - \alpha|^2). \quad (3.8)$$

According to Eqs. (3.1) and (3.3), in the presence of loss  $e^{\mathcal{L}_\Gamma t}(|\alpha\rangle\langle\alpha|) = |\eta^{1/2}\alpha\rangle\langle\eta^{1/2}\alpha|$ , and hence the conditional probability density simply rewrites

$$Q_\eta(\beta|\alpha) = \frac{1}{\pi} \exp(-|\beta - \eta^{1/2}\alpha|^2). \quad (3.9)$$

The constraint of fixed average power at the transmitter reads

$$\int d^2\alpha p(\alpha) \langle \alpha | a^\dagger a | \alpha \rangle = \int d^2\alpha p(\alpha) |\alpha|^2 = N, \quad (3.10)$$

where in the following  $N$  will generally denote the total mean photon number. We now maximize the mutual information (3.7) over all possible normalized probability densities  $p(\alpha)$  that satisfy the constraint (3.10). Eq. (3.7) can be simplified as follows

$$I = -\ln \pi - 1 - \int d^2\beta f(\beta) \ln f(\beta) , \quad (3.11)$$

where  $f(\beta)$  denotes the unconditioned or “*a posteriori*” probability, namely

$$f(\beta) = \int d^2\alpha p(\alpha) Q_\eta(\beta|\alpha) . \quad (3.12)$$

By transferring the (normalization and power) constraints from  $p(\alpha)$  to  $f(\beta)$ , we can maximize the mutual information with respect to  $f(\beta)$  through a variational calculus on Eq. (3.11). While normalization condition for  $p(\alpha)$  simply corresponds to normalization of  $f(\beta)$ , the fixed-power constraint needs the following algebra

$$\begin{aligned} N &= \int d^2\alpha p(\alpha) |\alpha|^2 \\ &= \int \frac{d^2\beta}{\eta} \int d^2\alpha p(\alpha) |\alpha|^2 \frac{1}{\pi} \exp\left(-\frac{|\beta|^2}{\eta} - \eta|\alpha|^2 + \beta\bar{\alpha} + \bar{\beta}\alpha\right) \\ &= \frac{1}{\eta} \int d^2\beta (|\beta|^2 - 1) f(\beta) , \end{aligned} \quad (3.13)$$

where the bar denotes the complex conjugate number. Hence, the variational equation for the mutual information writes

$$0 = \frac{\delta}{\delta f} \left[ I - \lambda \int d^2\beta f(\beta) - \frac{\mu}{\eta} \int d^2\beta (|\beta|^2 - 1) f(\beta) \right] , \quad (3.14)$$

with  $I$  given by Eq. (3.11), and with  $\lambda$  and  $\mu$  as Lagrange multipliers to be determined. One can easily check that Eq. (3.14) has the Gaussian solution

$$f(\beta) = \frac{1}{\pi(\eta N + 1)} \exp\left(-\frac{|\beta|^2}{\eta N + 1}\right) , \quad (3.15)$$

and from Eqs. (3.11) and (3.15) one obtains the capacity of the heterodyne channel in the presence of loss

$$C = \ln(1 + \eta N) . \quad (3.16)$$

Hence, the channel capacity depends only on the mean photon number  $\eta N$  at the receiver. Eqs. (3.12) and (3.15) give the optimal *a priori* probability density

$$p(\alpha) = \frac{1}{\pi N} \exp\left(-\frac{|\alpha|^2}{N}\right) , \quad (3.17)$$

which is manifestly independent on  $\eta$ , with the consequence that the optimal *a priori* probability for the lossless heterodyne channel is still optimal in the presence of loss. This result is due to the peculiar form of the master equation (3.1), which keeps coherent states as coherent. As we will show in the following, this will no longer hold true for the squeezed-state and the number-state channels.

### 3.2.2 Homodyne channel

The homodyne channel encodes a real variable  $x$  on the quadrature-squeezed state

$$|x\rangle_r = D(x)S(r)|0\rangle, \quad (3.18)$$

which is generated from the vacuum  $|0\rangle$  through the action of the displacement operator  $D(x)$  and of the squeezed operator  $S(r)$ , which are defined as follows

$$D(x) = \exp \left[ x (a^\dagger - a) \right] \quad (3.19)$$

$$S(r) = \exp \left[ \frac{r}{2} (a^{\dagger 2} - a^2) \right]. \quad (3.20)$$

The decoding is performed by homodyning a fixed quadrature, say  $\hat{X} \equiv (a + a^\dagger)/2$ . For lossless transmission, the conditional probability density of getting the value  $x'$  when the transmitted state is  $|x\rangle_r$  writes

$$Q(x'|x) = |\langle x'|x\rangle_r|^2 = \sqrt{\frac{1}{2\pi\Delta^2}} \exp \left[ -\frac{(x' - x)^2}{2\Delta^2} \right], \quad (3.21)$$

where  $|x'\rangle$  denotes the eigenstate of  $\hat{X}$ , and the variance is given by  $\Delta^2 = e^{-2r}/4$ . According to Shannon's theorem[79, 85] the optimal *a priori* probability  $p(x)$  for the ideal homodyne channel has the Gaussian form

$$p(x) = \sqrt{\frac{1}{2\pi\sigma^2}} \exp \left( -\frac{x^2}{2\sigma^2} \right), \quad (3.22)$$

with variance

$$\sigma^2 = \frac{N(N+1)}{2N+1}. \quad (3.23)$$

The fixed-power constraint is given by

$$N = \int dx p(x)_r \langle x|a^\dagger a|x\rangle_r = \int dx p(x)(x^2 + \sinh^2 r) = \sigma^2 + \sinh^2 r. \quad (3.24)$$

Hence, Eq. (3.23) corresponds to fix the fraction of squeezing photons at the value  $\sinh^2 r = N^2/(2N+1)$ . The capacity is given by

$$\begin{aligned} C &= \int dx \int dx' p(x) Q(x'|x) \ln \frac{Q(x'|x)}{\int d\tilde{x} p(\tilde{x}) Q(x'|\tilde{x})} \\ &= \frac{1}{2} \ln \left( 1 + \frac{\sigma^2}{\Delta^2} \right) = \ln(1 + 2N). \end{aligned} \quad (3.25)$$

By comparing Eq. (3.25) with Eq. (3.16), one finds that in the lossless case the capacity of the squeezed-state channel is always greater than that of the coherent-state channel, with one additional bit *per mode* for high average power ( $N \gg 1$ ).

In the presence of loss, by means of the relation (3.5) and the following normal-ordered representation of the quadrature projector

$$|x\rangle\langle x| = \delta(\hat{X} - x) = \int \frac{d\lambda}{2\pi} e^{-i\lambda x} e^{-\lambda^2/8} e^{i\lambda a^\dagger/2} e^{i\lambda a/2}, \quad (3.26)$$

one obtains the conditional probability density

$$\begin{aligned} Q_\eta(x'|x) &= \langle x'|e^{\mathcal{L}_r t}(|x\rangle_{rr}\langle x|)|x'\rangle = \text{Tr} \left[ e^{\mathcal{L}_r^\vee t} \left( \delta(\hat{X} - x') \right) |x\rangle_{rr}\langle x| \right] \\ &= \text{Tr} \left[ \int \frac{d\lambda}{2\pi} e^{-i\lambda x'} e^{-\lambda^2(1-\eta)/8} e^{i\eta^{1/2}\lambda\hat{X}} |x\rangle_{rr}\langle x| \right] \\ &= \sqrt{\frac{1}{2\pi\Delta_\eta^2}} \exp \left[ -\frac{(x' - \eta^{1/2}x)^2}{2\Delta_\eta^2} \right], \end{aligned} \quad (3.27)$$

where

$$\Delta_\eta^2 = \frac{1}{4} [1 - \eta(1 - e^{-2r})]. \quad (3.28)$$

For Gaussian *a priori* probability with variance  $(N - \sinh^2 r)$ , which satisfies the fixed-power constraint (3.24), the mutual information is given by

$$I = \frac{1}{2} \ln \left( 1 + \frac{4\eta(N - \sinh^2 r)}{1 - \eta(1 - e^{-2r})} \right). \quad (3.29)$$

Upon maximizing Eq. (3.29) with respect to  $\xi \equiv e^{-2r}$  we obtain

$$I = \frac{1}{2} \ln \left( 1 + \frac{4\xi N - (1 - \xi)^2}{\xi^2 + \frac{1-\eta}{\eta}\xi} \right) \quad (3.30)$$

with

$$\xi = \frac{\eta + \sqrt{1 + 4\eta(1 - \eta)N}}{(4N + 1)\eta + 1}. \quad (3.31)$$

The optimal number of squeezing photons is given by  $N_{sq} = (\xi + 1/\xi - 2)/4$ , and it is plotted versus  $N$  in Fig. 3.1 for some values of the attenuation  $\eta$ . One can see that the optimal fraction of squeezing photons rapidly decreases with attenuation. This means that for increasing loss it is more and more unprofitable to use much power to squeeze the quadrature of the signal, since the quantum noise of the state at the receiver approaches that of the coherent state. These results agree with previous investigations on the loss effects in terms of signal-to-noise ratio [80]. For the experimental techniques to obtain tunable squeezed light see Refs. [88, 89].

Figs. 3.2 and 3.3 are optimality capacity diagrams, which compare different channels giving the regions on the loss-power plane where each channel is optimal. The coherent-state channel is compared to the squeezed-state channel without and with

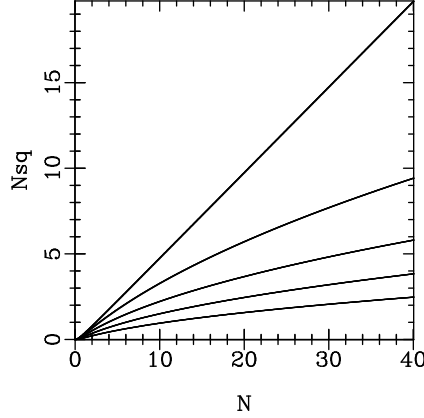


Figure 3.1: Number of squeezing photons that optimizes the lossy homodyne channel versus the total average number of photons, at different values of the attenuation factor  $\eta$ . From the top to the bottom, the plotted lines refer to  $\eta = 1, .95, .85, .7, .5$ .

loss-dependent optimization in Fig. 3.2 and Fig. 3.3, respectively. One can see that the optimization leads to a sizeable improvement of the mutual information, especially for strong attenuation and low power (see also Fig. 3.4), making the diagram symmetric around the  $\eta = 1/2$  vertical axis. Notice the location of the minimum at  $\eta = .5$  and  $N = 8$  on the boundary between the optimality regions in Fig. 3.3: this means that for mean power less than eight photons the squeezed-state channel always beats the coherent-state one, independently on attenuation.

Through a kind of exclusion principle for the information contents of quantum observables [87], Hall has proved an upper bound for the information that can be achieved by a homodyne channel subjected to Gaussian noise. Following Hall's method, here we prove the following upper bound for any lossy channel that uses homodyne detection

$$I \leq \ln(1 + 2\eta N) . \quad (3.32)$$

By denoting with  $S(\hat{A}|\hat{\rho})$  the entropy associated to the probability distribution  $\langle a|\hat{\rho}|a\rangle$  of the eigenvalue  $a$  of the observable  $\hat{A}$  when the state is  $\hat{\rho}$ , namely

$$S(\hat{A}|\hat{\rho}) = - \int da \langle a|\hat{\rho}|a\rangle \ln \langle a|\hat{\rho}|a\rangle , \quad (3.33)$$

the mutual information retrieved from the measurement of the observable  $\hat{A}$  on a member of the ensemble specified by the density matrix  $\hat{\rho} = \sum_i p_i \hat{\rho}_i$  is given by

$$I(\hat{A}|\hat{\rho}) = S(\hat{A}|\hat{\rho}) - \sum_i p_i S(\hat{A}|\hat{\rho}_i) . \quad (3.34)$$

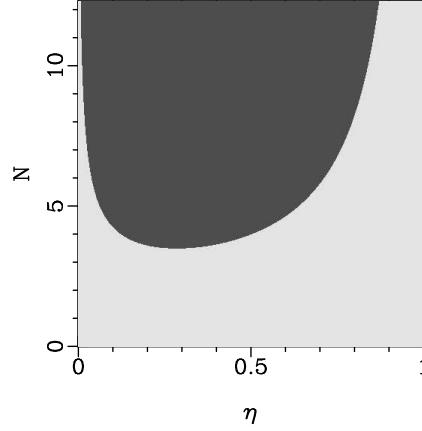


Figure 3.2: Optimality capacity diagram, which represents the region where the coherent-state channel is optimal (black area) and that where the squeezed-state channel is optimal instead (green area). Both channel are the customary ones, which were optimized for the lossless case.

A simple variational calculation gives the upper bounds

$$S(\hat{X}|\hat{\rho}) \leq \frac{1}{2} + \frac{1}{2} \ln(2\pi\langle\Delta\hat{X}^2\rangle_{\hat{\rho}}) \quad (3.35)$$

$$S(\hat{Y}|\hat{\rho}) \leq \frac{1}{2} + \frac{1}{2} \ln(2\pi\langle\Delta\hat{Y}^2\rangle_{\hat{\rho}}) \quad (3.36)$$

for the entropy associated to the conjugated quadratures  $\hat{X} = (a + a^\dagger)/2$  and  $\hat{Y} = (a - a^\dagger)/2i$ , the notation  $\langle\dots\rangle_{\hat{\rho}}$  representing the ensemble average with density operator  $\hat{\rho}$ .

Moreover, writing  $\hat{\rho}$  as a mixture of pure states

$$\hat{\rho} = \sum_j p_j |\psi_j\rangle\langle\psi_j|, \quad (3.37)$$

from the concavity of entropy one has

$$\begin{aligned} S(\hat{X}|e^{\mathcal{L}_{\text{r}}t}\hat{\rho}) &= S(e^{\mathcal{L}_{\text{r}}t}\hat{X}|\hat{\rho}) \geq \sum_j p_j S(e^{\mathcal{L}_{\text{r}}t}\hat{X}|(|\psi_j\rangle\langle\psi_j|)) \\ &\geq \inf_j S(e^{\mathcal{L}_{\text{r}}t}\hat{X}|(|\psi_j\rangle\langle\psi_j|)), \end{aligned} \quad (3.38)$$

and analogously for the other quadrature  $\hat{Y}$ . A derivation similar to that of Eq. (3.27) leads to the conditional probability

$$\begin{aligned} p(x|e^{\mathcal{L}_{\text{r}}t}(|\psi_j\rangle\langle\psi_j|)) &= \text{Tr} \left\{ \left[ \frac{2}{\pi(1-\eta)} \right]^{1/2} \exp \left[ -\frac{2(\eta^{1/2}\hat{X} - x)^2}{1-\eta} \right] |\psi_j\rangle\langle\psi_j| \right\} \\ &\equiv \text{Tr} \left[ G(\eta^{1/2}\hat{X} - x) |\psi_j\rangle\langle\psi_j| \right], \end{aligned} \quad (3.39)$$

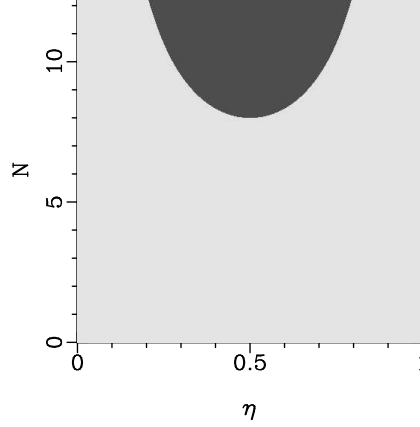


Figure 3.3: Optimality capacity diagram comparing the coherent-state channel to the squeezed-state channel in the presence of loss. Among the two channels, in the grey region the squeezed state channel has the highest capacity, whereas in the black region the coherent state channel is the best.

where we introduced the Gaussian operator-valued measure defined as follows

$$G(\eta^{1/2}\hat{X} - x) \equiv \left[ \frac{2}{\pi(1-\eta)} \right]^{1/2} \exp \left[ -\frac{2(\eta^{1/2}\hat{X} - x)^2}{1-\eta} \right]. \quad (3.40)$$

By varying over the bra  $\langle \psi_j |$  the following quantity

$$J = S \left( e^{\mathcal{L}_{\hat{r}}^{\chi t} \hat{X}} (|\psi_j\rangle\langle\psi_j|) \right) + S \left( e^{\mathcal{L}_{\hat{r}}^{\chi t} \hat{Y}} (|\psi_j\rangle\langle\psi_j|) \right) - \lambda (\langle\psi_j|\psi_j\rangle - 1), \quad (3.41)$$

one obtains the variational equation

$$0 = \frac{\delta J}{\delta \langle \psi_j |} = - \int dx G(\eta^{1/2}\hat{X} - x) \ln \left\{ \text{Tr} \left[ G(\eta^{1/2}\hat{X} - x) |\psi_j\rangle\langle\psi_j| \right] \right\} |\psi_j\rangle \\ - \int dy G(\eta^{1/2}\hat{Y} - y) \ln \left\{ \text{Tr} \left[ G(\eta^{1/2}\hat{Y} - y) |\psi_j\rangle\langle\psi_j| \right] \right\} |\psi_j\rangle - (\lambda + 2) |\psi_j\rangle, \quad (3.42)$$

where  $\lambda$  is the Lagrange multiplier for the normalization constraint relative to the state  $|\psi_j\rangle$ . It can be easily verified that the case of vacuum state  $|\psi_j\rangle \equiv |0\rangle$  satisfies Eq. (3.42). Then, from Eq. (3.38) along with the following relation

$$S \left( e^{\mathcal{L}_{\hat{r}}^{\chi t} \hat{O}} (|0\rangle\langle 0|) \right) = \frac{1}{2} - \frac{1}{2} \ln \left( \frac{2}{\pi} \right) \quad (3.43)$$

that holds for the quadrature operators  $\hat{O} = \hat{X}, \hat{Y}$ , one has

$$S \left( \hat{X} |e^{\mathcal{L}_{\hat{r}}^{\chi t} \hat{\rho}} \right) + S \left( \hat{Y} |e^{\mathcal{L}_{\hat{r}}^{\chi t} \hat{\rho}} \right) \geq 1 + \ln \left( \frac{\pi}{2} \right). \quad (3.44)$$

On the other hand, from Eqs. (3.35) and (3.36) one obtains

$$S \left( \hat{X} |e^{\mathcal{L}_{\hat{r}}^{\chi t} \hat{\rho}} \right) + S \left( \hat{Y} |e^{\mathcal{L}_{\hat{r}}^{\chi t} \hat{\rho}} \right) \leq 1 + \ln(2\pi) + \frac{1}{2} \ln \left( \langle \Delta \hat{X}^2 \rangle_{e^{\mathcal{L}_{\hat{r}}^{\chi t} \hat{\rho}}} \langle \Delta \hat{Y}^2 \rangle_{e^{\mathcal{L}_{\hat{r}}^{\chi t} \hat{\rho}}} \right). \quad (3.45)$$

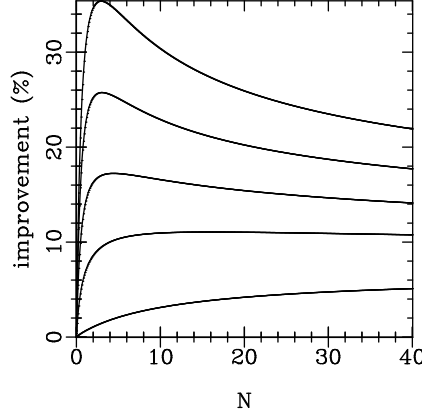


Figure 3.4: *Per cent* improvement of the mutual information versus the total average number of photons  $N$ , with  $\eta$ -independent optimization. The plotted lines refer to different values of the attenuation factor  $\eta$ . From the top to the bottom  $\eta = .15, .25, .4, .6, .9$ .

The product of the expectation values in Eq. (3.45) can be maximized as follows

$$\begin{aligned} \langle \Delta \hat{X}^2 \rangle_{e^{\mathcal{L}_{\mathbf{r}t} \hat{\rho}}} \langle \Delta \hat{Y}^2 \rangle_{e^{\mathcal{L}_{\mathbf{r}t} \hat{\rho}}} &= \left[ \eta \langle \Delta \hat{X}^2 \rangle_{\hat{\rho}} + \frac{1}{4}(1 - \eta) \right] \left[ \eta \langle \Delta \hat{Y}^2 \rangle_{\hat{\rho}} + \frac{1}{4}(1 - \eta) \right] \\ &\leq \frac{1}{4} \left[ \eta \left( \langle \hat{X}^2 \rangle_{\hat{\rho}} + \langle \hat{Y}^2 \rangle_{\hat{\rho}} \right) + \frac{1 - \eta}{2} \right]^2 \leq \frac{1}{4} \left( \eta \langle a^\dagger a \rangle_{\hat{\rho}} + \frac{1}{2} \right)^2, \end{aligned} \quad (3.46)$$

and we obtain

$$S \left( \hat{X} | e^{\mathcal{L}_{\mathbf{r}t} \hat{\rho}} \right) + S \left( \hat{Y} | e^{\mathcal{L}_{\mathbf{r}t} \hat{\rho}} \right) \leq 1 + \ln \left( \frac{\pi}{2} \right) + \ln \left( 1 + 2\eta \langle a^\dagger a \rangle_{\hat{\rho}} \right). \quad (3.47)$$

Finally, inequalities (3.44) and (3.47), together with Eq. (3.34) yield the information exclusion relation

$$I \left( \hat{X} | e^{\mathcal{L}_{\mathbf{r}t} \hat{\rho}} \right) + I \left( \hat{Y} | e^{\mathcal{L}_{\mathbf{r}t} \hat{\rho}} \right) \leq \ln(1 + 2\eta N) \quad (3.48)$$

where  $N = \langle a^\dagger a \rangle_{\hat{\rho}}$ . From Eq. (3.48) the bound (3.32) follows as a particular case. From the above derivation we see that the bound (3.32) holds for any lossy channel that employs homodyne detection.

The upper bound (3.32) is trivially achieved for  $\eta = 1$  by a Gaussian ensemble of squeezed states, however, in the presence of loss it is not reached by our optimized channel. As a matter of fact, there is still room for a slight improvement of the mutual information if one allows the squeezing  $r$  to vary as a function of the signal  $x$  in Eq. (3.18). However, such further optimization is not achievable analytically—due to the now non-Gaussian form of the conditional probability density—nor it can be worked out numerically, as no viable method is at hand.

### 3.2.3 Direct-detected channel

The ideal communication channel that uses direct detection of Fock states with thermal *a priori* probability

$$p_n^{\text{th}} = \frac{1}{1+N} \left( \frac{N}{1+N} \right)^n \quad (3.49)$$

achieves the ultimate quantum capacity (the Holevo's bound [90, 91]) with the constraint of fixed average number of photons  $N$ . The ultimate quantum capacity is given by

$$C = \ln(1+N) + N \ln \left( 1 + \frac{1}{N} \right) . \quad (3.50)$$

For ideal transmission the conditional probability density is given by the Kronecker delta  $\delta_{m,n}$ . In the presence of loss this is replaced by the binomial distribution

$$Q_{m,n}(\eta) = \binom{n}{m} \eta^m (1-\eta)^{n-m} , \quad (3.51)$$

which represents the probability of detecting  $m$  photons when the transmitted state is  $|n\rangle$ . The number-state channel is more sensitive to loss than the coherent-state and the squeezed-state ones.

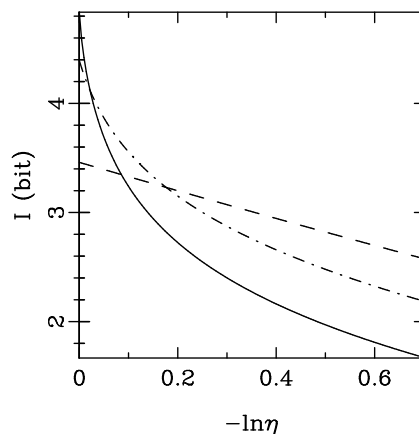


Figure 3.5: Mutual information versus attenuation for the number-state (full), the coherent-state (dashed), and the squeezed-state (dashed-dotted) channels. The fixed average number of photons is  $N = 10$ . The *a priori* probability densities are the customary ones for the lossless case [Eqs. (3.49), (3.17) and (3.22), respectively].

In Fig. 3.5 the mutual information for the three channels is plotted versus  $\eta$ , at fixed power  $N = 10$ , and with the customary *a priori* probabilities optimized for the lossless case [Eqs. (3.17), (3.22) and (3.49)]. One can see that at this power level a signal attenuation of 0.5 dB is sufficient to degrade the number-state channel below the capacity

of the coherent-state channel, whereas at higher power levels the effect is even more dramatic. The optimality capacity diagram in Fig. 3.6 compares the number-state with the coherent-state channels. One can see that in the presence of loss the number-state channel rapidly loses off its efficiency, especially for high power and strong attenuation.

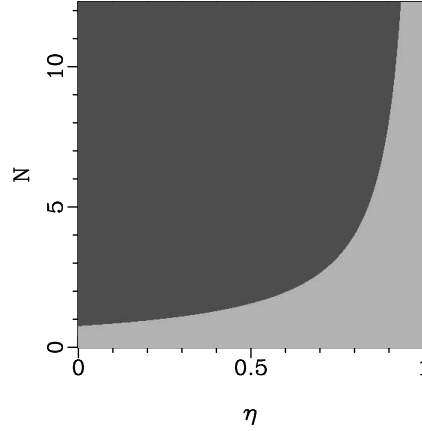


Figure 3.6: Optimality capacity diagram with  $\eta$ -independent optimization. Black region: the coherent-state channel is optimal; dark grey region: the number-state channel is optimal.

Now we address the problem of optimizing the *a priori* probability distribution in the presence of loss. In principle one could perform the optimization analytically by varying the information over the infinite set of variables  $\{p_n\}$ , however with no viable method for constraining each  $p_n$  to be nonnegative. For this reason we decided to carry out the optimization numerically, using the recursive Blahut's algorithm [92]. The recursion is given by

$$c_n^{(r+1)} = \exp \left( \sum_k Q_{k,n}(\eta) \ln \frac{Q_{k,n}(\eta)}{\sum_m p_m^{(r)} Q_{k,m}(\eta)} - \mu n \right), \quad (3.52)$$

$$p_n^{(r+1)} = p_n^{(r)} \frac{c_n^{(r)}}{\sum_m p_m^{(r)} c_m^{(r)}}, \quad (3.53)$$

where  $p_n^{(r)}$  is the *a priori* probability at the  $r$ th iteration,  $Q_{k,n}(\eta)$  is the conditional probability (3.51), and  $\mu$  is the Lagrange multiplier for the average-power constraint. The series are actually truncated to a finite dimension, corresponding to a maximum allowed number of photons. Blahut proved that the quantity

$$J^{(r)} = I^{(r)} - \mu N^{(r)} \quad (3.54)$$

increases versus  $r$ , and achieves the desired bound,  $I^{(r)}$  and  $N^{(r)}$  denoting the mutual information and the average photon number with the  $r$ th iterated *a priori* probability

$p_n^{(r)}$ . Then, for a given  $\mu$  one evaluates the limit of  $p_n^{(r)}$  for  $r \rightarrow \infty$  under the recursion (3.53), and determines the mutual information  $I$  and the mean photon number  $N$  for such limiting  $p_n^{(\infty)}$ : in this way the capacity versus power  $I = I(N)$  is obtained as parameterized by  $\mu$ .

Now we present some numerical results. Figs. 3.7 show the number probability distribution for different values of loss and power, evaluated by means of Blahut's recursive algorithm, stopped at  $10^5$  iterations. The Hilbert space has been truncated at dimension 200, however, truncation at 100 gives almost identical results. For stronger loss, the optimal *a priori* probability departs from the thermal-like behavior, with an enhanced vacuum probability. For loss  $\eta \lesssim .6$  (see Fig. 3.7) the probability plot develops gaps of zero probability at intermediate numbers of photons. This can be intuitively understood as the effect of a loss so strong that it becomes more convenient to use a smaller alphabet of well-spaced letters in order to achieve a better distinguishability at the receiver. The increase of the probability for the vacuum state comes clearly from the constant-energy constraint. Table 3.1 provides a list of numerical results pertaining to Figs. 3.7. It gives the *per cent* improvement of the mutual information after optimization, along with the absolute value of the mutual information for the optimized number-state channel, for the number-state channel with customary thermal probability and for the coherent-state channel at given value of the loss and of the mean photon number. Also the values of the quantities  $\epsilon_I$  and  $\epsilon_P$  are reported, for convergence estimation of Blahut's recursion (3.54). They are defined as the increment  $\epsilon_I = J^{(r)} - J^{(r-1)}$  of the quantity  $J^{(r)}$  in Eq. (3.54), and the distance  $\epsilon_P = \max_n |p_n^{(r)} - p_n^{(r-1)}|$  between probability plots, both  $\epsilon_I$  and  $\epsilon_P$  being evaluated at the last iteration step  $r = 10^5$ . One can see that, according to the small values of  $\epsilon_I$  and  $\epsilon_P$ , the algorithm is converging quite fast (indeed only 10 steps are usually sufficient to get an estimate of the capacity up to the second digit). With the occurrence of gaps in the *a priori* probability, the relative improvement of the mutual information increases even more dramatically, up to 70% for strong attenuation  $\eta = .15$ . At low power, this improvement allows the direct-detection channel to overcome the coherent-state channel capacity [see Figs. 3.7a,c,e,g,h and their pertaining numerical values in Table 3.1]. The optimality capacity diagram in Fig. 3.8 compares the optimized number-state channel with the coherent-state channel. Notice the difference with respect to Fig. 3.3: here the optimized number-state channel beats the heterodyne channel at power much lower than for the optimized squeezed-state channel in Fig. 3.3. As for the squeezed-state channel, the optimization makes the diagram more symmetric around the  $\eta = 1/2$  vertical axis.

plot	$\eta$	$N$	$I_{opt}$	$I_{th}$	$I_{coh}$	%	$\epsilon_P$	$\epsilon_I$
a)	.9	8.575	3.157	3.097	3.124	1.93	$2 \cdot 10^{-12}$	$1 \cdot 10^{-18}$
b)	.75	2.827	1.775	1.699	1.642	4.50	$4 \cdot 10^{-13}$	$1 \cdot 10^{-18}$
c)	.6	2.414	1.340	1.218	1.292	10.03	$1 \cdot 10^{-8}$	$1 \cdot 10^{-14}$
d)	.6	6.930	1.935	1.745	2.367	10.90	$2 \cdot 10^{-8}$	$6 \cdot 10^{-14}$
e)	.55	2.288	1.219	1.083	1.175	12.56	$8 \cdot 10^{-8}$	$7 \cdot 10^{-13}$
f)	.55	6.729	1.803	1.595	2.233	13.07	$1 \cdot 10^{-7}$	$2 \cdot 10^{-12}$
g)	.4	1.888	0.887	0.715	0.812	24.18	$6 \cdot 10^{-8}$	$2 \cdot 10^{-12}$
h)	.15	4.040	0.720	0.416	0.684	73.08	$8 \cdot 10^{-9}$	$2 \cdot 10^{-13}$

Table 3.1: Numerical values relative to the plots a-h of Fig. 3.7. The table lists the following quantities: attenuation factor ( $\eta$ ); average number of photons ( $N$ ); mutual information (in bits) ( $I_{opt}$ ) for the optimized number-state channel, ( $I_{th}$ ) for the number-state channel with customary thermal probability, ( $I_{coh}$ ) for the coherent-state channel; *per cent* improvement (%) of the mutual information due to the optimization; convergence parameters  $\epsilon_P$  and  $\epsilon_I$  (see text).

### 3.2.4 Summary of the results

We analyzed the detrimental effect of loss on narrow-band quantum-optical channels based on *i*) heterodyne detection of coherent states, *ii*) homodyne detection of squeezed states and *iii*) direct detection of number states. The main results are the following. The squeezed-state channel and, even more, the number-state channel, are both easily degraded by loss below the capacity of the coherent-state channel. Because of the peculiar form of the master equation for the loss, the coherent-state channel does not need optimization, and remains as the most efficient one at sufficiently high power.

The optimization of the squeezed-state channel leads to a sizeable improvement of the mutual information (over 30% for  $\eta = .15$  at low power). Correspondingly, the optimal fraction of squeezing photons rapidly decreases with attenuation. For total average number of photons  $N < 8$  the squeezed-state channel is always more efficient than the coherent-state one, independently on attenuation  $\eta$ . The optimization has been performed at constant squeezing, whereas the problem of optimizing a signal-dependent squeezing is still open.

With regard to the number-state channel, Blahut's recursive algorithm allows to evaluate the optimal *a priori* probability and the channel capacity. The improvement of the mutual information is considerable, achieving 70% for  $\eta = .15$ . The optimal *a priori* probability departs from the usual monotonic thermal-like distribution, and for  $\eta \lesssim .6$  it develops gaps of zero probability at intermediate number of photons. At low

power the optimization of the number-state channel makes its capacity better than that of the coherent-state channel.

A comprehensive view of the numerical results of this section is offered by the optimality capacity diagram in Fig. 3.9: there one can find the regions on the loss-power plane where the coherent-state, the optimized squeezed-state, and the optimized number-state channels are respectively optimal.

### 3.3 Equivalence between squeezed-state and twin-beam communication channels

As it was shown in the previous section, the maximum mutual information *per mode* for narrow-band linear bosonic channels under the constraint of fixed average power is achieved by the ideal number state channel with thermal input probabilities. Nevertheless, the generation of number eigenstates is quite hard (a novel method is however suggested in the Sec. 3.4) and, above all, a concrete realization of the ideal photon number amplifier that can assist the channel is still unknown. Hence, our interest is turned into squeezed-state channels, which are feasible and still lead to a satisfactory efficiency.

In this section we show a new communication scheme that is based on unconventional heterodyne detection on two-mode states—the displaced twin-beam states introduced in Sec. 2.3—and represents an alternative way to achieve the squeezed-state channel capacity [93]. It was already noticed the equivalence of a nondegenerate parametric amplifier with two parallel degenerate parametric amplifiers. Such equivalence has been also exploited to experimentally obtain a matched local oscillator for the detection of quadrature squeezing [94]. As regards communication purposes, we extend this equivalence to all the stages of the communication channel: the encoded state, the optimal amplifier for the channel, the master equation modeling the loss, and the output measurement scheme. The two equivalent schemes are the following.

- (i) a complex number is encoded on a twin-beam state generated by parametric down-conversion; decoding is achieved through unconventional heterodyne detection of both the signal and image-band modes which form the correlated twin beam;
- (ii) the real and the imaginary part of the complex number are independently encoded over two uncorrelated squeezed states pertaining two different modes; the states are decoded through ordinary homodyne detection on each mode separately.

The unitary transformation that connects the two communication schemes physically corresponds to the 50-50 frequency conversion between the two field modes. The twin-beam scheme is easier to obtain experimentally as compared to the squeezed-state

scheme, and also both the encoding and the decoding stage are simpler. As encoder one just needs parametric downconversion and coherent states, instead of squeezing. On the other hand, as decoder one has just one heterodyne detector versus a delicate balancing of two equal homodyne detectors. As compared to the single homodyne QS channel, the heterodyne one, by employing two field modes, carries a double amount of information.

### 3.3.1 The twin-beam communication scheme

The twin-beam communication scheme is based on unconventional heterodyne detection of the two-modes states  $|z\rangle\rangle_\lambda$  introduced in Sect. 2.3. We discuss the two-mode master equation that models both the effect of losses and a linear phase-insensitive amplification that assists the communication line. Then we derive a Fokker-Planck equation for the unconventional-heterodyne probability to evaluate the channel capacity.

The effect of losses on the communication channel can be modeled by the following master equation

$$\partial_t \hat{\rho} = \mathcal{L}_\Gamma \hat{\rho} \doteq \Gamma \left\{ (n_a + 1)L[a] + (n_b + 1)L[b] + n_a L[a^\dagger] + n_b L[b^\dagger] \right\} \hat{\rho}, \quad (3.55)$$

that generalizes Eq. (3.1) for two modes. The damping rate  $\Gamma$  is supposed to be equal for both modes, whereas the mean number of thermal photons  $n_a$  and  $n_b$  at the frequency of modes  $a$  and  $b$  can be neglected at optical frequencies. The absence of cross-terms that correlate the two modes is a consequence of the rotating-wave approximation assumed in the ordinary derivation of the master equation [95]. In a similar fashion, an active medium amplifier in the linear regime can be described by the superoperator

$$\mathcal{L}_\Lambda = \Lambda \left\{ (m_a + 1)L[a^\dagger] + (m_b + 1)L[b^\dagger] + m_a L[a] + m_b L[b] \right\}, \quad (3.56)$$

where  $\Lambda$  denotes the gain per unit time—i.e. the amplifier length—and  $m_a$  and  $m_b$  are related to the population inversion of the lasing levels at resonance with  $a$  and  $b$ , respectively. Finally, a parametric amplification distributed along the line with modes  $a$  and  $b$  correlated by a classical pump is represented by the following commutator

$$\mathcal{L}_K = K[a^\dagger b^\dagger - ab, \cdot], \quad (3.57)$$

where  $K$  is the gain per unit time and is related to the intensity of the pump. From Eq. (2.16) one obtains the following differential representation of modes

$$\begin{aligned} a|z\rangle\rangle &= \left( \frac{z}{2} - \partial_{\bar{z}} \right) |z\rangle\rangle, & a^\dagger|z\rangle\rangle &= \left( \frac{\bar{z}}{2} + \partial_z \right) |z\rangle\rangle, \\ b|z\rangle\rangle &= \left( \frac{\bar{z}}{2} - \partial_z \right) |z\rangle\rangle, & b^\dagger|z\rangle\rangle &= \left( \frac{z}{2} + \partial_{\bar{z}} \right) |z\rangle\rangle. \end{aligned} \quad (3.58)$$

Such representation converts a two-mode master equation of the general form

$$\begin{aligned} \mathcal{L} \hat{\rho}_t &= 2 \left\{ (A + C_a)L[a^\dagger] + (A + C_b)L[b^\dagger] + (B + C_a)L[a] + (B + C_b)L[b] \right\} \hat{\rho}_t \\ &+ K[a^\dagger b^\dagger - ab, \hat{\rho}_t] \end{aligned} \quad (3.59)$$

into the following Fokker-Planck equation

$$\partial_t P(z, \bar{z}; t) = \{Q(\partial_z z + \partial_{\bar{z}} \bar{z}) + 2D\partial_{z\bar{z}}^2\} P(z, \bar{z}; t), \quad (3.60)$$

where  $P(z, \bar{z}; t) \equiv \langle\langle z|\hat{\rho}_t|z\rangle\rangle$  denotes the (unconventional) heterodyne probability density, and the drift and diffusion terms are given by  $Q = B - A - K$  and  $D = A + B + C_a + C_b$ . Notice that the coefficients in the master equation (3.59) are not independent (the difference of the first two coefficients equals the difference of the last two in the curly brackets), and this is the condition under which all the derivatives in Eq. (3.58) gather to give the simple Fokker-Planck equation (3.60). Hence, when considering the effect of loss in Eq. (3.55), the assumption of equal damping for the two modes is crucial. Of course, the same argument holds true for the gain  $\Lambda$  in Eq. (3.56).

The solution of the Fokker-Planck equation (3.60) for a Gaussian initial probability density

$$P(z, \bar{z}; 0) = \frac{1}{\pi\Delta^2(0)} \exp\left(-\frac{|z-w|^2}{\Delta^2(0)}\right), \quad (3.61)$$

keeps the Gaussian form all the time, and writes

$$P(z, \bar{z}; t) = \frac{1}{\pi\Delta^2(t)} \exp\left(-\frac{|z-we^{-Qt}|^2}{\Delta^2(t)}\right), \quad (3.62)$$

where the ‘‘evolved’’ variance at time  $t$  is given by

$$\Delta^2(t) = \frac{D}{Q}(1 - e^{-2Qt}) + \Delta^2(0)e^{-2Qt}. \quad (3.63)$$

For a communication scheme using the states  $|w\rangle\rangle_\lambda$  of Sec. 2.3, one has  $\Delta^2(0) \equiv \Delta_\lambda^2 = (1 - \lambda)/(1 + \lambda)$ , according to Eq. (2.30). From Eq. (3.7), for *a priori* and conditional probability densities both Gaussian, i.e.

$$p(w) = \frac{1}{\pi\sigma^2} \exp\left(-\frac{|w|^2}{\sigma^2}\right) \quad (3.64)$$

$$p(w|z) = \frac{1}{\pi\Delta^2} \exp\left(-\frac{|z-gw|^2}{\Delta^2}\right), \quad (3.65)$$

the corresponding mutual information is given by

$$I = \ln\left(1 + \frac{g^2\sigma^2}{\Delta^2}\right). \quad (3.66)$$

The average number of photons *per* mode in the state  $|w\rangle\rangle_\lambda$  of Eq. (2.34) is given by

$$\frac{1}{2}\langle a^\dagger a + b^\dagger b \rangle = \frac{|w|^2}{4} + \frac{\lambda^2}{1 - \lambda^2}. \quad (3.67)$$

Then, the variance of the prior distribution for the twin-beam scheme under the constraint of fixed average power  $N$  reads

$$\sigma^2 = 4 \left( N - \frac{\lambda^2}{1 - \lambda^2} \right). \quad (3.68)$$

Hence, the mutual information transmitted at time  $t$  for a twin-beam channel modeled by the Fokker-Planck equation (3.60) is given by

$$I = \ln \left( 1 + \frac{4 \left( N - \frac{\lambda^2}{1 - \lambda^2} \right)}{\frac{D}{Q}(e^{2Qt} - 1) + \Delta_\lambda^2} \right). \quad (3.69)$$

In the lossless case, the mutual information is maximized by  $\lambda = N/(N + 1)$  to the value

$$I = 2 \ln(1 + 2N), \quad (3.70)$$

namely two times the mutual information for a single-mode squeezed state channel [compare Eq. (3.25)]. As noticed at the end of Sec. 3.2.2, here also the gain parameter  $\lambda$  could be allowed to vary as a function of the “displacement signal”  $z$ . One might achieve a little better capacity which, however, is not easy to be evaluated, because the conditional probability would not have a Gaussian form anymore. Moreover, such a varying parameter would be very difficult to get experimentally.

For a lossy channel with damping rate  $\Gamma$  and  $n_a = n_b = \bar{n}$  thermal photons one has  $D = \Gamma(2\bar{n} + 1)/2$  and  $Q = \Gamma/2$ . In this case, for  $\lambda = N/(N + 1)$ , Eq. (3.69) rewrites

$$I = \ln \left( 1 + \frac{4N(N + 1)}{1 + (2N + 1)(2\bar{n} + 1)(e^{\Gamma t} - 1)} \right). \quad (3.71)$$

Indeed, one could optimize the parameter  $\lambda$  as a function of the damping rate  $\Gamma$  as in Eqs. (3.29), (3.30) and (3.31) for the squeezed-state channel, with the correspondence

$$\lambda \rightarrow \tanh r, \quad e^{-\Gamma t} \rightarrow \eta. \quad (3.72)$$

The exponential erasure of information in Eq. (3.71) becomes linear using the master equation (3.59), with  $K = \Gamma/2$ , namely

$$I = \ln \left( 1 + \frac{4N(N + 1)}{1 + (2N + 1)(2\bar{n} + 1)\Gamma t} \right) \quad (3.73)$$

This case represents an ideal distributed parametric amplification that works against the detrimental effect of loss. Notice that, due to the energy of the pump, the condition of fixed average power is not strictly satisfied. Indeed, after a transient, the increase of the mean number of photons is approximately linear in time as follows

$$N(t) = \frac{1}{2} \left[ N(0) + \bar{n} - \frac{1}{2} + \left( N(0) - \bar{n} + \frac{1}{2} \right) e^{-2\Gamma t} + \Gamma(2\bar{n} + 1)t \right]. \quad (3.74)$$

In the following we will show the equivalence of the twin-beam channel with a communication scheme based on a couple of uncorrelated quadrature-squeezed states.

### 3.3.2 Equivalence with the squeezed-state channel

Let us consider the unitary transformation that describes a 50-50 frequency conversion device from mode  $a$  to mode  $b$ . Under suitable choice of phases, the corresponding unitary operator  $\hat{U}$  writes

$$\hat{U} = \exp \left[ \frac{\pi}{4} (ab^\dagger - a^\dagger b) \right] \quad (3.75)$$

so that the Heisenberg evolution of modes is given in matrix form as follows

$$\hat{U}^\dagger \begin{pmatrix} a \\ b \end{pmatrix} \hat{U} = \frac{1}{\sqrt{2}} \begin{pmatrix} 1 & -1 \\ 1 & 1 \end{pmatrix} \begin{pmatrix} a \\ b \end{pmatrix} \quad (3.76)$$

The action of the operator (3.75) on a twin-beam state is more easily evaluated using Eq. (2.25) for the twin beam with  $u = v = z/2$ . Since the vacuum state  $|0\rangle \otimes |0\rangle$  is an eigenvector of the frequency conversion operator (3.75) with eigenvalue 1, from the identity

$$e^A X e^{-A} = X + [A, X] + \frac{1}{2!} [A, [A, X]] + \dots \quad (3.77)$$

one has

$$\begin{aligned} \hat{U}|z\rangle\rangle_\lambda &= \left[ D_a \left( \frac{i \operatorname{Im} z}{\sqrt{2}} \right) S_a(\tanh^{-1} \lambda) \right] |0\rangle \otimes \left[ D_b \left( \frac{\operatorname{Re} z}{\sqrt{2}} \right) S_b(-\tanh^{-1} \lambda) \right] |0\rangle \\ &\equiv |i \operatorname{Im} z\rangle_\lambda \otimes |\operatorname{Re} z\rangle_{-\lambda}, \end{aligned} \quad (3.78)$$

where  $S_c(r)$  is the squeezing operator for the mode  $c = a, b$  in Eq. (3.20), and the squeezed state  $|\alpha\rangle_\lambda$  is defined as follows

$$|\alpha\rangle_\lambda = D_c(\alpha/\sqrt{2}) S_c(\tanh^{-1} \lambda) |0\rangle. \quad (3.79)$$

Hence, by means of frequency conversion the twin-beam state (2.25) disentangles into two squeezed states which are still related in intensity and phase. For modes  $a$  and  $b$  at the same frequency and different wave vectors or polarization, this “disentanglement” can be also achieved by means of a 50-50 beam splitter [96].

With regard to the effect of frequency conversion at the output of a lossy/amplified channel, notice that a superoperator of the form

$$\mathcal{L} = \alpha L[a] + \beta L[b] + \gamma L[a^\dagger] + \delta L[b^\dagger] + \mathcal{L}_K \quad (3.80)$$

undergoes the following transformation

$$\begin{aligned} \hat{U} \mathcal{L} \hat{U}^\dagger &= \frac{\alpha + \beta}{2} (L[a] + L[b]) + \frac{\gamma + \delta}{2} (L[a^\dagger] + L[b^\dagger]) + \frac{K}{2} [a^2 - a^{\dagger 2}, \cdot] \\ &- \frac{K}{2} [b^2 - b^{\dagger 2}, \cdot] + \frac{\alpha - \beta}{2} (\text{cross-terms}) + \frac{\gamma - \delta}{2} (\text{cross-terms}). \end{aligned} \quad (3.81)$$

We are not interested in the cross-terms in Eq. (3.81) that act jointly on  $\mathcal{H}_a \otimes \mathcal{H}_b$ , because they vanish when  $n_a = n_b$  and  $m_a = m_b$  in Eqs. (3.55) and (3.56), respectively. In this case one has

$$\hat{U}\mathcal{L}_\Gamma\hat{U}^\dagger = \mathcal{L}_\Gamma; \quad \hat{U}\mathcal{L}_\Lambda\hat{U}^\dagger = \mathcal{L}_\Lambda. \quad (3.82)$$

Thus, the 50-50 conversion leaves the superoperators  $\mathcal{L}_\Gamma$  and  $\mathcal{L}_\Lambda$  invariant. This means that the disentanglement of the twin beam occurs equivalently at whatever time during transmission. On the contrary, a distributed amplification with pump-correlated  $a$  and  $b$  is not invariant under the transformation (3.76). Indeed, a nondegenerate parametric amplifier followed by frequency conversion is equivalent to a couple of independent phase-sensitive amplifiers, as shown by the commutator terms in Eq. (3.81), namely

$$\hat{U}\mathcal{L}_K\hat{U}^\dagger = \mathcal{L}'_K = \frac{K}{2}[a^2 - a^{\dagger 2}, \cdot] - \frac{K}{2}[b^2 - b^{\dagger 2}, \cdot] \quad (3.83)$$

Notice that for  $K > 0$  the amplified quadrature components of the fields  $a$  and  $b$  through these commutators are  $\hat{Y}_a \equiv \hat{a}_{\pi/2}$  and  $\hat{X}_b \equiv \hat{b}_0$ , respectively, which are the right quadratures in order to enhance the signal carried by the couple of squeezed states (3.78). Of course, the communication scheme that encodes the information on states (3.78) needs two independent homodyne measurements of the quadratures  $\hat{Y}_a$  and  $\hat{X}_b$ .

We have shown the equivalence of the two channels with regard to the input states and the evolution master equation. It remains to show that also the final detection stage is equivalent in the two schemes. The unconventional heterodyne detection is described by the following orthogonal resolution of the identity

$$d\hat{\mu}(z, \bar{z}) = d^2z \delta^{(2)}(\hat{Z} - z) \equiv d^2z |z\rangle\langle\langle z|. \quad (3.84)$$

The unitary operator (3.75) transforms the orthogonal resolution (3.84) as follows

$$\begin{aligned} \hat{U}d\hat{\mu}(z, \bar{z})\hat{U}^\dagger &= d^2z \delta(\sqrt{2}\hat{X}_b - \text{Re}z) \delta(\sqrt{2}\hat{Y}_a - \text{Im}z) \\ &= dx dy \delta(\hat{X}_b - x) \delta(\hat{Y}_a - y), \quad z = \sqrt{2}(x + iy). \end{aligned} \quad (3.85)$$

The last orthogonal resolution in Eq. (3.85) is just the one corresponding to two independent homodyne measurements of quadratures  $\hat{X}_b$  and  $\hat{Y}_a$ .

In conclusion of this section, we also show the equivalence between the squeezed-state scheme and the twin-beam scheme at the level of Fokker-Planck equations. Using the homodyne probability density

$$P_a(y; t)P_b(x; t) = \text{Tr} \left[ \hat{\rho}_t |y\rangle_{\frac{\pi}{2}} \langle y| \otimes |x\rangle_{00} \langle x| \right] \quad (3.86)$$

the master equation

$$\begin{aligned} \mathcal{L}' \hat{\rho}_t &= 2 \left\{ A(L[a^\dagger] + L[b^\dagger]) + B(L[a] + L[b]) \right\} \hat{\rho}_t \\ &+ \frac{K}{2} [a^2 - a^{\dagger 2}, \hat{\rho}_t] - \frac{K}{2} [b^2 - b^{\dagger 2}, \hat{\rho}_t] \end{aligned} \quad (3.87)$$

can be written in the Fokker-Planck form

$$\partial_t \{P_a(y;t)P_b(x;t)\} = \left\{ Q(\partial_x x + \partial_y y) + \frac{D}{4}(\partial_{xx}^2 + \partial_{yy}^2) \right\} P_a(y;t)P_b(x;t) \quad (3.88)$$

with  $Q = B - A - K$  and  $D = A + B$ . In obtaining Eq. (3.88) we used the Wigner representation of both  $a$  and  $b$  modes given in Appendix A, and then evaluated the marginal integration over the quadratures  $\hat{X}_a$  and  $\hat{Y}_b$ . The equivalence of the Fokker-Planck equation (3.88) with Eq. (3.60) is evident, after the coordinate transformation

$$z = \sqrt{2}(x + iy), \quad \bar{z} = \sqrt{2}(x - iy), \quad (3.89)$$

and upon renaming the product of probabilities as follows

$$P'(z, \bar{z}; t) = \frac{1}{2} P_a\left(\frac{\text{Im}z}{\sqrt{2}}; t\right) P_b\left(\frac{\text{Re}z}{\sqrt{2}}; t\right). \quad (3.90)$$

Of course, Eq. (3.69) is valid also for the squeezed-state scheme, with parameter  $\lambda$  and variance  $\Delta_\lambda^2$  related to the squeezing parameter through Eqs. (3.78) and (2.30). The equivalence between the two communication channels is schematized in Fig. 3.10.

### 3.4 Optical Fock-state synthesizer

The generation of number states is of particular interest not only for quantum communication channels, but also for fundamental tests of Quantum Mechanics [6] as well as for relevant applications in quantum interferometry [82]. Up to now various methods for the generation of such states have been proposed both for traveling as well as for cavity fields. For traveling fields these methods are mainly based on highly nonlinear interactions [97], on conditional measurements [98], or on state engineering [99]. The experimental realizability or effectiveness of these proposals is often challenging. Less difficulties are involved in the generation of Fock states into cavity [100], *e.g.* using micromaser trapped states.

In this last section of the chapter, we address the problem of Fock state generation in a traveling mode. We suggest an optical device, feasible with current technology, based on a triggering photodetector and a ring cavity coupled to an external traveling wave through a cross-Kerr medium. Remarkably, the input states of the proposed setup are just customary coherent states. The scheme can also be used to engineer superpositions of few Fock states, which are crucial for optical quantum computers [101], and quantum

tomography of optical Hamiltonians [102]. As we will show, low quantum efficiency at the photodetector has no detrimental effect on the filtering process, but only reduces the state-synthesizing rate.

### 3.4.1 The experimental set-up

The schematic setup of the synthesizer is depicted in Fig. 3.11. The ring cavity is build by high reflectivity beam splitters. Here, for simplicity, we suppose that the beam splitters have the same transmissivity  $\tau$ . The cavity is fed by a coherent state in the mode  $a_1$ , whereas the mode  $a_2$  is left unexcited. Through the cross-Kerr interaction, the cavity mode  $d$  is coupled to an external traveling mode  $c_1$ , according to the unitary evolution [103]

$$\hat{U}_K = \exp(-i\chi t c_1^\dagger c_1 d^\dagger d), \quad (3.91)$$

$\chi$  being the nonlinear susceptibility of the medium and  $t$  the interaction time. The mode  $c_1$  is prepared in a coherent state, and a tunable phase shift  $\psi$  is also introduced in the cavity mode. At the output of the cavity the field is monitored by an avalanche photodetector. For the purpose of our scheme, we only need to verify the presence or absence of the field, at the output port of the cavity through the triggering photodiode D. Let us initially assume unit quantum efficiency at photodetection. The probability operator measure (POM)  $\hat{\Pi}_n$  at D is the two-value operator  $\hat{\Pi}_0 \doteq |0\rangle\langle 0|$  and  $\hat{\Pi}_1 \doteq \hat{I}_{b_2} - |0\rangle\langle 0|$ , where  $|0\rangle$  is the vacuum and  $\hat{I}_{b_2}$  is the identity for mode  $b_2$ . As we will show in the following, due to the very steep dependence of the cavity transmissivity on the total phase shift — including both cross Kerr interaction and phase  $\psi$  — the detection of the field at photodetector D guarantees that the free mode  $c_2$  (at the output of the Kerr medium) is reduced into a Fock state or a superposition of few Fock states.

The mode transformations of the ring cavity are [104]

$$\begin{cases} b_1 = \kappa(\varphi)a_1 + e^{i\varphi}\sigma(\varphi)a_2 \\ b_2 = \sigma(\varphi)a_1 + \kappa(\varphi)a_2 \end{cases}, \quad (3.92)$$

where the phase-dependent cavity transmissivity  $\sigma$  and reflectivity  $\kappa$  are given by

$$\begin{aligned} \kappa(\varphi) &\doteq \frac{\sqrt{1-\tau}(e^{i\varphi}-1)}{1-[1-\tau]e^{i\varphi}} \\ \sigma(\varphi) &\doteq \frac{\tau}{1-[1-\tau]e^{i\varphi}}, \end{aligned} \quad (3.93)$$

with  $|\kappa(\varphi)|^2 + |\sigma(\varphi)|^2 = 1$ . The transformations (3.92) and (3.93) are rigorously obtained by quantizing the e.m. field modes obtained by solving the Helmholtz equation of the etalon, as in Ref. [104], and taking the input/output modes of the asymptotic

free plane waves. However, a *naive* solution of the etalon as a loop of beam splitters gives the same result, with the internal modes having a reduced commutator (this point is well explained in Ref. [105]). For  $c_1$  in the Fock state  $|n\rangle$ , the total phase shift is  $\varphi = \psi - \chi nt \equiv \varphi_n$ . To simplify notation, we write  $\sigma_n \doteq \sigma(\varphi_n)$  and analogously for  $\kappa$ . Let us now consider the input state

$$\hat{\varrho}_{in} = |\alpha\rangle\langle\alpha| \otimes |0\rangle\langle 0| \otimes \hat{\nu}_{in}, \quad (3.94)$$

namely a generic state  $\hat{\nu}_{in}$  for mode  $c_1$ , a coherent state  $|\alpha\rangle$  for mode  $a_1$ , and vacuum for  $a_2$ . In the Schrödinger picture the output state can be written in the form

$$\hat{\varrho}_{out} = \sum_{n,m=0}^{\infty} \nu_{nm} |\kappa_n\alpha\rangle\langle\kappa_m\alpha| \otimes |\sigma_n\alpha\rangle\langle\sigma_m\alpha| \otimes |n\rangle\langle m|. \quad (3.95)$$

The process of filtering the desired Fock state from the input state  $\hat{\nu}_{in}$  is triggered by the photodetector D as follows. The probabilities corresponding to the outcomes 1 (detector D on) and 0 (detector D off) are given by

$$\begin{aligned} P_1 &= \text{Tr} \left[ \hat{\varrho}_{out} \hat{\Pi}_1 \right] = \sum_{n=0}^{\infty} \nu_{nn} \left( 1 - e^{-|\alpha|^2 |\sigma_n|^2} \right), \\ P_0 &= \text{Tr} \left[ \hat{\varrho}_{out} \hat{\Pi}_0 \right] = \sum_{n=0}^{\infty} \nu_{nn} e^{-|\alpha|^2 |\sigma_n|^2}. \end{aligned} \quad (3.96)$$

By means of Eq. (3.93) we have

$$|\sigma_n|^2 = \left[ 1 + 4 \frac{1-\tau}{\tau^2} \sin^2 \frac{\psi - \chi nt}{2} \right]^{-1}, \quad (3.97)$$

which is a periodic function sharply peaked at

$$n = \frac{\psi + 2\pi j}{\chi t} \doteq n^* + \frac{2\pi}{\chi t} j, \quad j \in \mathbb{Z}, \quad (3.98)$$

with unit maximum height and width of the same order of the beam splitter transmissivity  $\tau$  (typically  $\tau \sim 10^{-3} \div 10^{-6}$ ). The value  $n^*$  in Eq. (3.98) can be adjusted to an arbitrary integer by tuning the phase-shift  $\psi$  as a multiple of  $\chi t$ , whereas multiple resonances are avoided by using small nonlinearity  $\chi t \ll 1$ , so that the values of  $n$  satisfying Eq. (3.98) for  $j \neq 0$  correspond to vanishing matrix elements  $\nu_{ni} \simeq 0 \forall i$ . In this case for  $\tau \ll 1$  in Eq. (3.96) we have  $|\sigma_n|^2 \simeq \delta_{nn^*}$ , and the detection probability  $P_1$  rewrites

$$P_1 \simeq \nu_{n^*n^*} \left( 1 - e^{-|\alpha|^2} \right) \quad \tau \ll 1. \quad (3.99)$$

Notice that increasing the amplitude of  $\alpha$  will enhance the detection probability  $P_1$ . Moreover, one can optimize also the input state  $\hat{\nu}_{in}$  to achieve the highest  $\nu_{n^*n^*}$ . For example, in the case of a coherent input  $\hat{\nu}_{in} = |\beta\rangle\langle\beta|$ , one could select  $|\beta\rangle \simeq \sqrt{n^*}$ .

### 3.4.2 The output state reduction

We now evaluate the conditional state  $\hat{\nu}_{out}$  at the output of the Kerr medium for detector D on. One has

$$\hat{\nu}_{out} = \frac{1}{P_1} \text{Tr}_{a_1 a_2} [\hat{\rho}_{out} \hat{\Pi}_1] = \frac{e^{-|\alpha|^2}}{P_1} \sum_{n,m=0}^{\infty} \nu_{nm} e^{|\alpha|^2 \kappa_n \kappa_m^*} \left( e^{|\alpha|^2 \sigma_n \sigma_m^*} - 1 \right) |n\rangle \langle m| \quad (3.100)$$

where the partial trace is performed over the ring cavity modes. The argument  $\theta$  of  $\sigma(\theta) = |\sigma(\theta)| \exp[i\theta(\varphi)]$  is given by

$$\theta(\varphi) = \arctan \left[ \frac{\sin \varphi (1 - \tau)}{1 - (1 - \tau) \cos \varphi} \right]. \quad (3.101)$$

As already noticed, for  $\tau \ll 1$   $|\sigma_n|$  is nonzero only for  $n = n^*$ , and correspondingly we have  $\theta(\varphi_n) = 0$ . Therefore, for all practical purposes we can write  $\sigma_n \sigma_m^* \simeq |\sigma_n| |\sigma_m^*| \simeq \delta_{nn^*} \delta_{mm^*}$ , and the output state (3.100) becomes

$$\hat{\nu}_{out} \simeq |n^*\rangle \langle n^*|, \quad \tau \ll 1, \quad (3.102)$$

*i.e.* the Fock component  $|n^*\rangle$  has been filtered from the initial state  $\hat{\nu}_{in}$ .

In Fig. 3.12 we report the number distribution of the conditional output state  $\hat{\nu}_{out}$ , with  $\psi$  tuned to obtain  $|n^* = 4\rangle$  for different values of the beam splitter transmissivity.

We now show how the same setup may be used to produce superpositions of Fock states. By choosing higher nonlinearities, the quantity  $2\pi/(\chi t)$  decreases and  $|\sigma_n|^2$  can be significantly different from zero for more than one value of  $n$  corresponding to sizeable components of the input state  $\hat{\nu}_{in}$ . If there are only two of these “resonant” values  $n_1 = n^*$  and  $n_2 = n^* + 2\pi/\chi t$ , we have  $|\sigma_n| \simeq \delta_{nn_1} + \delta_{nn_2}$  and Eq. (3.99) rewrites as follows

$$P_1 \simeq (\nu_{n_1 n_1} + \nu_{n_2 n_2}) \left( 1 - e^{-|\alpha|^2} \right), \quad \tau \ll 1. \quad (3.103)$$

Accordingly, the conditional state after a successful photodetection becomes

$$\begin{aligned} \hat{\nu}_{out} \simeq & \frac{1}{\nu_{n_1 n_1} + \nu_{n_2 n_2}} \left[ \nu_{n_1 n_1} |n_1\rangle \langle n_1| + \nu_{n_2 n_2} |n_2\rangle \langle n_2| \right. \\ & \left. + \nu_{n_1 n_2} |n_1\rangle \langle n_2| + \nu_{n_2 n_1} |n_2\rangle \langle n_1| \right] \quad \tau \ll 1, \end{aligned} \quad (3.104)$$

which is a pure state if and only if  $\nu_{n_1 n_1} \nu_{n_2 n_2} = \nu_{n_1 n_2} \nu_{n_2 n_1}$ , namely for  $\hat{\nu}_{in}$  a coherent state.

In Fig. 3.13 we report the density matrix of the conditional output state  $\hat{\nu}_{out}$ , with  $\psi$  tuned to obtain a superposition of the Fock states  $|n_1 \equiv 10\rangle$  and  $|n_2 \equiv 20\rangle$  for different values of the beam splitter transmissivity. It is worth noting that the coefficients of the superposition in Eq. (3.104) are selected by the input state  $\hat{\nu}_{in}$ . Therefore, in

order to have a superposition with equal weights starting from a coherent state  $|\beta\rangle$ , it is sufficient to choose its amplitude in such a way that

$$|\beta|^2 = \left( \frac{n_1!}{n_2!} \right)^{\frac{1}{n_1 - n_2}}. \quad (3.105)$$

Notice, however, that with this choice of  $\beta$  we find a small contribution due to the term with  $j = 2$  in Eq. (3.98).

Let us now take into account the quantum efficiency  $\eta$  at the photodetector. In this case the POM  $\hat{\Pi}_n$  is replaced with  $\hat{\Pi}_n^{(\eta)}$ , where

$$\hat{\Pi}_0^{(\eta)} \doteq \sum_{k=0}^{\infty} (1 - \eta)^k |k\rangle\langle k|, \quad \hat{\Pi}_1^{(\eta)} \doteq I_{b_2} - \hat{\Pi}_0^{(\eta)}. \quad (3.106)$$

The probability  $P_1^{(\eta)}$  of having outcome 1 at the photodetector and the conditional output state now are the following

$$P_1^{(\eta)} = \text{Tr}[\hat{\Pi}_1^{(\eta)} \hat{\rho}_{out}] = \sum_{n=0}^{\infty} \nu_{nn} \left( 1 - e^{-\eta|\alpha|^2 |\sigma_n|^2} \right),$$

$$\hat{\rho}_{out}^{(\eta)} = \frac{e^{-|\alpha|^2}}{P_1^{(\eta)}} \sum_{n,m=0}^{\infty} \nu_{nm} e^{|\alpha|^2 [\kappa_n \kappa_m^* + \sigma_n \sigma_m^*]} \left( 1 - e^{-\eta|\alpha|^2 \sigma_n \sigma_m^*} \right) |n\rangle\langle m|. \quad (3.107)$$

Remarkably, low values for the quantum efficiency  $\eta$  can reinforce the process of filtering, though at the cost of lowering the probability  $P_1^{(\eta)}$  of photodetection. In fact,  $\eta$  scales the term  $\sigma_p \sigma_q^*$  in the exponential in Eq. (3.107), thus lowering the off-resonance contributions. In Fig. 3.14a we actually purify the superposition shown in Fig. 3.13a by lowering the quantum efficiency to the value  $\eta = 20\%$ . The probability of obtaining the state is correspondingly lowered from the value  $P_1 = 0.205$  to  $P_1^{(\eta)} = 0.116$ . An analogous argument holds for the dependence of the output state  $\hat{\rho}_{out}$  on the input coherent amplitude  $\alpha$ . In Fig. 3.14b we report the conditional state obtained by choosing  $\alpha = 3.58$ , which corresponds to the same detection probability  $P_1^{(\alpha)} = 0.116$ . Obviously the above discussion on the effect of non-unit quantum efficiency and on the intensity of the input coherent state  $|\alpha\rangle$  holds also for the generation of a single Fock states.

## 3.5 Conclusion

In this chapter we have determined the optimal *a priori* probabilities for the squeezed-state and the number-state channels. We showed that the optimal fraction of squeezing photons rapidly decreases with loss, with a relative improvement of the mutual information up to 30 % at low power for  $\eta = .15$ . For total mean photon number  $N < 8$  the optimized squeezed-state channel beats the coherent-state one at any value of the loss. Using the recursive Blahut's algorithm [92], we obtained an optimized *a priori* probability that departs from the usual monotonically-decreasing thermal-like behavior, and

that, for attenuation  $\eta \lesssim .6$ , develops gaps of zero probability at intermediate numbers of photons. The sizeable improvement of the mutual information—over 70 % for high attenuation at low power—partially stems the detrimental effect of loss.

With regard to the feasibility of the squeezed-state channel, we showed the equivalence of such a channel with a heterodyne scheme characterized by an easier implementation and based on the two-mode states we introduced in Sec. 2.3. The correspondence between the two channels holds also in the presence of loss and optimal amplification.

Finally, we suggested an effective scheme, feasible with current technology, to generate optical photon-number eigenstates in a traveling wave mode. The scheme uses on-off photodetection of the field mode exiting a high-Q cavity, which, in turn, is coupled to the the traveling-wave by nonlinear Kerr interaction. The input fields for the setup are customary coherent states. After a successful photodetection, the traveling mode is found in a photon-number eigenstate, or, for high Kerr nonlinearity, in a superposition of Fock states. We have shown that non-unit quantum efficiency at photodetection improves the quality of the state synthesis, however at the expenses of the synthesizing rate.

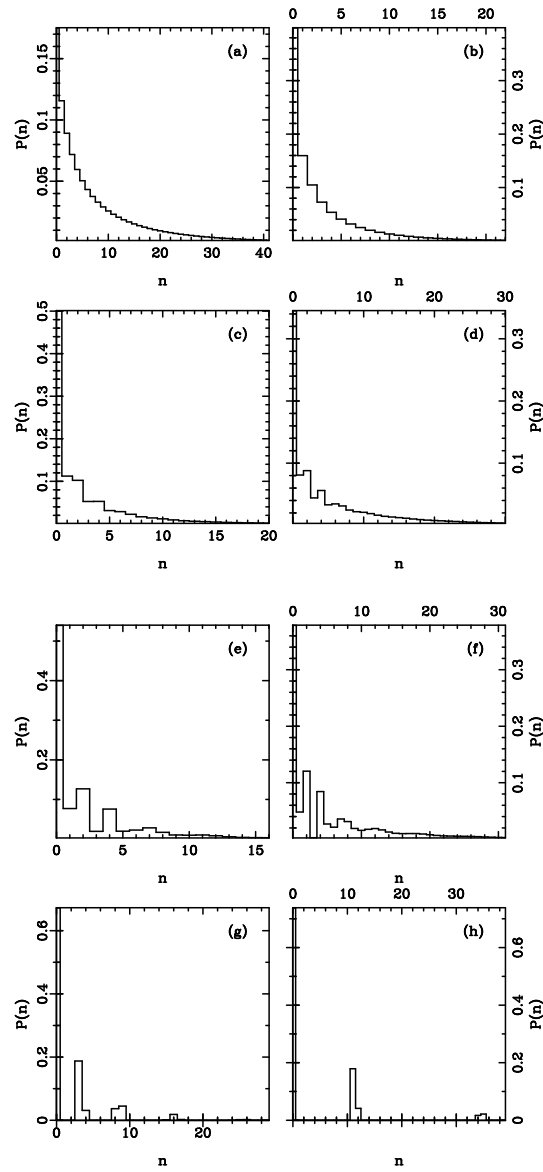


Figure 3.7: A *a priori* probability  $p(n)$  versus  $n$  for different values of the attenuation factor  $\eta$  and the average power  $N$ , optimized in the presence of loss. a)  $\eta = .9$ ,  $N = 8.575$ , b)  $\eta = .75$ ,  $N = 2.827$ , c)  $\eta = .6$ ,  $N = 2.414$ , d)  $\eta = .6$ ,  $N = 6.930$  e)  $\eta = .55$ ,  $N = 2.288$ , f)  $\eta = .55$ ,  $N = 6.729$ , g)  $\eta = .4$ ,  $N = 1.888$ , h)  $\eta = .15$ ,  $N = 4.040$  [see Table 3.1].

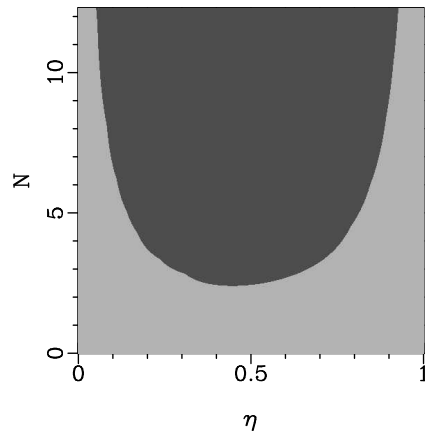


Figure 3.8: Optimality capacity diagram comparing the coherent-state with the optimized number-state channels. In the dark grey region the optimized number-state channel achieves a superior capacity, whereas in the black region it is the coherent-state channel the optimal one.

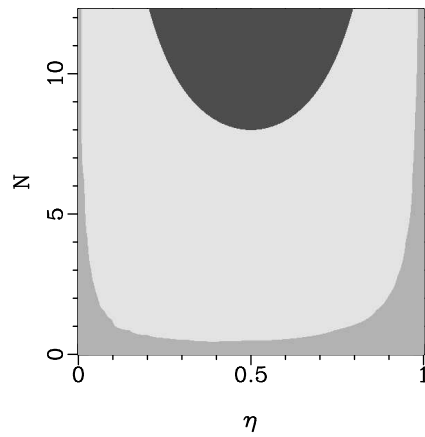


Figure 3.9: Optimality capacity diagram. In the black region the coherent-state channel has the highest capacity, in the light grey region the best channel is the optimized squeezed-state one. Finally, in the dark grey region the optimal channel is the optimized number-state one.

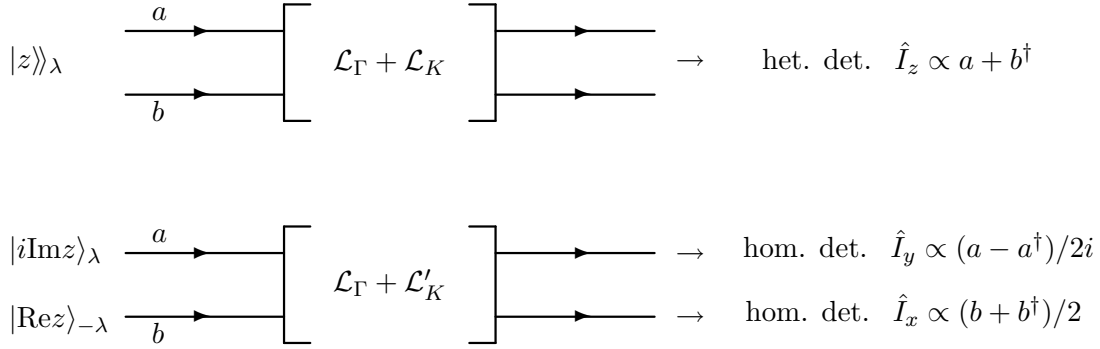


Figure 3.10: Equivalence between the channels transmitting twin-beam states  $|z\rangle\rangle_\lambda$  and couple of quadrature-squeezed states  $|i\text{Im}z\rangle_\lambda \otimes |\text{Re}z\rangle_{-\lambda}$ . The decoding measurements are the unconventional-heterodyne detection (complex photocurrent  $\hat{I}_z$ ) and two independent ordinary homodyne detections (real photocurrents  $\hat{I}_x$  and  $\hat{I}_y$ ), respectively. The superoperators  $\mathcal{L}_\Gamma$ ,  $\mathcal{L}_K$  and  $\mathcal{L}'_K$  model the loss in Eq. (3.55), the phase-insensitive amplification in Eq. (3.57) and the phase-sensitive amplification in Eq. (3.83), respectively. The equivalence between the two communication schemes is realized by the unitary transformation (3.76), namely a 50-50 frequency conversion.

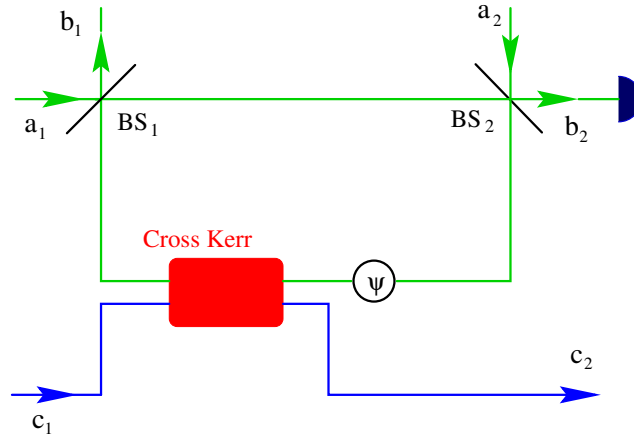


Figure 3.11: Schematic diagram of the setup for the generation of Fock states and superposition of Fock states.  $\text{BS}_1$  and  $\text{BS}_2$  denote high transmissivity beam splitters, and  $\psi$  a tunable phase shift. The cavity input modes  $a_1$  and  $a_2$  are placed in a coherent state and in the vacuum respectively. The box denotes the cross Kerr medium that couples the cavity mode  $d$  with the traveling free mode  $c_1$  which is initially prepared in a coherent state. After successful detection at the photodiode  $D$ , the output mode  $c_2$  is found in a Fock state or in a superposition of few Fock states.

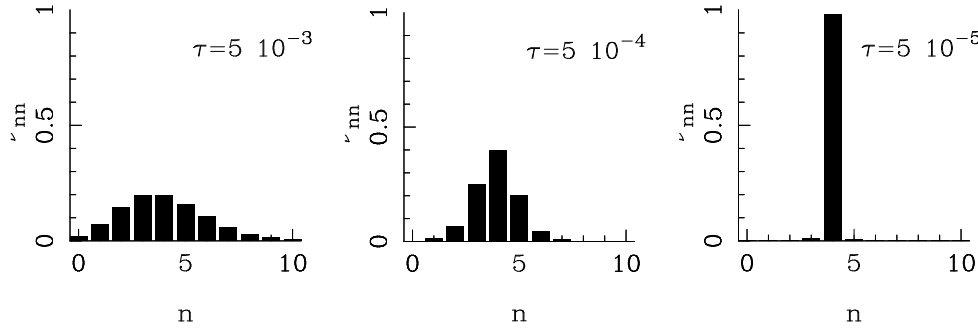


Figure 3.12: The number distribution of the conditional output state  $\hat{\nu}_{out}$  for different values of the BS transmissivity  $\tau$ , indicated on each plot. The parameters are chosen to select the number state  $|n^* \equiv 4\rangle$ , with  $\chi t = 0.01$  and  $\psi = 0.04$ . The modes  $a_1$  and  $c_1$  are both excited in a coherent state with real amplitude  $\alpha = 20$  and  $\beta = 2$ , respectively. The probabilities of obtaining the three states (i.e. the detection probability at D) are respectively  $P_1 = 0.99885$ ,  $0.4905$ ,  $0.1997$ .

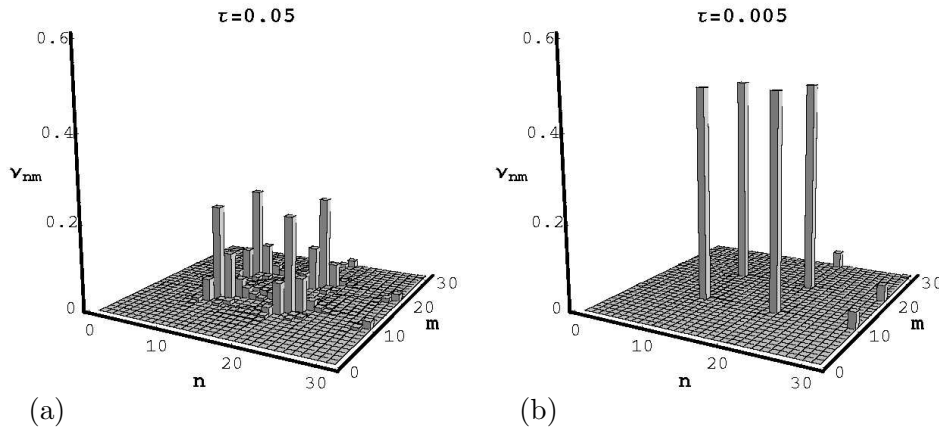


Figure 3.13: The density matrix of the conditional output state  $\hat{\nu}_{out}$  for different values of the BS transmissivity. The parameters are chosen to select the superposition  $2^{-1/2}(|10\rangle + |20\rangle)$ , that is  $\chi t = \pi/5$  and  $\psi = 0$ . The modes  $a_1$  and  $c_1$  are both excited in a coherent state with amplitude  $\alpha = 8.0$  and  $\beta = (20!/10!)^{1/20} \simeq 3.902$ , respectively. The detector has unit quantum efficiency. Notice the small components due to the Fock state  $|30\rangle$ . The probabilities of synthesizing these two states are  $P_1 = 0.205$ ,  $0.092$ , respectively.

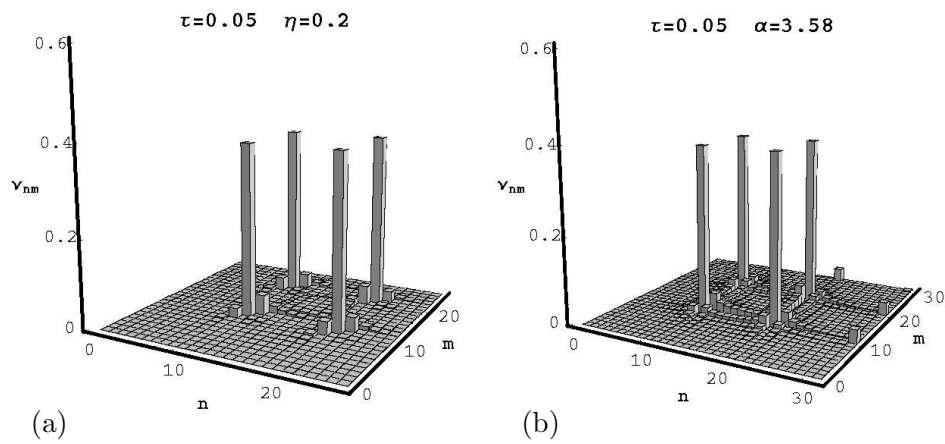


Figure 3.14: The density matrix of the conditional output state  $\hat{\nu}_{out}$  as in Fig. 3.13a. Here we show the matrix elements for lowered quantum efficiency  $\eta = 20\%$  in (a), and for lowered input amplitude  $\alpha = 3.58$  in (b). Notice, in both cases, the improvement over the state in Fig. 3.13a.



## Chapter 4

# Testing Quantum Mechanics

### 4.1 Introduction

This chapter is entirely devoted to some proposed experimental tests of Quantum Mechanics over radiation states generated by parametric processes in nonlinear media. The following tests are presented. i) An optical scheme that realizes the standard von Neumann measurement model, providing an indirect measurement of a quadrature of the field with controllable Gaussian state-reduction. Such a scheme represents an optical version of the measurement scheme for the position of a particle formulated in the last chapter of von Neumann's book [106]. ii) A novel method to generate mesoscopic quantum superpositions by *stimulated* down conversion in nonlinear  $\chi^{(2)}$  media. The scheme relies on feeding a nondegenerate parametric amplifier by a single-photon state, in a way that makes signal and idler paths indistinguishable. The amplification process is analyzed realistically by taking into account the effects of cavity losses, and the appearance of mesoscopic quantum superpositions at the output is demonstrated. iii) A homodyne detection scheme to verify Bell's inequality on correlated optical beams at the output of a nondegenerate parametric amplifier. The approach is based on tomographic measurement of the joint detection probabilities, which allows using high quantum-efficient detectors without supplementary hypotheses. iv) Finally, a test based on homodyne tomography to check the nonclassicality of quantum states even for rather low quantum efficiency. For single-mode states we check violations of inequalities involving the photon-number probability. For two-mode states we reconstruct some suitable number-operator functions. The nonclassicality test discriminates classical states from states that invalidate the Mandel's semiclassical formula of photon counting [141].

## 4.2 Optical von Neumann measurement

In the last chapter of his book [106] von Neumann formulated a measurement scheme for the position  $\hat{q}$  of a particle based on a coupling with another particle. The interaction Hamiltonian between the two particles—object and probe—is of the form  $\hat{H}_I = \hat{q}\hat{P}$ , product of the object position  $\hat{q}$  with the probe momentum  $\hat{P}$ . It is switched on with a very strong coupling and for a very short time, and immediately afterwards a measurement of the probe-particle position  $\hat{Q}$  is performed. By shifting the probe position  $\hat{Q}$  by an amount proportional to the object position  $\hat{q}$ , the coupling correlates the object position with the probe “pointer observable”  $\hat{Q}$ , through which the object position is obtained, thus leaving the particle available for a forthcoming measure.

Originally, von Neumann introduced his model in order to discuss the repeatability hypothesis suggested by the Compton-Simons experiment. After, it remained as a reference point for theoretical models of repeatable measurements, an ideal “gedanken microscope” with controllable disturbance on the system (see, for example, Refs. [69] and [107], where the von Neumann model is considered in relation to the problem of position measurements below the standard quantum limit).

Is it possible to achieve this model experimentally? As a particle Hamiltonian, the  $\hat{q}\hat{P}$  interaction is rather artificial. However, we will show that in the domain of quantum optics, one can achieve the von Neumann measurement (i.e. with the same probability distribution and the same “state-reduction”) without the need of either realizing the precise form of the von Neumann Hamiltonian, or of experimentally achieving the impulsive limit [108]. The scheme we present is made of simple optical elements, as laser sources, beam splitters, and phase sensitive amplifiers, along with a feedback mechanism that uses a Pockels cell. We will employ a “pre-amplification” of the signal state and a “pre-squeezing” of the probe state: this is the basic idea to improve the quality of a quantum measurement [109], that has already been implemented in the realm of back-action evading measurements [110, 111, 112, 113].

### 4.2.1 A feasible interaction Hamiltonian

For a single mode of the radiation field, the optical observables that correspond to particle position  $\hat{q}$  and momentum  $\hat{p}$  are represented by any two conjugated quadratures  $\hat{x}_\phi$ , and  $\hat{x}_{\phi+\pi/2}$ , with commutator  $[\hat{x}_\phi, \hat{x}_{\phi+\pi/2}] = i/2$ , the generic quadrature being defined as follows

$$\hat{x}_\phi = \frac{1}{2} \left( a^\dagger e^{i\phi} + a e^{-i\phi} \right). \quad (4.1)$$

The quadrature  $\hat{x}_\phi$  can be ideally measured by means of a homodyne detector, in the limit of strong coherent local oscillator (LO),  $\phi$  being the phase of the signal mode

relative to the LO [34]. In Eq. (4.1),  $a$  and  $a^\dagger$  are the bosonic annihilation and creation operators of the field mode of interest, with commutation  $[a, a^\dagger] = 1$ .

The standard von Neumann measurement model is based on an impulsive interaction Hamiltonian  $\hat{q}\hat{P}$  with the probe-particle prepared in a Gaussian wave packet. In the framework of repeatable measurements, according to Sec. 2.4.1, such a measurement scheme is described by the Gaussian reduction operator

$$\hat{\Omega}(q) = \left( \frac{1}{2\pi\Delta^2} \right)^{1/4} \exp \left[ -\frac{(q - \hat{q})^2}{4\Delta^2} \right]. \quad (4.2)$$

From Eqs. (2.40) and (2.41) it follows that the experimental probability density  $p(q) = \text{Tr}[\hat{\rho}\hat{\Omega}^\dagger(q)\hat{\Omega}(q)]$  is just a Gaussian convolution of the ideal probability distribution  $\langle q|\hat{\rho}|q\rangle$ , with additional r.m.s. noise given by  $\Delta$  (for interaction time  $\tau = \kappa^{-1}$  with  $\kappa$  the interaction strength,  $\Delta^2$  is simply given by the variance of the probe-particle Gaussian wave-packet).

Now we present the quantum-optical scheme that performs the standard von Neumann measurement of the quadrature  $\hat{x}_\phi$  of the radiation field in Eq. (4.1). In the following we will consider a fixed phase  $\phi$ , using the short notation  $\hat{x} = \hat{x}_\phi$ ,  $\hat{y} = \hat{x}_{\phi+\pi/2}$ . In a fully optical measurement scheme the simplest choice for a measuring probe is just another mode of the field. We consistently use capital letters for the probe operators: thus,  $\hat{A}$  and  $\hat{A}^\dagger$  will denote the annihilation and creation operators of the probe mode, whereas  $\hat{X}$  and  $\hat{Y}$  will be used to represent any couple of conjugated quadratures of the probe for fixed phase  $\phi'$ . With this notation, the optical equivalent of the standard von Neumann Hamiltonian (for indirectly measuring the quadrature  $\hat{x}$  by probing  $\hat{X}$ ) is given by

$$\hat{H} = \hat{x}\hat{Y}. \quad (4.3)$$

Notice that the choice of the phases  $\phi$  and  $\phi'$  is totally free, and is ultimately related to the definition itself of the annihilation and creation operators of the two modes. From the definition (4.1) of  $\hat{x}_\phi$  we can immediately see that, independently on the frequency of the two field modes, the Hamiltonian (4.3) cannot be realized in the rotating wave approximation, due to the counter-rotating terms  $\hat{A}\hat{a}$  and  $\hat{A}^\dagger\hat{a}^\dagger$ . On the other hand, an impulsive realization of this Hamiltonian, as in the original formulation of von Neumann, again is not feasible in the optical domain, because it would require switching the interaction faster than the optical frequency. However, as we will show in the following, we don't need to realize the Hamiltonian (4.3) in order to achieve the von Neumann measurement.

Instead of the Hamiltonian (4.3) we consider the interaction of the two field modes at a beam splitter. This is described by the unitary evolution operator

$$\hat{U} = \exp \left[ \text{atan} \sqrt{\frac{1-\eta}{\eta}} \left( \hat{a}\hat{b}^\dagger - \hat{a}^\dagger\hat{b} \right) \right]. \quad (4.4)$$

The unitary evolution operator (4.4) has no counter-rotating terms: in the following we will take both modes at the same frequency, so that the operator (4.4) will retain its time-independent form also in the interaction picture (the simple form of the operator (4.4) holds for an appropriate choice of the modal phases, which can be achieved by just changing optical path lengths). Expressed as a function of the field quadratures, the unitary operator  $\hat{U}$  reads

$$\hat{U} = \exp \left[ 2i \operatorname{atan} \sqrt{\frac{1-\eta}{\eta}} \left( \hat{y}\hat{X} - \hat{x}\hat{Y} \right) \right]. \quad (4.5)$$

The operator in Eq. (4.5) can be conveniently factorized into the product of elemental unitary evolutions by exploiting the realization of the  $su(2)$  algebra  $\hat{J}_+ \equiv 2i\hat{y}\hat{X}$ ,  $\hat{J}_- \equiv 2i\hat{x}\hat{Y}$ ,  $\hat{J}_z \equiv i(\hat{X}\hat{Y} - \hat{x}\hat{y})$ , where one can easily verify the  $su(2)$  commutation relations  $[\hat{J}_+, \hat{J}_-] = 2\hat{J}_z$ ,  $[\hat{J}_z, \hat{J}_\pm] = \pm\hat{J}_\pm$ . Using the BCH formula for the  $SU(2)$  group the operator  $\hat{U}$  can be written as follows <sup>1</sup>

$$\hat{U} = e^{2i\sqrt{\frac{1-\eta}{\eta}}\hat{y}\hat{X}} \eta^{i(\hat{x}\hat{y} - \hat{X}\hat{Y})} e^{-2i\sqrt{\frac{1-\eta}{\eta}}\hat{x}\hat{Y}}. \quad (4.6)$$

The last factor on the right of Eq. (4.6) has the same form of the von Neumann unitary evolution for Hamiltonian (4.3). The physical meaning of other two factors will become clear after evaluating the reduction operator  $\hat{\Omega}(x)$  corresponding to the unitary evolution in Eq. (4.6).

Let  $|\varphi\rangle$  be the state preparation of the probe mode before the measurement, (the state of the field mode  $A$  that enters one port of the beam splitter), and let us denote by  $|x\rangle$  the eigenvectors of the quadrature  $\hat{X}$  effectively measured at one output port of the beam splitter by means of a homodyne detector. Then,  $\hat{\Omega}(x)$  can be evaluated through the following steps

$$\begin{aligned} \hat{\Omega}(x) &= \langle x | e^{2i\sqrt{\frac{1-\eta}{\eta}}\hat{X}\hat{y}} \eta^{i(\hat{x}\hat{y} - \hat{X}\hat{Y})} e^{-2i\sqrt{\frac{1-\eta}{\eta}}\hat{x}\hat{Y}} | \varphi \rangle \\ &= e^{2i\sqrt{\frac{1-\eta}{\eta}}x\hat{y}} \eta^{i\hat{x}\hat{y}} \langle x | \eta^{-i\hat{X}\hat{Y}} e^{-2i\sqrt{\frac{1-\eta}{\eta}}\hat{x}\hat{Y}} | \varphi \rangle \\ &= e^{2i\sqrt{\frac{1-\eta}{\eta}}x\hat{y}} \eta^{i\hat{x}\hat{y}} e^{-\ln \eta^{1/2} x \partial_x} e^{-\sqrt{\frac{1-\eta}{\eta}}\hat{x}\partial_x} \varphi(x) \\ &= \hat{D}_a^\dagger \left( \sqrt{\frac{1-\eta}{\eta}} x \right) \hat{S}_a^\dagger \left( \ln \eta^{1/2} \right) \eta^{-1/4} \varphi \left[ \eta^{-1/2} \left( x - (1-\eta)^{1/2} \hat{x} \right) \right], \quad (4.7) \end{aligned}$$

where  $\hat{S}_a(r)$  and  $\hat{D}_a(\alpha)$  denote the squeezing and displacement operators of the mode  $a$ , namely

$$\hat{S}_a(r) = e^{-ir(\hat{x}\hat{y} + \hat{y}\hat{x})}, \quad \hat{D}_a(\alpha) = e^{\alpha a^\dagger - \bar{\alpha} a}, \quad (4.8)$$

---

<sup>1</sup>Notice that the fact that our realization of the  $su(2)$  algebra does not preserve hermitian conjugation is irrelevant for the group multiplication, as in the BCH formula we are actually using the complexification of the group.

and we used the quadrature differential representation

$$\langle x|f(\hat{X}, \hat{Y})|\varphi\rangle = f\left(x, -\frac{i}{2}\partial_x\right)\varphi(x); \quad \varphi(x) \equiv \langle x|\varphi\rangle. \quad (4.9)$$

The squeezing and displacement unitary operators that appear in the last step of Eq. (4.7) represent an additional back action from the measurement, i.e. they just change the state-reduction by an additional unitary evolution, but they do not change the probability operator-valued measure (POM), which for the reduction operator (4.7) is given by

$$d\hat{\mu}_\eta(x) = dx \hat{\Omega}^\dagger(x)\hat{\Omega}(x) = dx \eta^{-1/2} \left| \varphi \left[ \eta^{-1/2} \left( x - (1-\eta)^{1/2} \hat{x} \right) \right] \right|^2. \quad (4.10)$$

For very high reflectivity at the beam splitter  $\eta \rightarrow 0$  and with the probe prepared in the vacuum state  $|\varphi\rangle \equiv |0\rangle$ , Eq. (4.10) would approach the Gaussian von Neumann POM from Eqs. (2.40) and (4.2) with variance  $\Delta = \sqrt{\eta}/2$ . However, the reduction operator (4.7) is still different from that in Eq. (4.2), and in order to make them equal we need to remove the squeezing and the displacement back-action terms.

The displacement term is a unitary transformation that depends on the measurement outcome, and hence it can be compensated by an appropriate feedback device. On the other hand, the squeezing term can be balanced by an inverse squeezing transformation of the mode  $a$  performed after the displacing feedback: this will be the last transformation on the mode  $a$ , and we will refer to it as *back-squeezing*. For vanishing  $\eta$  one would need increasingly large back-squeezing, and it may be more convenient to compensate the vanishing  $\eta$  by squeezing the probe state  $|\varphi\rangle$ . In fact, squeezing transforms the quadrature  $\hat{x}$  as follows

$$\hat{x} \rightarrow \hat{S}_a^\dagger(r) \hat{x} \hat{S}_a(r) = e^r \hat{x}. \quad (4.11)$$

Hence the factor  $(1-\eta)^{1/2}$  in the POM (4.10) can be removed by *pre-squeezing* the initial state of the system with squeezing parameter  $r = -\frac{1}{2} \ln(1-\eta)$ . Such pre-squeezing modifies the reduction operator  $\hat{\Omega}(x)$  in Eq. (4.7) into the following one

$$\hat{\Omega}(x) \rightarrow \hat{\tilde{\Omega}}(x) = \eta^{-1/4} \varphi \left[ \eta^{-1/2} (x - \hat{x}) \right], \quad (4.12)$$

where now we have changed the back-squeezing as follows

$$\hat{S}_a^\dagger(\ln \eta^{1/2}) \longrightarrow \hat{S}_a^\dagger(\ln \eta^{1/2}) \hat{S}_a[\ln(1-\eta)^{-1/2}] = \hat{S}_a^\dagger \left[ \frac{1}{2} \ln(\eta(1-\eta)) \right]. \quad (4.13)$$

Then, in order to get a tunable variance for the reduction operator, one can change the state preparation  $|\varphi\rangle$  of the probe. For the squeezed vacuum

$$|\varphi\rangle = \hat{S}_A(\ln \sigma^{1/2})|0\rangle, \quad (4.14)$$

the reduction operator (4.12) becomes

$$\hat{\Omega}(x) = \left( \frac{2}{\pi\eta\sigma} \right)^{\frac{1}{4}} \exp \left[ -\frac{(x - \hat{x})^2}{\eta\sigma} \right], \quad (4.15)$$

and the operator  $\hat{\Omega}(x)$  in Eq. (4.15) is of the same form of the von Neumann one in Eq. (4.2), with  $\Delta = \sqrt{\eta\sigma}/2$ .

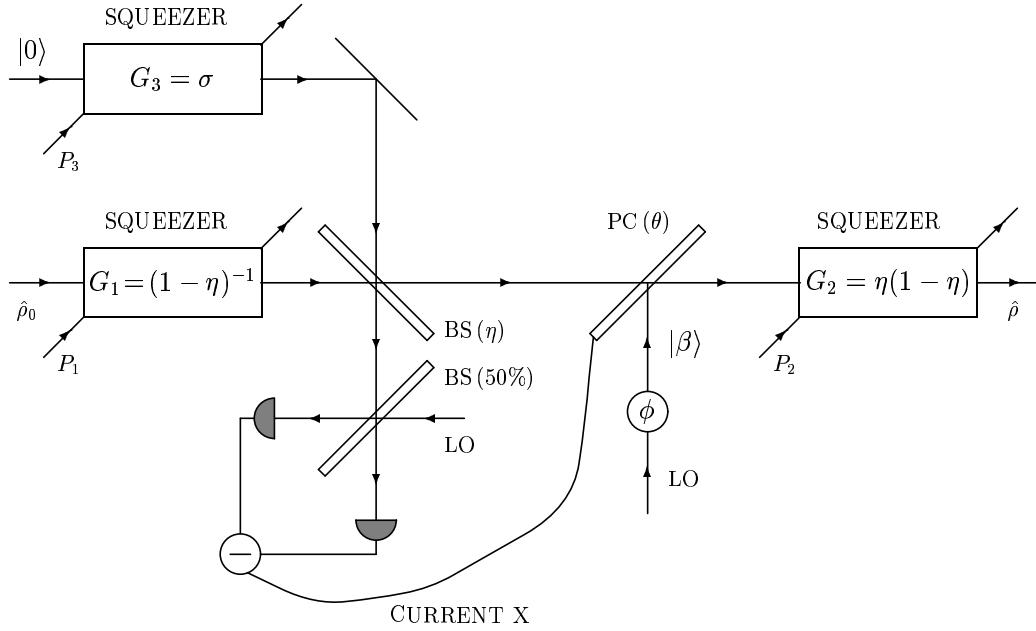


Figure 4.1: Outline of the proposed experimental setup to realize a von Neumann measurement of a quadrature of the electromagnetic field. BS denote a beam splitter;  $PC(\theta)$  denotes a Pockels cell with transmissivity  $\theta$ .

The experimental set-up to perform the optical von Neumann measurement is sketched in Fig. 4.1. The pre-squeezing and back-squeezing transformation described by the unitary operators

$$\hat{S}_a^1 \left[ -\frac{1}{2} \ln(1 - \eta) \right], \quad \hat{S}_a^2 \left[ \frac{1}{2} \ln(\eta(1 - \eta)) \right], \quad (4.16)$$

are the two extremal steps of the sequence of optical operations on the system mode. They can be accomplished by two phase-sensitive amplifiers (PSA) [114] with gains  $G_1 = (1 - \eta)^{-1}$  and  $G_2 = \eta(1 - \eta)$ , respectively. The PSA ideally amplifies the quadratures of the field with a phase-dependent gain, namely  $\hat{x}'_\phi = G^{-1/2} \hat{x}_\phi$ ,  $\hat{x}'_{\phi+\pi/2} = G^{1/2} \hat{x}_{\phi+\pi/2}$ , and it can be attained through degenerate three- or four-wave mixing. In the same way the probe state (4.14) can be achieved using a third PSA that amplifies

an input vacuum field with gain  $G_3 = \sigma$ . After the first squeezing, the state of the  $a$  mode is entangled with the squeezed vacuum state (4.14) of the  $A$  mode through the beam splitter with transmissivity  $\sqrt{\eta}$ , and at the reflected output beam the quadrature  $\hat{X}$  is homodyne detected. The displacement  $\hat{D}\left(\sqrt{\frac{1-\eta}{\eta}}x\right)$  is achieved by combining the transmitted beam with a strong coherent LO  $|\beta\rangle$  ( $\beta \rightarrow \infty$ ) in a beam splitter with a transmissivity  $\theta \rightarrow 1$ , such that  $|\beta|\sqrt{1-\theta} = \sqrt{\frac{1-\eta}{\eta}}x$ , as already shown in Sec. 1.3.1.

The parametric dependence on the homodyne outcome  $x$  is carried out by driving the LO with the homodyne photocurrent, for example by stimulating the laser that provides the LO by the photodetection current itself. However, this method is expected to fail for small “photocurrents”  $x$ , because it would bring the LO laser below threshold, thus losing the phase of  $\beta$ . A better way to achieve this feedback is to provide a current-dependent transmissivity  $\theta(x)$  for the beam-splitter, making use, for example, of a Pockels cell, and working in the linearity regime  $\theta \propto x$  of the cell. A similar feedback mechanism has been experimentally implemented in Ref. [115]. Of course, good phase coherence between the PSA pumps and the LO may be technically difficult to achieve. Finally, also notice that the quadrature phase  $\phi$  can be changed in many different ways by tuning any one of the relative phase-shifts between the pumps and the LO.

### 4.3 Amplification of entanglement

The recent developments in quantum optics and in light manipulation of atoms and ions have renewed the interest in the basic laws of quantum mechanics. In these frameworks, the two features that play a major role are the superposition principle and the existence of nonlocal correlations among separate physical systems. As a matter of fact, the phenomenon of entanglement and the generation of Schrödinger cats are at the heart of many crucial experiments [116, 117, 118], both in the realm of fundamentals and for potential applications in modern technology. Among these, we mention the developments in quantum computation [119], quantum cryptography [120], and quantum teleportation [116].

Entangled photon pairs can be produced by spontaneous down-conversion [121], and are used for many purposes, including test of Bell’s inequality and secure quantum key distribution. The same process also allows to generate entangled states with higher number of photons, and the corresponding photon distribution has been measured by means of quantum homodyne tomography [122]. A number of schemes have been also suggested with the aim of generating optical Schrödinger cats, namely superpositions of mesoscopic distinguishable states of the radiation field [123, 117, 118].

Further interest has been found in the generation of states that gather both the entanglement feature and the mesoscopic character of superpositions. In such direction,

it has been suggested in Ref. [124] a scheme for the generation of mesoscopic quantum superpositions based on quantum injection into a non-degenerate parametric amplifier operating in an entangled configuration. The above scheme have been also analyzed in details [125] in the case of parametric oscillations, i.e. when the nonlinear crystals are placed into optical cavities. This latest extension leads to a large enhancement of the number of generated photons.

In this section, we suggest a novel method to generate mesoscopic quantum superpositions, which is based on the process of stimulated down-conversion in nonlinear  $\chi^{(2)}$  crystal. The scheme maintains the original idea of Ref. [124], namely that of a quantum injection into an optical amplifier, however with two main novelties. On one hand, the dynamics of the amplifier is restricted to two modes only, which share the entanglement on two different wave vectors. This leads to the generation of a mesoscopic superposition that is quite robust against decoherence. On the other hand, the *seed* photon is injected into the crystal in a way that makes the signal and the idler paths indistinguishable. The subsequent amplification process preserves the path indistinguishability, and enhances the number of photons of the output entangled state to mesoscopic scale. In the following we describe how to generate the quantum seed through the reduction of a down-converted pair of photons by a triggering photodetector behind a polarizing filter. We then show the main features of the mesoscopic entangled superposition that results from ideal stimulated down-conversion. A feasible measurement to reveal such quantum superposition is also suggested. The amplification process is finally analyzed realistically by taking into account the effects of cavity losses, and the whole dynamics of the device is numerically studied by means of Monte Carlo simulations. The appearance of mesoscopic entangled superpositions at the output, and their robustness against decoherence are demonstrated.

### 4.3.1 Generation of the seed state

A non-degenerate optical parametric amplifier (NOPA) consists of a  $\chi^{(2)}$  nonlinear optical crystal cut for type II phase-matching. The crystal couples orthogonal polarization modes according to the effective Hamiltonian

$$\hat{H} = i\kappa \left[ (a_{\parallel}^{\dagger} b_{\perp}^{\dagger} - a_{\parallel} b_{\perp}) + (a_{\perp}^{\dagger} b_{\parallel}^{\dagger} - a_{\perp} b_{\parallel}) \right], \quad (4.17)$$

where  $\kappa$  represents the effective nonlinear coupling, and  $a$  and  $b$  denotes modes with wave vectors satisfying the phase-matching condition  $\mathbf{k}_a + \mathbf{k}_b = \mathbf{k}_p$ ,  $\mathbf{k}_p$  being the wave vector of the pump. The symbols  $\parallel$  and  $\perp$  denote an arbitrary pair of orthogonal polarizations, the Hamiltonian (4.17) being invariant with respect to a global rotation of the polarization reference.

For weak pumping and short interaction time  $\tau$ , the state exiting the NOPA by

spontaneous down conversion (SPDC) can be well approximated by

$$|\Psi\rangle = \frac{1}{\sqrt{1 + (\kappa\tau)^2}} \left\{ |0\rangle + \frac{\kappa\tau}{\sqrt{2}} [ |1\rangle_{a\parallel} |0\rangle_{a\perp} |0\rangle_{b\parallel} |1\rangle_{b\perp} + |0\rangle_{a\parallel} |1\rangle_{a\perp} |1\rangle_{b\parallel} |0\rangle_{b\perp} ] \right\}, \quad (4.18)$$

where  $|0\rangle$  denotes the vacuum state and  $|n\rangle_i$  the state with  $n$  photons in the  $i$ -th mode. The state  $|\Psi\rangle$  in Eq. (4.18) is a two-photon entangled state that shows perfect correlations between wave-vector and polarization.

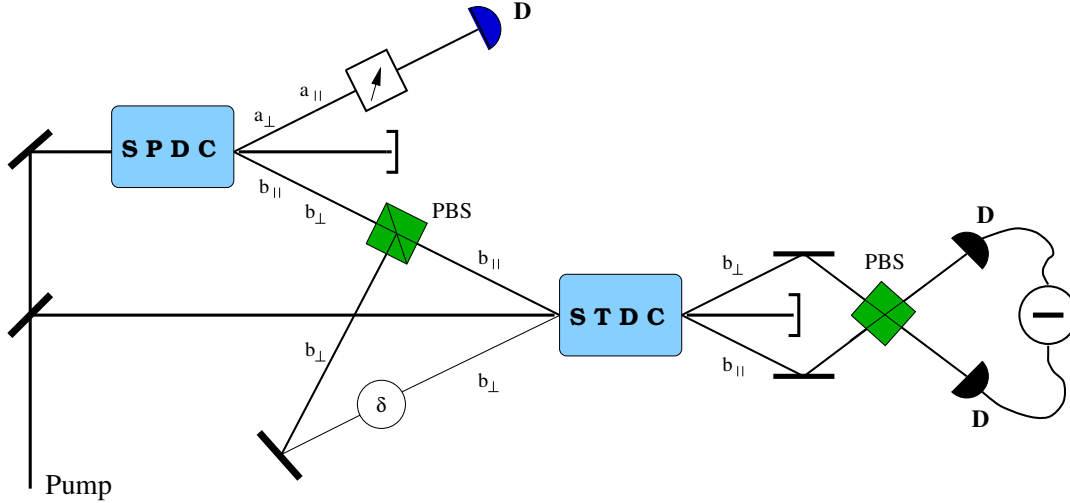


Figure 4.2: Schematic diagram of the setup for the generation of mesoscopic entangled quantum superpositions by the parametric amplification of a single photon state prepared in a way that makes signal and idler paths indistinguishable. In the first part a two-mode one-photon state is prepared by a conditional measurement on a down converted (SPDC) Bell-type state. The reduced two modes  $b$  are spatially separated by a polarizing beam splitter (PBS), and then redirected to the second crystal with the proper wave vectors to satisfy phase-matching conditions. The input state for the second crystal is thus given by  $|\Phi\rangle = \frac{1}{\sqrt{2}}(|1\rangle_{b\parallel} |0\rangle_{b\perp} + e^{i\delta} |0\rangle_{b\parallel} |1\rangle_{b\perp})$ . This quantum injection triggers a stimulated down-conversion process (STDC) which leads to the desired mesoscopic quantum superposition. Both spontaneous and stimulated down conversion takes place in non-degenerate optical amplifiers (NOPA) consisting of nonlinear  $\chi^{(2)}$  crystals cut for type II phase-matching. In the last stage of the setup the output beams from the second crystal are mixed in polarizing beam splitter (PBS) and then detected. The mean value of the difference photocurrent gives the second order correlation function  $C^{(2)}$  defined in Eq. (4.28) of the text.

Let us now consider the conditional measurement scheme depicted in the left part of Fig. 4.2. One of the down-converted beams passes through a polarization filter, and then it is detected. The filter selects the polarization in a fixed direction, say  $\perp$ , so that when a photon is revealed by detector  $D$  the state at modes  $b$  is reduced to a single photon with the orthogonal polarization, say  $\parallel$ . The same state reduction obviously happens for any other orientation of the polarization filter. After reduction,

the modes  $b$  enter a polarizing beam splitter (PBS) with axis oriented at  $45^\circ$  relative to the first analyzer. According to PBS evolution, orthogonal polarization components are spatially separated, and the resulting state can be written

$$|\Phi\rangle = \frac{1}{\sqrt{2}} \left\{ |1\rangle_{b\parallel} |0\rangle_{b\perp} + e^{i\delta} |0\rangle_{b\parallel} |1\rangle_{b\perp} \right\}, \quad (4.19)$$

where  $\delta$  is a tunable phase-shift which results from the difference in the optical paths of the two modes. Notice that the state in Eq. (4.19) is not an entangled state in a strict sense [126]. Actually, it describes just a single-photon state with polarization rotated by  $45^\circ$ . However, the main point of our scheme is that the PBS scatters the photon in two directions (depending on polarization  $\parallel$  and  $\perp$ ) with equal probability amplitude, thus making the two possible paths of the photon indistinguishable. As we will show in the following, such path indistinguishability plays the role of a *quantum seed*, which makes the parametric amplification of the state (4.19) a novel source of mesoscopic entangled quantum superpositions.

### 4.3.2 From path indistinguishability to mesoscopic entanglement

Here we analyze the parametric amplification which takes place in the second crystal of our scheme (see Fig. 4.2). For this crystal the input signal is not the e.m. vacuum but the single-photon state of Eq. (4.19). Therefore, we are dealing with a kind of *stimulated* down-conversion process.

After the polarizing beam splitter, the two polarization modes in the state (4.19) have been spatially separated, and can be directed to the second crystal with the proper wave vectors in order to satisfy phase-matching conditions. In such a way, the dynamics in the second crystal only involves modes  $b_{\parallel}$  and  $b_{\perp}$ , according to the following interaction Hamiltonian

$$\hat{H}_I = i\kappa(b_{\parallel}^{\dagger}b_{\perp}^{\dagger} - b_{\parallel}b_{\perp}). \quad (4.20)$$

The use of the polarizing beam splitter before the second crystal is a relevant point of our scheme. On one hand, it allows to restrict the NOPA dynamics to two modes only, on the other hand, it is the key ingredient to make the two paths for the photon indistinguishable, thus leading to the initial quantum seed described in Eq. (4.19). Notice that in the original scheme of Refs. [124, 125] all the four modes of Hamiltonian (4.17) are involved in the amplification stage. Such four-mode entanglement is in principle very interesting, however the presence of many modes makes the effect of losses more detrimental, thus leading to a more stringent decoherence. For this reason we believe that our scheme should be more effective in generating mesoscopic quantum superpositions.

The amplifier described by Hamiltonian (4.20) is characterized by the gain  $\mathcal{G}$ , which is given by  $\mathcal{G} = \cosh^2(\kappa\tau)$ ,  $\tau$  being the interaction time. In the case of ideal amplification

(no losses), the state at the output writes

$$|\Phi_{OUT}\rangle = \frac{1}{\sqrt{2\mathcal{G}}} \sum_{n=0}^{\infty} \left(\frac{\mathcal{G}-1}{\mathcal{G}}\right)^{n/2} \sqrt{1+n} \left\{ |n+1\rangle_{\parallel} |n\rangle_{\perp} + e^{i\delta} |n\rangle_{\parallel} |n+1\rangle_{\perp} \right\}. \quad (4.21)$$

The state in Eq. (4.21) describes two highly correlated and spatially separated beams. For large enough gain it represents a kind of mesoscopic entangled quantum superposition, whose mean photon number is given by

$$\langle \Phi_{OUT} | b_{\perp}^{\dagger} b_{\perp} + b_{\parallel}^{\dagger} b_{\parallel} | \Phi_{OUT} \rangle = 4\mathcal{G} - 3. \quad (4.22)$$

We now evaluate the two-mode Wigner function, which is defined as follows

$$\begin{aligned} W(x_1, y_1; x_2, y_2) &= \int_{\mathbb{R}} d\mu_1 \int_{\mathbb{R}} d\nu_1 \int_{\mathbb{R}} d\mu_2 \int_{\mathbb{R}} d\nu_2 e^{2i(\nu_1 x_1 - \mu_1 y_1 + \nu_2 x_2 - \mu_2 y_2)} \times \\ &\times \text{Tr} \left\{ \hat{\rho} \hat{D}_{b_{\perp}}(\mu_1 + i\nu_1) \hat{D}_{b_{\parallel}}(\mu_2 + i\nu_2) \right\}. \end{aligned} \quad (4.23)$$

In Eq. (4.23) the variables  $(x_1, y_1)$  and  $(x_2, y_2)$  pertain to modes  $b_{\perp}$  and  $b_{\parallel}$  respectively, and  $\hat{D}_{b_j}(z) = \exp[zb_j^{\dagger} - \bar{z}b_j]$  denotes the displacement operator for mode  $b_j$ ,  $j = \parallel, \perp$ . For  $\hat{\rho} = |\Phi_{OUT}\rangle\langle\Phi_{OUT}|$  one obtains

$$\begin{aligned} W_{\tau}(x_1, y_1; x_2, y_2) &= \\ &\frac{8}{\pi^2} \exp \left[ - (4\mathcal{G} - 2) (x_1^2 + x_2^2 + y_1^2 + y_2^2) - 8\sqrt{\mathcal{G}(\mathcal{G} - 1)} (X_1 x_2 + Y_1 y_2) \right] \\ &\times \left[ e^{-2\kappa\tau} (X_1 - x_2)^2 + e^{-2\kappa\tau} (Y_1 - y_2)^2 - \frac{1}{2} \right], \end{aligned} \quad (4.24)$$

where

$$\begin{cases} X_1 = x_1 \cos \delta + y_1 \sin \delta \\ Y_1 = -x_1 \sin \delta + y_1 \cos \delta \end{cases} \quad (4.25)$$

As it can be easily checked, the Wigner function in Eq. (4.24) shows negative values in a sizeable region of the phase space, thus revealing the genuine nonclassical nature of the state resulting from stimulated down-conversion.

The high degree of entanglement of  $|\Phi_{OUT}\rangle$  is easily revealed also by the two-mode photon number distribution, which, for any value of the phase-shift  $\delta$ , reads as follows

$$\begin{aligned} P(n, m) &= \left| \langle n |_{\perp} \langle m | \Phi_{OUT} \rangle \right|^2 \\ &= \frac{1}{2\mathcal{G}^2} \left(\frac{\mathcal{G}-1}{\mathcal{G}}\right)^{n-1} \left[ n \delta_{m, n-1} + (n+1) \frac{\mathcal{G}-1}{\mathcal{G}} \delta_{m, n+1} \right], \end{aligned} \quad (4.26)$$

where  $\delta_{kl}$  denotes Kronecker delta. The two-mode number probability  $P(n, m)$  is reported in Fig. 4.3 for two different values of the gain  $\mathcal{G}$ . The high degree of correlations in  $P(n, m)$  is apparent. Notice that the location of the peaks linearly increases with the gain  $\mathcal{G}$ .

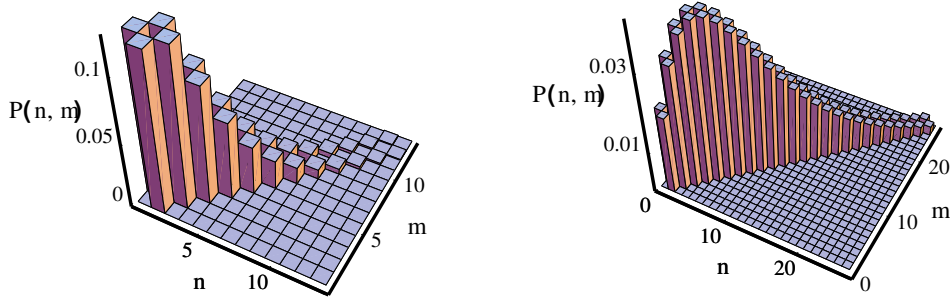


Figure 4.3: The two-mode photon distribution  $P(n, m)$  for two different values of the gain  $\mathcal{G}$ ,  $\mathcal{G} = 2$  on the left and  $\mathcal{G} = 5$  on the right.

It should be emphasized that the distributions in Fig. 4.3 are very different from the corresponding distribution of the so-called twin-beam state

$$|\Phi_{TWB}\rangle = \frac{1}{\sqrt{\mathcal{G}}} \sum_{n=0}^{\infty} \left(\frac{\mathcal{G}-1}{\mathcal{G}}\right)^{n/2} |n\rangle_{\parallel} |n\rangle_{\perp}, \quad (4.27)$$

which results from spontaneous down-conversion. In the case of twin-beam the photon number probability  $P(n, m)$  is just a two-mode thermal distribution  $P(n, m) = \delta_{m,n} \mathcal{G}^{-1-n} (\mathcal{G}-1)^n$ , and the quantum correlation involves only the photon number fluctuations, which are amplified by down-conversion process. Actually, the Wigner function of the twin-beam (i.e. the output state without the quantum injection) is positive over the whole phase space.

As a feasible measurement to check the generation of the mesoscopic superposition  $|\Phi_{OUT}\rangle$  we suggest the detection of the second order correlation function

$$C^{(2)} = \text{Tr} \left\{ \hat{\rho} \left( b_{\parallel}^{\dagger} b_{\perp} + b_{\parallel} b_{\perp}^{\dagger} \right) \right\}. \quad (4.28)$$

which can be accomplished by the following interference experiment. The output beams from the amplifier should be mixed in a further polarizing beam splitter, and then the difference photocurrent is detected, as in customary homodyne detection scheme (see Fig. 4.2). Using Eq. (4.21) it results

$$\langle \Phi_{OUT} | b_{\parallel}^{\dagger} b_{\perp} + b_{\parallel} b_{\perp}^{\dagger} | \Phi_{OUT} \rangle = \frac{1}{2} (8\mathcal{G} - 5) \cos \delta, \quad (4.29)$$

that is, one has interference fringes with amplitude and modulation that depend on the amplification gain and on the optical paths of the input beams, respectively. It is worth noticing that without quantum injection, i.e. for the twin-beam there is no interference effect, we have

$$\langle \Phi_{TWB} | b_{\parallel}^{\dagger} b_{\perp} + b_{\parallel} b_{\perp}^{\dagger} | \Phi_{TWB} \rangle = 0. \quad (4.30)$$

We also point out that the measurement of  $C^{(2)}$  is not a kind of coincidence detection. The effect of nonunit quantum efficiency of the photodetectors is simply a rescaling and no post-selection strategy is involved.

### 4.3.3 Dynamics of the stimulated down-conversion process

We have analyzed the stimulated down-conversion process in the ideal case of perfect amplification, namely without taking into account the effects of losses. Here, we consider a more realistic situation and study whether the state  $|\Phi_{OUT}\rangle$  of Eq. (4.21) can be actually approached when losses unavoidably introduce decoherence effects.

The realistic amplification process is described in terms of the two-mode Master equation

$$\frac{d\hat{\rho}_t}{dt} \equiv \mathcal{L}\hat{\rho}_t = -i[\hat{H}_I, \hat{\rho}_t] + \Gamma(L[b_\perp]\hat{\rho}_t + L[b_\parallel]\hat{\rho}_t), \quad (4.31)$$

where  $\hat{\rho}_t \equiv \hat{\rho}(t)$ ,  $\hat{H}_I$  is the interaction Hamiltonian given in Eq. (4.20),  $\Gamma$  denotes the damping rate of the optical cavity, and  $L[\hat{O}]$  is the Lindblad superoperator

$$L[\hat{O}]\hat{\rho}_t = \hat{O}\hat{\rho}_t\hat{O}^\dagger - \frac{1}{2}\hat{O}^\dagger\hat{O}\hat{\rho}_t - \frac{1}{2}\hat{\rho}_t\hat{O}^\dagger\hat{O},$$

which describes cavity losses.

The Hamiltonian  $\hat{H}_I$  in the Master equation (4.31) strongly correlates the two modes. Thus, in principle, we are in presence of a quite complicated dynamics. However, notice that the unitary transformation

$$\hat{V} = \exp\left\{\frac{\pi}{4}\left(b_\perp^\dagger b_\parallel - b_\perp b_\parallel^\dagger\right)\right\} \quad (4.32)$$

“disentangles” the Hamiltonian  $\hat{H}_I$  in two squeezing Hamiltonians for the two modes respectively, in formula

$$\hat{V}\hat{H}_I\hat{V}^\dagger = \frac{i\kappa}{2}\left(b_\perp^{\dagger 2} - b_\perp^2\right) - \frac{i\kappa}{2}\left(b_\parallel^{\dagger 2} - b_\parallel^2\right). \quad (4.33)$$

At the same time, the sum of the Lindblad terms is left unchanged by the transformation (4.32), namely

$$\hat{V}\{L[b_\perp] + L[b_\parallel]\}\hat{V}^\dagger = L\left[\frac{b_\perp - b_\parallel}{\sqrt{2}}\right] + L\left[\frac{b_\parallel + b_\perp}{\sqrt{2}}\right] = L[b_\perp] + L[b_\parallel]. \quad (4.34)$$

Therefore, the solution  $\hat{\rho}_t$  of Eq. (4.31) can be written as

$$\hat{\rho}_t = \hat{V}^\dagger \hat{\rho}'_t \hat{V}, \quad (4.35)$$

$\hat{\rho}'_t$  being the solution of the “disentangled” Master equation

$$\frac{d\hat{\rho}'_t}{dt} = \left(\mathcal{L}_{b_\perp} + \mathcal{L}_{b_\parallel}\right) \hat{\rho}'_t = \frac{\kappa}{2}\left[b_\perp^{\dagger 2} - b_\perp^2, \hat{\rho}'_t\right] + \Gamma L[b_\perp]\hat{\rho}'_t - \frac{\kappa}{2}\left[b_\parallel^{\dagger 2} - b_\parallel^2, \hat{\rho}'_t\right] + \Gamma L[b_\parallel]\hat{\rho}'_t \quad (4.36)$$

The master equation (4.36) can be transformed into a Fokker-Planck equation for the two-mode Wigner function  $W'_t(x_1, y_1; x_2, y_2)$ . Using the differential representation of

the superoperators in (4.36) the corresponding Fokker-Planck equation reads as follows

$$\begin{aligned} \partial_\tau W'_\tau(x_1, y_1; x_2, y_2) = & \left[ \frac{1}{8} (\partial_{x_1 x_1}^2 + \partial_{y_1 y_1}^2 + \partial_{x_2 x_2}^2 + \partial_{y_2 y_2}^2) + \right. \\ & \left. + \gamma_+ (\partial_{x_1} x_1 + \partial_{y_2} y_2) + \gamma_- (\partial_{x_2} x_2 + \partial_{y_1} y_1) \right] W'_\tau(x_1, y_1; x_2, y_2), \end{aligned} \quad (4.37)$$

where  $\tau$  denotes the rescaled time  $\tau = \Gamma t$ , and the drift terms  $\gamma_+$  and  $\gamma_-$  are given by

$$\gamma_+ = \frac{1}{2} \left( 1 + \frac{2\kappa}{\Gamma} \right), \quad \gamma_- = \frac{1}{2} \left( 1 - \frac{2\kappa}{\Gamma} \right). \quad (4.38)$$

The solution of Eq. (4.37) can be written as

$$\begin{aligned} W'_\tau(x_1, y_1; x_2, y_2) = & \int_{\mathbb{R}} dx'_1 \int_{\mathbb{R}} dx'_2 \int_{\mathbb{R}} dy'_1 \int_{\mathbb{R}} dy'_2 W'_0(x'_1, y'_1; x'_2, y'_2) \times \\ & \times G_\tau(x_1|x'_1) G_\tau(x_2|x'_2) G_\tau(y_1|y'_1) G_\tau(y_2|y'_2), \end{aligned} \quad (4.39)$$

where  $W'_0(x_1, y_1; x_2, y_2)$  is the Wigner function at  $\tau = 0$ , and the Green functions  $G_\tau(x_j|x'_j)$  are given by

$$G_\tau(x_j|x'_j) = \frac{1}{\sqrt{2\pi\sigma_j^2}} \exp \left[ -\frac{(x_j - x'_j e^{-\frac{1}{2}\gamma_j\tau})^2}{2\sigma_j^2} \right], \quad \sigma_j^2 = \frac{1}{4\gamma_j} (1 - e^{-\gamma_j\tau}). \quad (4.40)$$

Remarkably, the diffusion coefficients  $\sigma_j^2$  remains positive for all times, both below ( $2\kappa < \Gamma$ ) and above ( $2\kappa > \Gamma$ ) threshold. However, from the physical point of view, Eq. (4.37) provides a good description of the amplifier above threshold only for short times, namely when saturation effects can be neglected.

Of course, Eq. (4.37) admits a stationary solution only below threshold: such a solution can be easily derived from Eqs. (4.38-4.39) and, independently on the initial state, has the Gaussian form

$$W'_{\text{stat}}(x_1, y_1; x_2, y_2) = \frac{16\gamma_+\gamma_-}{\pi} \exp \left[ -4\gamma_+(x_1^2 + y_2^2) - 4\gamma_-(x_2^2 + y_1^2) \right], \quad (4.41)$$

corresponding to the (factorized) squeezed thermal density matrix given by

$$\hat{\rho}'_{\text{stat}} = \left[ S_\perp(r) \hat{\nu}_{\perp\bar{N}} S_\perp^\dagger(r) \right] \otimes \left[ S_\parallel(-r) \hat{\nu}_{\parallel\bar{N}} S_\parallel^\dagger(-r) \right]. \quad (4.42)$$

In Eq. (4.42)  $\hat{S}_j(r) = \exp[\frac{r}{2}(b_j^{\dagger 2} - b_j^2)]$  denotes the squeezing operator for mode  $b_j$ ,  $j = \parallel, \perp$ , whereas  $\hat{\nu}_{j\bar{N}}$  is the density matrix of a thermal state with  $\bar{N}$  thermal photons

$$\hat{\nu}_{j\bar{N}} = \frac{1}{1 + \bar{N}} \left( \frac{\bar{N}}{1 + \bar{N}} \right)^{b_j^\dagger b_j}. \quad (4.43)$$

Both the squeezing parameter  $r$  and the thermal photon number  $\bar{N}$  in Eq. (4.42) only depend on the ratio between  $2\kappa$  and  $\Gamma$ , in formula

$$r = \frac{1}{4} \log \frac{\gamma_+}{\gamma_-} \quad 2\bar{N} + 1 = \frac{1}{2} \frac{1}{\sqrt{\gamma_+ \gamma_-}}. \quad (4.44)$$

The stationary solution  $\hat{\rho}_{stat}$  for the original Master equation (4.31) can be obtained through Eq. (4.33), and it is given by

$$\hat{\rho}_{stat} = \exp \left[ 2r(b_{\perp}^{\dagger} b_{\parallel}^{\dagger} - b_{\perp} b_{\parallel}) \right] \left[ \hat{\nu}_{\perp \bar{N}} \otimes \hat{\nu}_{\parallel \bar{N}} \right] \exp \left[ -2r(b_{\perp}^{\dagger} b_{\parallel}^{\dagger} - b_{\perp} b_{\parallel}) \right]. \quad (4.45)$$

Let us now consider the more interesting case of amplification above threshold. The Wigner function  $W_{\tau}(x_1, y_1; x_2, y_2)$  corresponding to the evolved density matrix  $\hat{\rho}_{\tau}$  can be obtained from  $W'_{\tau}(x_1, y_1; x_2, y_2)$  by noticing that the unitary transformation  $\hat{V}$  in (4.32) just corresponds, at all times, to a rotation in the four-dimensional space for the Wigner function, more explicitly

$$W_{\tau}(x_1, y_1; x_2, y_2) = W'_{\tau} \left( \frac{x_1 + x_2}{\sqrt{2}}, \frac{y_1 + y_2}{\sqrt{2}}; \frac{x_2 - x_1}{\sqrt{2}}, \frac{y_2 - y_1}{\sqrt{2}} \right). \quad (4.46)$$

The recipe to solve the dynamics of the amplifier is thus the following: starting from the Wigner function  $W_0(x_1, y_1; x_2, y_2)$  of the initial state one evaluates  $W'_0(x_1, y_1; x_2, y_2)$  by the inverse rotation of that of Eq. (4.46), namely

$$W'_0(x_1, y_1; x_2, y_2) = W_0 \left( \frac{x_1 - x_2}{\sqrt{2}}, \frac{y_1 - y_2}{\sqrt{2}}; \frac{x_2 + x_1}{\sqrt{2}}, \frac{y_2 + y_1}{\sqrt{2}} \right). \quad (4.47)$$

Then, one makes  $W'_0(x_1, y_1; x_2, y_2)$  evolve according to Eq. (4.39), and finally recovers  $W_{\tau}(x_1, y_1; x_2, y_2)$  by means of Eq. (4.46). Following this recipe we have numerically simulated the whole evolution, starting from the Wigner function of the state (4.19), namely

$$W_0(x_1, y_1; x_2, y_2) = \frac{8}{\pi^2} \exp \left[ -2(x_1^2 + x_2^2 + y_1^2 + y_2^2) \right] \times \left[ (x_1 \cos \delta + y_1 \sin \delta - x_2)^2 + (y_1 \cos \delta - x_1 \sin \delta - y_2)^2 - \frac{1}{2} \right]. \quad (4.48)$$

The input state is nonclassical and exhibits negative values in the Wigner function. Anyhow, the Green evolution can be performed by standard Monte Carlo techniques, by evolving separately the positive and negative parts of the Wigner function, which are not mixed by the Fokker-Planck equation (4.37).

In Fig. 4.4 we report the two-mode number probability  $P(n, m)$  for two different values of the ratio between gain and loss parameters  $2\kappa/\Gamma$  and for  $\delta = 0$ . Both plots refer to amplification above threshold, where the effectiveness of the process is apparent. We have chosen short interaction times, in order to make saturation effects negligible. Notice that the main effect of losses is the appearance of further subdiagonal terms,

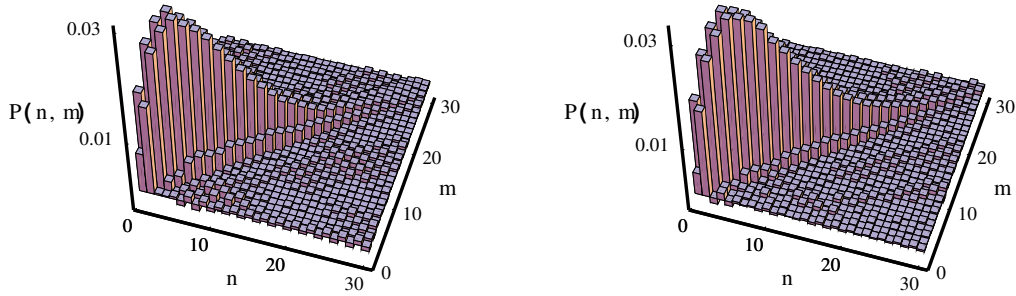


Figure 4.4: The two-mode photon distribution  $P(n, m)$  for  $\delta = 0$  and for  $2\kappa/\Gamma = 30$  (top) and  $2\kappa/\Gamma = 50$  (bottom). The corresponding interaction time is given by  $\tau = 0.1$  and  $\tau = 0.06$  respectively. We report two views for each distribution. Though the effective gain  $\frac{2\kappa}{\Gamma}\tau$  is the same for both cases the amplification process is more effective well above threshold. In comparison with the ideal case of Fig. 4.3 the main effect of losses is the appearance of subdiagonal terms, however without affecting the high correlation between the modes.

however without affecting the high correlation between the modes. On the other hand, the amplification below threshold cannot stem the detrimental effect of losses, and the field state rapidly approaches the thermal-squeezed state of Eq. (4.42).

By varying the optical path of the input beams, namely the value of  $\delta$  we have also evaluated the correlation function  $C^{(2)}$  defined in Eq. (4.28). In Fig. 4.5 we report  $C^{(2)}$  for different values of the effective gain  $\frac{2\kappa}{\Gamma}\tau$ . By inspecting the dependence of  $C^{(2)}$  on the phase-shift  $\delta$  in Fig. 4.5 one immediately argues that in a wide range of working regimes the effects of losses does not wash out interference fringes.

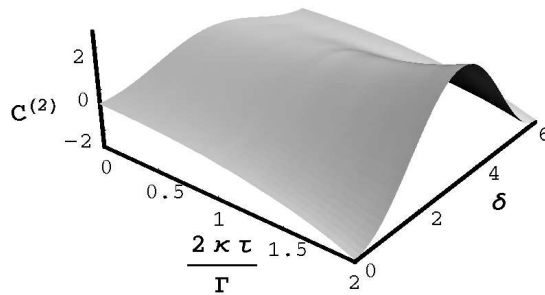


Figure 4.5: The correlation function  $C^{(2)}$  as a function of the ratio  $2\kappa\tau/\Gamma$  and the phase-shift  $\delta$ . Compare Eq. (4.29) for the lossless case.

## 4.4 Tomographic test of Bell's inequality

In 1935 Einstein, Podolsky and Rosen [127] proved the incompatibility among three hypotheses: 1) quantum mechanics is correct; 2) quantum mechanics is complete; 3) the following criterion of local reality holds: “If, without in any way disturbing a system, we can predict with certainty [...] the value of a physical quantity, then there exists an element of physical reality corresponding to this quantity.” The paper opened a long and as yet unsettled debate about which one of the three hypotheses should be discarded. While Einstein suggested to abandon the completeness of quantum mechanics, Bohr [128] refused the criterion of reality. The most important step forward in this debate was Bell's theorem of 1965 [129], which proved that there is an intrinsic incompatibility between the assumptions 1) and 3), namely the correctness of quantum mechanics and Einstein's “criterion of reality”. In Bell's approach, a source produces a pair of correlated particles, which travel along opposite directions and impinge into two detectors. The two detectors measure two dichotomic observables  $A(\alpha)$  and  $B(\beta)$  respectively,  $\alpha$  and  $\beta$  denoting experimental parameters which can be varied over different trials, typically the polarization/spin angle of detection at each apparatus. Assuming that each measurement outcome is determined by the experimental parameters  $\alpha$  and  $\beta$  and by an “element of reality” or “hidden variable”  $\lambda$ , Bell proved an inequality which holds for any theory that satisfies Einstein's “criterion of reality”, while it is violated by quantum mechanics. Such a fundamental inequality, which allows an experimental discrimination between local hidden-variable theories and quantum mechanics, has been the focus of interest in a number of experimental works [130].

Unfortunately, Bell's proof is based on two conditions which are difficult to achieve experimentally. The first is the feasibility of an experimental configuration yielding perfect correlation; the second is the possibility of approaching an ideal measurement, which itself does not add randomness to the outcome. Since 1969, attention was focused on improving the correlation of the source on one hand, and, on the other, on deriving more general inequalities that take into account detection quantum efficiency or circumvent the problem, however, at the cost of introducing supplementary hypotheses (see Refs. [131]), as the well known “fair sampling” assumption. Anyhow it was clear also to the authors of the same Refs. [131] that these assumptions are questionable, and, as a matter of fact, it was proved [132] that in all performed experimental checks the results can be reproduced in the context of Einstein's assumptions if quantum efficiency of detectors is less than 82.3%.

In a typical experiment the source emits a pair of correlated photons and two detectors separately check the presence of the two photons after polarizing filters at angles  $\alpha$  and  $\beta$ , respectively. Alternatively, one can use four photodetectors with polarizing beam splitters in front, with the advantage of checking through coincidence counts

that photons come in pairs. Let us denote by  $p_{\alpha,\beta}$  the joint probability of finding one photon at each detector with polarization angle  $\alpha$  and  $\beta$ , respectively. In terms of the correlation function

$$C(\alpha, \beta) = p_{\alpha,\beta} + p_{\bar{\alpha},\bar{\beta}} - p_{\bar{\alpha},\beta} - p_{\alpha,\bar{\beta}}, \quad (4.49)$$

Bell's inequality [129] writes as follows

$$B(\alpha, \beta, \alpha', \beta') \doteq |C(\alpha, \beta) - C(\alpha, \beta')| + |C(\alpha', \beta') + C(\alpha', \beta)| \leq 2, \quad (4.50)$$

$\bar{\alpha}$  and  $\bar{\beta}$  being the polarization angles orthogonal to  $\alpha$  and  $\beta$  respectively. In this section we propose a new kind of test for Bell's inequality based on quantum homodyne tomography [133, 134] (for a review see Ref. [135]). In our set-up the photodetectors are replaced by homodyne detectors, which along with the tomographic technique can be regarded as a black box for measuring the joint probabilities  $p_{\alpha,\beta}$  [136, 137]. The main advantage of the tomographic test is that it allows using linear photodiodes with quantum efficiency  $\eta$  higher than 90% [138]. On the other hand, the method works effectively even with  $\eta$  as low as 70%, without the need of a "fair sampling" assumption, since all data are collected in a single experimental run. With respect to the customary homodyne technique, which in the present case would need many beam splitters and local oscillators (LO) that are coherent with each other, the set-up is greatly simplified by using the recent self-homodyne technique [122].

#### 4.4.1 The experimental set-up

The apparatus for generating the correlated beams is a  $\chi^{(2)}$  nonlinear crystal, cut for Type-II phase-matching, acting as a nondegenerate optical parametric amplifier (NOPA), as already introduced in the previous section. The NOPA is injected with excited coherent states (see Fig. 4.6) in modes  $c_{\leftrightarrow}, c_{\uparrow}, d_{\leftrightarrow}, d_{\uparrow}$  all with equal intensities and at the same frequency  $\omega_0$ ,  $c$  and  $d$  denoting mode operators for the two different wave-vector directions, and  $\uparrow$  and  $\leftrightarrow$  representing vertical and horizontal polarization, respectively. The NOPA is pumped at the second harmonic  $2\omega_0$ .

At the output of the amplifier four photodetectors separately measure the intensities  $\hat{I}_{a_{\uparrow}}, \hat{I}_{b_{\leftrightarrow}}, \hat{I}_{a_{\leftrightarrow}}, \hat{I}_{b_{\uparrow}}$  of the mutual orthogonal polarization components of the fields propagating at different wave vectors. A narrow band of the photocurrent is selected, centered around frequency  $\Omega \ll \omega_0$  (typically  $\omega_0$  is optical/infrared, whereas  $\Omega$  is a radio frequency). In the process of direct detection, the central modes  $c_{\uparrow,\leftrightarrow}$  and  $d_{\uparrow,\leftrightarrow}$  beat with  $\omega_0 \pm \Omega$  sidebands, thus playing the role of the local oscillator of homodyne detectors. The four photocurrents  $\hat{I}_{a_{\uparrow}}, \hat{I}_{b_{\leftrightarrow}}, \hat{I}_{a_{\leftrightarrow}}, \hat{I}_{b_{\uparrow}}$  yield the value of the quadratures of the four modes [122]

$$s_{\pi} = \frac{1}{\sqrt{2}} \left( a_{\pi(+)} + a_{\pi(-)} \right), \quad s = \{a, b\}, \quad \pi = \{\leftrightarrow, \uparrow\}, \quad (4.51)$$

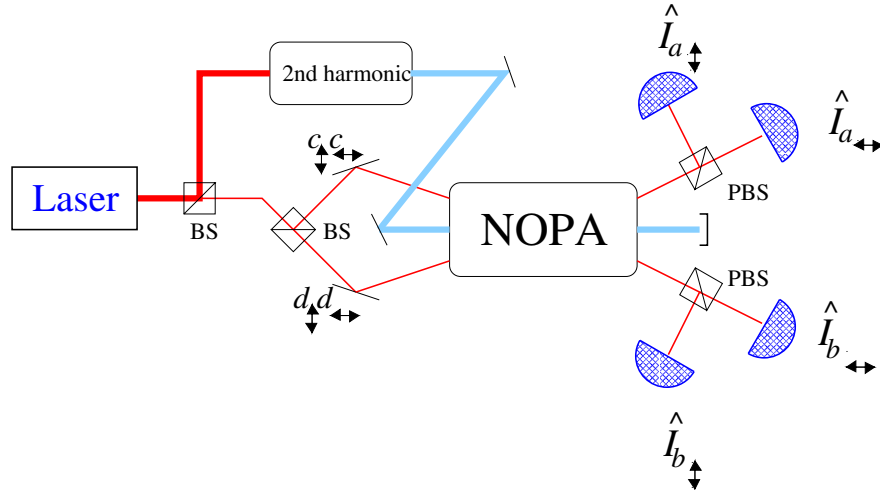


Figure 4.6: Experimental set-up for the tomographic test of Bell's inequality. PBS and BS denote 'polarizing beam splitter' and 'conventional beam splitter' respectively. Input radiation modes  $a_{\uparrow}$ ,  $b_{\leftrightarrow}$ ,  $a_{\leftrightarrow}$  and  $b_{\uparrow}$  are in the vacuum state, while modes  $c_{\uparrow}$ ,  $c_{\leftrightarrow}$ ,  $d_{\uparrow}$ ,  $d_{\leftrightarrow}$  (at laser frequency  $\omega_0$ ) are in a coherent state. At the output of the nondegenerate parametric amplifier (NOPA) the four photocurrents  $\hat{I}$  at radiofrequency  $\Omega$  are measured, yielding the value of quadratures of the field modes  $a_{\uparrow}$ ,  $b_{\leftrightarrow}$ ,  $a_{\leftrightarrow}$  and  $b_{\uparrow}$ . The outcome quadratures are then used to reconstruct the probabilities of interest through quantum tomography.

where  $a_{\pi}(\pm)$  and  $b_{\pi}(\pm)$  denote the sideband modes at frequency  $\omega_0 \pm \Omega$ , which are in the vacuum state at the input of the NOPA. The quadrature is defined by the operator  $\hat{x}_{\phi} \doteq \frac{1}{2}(ae^{-i\phi} + a^{\dagger}e^{i\phi})$ , where  $\phi$  is the relative phase between the signal and the local oscillator. The value of the quadratures is used as input data for the tomographic measurement of the correlation function  $C(\alpha, \beta)$ .

The direction of polarizers  $(\alpha, \beta)$  in the experimental set-up does not need to be varied over different trials, because, as we will show in the following, such direction can be changed tomographically.

We will now enter into details on the state at the output of the NOPA and on the tomographic detection. In terms of the field modes in Eq. (4.51) the spontaneous down-conversion at the NOPA is described by the unitary evolution operator

$$\hat{U}(\xi) = \exp \left[ \xi \left( a_{\uparrow}^{\dagger} b_{\leftrightarrow}^{\dagger} + e^{i\varphi} a_{\leftrightarrow}^{\dagger} b_{\uparrow}^{\dagger} \right) - \text{h. c.} \right], \quad (4.52)$$

where  $\xi = \chi^{(2)}\gamma L/c$  is the rescaled interaction time written in terms of the nonlinear susceptibility  $\chi^{(2)}$  of the medium, the crystal length  $L$ , the pump amplitude  $\gamma$  and the speed  $c$  of light in the medium, whereas  $\varphi$  represents the relative phase between the orthogonal polarization components of the pump field. The state at the output of the NOPA writes as follows

$$|\psi\rangle = (1 - |\Lambda|^2)^{\frac{1}{2}} \sum_{n=0}^{\infty} \sum_{m=0}^{\infty} \Lambda^{n+m} e^{i\varphi m} |n, n, m, m\rangle \equiv |\psi_{1,2}\rangle \otimes |\psi_{3,4}\rangle, \quad (4.53)$$

where  $\Lambda = \xi/|\xi| \tanh|\xi|$  and  $|i, l, m, n\rangle$  represents the common eigenvector of the number operators of modes  $a_{\uparrow}, b_{\leftrightarrow}, a_{\leftarrow}, b_{\downarrow}$ , with eigenvalues  $i, l, m$  and  $n$ , respectively. The average photon number *per* mode is given by  $N = |\Lambda|^2/(1 - |\Lambda|^2)$ . The four-mode state vector in Eq. (4.53) factorizes into a couple of twin beams  $|\psi_{1,2}\rangle$  and  $|\psi_{3,4}\rangle$ , each one entangling a couple of spatially divergent modes ( $a_{\uparrow}, b_{\leftrightarrow}$  and  $a_{\leftarrow}, b_{\downarrow}$ , respectively). Notice that conventional experiments, concerning a two-photon polarization-entangled state generated by spontaneous down-conversion, consider a four-mode entangled state which corresponds to keeping only the first-order terms of the sums in Eq. (4.53), and to ignoring the vacuum component, as only intensity correlations are usually measured. Here, on the contrary, we measure the joint probabilities on the state (4.53) to test Bell's inequality through homodyne tomography, which yields the value of  $B(\alpha, \beta, \alpha', \beta')$  in Eq. (4.50).

#### 4.4.2 Homodyning Bell's inequality

The tomographic technique is a kind of universal detector, which can measure any observable  $\hat{O}$  of the field, by averaging a suitable “pattern” function  $\mathcal{R}[\hat{O}](x, \phi)$  over homodyne data  $x$  at random phase  $\phi$ , namely

$$\langle \hat{O} \rangle = \mathcal{AV}\{\mathcal{R}[\hat{O}](x, \phi)\} . \quad (4.54)$$

The “pattern” function is obtained through the trace-rule [139]

$$\mathcal{R}[\hat{O}](x, \phi) = \text{Tr} \left[ \hat{O} K_{\eta}(x - \hat{x}_{\phi}) \right] , \quad (4.55)$$

where  $K_{\eta}(x)$  is the distribution

$$K_{\eta}(x) = \frac{1}{2} \text{Re} \int_0^{+\infty} dr r \exp \left( \frac{1 - \eta}{8\eta} r^2 + irx \right) \quad (4.56)$$

which is derived in Ref. [140]. For factorized many-mode operators  $\hat{O} = \hat{O}_1 \otimes \hat{O}_2 \otimes \dots \otimes \hat{O}_n$  the pattern function is just the product of those corresponding to each single-mode operator  $\hat{O}_1, \dots, \hat{O}_n$  labeled by variables  $(x_1, \phi_1), \dots, (x_n, \phi_n)$ . By linearity the pattern function is extended to generic many-mode operators.

Now we consider which observables are involved in testing Bell's inequality (4.50). Let us denote by  $p_{\alpha, \beta}(i, l, m, n)$  the probability of having  $i, l, m, n$  photons in modes  $a_{\uparrow}, b_{\leftrightarrow}, a_{\leftarrow}, b_{\downarrow}$  for the “rotated” state

$$|\psi\rangle_{\alpha, \beta} \equiv \hat{U}_{1,3}(\alpha) \hat{U}_{2,4}(\beta) |\psi\rangle , \quad (4.57)$$

$\hat{U}_{1,3}(\alpha)$  and  $\hat{U}_{2,4}(\beta)$  being the unitary operators

$$\hat{U}_{1,3}(\alpha) = \exp \left[ \alpha \left( a_{\downarrow}^{\dagger} a_{\leftarrow} - a_{\uparrow} a_{\leftrightarrow}^{\dagger} \right) \right] , \quad (4.58)$$

$$\hat{U}_{2,4}(\beta) = \exp \left[ \beta \left( b_{\downarrow}^{\dagger} b_{\leftrightarrow} - b_{\uparrow} b_{\leftarrow}^{\dagger} \right) \right] . \quad (4.59)$$

The probabilities in Eq. (4.49) can be written as  $p_{\alpha,\beta} = p_{\alpha,\beta}(1,1)$ ,  $p_{\bar{\alpha},\bar{\beta}} = p_{\alpha,\beta}(0,0)$ ,  $p_{\bar{\alpha},\beta} = p_{\alpha,\beta}(0,1)$ , and  $p_{\alpha,\bar{\beta}} = p_{\alpha,\beta}(1,0)$ , with

$$p_{\alpha,\beta}(n,m) = \frac{p_{\alpha,\beta}(n,1-m,1-n,m)}{P(1,1)}, \quad (4.60)$$

and  $\{n,m = 0,1\}$ . The denominator  $P(1,1)$  in Eq. (4.60) represents the absolute probability of having at the output of the NOPA one photon in modes  $a_{\uparrow}, a_{\leftrightarrow}$  and one photon in modes  $b_{\uparrow}, b_{\leftrightarrow}$ , independently on the polarization, namely

$$P(1,1) = \sum_{n=0,1} \sum_{m=0,1} p_{\alpha,\beta}(n,1-m,1-n,m). \quad (4.61)$$

Notice that our procedure does not need a fair sampling assumption, since we measure in only one run, both the numerator and the denominator of Eq. (4.60), namely we do not have to collect auxiliary data to normalize probabilities. On the other hand, since we can exploit quantum efficiencies as high as  $\eta = 90\%$  or more, and the tomographic pattern functions already take into account  $\eta$ , we do not need supplementary hypothesis for it.

The observables that correspond to probabilities  $p_{\alpha,\beta}(i,l,m,n)$  in Eqs. (4.60) and (4.61) are the projectors

$$\begin{aligned} & |i,l,m,n\rangle_{\alpha,\beta} \langle i,l,m,n| \\ & = \hat{U}_{1,3}^{\dagger}(\alpha) \hat{U}_{2,4}^{\dagger}(\beta) |i,l,m,n\rangle \langle i,l,m,n| \hat{U}_{2,4}(\beta) \hat{U}_{1,3}(\alpha). \end{aligned} \quad (4.62)$$

After a straightforward calculation using Eqs. (4.60), (4.61) and (4.62), one obtains that  $P(1,1)$  is measured through the following average  $\mathcal{AV}$  of homodyne data

$$P(1,1) = \mathcal{AV} \{ (K_1^1 K_0^3 + K_0^1 K_1^3) (K_1^2 K_0^4 + K_0^2 K_1^4) \}, \quad (4.63)$$

where  $K_n^j$  denotes the diagonal ( $n = 0,1$ ) tomographic kernel function for mode  $j$ , namely

$$K_n^j \equiv \langle n | K_{\eta}(x - \hat{x}_{\phi_j}) | n \rangle. \quad (4.64)$$

The probabilities in the numerator of Eq. (4.60) are given by the average of a lengthy expression, which depends on both the diagonal terms (4.64) and the following off-diagonal terms

$$K_+^j \equiv \langle 0 | K_{\eta}(x - \hat{x}_{\phi_j}) | 1 \rangle, \quad K_-^j \equiv \langle 1 | K_{\eta}(x - \hat{x}_{\phi_j}) | 0 \rangle = (K_+^j)^*. \quad (4.65)$$

Here we report the final expression for  $C(\alpha,\beta)$  of Eq. (4.49)

$$\begin{aligned} C(\alpha,\beta) &= \frac{1}{P(1,1)} \times \\ & \mathcal{AV} \left\{ [\cos(2\alpha) (K_1^1 K_0^3 - K_0^1 K_1^3) + \sin(2\alpha) (K_+^1 K_-^3 + K_-^1 K_+^3)] \times \right. \\ & \left. [\cos(2\beta) (K_0^2 K_1^4 - K_1^2 K_0^4) + \sin(2\beta) (K_+^2 K_-^4 + K_-^2 K_+^4)] \right\}. \end{aligned} \quad (4.66)$$

Caution must be taken in the estimation of the statistical error, because  $C(\alpha, \beta)$ —and thus  $B(\alpha, \beta, \alpha', \beta')$  in Eq. (4.50)—are non linear averages (they are ratios of averages). The error is obtained from the variance calculated upon dividing the set of data into large statistical blocks. However, since the nonlinearity of  $B$  introduces a systematic error which is vanishingly small for increasingly larger sets of data, the estimated mean value of  $B$  is obtained from the full set of data, instead of averaging the mean value of blocks.

#### 4.4.3 Numerical results

We now present some numerical results obtained from Monte–Carlo simulations of the proposed experiment.

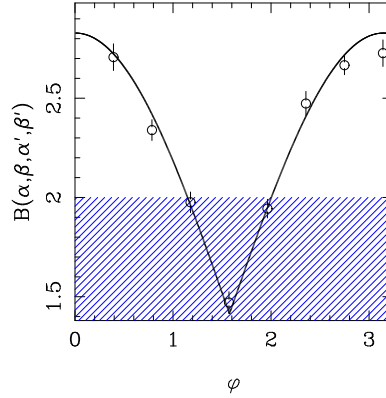


Figure 4.7: Plot of  $B(\alpha, \beta, \alpha', \beta')$  vs the phase  $\varphi$  in the state of Eq. (4.53) for a simulated experiment. The shaded area represents the classical region for  $B$ . The parameters of the simulation are:  $\alpha = 0$ ;  $\beta = \frac{3}{8}\pi$ ;  $\alpha' = \frac{\pi}{4}$ ;  $\beta' = \frac{\pi}{8}$ ; quantum efficiency  $\eta = 85\%$ ; average photon number *per* mode  $N = .5$ . A total number of  $10^6$  homodyne data (divided into 20 statistical blocks) has been used.

For the simulation we use the theoretical homodyne probability pertaining to the state  $|\psi\rangle$  in Eq. (4.53) which, for each factor  $|\psi_{i,j}\rangle$ , is given by

$$p_{\eta}(x_i, x_j; \phi_i, \phi_j) = \frac{2 \exp \left[ -\frac{(x_i + x_j)^2}{d_{z_{ij}}^2 + 4\Delta_{\eta}^2} - \frac{(x_i - x_j)^2}{d_{-z_{ij}}^2 + 4\Delta_{\eta}^2} \right]}{\pi \sqrt{(d_{z_{ij}}^2 + 4\Delta_{\eta}^2)(d_{-z_{ij}}^2 + 4\Delta_{\eta}^2)}}, \quad (4.67)$$

where  $x_i$  ( $i = 1, 2, 3, 4$ ) is the outcome of the homodyne measurement for quadrature of the  $i$ -th mode at phase  $\phi_i$ , and

$$z_{ij} = e^{-i(\phi_i + \phi_j)} \Lambda, \quad d_{\pm z_{ij}}^2 = \frac{|1 \pm z_{ij}|^2}{1 - |z_{ij}|^2}, \quad \Delta_{\eta}^2 = \frac{1 - \eta}{4\eta}. \quad (4.68)$$

In Fig. 4.7 we present the simulation results for  $B$  in Eq. (4.50) vs the phase  $\varphi$  in the state of Eq. (4.53). The full line represents the value of  $B$  in Eq. (4.50) with the

quantum theoretical value  $C(\alpha, \beta)$  given by

$$C(\alpha, \beta) = \cos \varphi \sin 2\alpha \sin 2\beta - \cos 2\alpha \cos 2\beta . \quad (4.69)$$

Quantum efficiency  $\eta = 85\%$  has been used, nonetheless notice that for  $\varphi = \pi$  (corresponding to a maximum violation with respect to the classical bound 2), the obtained value is over  $10 \sigma$  distant from the bound. By increasing the number of homodyne data, it is possible to obtain good results also for lower quantum efficiency. In fact, by increasing the number of data to  $8 \cdot 10^8$ , a value of  $B(0, \frac{3}{8}\pi, \frac{\pi}{4}, \frac{\pi}{8}) = 2.834 \pm 0.268$  has been obtained for  $N = .5$ ,  $\varphi = \pi$ , and  $\eta$  as low as 65%. This result is to be compared with the quantum theoretical value of  $2\sqrt{2}$ .

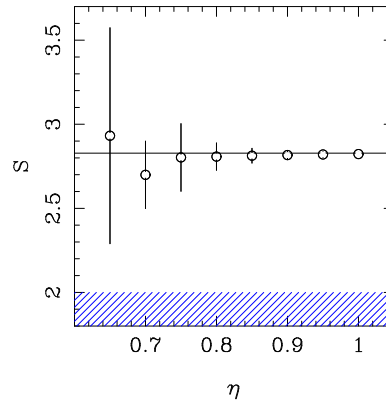


Figure 4.8: Plot of  $B(\alpha, \beta, \alpha', \beta')$  vs the quantum efficiency of the detectors for a series of simulated experiments. The shaded area represents the classical region for  $B$ . The parameters of the simulations are:  $\alpha = 0$ ;  $\beta = \frac{3}{8}\pi$ ;  $\alpha' = \frac{\pi}{4}$ ;  $\beta' = \frac{\pi}{8}$ ;  $\varphi = \pi$ ;  $N = .5$ . A total number of  $6 \cdot 10^7$  homodyne data (in 20 statistical blocks) has been used for each simulation.

For an order of magnitude of the data acquisition rate in a real experiment, one can consider that in a typical set-up with a NOPA pumped by a  $2^{nd}$  harmonic of a Q-switched mode-locked Nd:YAG the pulse repetition rate is 80 MHz, with a 7 ps pulse duration, the effective number of data depending on the speed of the boxcar integrator.

In Fig. 4.8 the results of the measurement of  $B$ , for different simulated experiments using the same number of data, are presented for different detector efficiencies  $\eta$ . Notice how the error bars decrease *versus*  $\eta$ .

The numerical results based on Monte-Carlo simulations confirm the feasibility of the experiment, showing violations of Bell's inequality for over  $10 \sigma$  with detector quantum efficiency  $\eta = 85\%$ .

## 4.5 Tomographic measurement of the nonclassicality of radiation states

In the previous section we used homodyne tomography to check a particular kind of nonclassical feature of quantum states, namely the quantum nonlocal correlations. As we will show in this section, homodyne tomography allows to test more generally the nonclassicality of radiation states, even when quantum efficiency at homodyne detectors is rather low.

The concept of nonclassical states of light has drawn much attention in quantum optics [141, 142, 143, 35, 5, 144, 145, 146, 147, 6, 148]. The customary definition of nonclassicality is given in terms of the Glauber-Sudarshan  $P$  function: a nonclassical state does not admit a regular positive  $P$ -function representation, namely, it cannot be written as a statistical mixture of coherent states. Such states produce effects that have no classical analogue. These kinds of states are of fundamental relevance not only for the demonstration of the inadequacy of classical description, but also for applications, e.g., in the realms of information transmission and interferometric measurements [5, 144, 6].

Here we are interested in testing the nonclassicality of radiation states by means of an operational criterion, which is based on a set of quantities that can be measured experimentally with some given level of confidence, even in the presence of loss, noise, and less-than-unity quantum efficiency [149]. The positivity of the  $P$  function itself cannot be adopted as a test, since there is no method available to measure it. The  $P$  function is a Fourier transform on the complex plane of the generating function for the normal-ordered moments (see Appendix A). In principle, it could be recovered by measuring all the quadrature components of the field, and subsequently performing an (deconvolved) inverse Radon transform [150]. Currently, there is a well-established quantitative method for such a universal homodyne measurement, and it is usually referred to as quantum homodyne tomography (see Ref. [135] for a review). However, as proven in Ref. [139], only the generalized Wigner functions of order  $s < 1 - \eta^{-1}$  can be measured,  $\eta$  being the quantum efficiency of homodyne detection. Hence, through this technique, all functions from  $s = 1$  to  $s = 0$  cannot be recovered, i.e., we cannot obtain the  $P$  function and all its smoothed convolutions up to the customary Wigner function. For the same reason, the nonclassicality parameter proposed by Lee [146], namely, the maximum  $s$ -parameter that provides a positive distribution, cannot be experimentally measured.

Among the many manifestations of nonclassical effects, one finds squeezing, anti-bunching, even-odd oscillations in the photon-number probability, and negativity of the Wigner function [142, 143, 35, 5, 6, 3, 4, 26]. Any of these features alone, however, does not represent the univocal criterion we are looking for. Neither squeezing nor anti-bunching provides a necessary condition for nonclassicality [145]. The negativity of the

Wigner function, which is well exhibited by the Fock states and the Schrödinger-cat-like states, is absent for the squeezed states. As for the oscillations in the photon-number probability, some even-odd oscillations can be simply obtained by using a statistical mixture of coherent states [151].

Many authors [145, 147, 148] have adopted the nonpositivity of the phase-averaged  $P$  function

$$F(I) = \frac{1}{2\pi} \int_0^{2\pi} d\phi P(I^{1/2} e^{i\phi}) \quad (4.70)$$

as the definition for a nonclassical state, since  $F(I) < 0$  invalidates Mandel's semiclassical formula [141] of photon counting, i.e., it does not allow a classical description in terms of a stochastic intensity. Of course, some states can exhibit a “weak” nonclassicality [148], namely, a positive  $F(I)$ , but with a non-positive  $P$  function (a relevant example being a coherent state undergoing Kerr-type self-phase modulation). However, from the point of view of the detection theory, such “weak” nonclassical states still admit a classical description in terms of having the intensity probability  $F(I) > 0$ . For this reason, we adopt nonpositivity of  $F(I)$  as the definition of nonclassicality.

#### 4.5.1 Single-mode nonclassicality

The authors of Refs. [145, 147, 148] have recognized relations between  $F(I)$  and generalized moments of the photon distribution, which, in turn, can be used to test the nonclassicality. The problem is reduced to an infinite set of inequalities that provide both necessary and sufficient conditions for nonclassicality [147]. In terms of the photon-number probability  $p(n) = \langle n | \hat{\rho} | n \rangle$  of the state with density matrix  $\hat{\rho}$ , the simplest sufficient condition involves the following three-point relation for  $p(n)$  [147, 148]

$$B(n) \equiv (n+2)p(n)p(n+2) - (n+1)[p(n+1)]^2 < 0. \quad (4.71)$$

Higher-order sufficient conditions involve five-, seven-, ...,  $(2k+1)$ -point relations, always for adjacent values of  $n$ . It is sufficient that just one of these inequalities be satisfied in order to assure the negativity of  $F(I)$ . Notice that for a coherent state  $B(n) = 0$  identically for all  $n$ .

The relation in Eq. (4.71) can be easily obtained by considering the expression for the number probability  $p(n)$  in terms of  $F(I)$

$$p(n) = \pi \int dI F(I) \frac{e^{-I} I^n}{n!}, \quad (4.72)$$

and noticing that for a classical state with  $F(I) \geq 0$  the average of the polynomial  $I^n(I-x)^2$  is nonnegative for any real value of  $x$ .

In the following we show that quantum tomography can be used as a powerful tool for performing the nonclassicality test in Eq. (4.71). For less-than-unity quantum

efficiency ( $\eta < 1$ ), we rely on the concept of a “noisy state”  $\hat{\rho}_\eta$ , wherein the effect of quantum efficiency is ascribed to the quantum state itself rather than to the detector. In this model, the effect of quantum efficiency is treated in a Schrödinger-like picture, with the state evolving from  $\hat{\rho}$  to  $\hat{\rho}_\eta$ , and with  $\eta$  playing the role of a time parameter. Such lossy evolution is described by the master equation

$$\partial_t \hat{\rho}(t) = \Gamma L[a] \hat{\rho}(t) \equiv \frac{\Gamma}{2} \left\{ 2a \hat{\rho}(t) a^\dagger - a^\dagger a \hat{\rho}(t) - \hat{\rho}(t) a^\dagger a \right\}, \quad (4.73)$$

wherein  $\hat{\rho}(t) \equiv \hat{\rho}_\eta$  with  $t = -\ln \eta / \Gamma$ .

For the nonclassicality test, reconstruction in terms of the noisy state has many advantages over the true-state reconstruction. In fact, for nonunit quantum efficiency  $\eta < 1$  the tomographic method introduces errors for  $p(n)$  which are increasingly large versus  $n$ , with the additional limitation that quantum efficiency must be greater than the minimum value  $\eta = 0.5$  [140, 152]. On the other hand, the reconstruction of the noisy-state probabilities  $p_\eta(n) = \langle n | \hat{\rho}_\eta | n \rangle$  does not suffer such limitations, and even though all quantum features are certainly diminished in the noisy-state description, nevertheless the effect of nonunit quantum efficiency does not change the sign of the  $P$  function, but only rescales it as follows

$$P(z) \rightarrow P_\eta(z) = \frac{1}{\eta} P(z/\eta^{1/2}). \quad (4.74)$$

Hence, the inequality (4.71) still represents a sufficient condition for nonclassicality when the original probabilities  $p(n) = \langle n | \hat{\rho} | n \rangle$  are replaced with the noisy-state probabilities  $p_\eta(n) = \langle n | \hat{\rho}_\eta | n \rangle$ , the latter being given by the Bernoulli convolution

$$p_\eta(n) = \sum_{k=n}^{\infty} \binom{k}{n} \eta^n (1-\eta)^{k-n} p(k). \quad (4.75)$$

Hence, when referred to the noisy-state probabilities  $p_\eta(n)$ , the inequality in Eq. (4.71) keeps its form and simply rewrites as follows

$$B_\eta(n) \equiv (n+2)p_\eta(n)p_\eta(n+2) - (n+1)[p_\eta(n+1)]^2 < 0. \quad (4.76)$$

According to Eq. (4.76), the quantity  $B_\eta(n)$  is nonlinear in the density matrix. This means that  $B_\eta(n)$  cannot be measured by averaging a suitable kernel function over the homodyne data, as for any other observable [139]. Hence, in the evaluation of  $B_\eta(n)$  one needs to reconstruct tomographically the photon-number probabilities, using the kernel functions of Eq. (4.64) which are given explicitly by

$$K_\eta^{(n)}(x) = 2\kappa^2 e^{-\kappa^2 x^2} \sum_{\nu=0}^n \frac{(-)^\nu}{\nu!} \binom{n}{n-\nu} (2\nu+1)! \kappa^{2\nu} \operatorname{Re} \{ D_{-(2\nu+2)}(-2i\kappa x) \}, \quad (4.77)$$

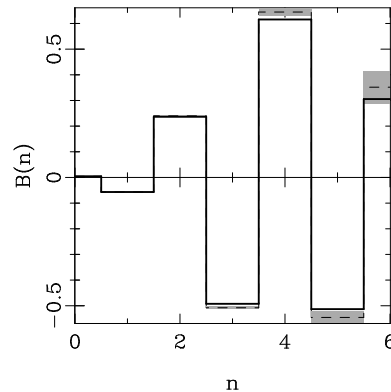


Figure 4.9: Tomographic measurement of  $B(n)$  (dashed trace) with the respective error bars (superimposed in grey-shade) along with the theoretical values (solid trace) for a Schrödinger-cat state with average photon number  $\bar{n} = 5$ . The quantum efficiency is  $\eta = 0.8$  and the number of simulated experimental data used for the reconstruction is  $10^7$ .

where  $D_\sigma(z)$  denotes the parabolic cylinder function and  $\kappa = \sqrt{\eta/(2\eta - 1)}$ . The derivation of Eq. (4.77) can be found in Ref. [140]. The true-state probabilities  $p(n)$  are obtained by averaging the kernel function in Eq. (4.77) over the homodyne data. On the other hand, the noisy-state probabilities  $p_\eta(n)$  are obtained by using the kernel function in Eq. (4.77) for  $\eta = 1$ , namely without recovering the convolution effect of nonunit quantum efficiency. Notice that the expression (4.77) does not depend on the phase of the quadrature. Hence, the knowledge of the phase of the local oscillator in the homodyne detector is not needed for the tomographic reconstruction, and it can be left fluctuating in a real experiment.

Regarding the estimation of statistical errors, they are generally obtained by dividing the set of homodyne data into blocks. However, as in the case of the Sec. 4.4, the nonlinear dependence on the photon number probability introduces a systematic error that is vanishingly small for increasingly larger sets of data. Therefore, the estimated value of  $B(n)$  has been obtained from the full set of data, instead of averaging the mean value of the different statistical blocks.

In Figs. 4.9–4.15 we present some numerical results that are obtained by a Monte–Carlo simulation of a quantum tomography experiment. The nonclassicality criterion is tested either on a Schrödinger-cat state  $|\psi(\alpha)\rangle \propto (|\alpha\rangle + |-\alpha\rangle)$  or on a squeezed state  $|\alpha, r\rangle \equiv D(\alpha)S(r)|0\rangle$ , wherein  $|\alpha\rangle$ ,  $D(\alpha)$ , and  $S(r)$  denote a coherent state with amplitude  $\alpha$ , the displacement operator  $D(\alpha) = e^{\alpha\hat{a}^\dagger - \bar{\alpha}\hat{a}}$ , and the squeezing operator  $S(r) = e^{r(\hat{a}^{\dagger 2} - \hat{a}^2)/2}$ , respectively. Figs. 4.9–4.11 show tomographically-obtained values of  $B(n)$ , with the respective error bars superimposed, along with the theoretical values for a Schrödinger-cat state, for a phase-squeezed state ( $r > 0$ ), and for an amplitude-squeezed state ( $r < 0$ ), respectively. For the same set of states the results for  $B_\eta(n)$  [cf.

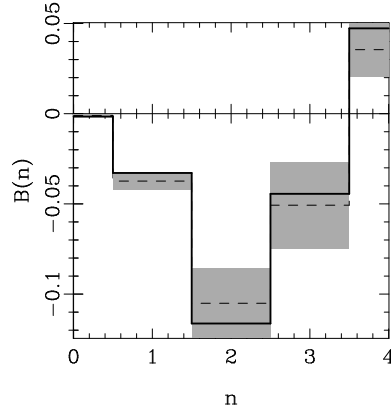


Figure 4.10: Tomographic measurement of  $B(n)$  (dashed trace) with the respective error bars (superimposed in grey-shade) along with the theoretical values (solid trace) for a phase-squeezed state with  $\bar{n} = 5$  and  $\bar{n}_{\text{sq}} = \sinh^2 r = 3$  squeezing photons. The quantum efficiency is  $\eta = 0.8$  and  $10^7$  simulated experimental data have been used for the reconstruction.

Eq. (4.76)] obtained by tomographic reconstruction of the noisy state are reported in Figs. 4.12–4.14. Let us compare the statistical errors that affect the two measurements, namely, those of  $B(n)$  and  $B_\eta(n)$  on the original and the noisy states, respectively. In the first case (Figs. 4.9–4.11) the error increases with  $n$ , whereas in the second (Figs. 4.12–4.14) it remains nearly constant, albeit with less marked oscillations in  $B_\eta(n)$  than those in  $B(n)$ . Fig. 4.15 shows tomographically-obtained values of  $B_\eta(n)$  for the phase-squeezed state (cf. Fig. 4.13), but for a lower quantum efficiency  $\eta = 0.4$ . Notice that, in spite of the low quantum efficiency, the nonclassicality of such a state is still experimentally verifiable, as  $B_\eta(0) < 0$  by more than five standard deviations. In contrast, for coherent states one obtains small statistical fluctuations around zero for all  $n$ . We remark that the simpler test of checking for antibunching or oscillations in the photon-number probability in the case of the phase-squeezed state considered here (Figs. 4.10, 4.13, and 4.15) would not reveal the nonclassical features of such a state.

### 4.5.2 Two-mode nonclassicality

Quantum homodyne tomography can also be employed to test the nonclassicality of two-mode states. For a two-mode state nonclassicality is defined in terms of nonpositivity of the following phase-averaged two-mode  $P$ -function [148]

$$F(I_1, I_2, \phi) = \frac{1}{2\pi} \int_0^{2\pi} d\phi_1 P(I_1^{1/2} e^{i\phi_1}, I_2^{1/2} e^{i(\phi_1 + \phi)}). \quad (4.78)$$

A sufficient condition for nonclassicality is found in Ref. [148] as the following

$$C = \langle (\hat{n}_1 - \hat{n}_2)^2 \rangle - (\langle \hat{n}_1 - \hat{n}_2 \rangle)^2 - \langle \hat{n}_1 + \hat{n}_2 \rangle < 0, \quad (4.79)$$

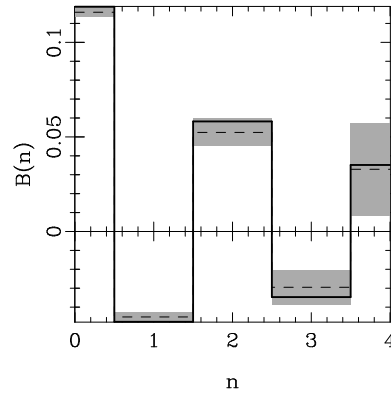


Figure 4.11: Same as in Fig. 4.10, but for an amplitude-squeezed state.

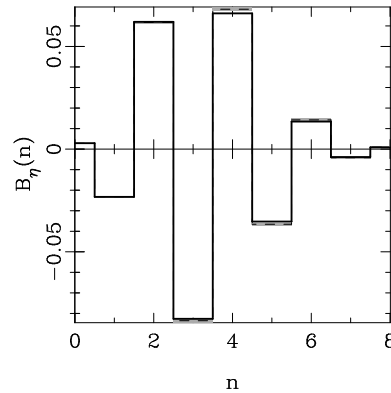


Figure 4.12: Tomographic measurement of  $B_\eta(n)$  for a Schrödinger-cat state with  $\bar{n} = 5$ , degraded by a quantum efficiency  $\eta = 0.8$ . The number of simulated experimental data is  $10^7$ .

where  $\hat{n}_1$  and  $\hat{n}_2$  are the photon-number operators of the two modes.

A tomographic test of the inequality in Eq. (4.79) can be performed by averaging the kernel functions for the operators in the ensemble averages in Eq. (4.79) over the two-mode homodyne data. For the normal-ordered field operators one can use the Richter formula in Ref. [153], namely

$$\mathcal{R}[a^{\dagger n} a^m](x, \phi) = e^{i(m-n)\phi} \frac{H_{n+m}(\sqrt{2\eta}x)}{\sqrt{(2\eta)^{n+m} \binom{n+m}{n}}}, \quad (4.80)$$

$H_n(x)$  denoting the Hermite polynomial and  $\phi$  being the phase of the fields with respect to the local oscillator of the homodyne detector. Again, as for the kernel function in Eq. (4.77), the value  $\eta = 1$  is used to reconstruct the ensemble averages of the noisy state  $\hat{\rho}_\eta$ . Notice that for  $n = m$  Eq. (4.80) is independent on the phase  $\phi$ , and hence no phase knowledge is needed to reconstruct the ensemble averages in Eq. (4.79). As an

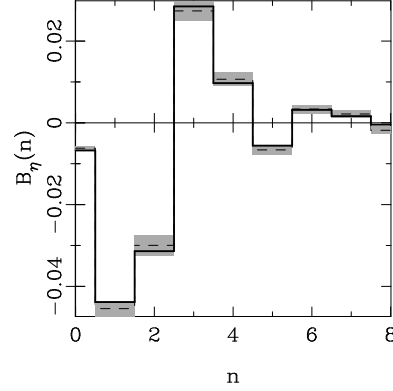


Figure 4.13: Tomographic measurement of  $B_\eta(n)$  (dashed trace) with the respective error bars (superimposed in grey-shade) along with the theoretical values (solid trace) for a phase-squeezed state, which has  $\bar{n} = 5$  and  $\bar{n}_{\text{sq}} = \sinh^2 r = 3$  squeezing photons, and which has been degraded by a quantum efficiency  $\eta = 0.8$ . For the reconstruction a sample of  $10^7$  simulated experimental data have been used.

example, we consider the twin-beam state at the output of a nondegenerate parametric amplifier

$$|\chi\rangle \equiv (1 - |\lambda|^2) \sum_{n=0}^{\infty} \lambda^n |n\rangle \otimes |n\rangle, \quad (4.81)$$

where  $|n\rangle \otimes |n\rangle$  denotes the joint eigenvector of the number operators of the two modes with equal eigenvalue  $n$ , and the parameter  $\lambda$  is related to the gain  $G$  of the amplifier by the relation  $|\lambda|^2 = 1 - G^{-1}$ . The theoretical value of  $C$  for the state in Eq. (4.81) is  $C = -2|\lambda|^2/(1 - |\lambda|^2) < 0$ . A tomographic reconstruction of the twin-beam state in Eq. (4.81) is particularly facilitated by the self-homodyning scheme described in Sec. 4.4.1. With regard to the effect of quantum efficiency  $\eta < 1$ , the same argument still holds as for the single-mode case: one can evaluate  $C_\eta$  for the twin-beam state that has been degraded by the effect of loss. In this case, the theoretical value of  $C_\eta$  is simply rescaled to  $C_\eta = -2\eta^2|\lambda|^2/(1 - |\lambda|^2)$ .

In Fig. 4.16 we report  $C_\eta$  vs.  $1 - \eta$ ,  $\eta$  ranging from 1 to 0.3 in steps of 0.05, for the twin-beam state in Eq. (4.81) with  $|\lambda|^2 = 0.5$ , corresponding to the total average photon number equal to 2. The values of  $C_\eta$  result from a Monte-Carlo simulation of a homodyne tomography experiment with a sample of  $4 \times 10^5$  data, using the theoretical joint homodyne probability of the state  $|\chi\rangle$ , namely the probability  $p_\eta(x_1, x_2, \phi_1, \phi_2)$  given by Eq. (4.67),  $\phi_1$  and  $\phi_2$  denoting the phases of the two modes relative to the respective local oscillator. Notice that the nonclassicality test in terms of the noisy state gives values of  $C_\eta$  that are increasingly near the classically positive region for decreasing quantum efficiency  $\eta$ . However, the statistical error remains constant and is sufficiently small to allow recognition of the nonclassicality of the twin-beam state in

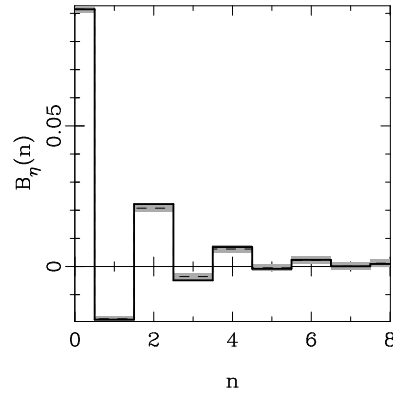


Figure 4.14: Same as in Fig. 4.13, but for an amplitude-squeezed state.

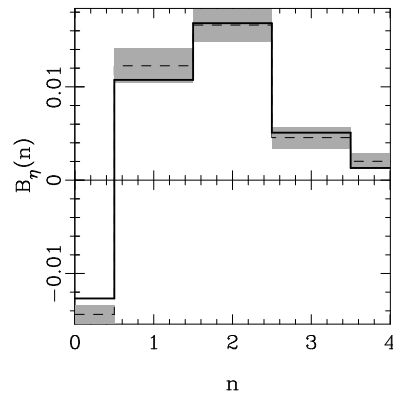


Figure 4.15: Same as in Fig. 4.13, but here for a quantum efficiency of  $\eta = 0.4$ , and a sample of  $5 \times 10^7$  simulated experimental data.

Eq. (4.81) up to  $\eta = 0.3$ . As in the single-mode test, the tomographic reconstruction does not need the knowledge of the phase of the local oscillator. We conclude that the proposed nonclassicality test should be easy to perform experimentally.

## 4.6 Conclusion

In this chapter we have proposed several experimental set-ups in the realm of the quantum theory of measurement.

We presented a quantum-optical scheme that realizes the standard von Neumann model, a model for repeatable quantum measurements with controlled state-reduction. Our scheme uses simple optical elements, like beam-splitters and squeezers. We have seen that, contrarily to the customary modeling of repeatable measurements, there is

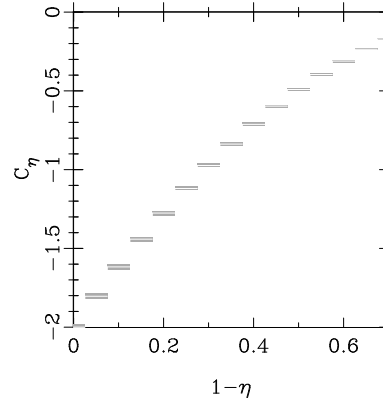


Figure 4.16: Tomographic measurement of  $C_\eta$  as defined in Eq. (4.79) and modified by the quantum efficiency for the twin-beam state in Eq. (4.81). The respective error bars are shown in the grey shade and  $|\lambda|^2 = 0.5$  corresponding to an average of 2 total photons. The results are shown for various values of the quantum efficiency  $\eta$  (in steps of 0.05) and for each value of  $\eta$  the number of simulated data is  $4 \times 10^5$ .

no need of working in a ultra-short pulsed regime. We have also shown how the precise form of the state reduction can be engineered by means of a feedback mechanism that uses a Pockels cell: we think that this method can be of use in more general situations, for controlling the back-action of a quantum measurement.

Then we suggested a novel method to generate mesoscopic entangled superposition of quantum states by stimulated down conversion. Our scheme has been inspired by the quantum injection concept suggested in Ref. [124]. The setup relies on feeding a non-degenerate parametric amplifier by a single-photon state, however making signal and idler paths indistinguishable. We analyzed the full amplification process taking into account the effects of cavity losses. The main result is the appearance of mesoscopic quantum superpositions for the amplifier working well above threshold and with a short interaction time. The entanglement is shared by a couple of spatially separated field modes. The resulting superposition turns out to be robust against decoherence and can be revealed by a simple interference measurement.

The last two experimental set-ups are based on quantum homodyne tomography. We proposed a test of Bell's inequality, based on self-homodyne tomography. The rather simple experimental apparatus is mainly composed of a nondegenerate optical parametric amplifier and four photodiodes. The experimental data are collected through a self-homodyne scheme and processed by quantum tomography. No supplementary hypotheses are introduced, a quantum efficiency  $\eta$  as high as 90% is currently available, and, anyway,  $\eta$  as low as 70% is tolerated for  $10^6 \div 10^7$  experimental data. The numerical results based on Monte-Carlo simulations confirm the feasibility of the experiment, showing violations of Bell's inequality for over  $10 \sigma$  with detector quantum

efficiency  $\eta = 85\%$ . More generally, quantum homodyne tomography allows one to perform nonclassicality tests that invalidate Mandel's semiclassical formula of photon counting for various single- and two-mode radiation states, even when the quantum efficiency of homodyne detection is rather low. The method involves reconstruction of the photon-number probability or of some suitable function of the number operators pertaining to the noisy state, namely, the state degraded by the less-than-unity quantum efficiency. The noisy-state reconstruction is affected by the statistical errors; however, they are sufficiently small that the nonclassicality of the state can be tested even for low values of  $\eta$ . For the cases considered in this chapter, we have shown that the nonclassicality of the states can be proven (deviation from classicality by many error bars) with  $10^5$ – $10^7$  homodyne data.



# Conclusions

In this thesis we have shown many different applications of the parametric amplification of light through nonlinear media in the realm of quantum communication and measurement. The very wide spectrum of such applications proves that it is worth making many efforts to improve the effectiveness of parametric processes and the efficiency of quantum measurements. In fact, the generation of states of light with tunable nonclassical features is a crucial requirement to improve both the sensitivity in interferometric devices and the capacity in optical communication channels, with respect to the classical performances.

The theoretical treatment of parametric processes in nonlinear media is usually drawn within the parametric approximation by replacing one or more bosonic modes with c-numbers representing classical undepleted pumps. We discussed thoroughly the validity of such approximation in Chap. 1. We showed that the regime of validity of the parametric approximation is very large, including also the case of weak pump with  $1 \div 10$  mean photon number. We found that the degree of coherence of the pump *after* the interaction rather than its undepletion discriminates the working regimes of parametric amplifiers. In terms of the pump Fano factor we found that a deviation from the coherent level smaller than 10% guarantees an overlap larger than 99% between the states predicted within the parametric approximation and those evaluated by the exact Hamiltonian.

As shown in Chap. 2, the parametric amplification of light is effective in generating radiation states with good phase properties for interferometric and communication purposes. We found an interaction scheme to generate the phase-coherent states by nonlinear  $\chi^{(2)}$  media. The scheme is based on spontaneous parametric downconversion followed by upconversion of the resulting twin beam. Among the single-mode radiation states, the phase-coherent states are optimal phase states for both the Süssmann and the reciprocal peak likelihood measure of phase uncertainty. Moreover, they maintain phase coherence under phase amplification such that they are privileged states for phase-based communication channels. The second proposal of Chap. 2 is an experimental scheme for the generation of two-mode states that approach the eigenstates of

the heterodyne detector. These states are essentially generated by parametric down-conversion of coherent sources, and are shown to achieve the ideal phase sensitivity (inversely proportional to the mean photon number). We addressed more generally the problem of the phase measurement in the realm of estimation theory, along with the derivation of the optimal positive operator-valued measure and the optimal input state.

The application of parametric processes for quantum optical communication channel has been the subject of Chap. 3. First of all we considered the effect of loss on the communication channels based on heterodyne detection of coherent states, on homodyne detection of squeezed states and on direct detection of Fock states, and optimized the *a priori* probability in the presence of loss. Then, with regard to the generation of the squeezed states and the number states involved in the nonclassical channels, we suggested the following solution. On one hand, we showed the equivalence between a couple of customary squeezed-state channels and a more easily achievable communication channel based on the two-mode heterodyne states we introduced in Chap. 1. On the other hand, we presented an experimental scheme to synthesize number states (and also superpositions of number states) through a ring cavity coupled to a coherent traveling wave by a cross-Kerr medium.

Parametric interactions deserve some attention also for their promising possibilities to allow a number of fundamental tests of Quantum Mechanics. We proposed the following experimental tests in Chap. 4. An optical scheme that realizes von Neumann's measurement model for the position of a particle, with tunable Gaussian state reduction. A method to generate mesoscopic quantum superpositions by parametric amplification of the path indistinguishability of a single-photon state. A tomographic test of Bell's inequality on correlated optical beams at the output of a nondegenerate parametric amplifier. Finally, a nonclassicality test based on homodyne tomography that discriminates classical radiation from states that invalidates Mandel's semiclassical formula of photon counting.

# Appendix A

## Trace formula for generalized Wigner functions

### A.1 Introduction

In this appendix we derive simple formulas connecting the generalized Wigner functions for  $s$ -ordering with the density matrix, and *vice-versa*. These formulas proved very useful for quantum mechanical applications, as, for example, for connecting master equations with Fokker-Planck equations, or for evaluating the quantum state from Monte Carlo simulations of Fokker-Planck equations, and finally for studying positivity of the generalized Wigner functions in the complex plane [154].

Since Wigner's pioneering work [155], generalized phase-space techniques have proved very useful in various branches of physics [156]. As a method for expressing the density operator in terms of  $c$ -number functions, the Wigner functions often lead to considerable simplification of the quantum equations of motion, as for example, transforming operator master equations into more amenable Fokker-Planck differential equations (see, for example, Ref. [95]). By the Wigner function one can express quantum-mechanical expectation values in form of averages over the complex plane (the classical phase-space), the Wigner function playing the role of a  $c$ -number quasi-probability distribution, which generally can also have negative values. More precisely, the original Wigner function allows to easily evaluate expectations of symmetrically ordered products of the field operators, corresponding to the Weyl's quantization procedure [157]. However, with a slight change of the original definition, one defines generalized  $s$ -ordered Wigner function  $W_s(\alpha, \bar{\alpha})$ , as follows [158]

$$W_s(\alpha, \bar{\alpha}) \doteq \int \frac{d^2\lambda}{\pi^2} e^{\alpha\bar{\lambda} - \bar{\alpha}\lambda + \frac{s}{2}|\lambda|^2} \text{Tr}[D(\lambda)\hat{\rho}] \quad (\text{A.1})$$

where the integral is performed on the complex plane with measure  $d^2\lambda = d\text{Re}\lambda d\text{Im}\lambda$ ,  $D(\alpha) = e^{\alpha a^\dagger - \bar{\alpha} a}$  denotes the displacement operator, and  $a$  and  $a^\dagger$  ( $[a, a^\dagger] = 1$ ) are

the annihilation and creation operators of the field mode of interest. Then, using the Wigner function in Eq. (A.1) one can evaluate  $s$ -ordered expectation values of the field operators through the following relation

$$\text{Tr}[:(a^\dagger)^n a^m :_s \hat{\rho}] = \int d^2\alpha W_s(\alpha, \bar{\alpha}) \bar{\alpha}^n \alpha^m . \quad (\text{A.2})$$

It is easy to show that the particular cases  $s = -1, 0, 1$  lead to *antinormal*, *symmetrical*, and *normal* ordering, respectively, in which cases the generalized Wigner function  $W_s(\alpha, \bar{\alpha})$  historically was denoted with the following symbols and names

$$W_s(\alpha, \bar{\alpha}) = \begin{cases} \frac{1}{\pi} Q(\alpha, \bar{\alpha}) & \text{for } s=-1 \text{ “}Q \text{ function”} \\ W(\alpha, \bar{\alpha}) & \text{for } s=0 \text{ (usual Wigner function)} \\ P(\alpha, \bar{\alpha}) & \text{for } s=1 \text{ “}P \text{ function”} \end{cases} \quad (\text{A.3})$$

For the normal ( $s = 1$ ) and antinormal ( $s = -1$ ) orderings, the following two simple relations between the generalized Wigner function and the density matrix are well known

$$Q(\alpha, \bar{\alpha}) \equiv \langle \alpha | \hat{\rho} | \alpha \rangle , \quad (\text{A.4})$$

$$\hat{\rho} = \int d^2\alpha P(\alpha, \bar{\alpha}) |\alpha\rangle \langle \alpha| , \quad (\text{A.5})$$

where  $|\alpha\rangle$  denotes the customary coherent state  $|\alpha\rangle = D(\alpha)|0\rangle$ ,  $|0\rangle$  being the vacuum state of the field. Among the three particular representations (A.3), it is also well known that the  $Q$  function is positively definite and infinitely differentiable (it actually represents the probability distribution for ideal joint measurements of position and momentum of the harmonic oscillator: see, for example, Ref. [34]). On the other hand, the  $P$  function is known to be possibly highly singular, and the only pure states for which it is positive are the coherent states [159]. Finally, the usual Wigner function has the remarkable property of providing the probability distributions of the quadratures of the field in form of marginal distributions, namely

$$\int d\text{Im}\alpha W(\alpha e^{i\phi}, \bar{\alpha} e^{-i\phi}) = {}_\phi \langle \text{Re}\alpha | \hat{\rho} | \text{Re}\alpha \rangle_\phi , \quad (\text{A.6})$$

where  $|x\rangle_\phi$  stands for the eigenstates of the field quadrature  $\hat{X}_\phi = (a^\dagger e^{i\phi} + \text{h.c.})/2$  (any couple of conjugated quadratures  $\hat{X}_\phi, \hat{X}_{\phi+\pi/2}$ , with  $[\hat{X}_\phi, \hat{X}_{\phi+\pi/2}] = i/2$ , are equivalent to the position and momentum of a harmonic oscillator). Usually, negative values of the Wigner function are viewed as signature of a nonclassical state (one of the more eloquent examples is given by the Schrödinger-cat states [70] whose Wigner function is characterized by rapid oscillations around the origin of the complex plane). From Eq. (A.1) one can see that all  $s$ -ordered Wigner functions are related to each other through the convolution relation

$$W_s(\alpha, \bar{\alpha}) = \int d^2\beta W_{s'}(\beta, \bar{\beta}) \frac{2}{\pi(s' - s)} \exp\left(-\frac{2}{s' - s} |\alpha - \beta|^2\right) \quad (\text{A.7})$$

$$= \exp\left(\frac{s' - s}{2} \frac{\partial^2}{\partial \alpha \partial \bar{\alpha}}\right) W_{s'}(\alpha, \bar{\alpha}), \quad (s' > s). \quad (\text{A.8})$$

Equation (A.7) shows the positiveness of the generalized Wigner function for  $s < -1$ , as a consequence of the positiveness of the  $Q$  function. From a qualitative point of view, the maximum value of  $s$  keeping the generalized Wigner functions as positive can be considered as an indication of the classical nature of the physical state.

## A.2 Three equivalent trace forms

In the following we derive three equivalent trace forms that connect  $s$ -ordered Wigner functions with the density matrix, namely the identities

$$W_s(\alpha, \bar{\alpha}) = \frac{2}{\pi(1-s)} e^{-\frac{2}{1-s}|\alpha|^2} \text{Tr} \left[ \left(\frac{s+1}{s-1}\right)^{a^\dagger a} e^{\frac{2}{1-s}\bar{\alpha}a} \hat{\rho} e^{\frac{2}{1-s}a\alpha^\dagger} \right], \quad (\text{A.9})$$

$$= \frac{2}{\pi(1-s)} e^{\frac{2}{1+s}|\alpha|^2} \text{Tr} \left[ \left(\frac{s+1}{s-1}\right)^{a^\dagger a} e^{-\frac{2}{1+s}a\alpha^\dagger} \hat{\rho} e^{-\frac{2}{1+s}\bar{\alpha}a} \right], \quad (\text{A.10})$$

$$= \frac{2}{\pi(1-s)} e^{-\frac{2s}{1-s^2}|\alpha|^2} \text{Tr} \left[ \left(\frac{s+1}{1-s}\right)^{\frac{1}{2}a^\dagger a} D\left(\frac{2\alpha}{\sqrt{1-s^2}}\right) \left(\frac{s+1}{1-s}\right)^{\frac{1}{2}a^\dagger a} (-)^{a^\dagger a} \hat{\rho} \right]. \quad (\text{A.11})$$

Equations (A.9-A.10) can be compared with the Cahill-Glauber formula [158]

$$W_s(\alpha, \bar{\alpha}) = \frac{2}{\pi(1-s)} \text{Tr} \left\{ : \exp \left[ -\frac{2}{1-s}(\bar{\alpha} - a^\dagger)(\alpha - a) \right] : \hat{\rho} \right\}, \quad (\text{A.12})$$

where the colons denote the usual normal ordering; Eq. (A.11) represents a generalization of the formula [160]

$$W(\alpha, \bar{\alpha}) = \frac{2}{\pi} \text{Tr} \left[ \hat{\rho} D(2\alpha) \exp(i\pi a^\dagger a) \right]. \quad (\text{A.13})$$

Vice versa, the density matrix can be recovered from the generalized Wigner functions using the following expression

$$\hat{\rho} = \frac{2}{1+s} \int d^2\alpha W_s(\alpha, \bar{\alpha}) e^{-\frac{2}{1+s}|\alpha|^2} \exp\left(\frac{2\alpha}{1+s}a^\dagger\right) \left(\frac{s-1}{s+1}\right)^{a^\dagger a} \exp\left(\frac{2\bar{\alpha}}{1+s}a\right). \quad (\text{A.14})$$

The proof of our statements requires the following identity

$$e^{a^\dagger \partial_{\bar{\alpha}}} |0\rangle \langle 0| e^{a\partial_{\alpha}} \Big|_{\alpha=\bar{\alpha}=0} e^{|\alpha|^2 + \bar{\alpha}\lambda - \alpha\bar{\lambda} - \frac{1}{2}|\lambda|^2} = D(\lambda), \quad (\text{A.15})$$

which is proved at the end of this section. Then, through the following steps:

$$W_s(\alpha, \bar{\alpha}) = \int \frac{d^2\lambda}{\pi^2} e^{\alpha\bar{\lambda} - \bar{\alpha}\lambda + \frac{s}{2}|\lambda|^2} \text{Tr}[D(\lambda)\hat{\rho}]$$

$$\begin{aligned}
&= \int \frac{d^2\lambda}{\pi^2} e^{\alpha\bar{\lambda} - \bar{\alpha}\lambda} \text{Tr} \left[ e^{a^\dagger \partial_{\bar{\beta}}} |0\rangle \langle 0| e^{a \partial_{\beta}} \hat{\rho} \right] \Bigg|_{\beta=\bar{\beta}=0} e^{|\beta|^2 + \bar{\beta}\lambda - \beta\bar{\lambda} + \frac{1}{2}(s-1)|\lambda|^2} \\
&= \frac{2}{\pi(1-s)} \text{Tr} \left[ e^{a^\dagger \partial_{\bar{\beta}}} |0\rangle \langle 0| e^{a \partial_{\beta}} \hat{\rho} \right] \Bigg|_{\beta=\bar{\beta}=0} e^{-\frac{1+s}{1-s}|\beta|^2 - \frac{2}{1-s}(|\alpha|^2 - \alpha\bar{\beta} - \bar{\alpha}\beta)} \\
&= \frac{2}{\pi(1-s)} e^{-\frac{2}{1-s}|\alpha|^2} \text{Tr} \left[ e^{\frac{2}{1-s}\alpha a^\dagger} \left( -\frac{1+s}{1-s} \right)^{a^\dagger a} e^{\frac{2}{1-s}\bar{\alpha} a} \hat{\rho} \right],
\end{aligned}$$

one proves Eq. (A.9). Continuing from the last result we have

$$\begin{aligned}
W_s(\alpha, \bar{\alpha}) &= \frac{2}{\pi(1-s)} e^{-\frac{2}{1-s}|\alpha|^2} \times \\
&\text{Tr} \left[ \left( \frac{1+s}{1-s} \right)^{\frac{1}{2}a^\dagger a} \left( \frac{1-s}{1+s} \right)^{\frac{1}{2}a^\dagger a} e^{\frac{2}{1-s}\alpha a^\dagger} \left( -\frac{1+s}{1-s} \right)^{a^\dagger a} e^{\frac{2}{1-s}\bar{\alpha} a} \left( \frac{1-s}{1+s} \right)^{\frac{1}{2}a^\dagger a} \left( \frac{1+s}{1-s} \right)^{\frac{1}{2}a^\dagger a} \hat{\rho} \right] \\
&= \frac{2}{\pi(1-s)} e^{-\frac{2}{1-s}|\alpha|^2} \text{Tr} \left[ \left( \frac{1+s}{1-s} \right)^{\frac{1}{2}a^\dagger a} e^{\frac{2}{\sqrt{1-s^2}}\alpha a^\dagger} (-)^{a^\dagger a} e^{\frac{2}{\sqrt{1-s^2}}\bar{\alpha} a} \left( \frac{1+s}{1-s} \right)^{\frac{1}{2}a^\dagger a} \hat{\rho} \right] \\
&= \frac{2}{\pi(1-s)} e^{-\frac{2s}{1-s^2}|\alpha|^2} \text{Tr} \left[ \left( \frac{1+s}{1-s} \right)^{\frac{1}{2}a^\dagger a} D \left( \frac{2\alpha}{\sqrt{1-s^2}} \right) \left( \frac{1+s}{1-s} \right)^{\frac{1}{2}a^\dagger a} (-)^{a^\dagger a} \hat{\rho} \right],
\end{aligned}$$

which proves Eq. (A.11). Equation (A.10) is derived from the following identities

$$\begin{aligned}
e^{\frac{2\alpha}{1-s}a^\dagger} \left( \frac{s+1}{s-1} \right)^{a^\dagger a} e^{\frac{2\bar{\alpha}}{1-s}a} &= \left( \frac{s+1}{s-1} \right)^{a^\dagger a} e^{-\frac{2\alpha}{1+s}a^\dagger} e^{\frac{2\bar{\alpha}}{1-s}a}, \\
e^{\frac{4|\alpha|^2}{1-s^2}} \left( \frac{s+1}{s-1} \right)^{a^\dagger a} e^{\frac{2\bar{\alpha}}{1-s}a} e^{-\frac{2\alpha}{1+s}a^\dagger} &= e^{\frac{4|\alpha|^2}{1-s^2}} e^{-\frac{2\bar{\alpha}}{1+s}a} \left( \frac{s+1}{s-1} \right)^{a^\dagger a} e^{-\frac{2\alpha}{1+s}a^\dagger}.
\end{aligned}$$

As a check, from Eqs. (A.9-A.11) one can easily recover the usual definition of the Wigner function (A.1) for  $s = 0$ , and Eq. (A.4) for the  $Q$  function ( $s = -1$ ), namely

$$\begin{aligned}
W_{-1}(\alpha, \bar{\alpha}) &= \frac{1}{\pi} e^{-|\alpha|^2} \text{Tr} \left[ (-O^+)^{a^\dagger a} e^{\bar{\alpha} a} \hat{\rho} e^{\alpha a^\dagger} \right] = \frac{1}{\pi} e^{-|\alpha|^2} \text{Tr} \left[ |0\rangle \langle 0| e^{\bar{\alpha} a} \hat{\rho} e^{\alpha a^\dagger} \right] \\
&= \frac{1}{\pi} Q(\alpha, \bar{\alpha}).
\end{aligned}$$

The inversion formula (A.14) is obtained using Eq. (A.11) and the following formula [158]

$$\hat{O} = \int \frac{d^2\alpha}{\pi} \text{Tr}[\hat{O}D(\alpha)] D^\dagger(\alpha), \quad (\text{A.16})$$

that holds true for any Hilbert-Schmidt operator  $\hat{O}$ , and hence for a (trace-class) density matrix. One has

$$\left( \frac{s+1}{1-s} \right)^{\frac{1}{2}a^\dagger a} (-)^{a^\dagger a} \hat{\rho} \left( \frac{s+1}{1-s} \right)^{\frac{1}{2}a^\dagger a}$$

$$\begin{aligned}
&= \int \frac{d^2\alpha}{\pi} \text{Tr} \left[ D(\alpha) \left( \frac{s+1}{1-s} \right)^{\frac{1}{2}a^\dagger a} (-)^{a^\dagger a} \hat{\rho} \left( \frac{s+1}{1-s} \right)^{\frac{1}{2}a^\dagger a} \right] D^\dagger(\alpha) \\
&= \frac{4}{1-s^2} \int \frac{d^2\alpha}{\pi} W_s(\alpha, \bar{\alpha}) \frac{\pi(1-s)}{2} e^{\frac{2s}{1-s^2}|\alpha|^2} D^\dagger \left( \frac{2\alpha}{\sqrt{1-s^2}} \right). \quad (\text{A.17})
\end{aligned}$$

Hence,

$$\begin{aligned}
\hat{\rho} &= \frac{2}{1+s} \int d^2\alpha W_s(\alpha, \bar{\alpha}) e^{\frac{2s}{1-s^2}|\alpha|^2} \left( \frac{1-s}{1+s} \right)^{\frac{1}{2}a^\dagger a} (-)^{a^\dagger a} D^\dagger \left( \frac{2\alpha}{\sqrt{1-s^2}} \right) \left( \frac{1-s}{1+s} \right)^{\frac{1}{2}a^\dagger a} \\
&= \frac{2}{1+s} \int d^2\alpha W_s(\alpha, \bar{\alpha}) e^{-\frac{2}{1+s}|\alpha|^2} \left( \frac{1-s}{1+s} \right)^{\frac{1}{2}a^\dagger a} e^{\frac{2\alpha}{\sqrt{1-s^2}}a^\dagger} (-)^{a^\dagger a} e^{\frac{2\bar{\alpha}}{\sqrt{1-s^2}}a} \left( \frac{1-s}{1+s} \right)^{\frac{1}{2}a^\dagger a},
\end{aligned}$$

and then the result follows easily. In particular, for  $s = 0$  one has the inverse of the Glauber formula

$$\hat{\rho} = 2 \int d^2\alpha W(\alpha, \bar{\alpha}) D(2\alpha) (-)^{a^\dagger a}, \quad (\text{A.18})$$

whereas for  $s = 1$  one recovers the relation (A.5) that defines the  $P$  function.

The trace form of Eqs.(A.9-A.10-A.11) can be used for an analysis of positivity of the Wigner function, usually a quite difficult task, as confirmed in Ref. [161]. In particular, from Eq. (A.9) one can immediately see that for  $s < 1$  (namely, with the only exception of the  $P$  function) the  $s$ -Wigner function can become negative, because the operator  $e^{\frac{2}{1-s}\bar{\alpha}a} \hat{\rho} e^{\frac{2}{1-s}a\alpha^\dagger}$  is positive-definite, whereas the preceding factor  $\left(\frac{s+1}{s-1}\right)^{a^\dagger a}$  is negative for  $s < 1$ , and positivity is guaranteed only for products of positive operators. On the other hand, from Eq. (A.11) one can easily see that there is always a state (the eigenstate of  $a^\dagger a$  with odd eigenvalue) that makes the  $s$ -Wigner function at  $\alpha = 0$  negative for  $s < 0$ .

### A.3 Differential Wigner representations

The representations (A.9,A.10) for the generalized Wigner functions also provide the easiest way to derive differential representations for boson operators acting on a density matrix. By defining, analogously to Eq. (A.1), the generalized *Wigner symbol* for any operator  $\hat{O}$ ,

$$W_s(\alpha, \bar{\alpha} | \hat{O}) \doteq \int \frac{d^2\lambda}{\pi^2} e^{\alpha\bar{\lambda} - \bar{\alpha}\lambda + \frac{s}{2}|\lambda|^2} \text{Tr}[D(\lambda)\hat{O}], \quad (\text{A.19})$$

from Eqs. (A.9,A.10) one immediately derives the relations

$$\begin{aligned}
W_s(\alpha, \bar{\alpha} | a\hat{\rho}) &= e^{-\frac{2}{1-s}|\alpha|^2} \frac{1-s}{2} \partial_{\bar{\alpha}} e^{\frac{2}{1-s}|\alpha|^2} W_s(\alpha, \bar{\alpha}), \\
&= \left( \alpha + \frac{1-s}{2} \partial_{\bar{\alpha}} \right) W_s(\alpha, \bar{\alpha}) \quad (\text{A.20})
\end{aligned}$$

$$\begin{aligned}
W_s(\alpha, \bar{\alpha} | a^\dagger \hat{\rho}) &= e^{\frac{2}{1+s}|\alpha|^2} \left( -\frac{1+s}{2} \partial_\alpha \right) e^{-\frac{2}{1+s}|\alpha|^2} W_s(\alpha, \bar{\alpha}) \\
&= \left( \bar{\alpha} - \frac{1+s}{2} \partial_\alpha \right) W_s(\alpha, \bar{\alpha}), \tag{A.21}
\end{aligned}$$

and analogous relations for right multiplication by the boson operator. More generally, one can write a differential representation for any *super-operator*—i.e. right or left multiplication by an operator  $\hat{O}$ —namely

$$W_s(\alpha, \bar{\alpha} | \hat{O} \hat{\rho}) \doteq F_s[\hat{O} \cdot] W_s(\alpha, \bar{\alpha}), \quad W_s(\alpha, \bar{\alpha} | \hat{\rho} \hat{O}) \doteq F_s[\cdot \hat{O}] W_s(\alpha, \bar{\alpha}), \tag{A.22}$$

where  $\hat{O} \cdot$  and  $\cdot \hat{O}$  denote left and right multiplication by the operator  $\hat{O}$ , respectively, and  $F_s$  are differential forms functions of  $\alpha$ ,  $\bar{\alpha}$ ,  $\partial_\alpha$  and  $\partial_{\bar{\alpha}}$  with the following properties

$$F_s[\hat{O}_1 \hat{O}_2 \cdot] = F_s[\hat{O}_1 \cdot] F_s[\hat{O}_2 \cdot], \tag{A.23}$$

$$F_s[\cdot \hat{O}_1 \hat{O}_2] = F_s[\cdot \hat{O}_2] F_s[\cdot \hat{O}_1]. \tag{A.24}$$

$$[F_s[\cdot \hat{O}_1], F_s[\hat{O}_2 \cdot]] = 0, \tag{A.25}$$

$$F_s[\cdot \hat{O}] = \bar{F}_s[\hat{O}^\dagger \cdot]. \tag{A.26}$$

The functional forms of the basic super-operators are summarized in Table A.1. The representations of  $\cdot a^\dagger$  and  $\cdot a$  can be easily obtained from those of  $a \cdot$  and  $a^\dagger \cdot$  using identities (A.26). Eq. (A.25) is just the obvious statement that “left multiplication commutes with right multiplication” (for  $a$  and  $a^\dagger$  this corresponds to the identity  $[\partial_\alpha + \kappa \bar{\alpha}, \partial_{\bar{\alpha}} + \kappa \alpha] = 0$ ). Then, the differential representation of higher-order super-

Super-operator	$F_s$
$a \cdot$	$\alpha + \frac{1-s}{2} \partial_{\bar{\alpha}}$
$a^\dagger \cdot$	$\bar{\alpha} - \frac{1+s}{2} \partial_\alpha$
$\cdot a$	$\alpha - \frac{1+s}{2} \partial_{\bar{\alpha}}$
$\cdot a^\dagger$	$\bar{\alpha} + \frac{1-s}{2} \partial_\alpha$
$a \cdot a^\dagger$	$ \alpha ^2 + \frac{1-s}{2}(1 + \alpha \partial_\alpha + \bar{\alpha} \partial_{\bar{\alpha}}) + \left(\frac{1-s}{2}\right)^2 \partial_{\alpha \bar{\alpha}}$
$a^\dagger \cdot a$	$ \alpha ^2 - \frac{1+s}{2}(1 + \alpha \partial_\alpha + \bar{\alpha} \partial_{\bar{\alpha}}) + \left(\frac{1+s}{2}\right)^2 \partial_{\alpha \bar{\alpha}}$
$a^\dagger a \cdot$	$ \alpha ^2 + \frac{1}{2}[(1-s)\bar{\alpha} \partial_{\bar{\alpha}} - (1+s)\alpha \partial_\alpha - (1+s) - \frac{1}{2}(1-s^2)\partial_{\alpha \bar{\alpha}}]$
$\cdot a^\dagger a$	$ \alpha ^2 + \frac{1}{2}[(1-s)\alpha \partial_\alpha - (1+s)\bar{\alpha} \partial_{\bar{\alpha}} - (1+s) - \frac{1}{2}(1-s^2)\partial_{\alpha \bar{\alpha}}]$

Table A.1: Differential Wigner representation of some super-operators

operators is easily obtained from the composition rules (A.23) and (A.24).

Using the differential representation for Bose super-operators, one can convert master equations into (possibly high order) Fokker-Planck equations. For example, the

master equation of the damped harmonic oscillator (damping coefficient  $\gamma$  and thermal photons  $\bar{n}$ )

$$\partial_t \hat{\rho} = -\frac{\gamma}{2}(\bar{n} + 1)(a^\dagger a \hat{\rho} + \hat{\rho} a^\dagger a - 2a \hat{\rho} a^\dagger) - \frac{\gamma}{2}\bar{n}(a a^\dagger \hat{\rho} + \hat{\rho} a a^\dagger - 2a^\dagger \hat{\rho} a), \quad (\text{A.27})$$

can be converted into the equivalent Fokker-Planck equation for the  $s$ -ordered Wigner function

$$\partial_t W_s(\alpha, \bar{\alpha}) = \frac{\gamma}{2} [\partial_\alpha \alpha + \partial_{\bar{\alpha}} \bar{\alpha} + (2\bar{n} + 1 - s) \partial_{\alpha \bar{\alpha}}] W_s(\alpha, \bar{\alpha}). \quad (\text{A.28})$$

In order to solve Fokker-Planck equations, one can use very efficient Monte-Carlo Green-function simulation methods (see, for example, Ref. [162]), choosing the parameter  $s$  such that both the Wigner function and the diffusion coefficient remain positive during the evolution. Then, from the inversion Eq. (A.14) one can recover the matrix elements  $\langle n | \hat{\rho} | m \rangle$  of the operator  $\hat{\rho}$  in form of Monte-Carlo integrals of Laguerre polynomials.

In conclusion, we have presented simple trace formulas that connect the generalized Wigner functions with the density matrix, and *vice-versa*, and we have shown how they can be practically used for: *i*) studying positivity of the generalized Wigner functions; *ii*) connecting master equations with Fokker-Planck equations; *iii*) evaluating the quantum state in Monte Carlo simulations of Fokker-Planck equations.

### Proof of identity (A.15)

From the relation

$$\left. \frac{\partial_\alpha^n \partial_{\bar{\alpha}}^m}{\alpha = \bar{\alpha} = 0} \right| e^{|\alpha|^2} = \delta_{nm} n!, \quad (\text{A.29})$$

one has

$$\begin{aligned} e^{a^\dagger \partial_{\bar{\alpha}}} |0\rangle \langle 0| e^{a \partial_\alpha} \left| e^{|\alpha|^2} \right|_{\alpha = \bar{\alpha} = 0} &= \sum_{n,m=0}^{\infty} (a^\dagger)^n |0\rangle \langle 0| a^m \left. \frac{\partial_\alpha^n \partial_{\bar{\alpha}}^m}{n! m!} \right|_{\alpha = \bar{\alpha} = 0} e^{|\alpha|^2} \\ &= \sum_{n=0}^{\infty} (a^\dagger)^n |0\rangle \langle 0| a^n \frac{1}{n!} = \sum_{n=0}^{\infty} |n\rangle \langle n| = \hat{1}. \end{aligned} \quad (\text{A.30})$$

Hence, using the identities

$$e^{a^\dagger \partial_{\bar{\alpha}}} e^{\bar{\alpha} \lambda} = e^{\lambda(a^\dagger + \bar{\alpha})} e^{a^\dagger \partial_{\bar{\alpha}}}, \quad e^{a \partial_\alpha} e^{-\alpha \bar{\lambda}} = e^{-\bar{\lambda}(a + \alpha)} e^{a \partial_\alpha}, \quad (\text{A.31})$$

one obtains

$$\begin{aligned} e^{a^\dagger \partial_{\bar{\alpha}}} |0\rangle \langle 0| e^{a \partial_\alpha} \left| e^{|\alpha|^2 + \bar{\alpha} \lambda - \alpha \bar{\lambda} - \frac{1}{2} |\lambda|^2} \right|_{\alpha = \bar{\alpha} = 0} \\ = e^{-\frac{1}{2} |\lambda|^2} e^{\bar{\alpha} \lambda - \alpha \bar{\lambda}} e^{a^\dagger \lambda} e^{a^\dagger \partial_{\bar{\alpha}}} |0\rangle \langle 0| e^{a \partial_\alpha} \left| e^{|\alpha|^2} e^{-\bar{\lambda} \alpha} \right|_{\alpha = \bar{\alpha} = 0} \\ = e^{-\frac{1}{2} |\lambda|^2} e^{a^\dagger \lambda} e^{-a \bar{\lambda}} = D(\lambda). \end{aligned} \quad (\text{A.32})$$



## Appendix B

# On the correspondence between classical and quantum measurements

### B.1 Introduction

In the standard formulation of Quantum Mechanics an abstract concept of physical observable is formulated in terms of real eigenvalues and sharp probability distributions, which leads to the well known correspondence between observables and self-adjoint operators on the Hilbert space [106]. A natural extension of this formulation is based on the general concept of positive operator-valued measure (POM) [163, 47], which allows the description of joint measurements of non-commuting observables, with generally complex eigenvalues and probability distributions that are not sharp for any quantum state. From an operational point of view, however, we have no prescription on how to achieve the ideal quantum measurement (i.e. with minimum noise) of a generic operator, and the problem of finding a *universal detector* is still an open one. Quantum homodyne tomography—the only known method for measuring the state itself of the field—can also be regarded as a kind of universal detection [139], however it is far from being ideal, due to the occurrence of statistical measurement errors that are intrinsic of the method.

In this appendix we study the possibility of achieving the ideal measurement of an observable  $\hat{O} = \hat{O}(a, a^\dagger)$  of one mode of the electromagnetic field by means of a fixed detection scheme—the heterodyne detector—after ideal preamplification  $\hat{O} \rightarrow g\hat{O}$  of the observable  $\hat{O}$ ,  $g$  denoting the amplifier gain, seeking a connection between the problem of measuring  $\hat{O}$  and that of amplifying  $\hat{O}$  ideally. As heterodyne detection corresponds to the ideal joint measurement of the canonical pair  $\hat{q} = \frac{1}{2}(a^\dagger + a)$  and  $\hat{p} = \frac{i}{2}(a^\dagger - a)$  of a harmonic oscillator in the phase space, in this way we also try to set

a link between classical and quantum measurements. We will give a necessary and sufficient condition that establishes when the preamplified-heterodyne detection scheme approaches the ideal quantum measurement of  $\hat{O}$  in the limit of infinite gain. We show that such condition is satisfied for the photon number operator  $a^\dagger a$ —corresponding to the function  $f(\alpha, \bar{\alpha}) = |\alpha|^2$  of the heterodyne outcome  $\alpha \in \mathbb{C}$ —and for the quadrature operator  $\hat{X}_\phi = (a^\dagger e^{i\phi} + a e^{-i\phi})/2$ —corresponding to the function  $f(\alpha, \bar{\alpha}) = \text{Re}(\alpha e^{-i\phi})$ . For the photon number operator  $a^\dagger a$  the amplification scheme also achieves the transition from the continuous spectrum  $|\alpha|^2 \in \mathbb{R}$  to the discrete spectrum  $\mathbb{S}_{a^\dagger a} \equiv \mathbb{N}$  of  $a^\dagger a$ . Moreover, for both operators  $a^\dagger a$  and  $\hat{X}_\phi$  the method is also robust to nonunit quantum efficiency of the heterodyne detector. On the other hand, we will see that the preamplified-heterodyne scheme does not work for arbitrary observable of the field. As a counterexample, we show that, unexpectedly, the simple quadratic function of the field  $\hat{K} = i(a^{\dagger 2} - a^2)/2$  has no corresponding polynomial function  $f(\alpha, \bar{\alpha})$ —including the obvious choice  $f = \text{Im}(\alpha^2)$ —which allows the measurement of  $\hat{K}$  through the preamplified-heterodyne measurement scheme.

## B.2 Heterodyne detection

In the following we derive the POM of the heterodyne measurement of a function  $f$  of the field, for generally nonunit quantum efficiency.

Heterodyne detection corresponds to measuring the complex field  $\hat{Z} = a + b^\dagger$ ,  $a$  and  $b$  denoting the signal and the image-band modes of the detector, respectively. The measurement is an exact joint measurement of the commuting observables  $\text{Re } \hat{Z}$  and  $\text{Im } \hat{Z}$ , but can also be regarded as the joint measurement of the non commuting operators  $\text{Re } a$  and  $\text{Im } a$ , by considering the image-band mode in the vacuum state. In this way the vacuum fluctuations of  $b$  introduce an additional 3dB noise, which can be proved to be the minimum added noise in an ideal joint measurement of a conjugated pair of non commuting observables [66].

The probability density in the complex plane  $p(\alpha, \bar{\alpha})$  for heterodyne detection is given by the Fourier transform of the generating function of the moments of  $\hat{Z}$ , namely

$$p(\alpha, \bar{\alpha}) = \int \frac{d^2 \lambda}{\pi^2} \langle e^{\lambda \hat{Z}^\dagger - \bar{\lambda} \hat{Z}} \rangle e^{\bar{\lambda} \alpha - \lambda \bar{\alpha}} \doteq \langle \delta^{(2)}(\alpha - \hat{Z}) \rangle, \quad (\text{B.1})$$

where the overbar denotes the complex conjugate,  $d^2 \lambda = d\text{Re } \lambda d\text{Im } \lambda$ ,  $\langle \dots \rangle$  represents the ensemble quantum average on both signal and image-band modes, and  $\delta^{(2)}(\alpha)$  is the Dirac delta-function in the complex plane. The partial trace over the image-band mode in Eq. (B.1) can be evaluated as follows

$$\begin{aligned} \langle e^{\lambda \hat{Z}^\dagger - \bar{\lambda} \hat{Z}} \rangle &= \text{Tr}_a \left[ \hat{\rho} \hat{D}_a(\lambda) \right] {}_b \langle 0 | \hat{D}_b(-\bar{\lambda}) | 0 \rangle_b = \text{Tr}_a \left[ \hat{\rho} \hat{D}_a(\lambda) \right] e^{-\frac{1}{2} |\lambda|^2} \\ &\doteq \text{Tr}_a \left[ \hat{\rho} : \hat{D}_a(\lambda) :_A \right], \end{aligned} \quad (\text{B.2})$$

where  $\hat{D}(\alpha) = \exp(\alpha a^\dagger - \bar{\alpha} a)$  denotes the displacement operator ( $\hat{D}_a$  for mode  $a$  and  $\hat{D}_b$  for mode  $b$ ),  $|0\rangle_b$  represents the vacuum for mode  $b$  only,  $\hat{\rho}$  is the density matrix for the signal mode, and  $: :_A$  denotes anti-normal ordering. The probability density *vs* the outcome  $\alpha$  is given by

$$d^2\alpha p(\alpha, \bar{\alpha}) = \text{Tr} [\hat{\rho} d\hat{\mu}(\alpha, \bar{\alpha})] , \quad (\text{B.3})$$

where POM  $d\hat{\mu}(\alpha, \bar{\alpha})$  can be written as follows

$$\begin{aligned} d\hat{\mu}(\alpha, \bar{\alpha}) &= d^2\alpha \int \frac{d^2\lambda}{\pi^2} e^{\bar{\lambda}\alpha - \lambda\bar{\alpha}} : \hat{D}(\lambda) :_A \\ &= d^2\alpha \int \frac{d^2\beta}{\pi} \int \frac{d^2\lambda}{\pi^2} e^{\bar{\lambda}(\alpha-\beta) - \lambda(\bar{\alpha}-\bar{\beta})} |\beta\rangle\langle\beta| \\ &= \frac{d^2\alpha}{\pi} |\alpha\rangle\langle\alpha| \doteq d^2\alpha : \delta^{(2)}(\alpha - a) :_A , \end{aligned} \quad (\text{B.4})$$

using the resolution of the identity in terms of coherent states  $\hat{1} = \int \frac{d^2\beta}{\pi} |\beta\rangle\langle\beta|$ .

In a ‘‘classical’’ measurement of the function  $w = f(\alpha, \bar{\alpha})$  on the phase space, one evaluates the function  $f$  of the outcome  $\alpha$  of the complex photocurrent  $\hat{Z}$ . Correspondingly, the probability distribution of  $w$  is given by the marginal probability density

$$p(w) = \int d^2\alpha p(\alpha, \bar{\alpha}) \delta(w - f(\alpha, \bar{\alpha})) . \quad (\text{B.5})$$

The POM  $d\hat{H}_f(w)$  that provides such probability density is the marginal POM of  $d\hat{\mu}(\alpha, \bar{\alpha})$ , and can be written as follows

$$d\hat{H}_f(w) = dw \int d\hat{\mu}(\alpha, \bar{\alpha}) \delta(w - f(\alpha, \bar{\alpha})) = dw : \delta(w - f(a, a^\dagger)) :_A . \quad (\text{B.6})$$

In this way one has a correspondence rule between POM’s  $d\hat{H}_f(w)$  and classical observables  $w = f(\alpha, \bar{\alpha})$  on the phase space  $\alpha \in \mathbb{C}$ .

The quantum efficiency  $\eta$  of the heterodyne detector can be taken into account by introducing auxiliary vacuum field modes for both the signal and the idler, and by rescaling the output photocurrent by an additional factor  $\eta^{1/2}$ . The overall effect resorts to a Gaussian convolution of the ideal POM with variance  $\Delta_\eta^2 = (1 - \eta)/\eta$ . Then, the POM in Eq. (B.6) rewrites

$$d\hat{H}_f(w) = dw \Gamma_{\frac{1-\eta}{\eta}} \left[ : \delta(w - f(a, a^\dagger)) :_A \right] , \quad (\text{B.7})$$

where  $\Gamma_{\sigma^2}$  denotes the completely positive (CP) map that describes the effect of additional Gaussian noise of variance  $\sigma^2$ , namely

$$\Gamma_{\sigma^2}[\hat{A}] = \int \frac{d^2\beta}{\pi\sigma^2} e^{-\frac{|\beta|^2}{\sigma^2}} \hat{D}(\beta) \hat{A} \hat{D}^\dagger(\beta) , \quad (\text{B.8})$$

for any operator  $\hat{A}$ . We do not know *a priori* if the measurement described by the POM in Eq. (B.6) or (B.7) corresponds to an approximate quantum measurement of

some observable of the field. We can argue that, for example, for  $f(\alpha, \bar{\alpha}) = |\alpha|^2$  the measurement would approximate the ideal detection of the number of photons  $a^\dagger a$ . In the following we give a necessary and sufficient condition to establish when the heterodyne POM  $d\hat{H}_f(w)$  approaches the ideal quantum measurement of an observable  $\hat{O}$  by preamplifying the heterodyne through an ideal amplifier of  $\hat{O}$  in the limit of infinite amplifier gain. In the following section we introduce the general concept of ideal amplification of an observable, and prove that it can be always achieved by a unitary transformation.

### B.3 Ideal amplification of quantum observables

For a given selfadjoint operator  $\hat{W}$ , the *ideal amplifier* of  $\hat{W}$  is a device that achieves the transformation

$$\mathcal{A}_g^{(\hat{W})}(\hat{W}) = g\hat{W}, \quad (\text{B.9})$$

where  $g > 1$  denotes the gain of the amplifier. The transformation (B.9) is to be regarded as the Heisenberg-picture evolution of the field throughout the device when the transformation is applied to  $\hat{W}$ . If the spectrum  $\mathbb{S}_{\hat{W}}$  of  $\hat{W}$  is  $\mathbb{S}_{\hat{W}} = \mathbb{R}$  or  $\mathbb{S}_{\hat{W}} = \mathbb{R}^+$ , the evolution  $\mathcal{A}_g^{(\hat{W})}$  can be written as follows

$$\mathcal{A}_g^{(\hat{W})}(|w\rangle\langle w|) = g^{-1}|g^{-1}w\rangle\langle g^{-1}w|, \quad (\text{B.10})$$

where  $|w\rangle$  denotes the eigenvector of  $\hat{W}$  pertaining to the eigenvalue  $w \in \mathbb{S}_{\hat{W}}$ . The corresponding Schrödinger-picture of the evolution (B.10) is given by the dual map

$$\mathcal{A}_g^{\vee(\hat{W})}(|w\rangle\langle w|) = g|gw\rangle\langle gw|, \quad (\text{B.11})$$

where  $|w\rangle$  now has to be regarded as a (Dirac-sense) normalized state vector. For integer spectrum  $\mathbb{S}_{\hat{W}} = \mathbb{N}$  or  $\mathbb{S}_{\hat{W}} = \mathbb{Z}$  Eq. (B.10) rewrites as follows

$$\mathcal{A}_g^{(\hat{W})}(|n\rangle\langle n|) = |g^{-1}n\rangle\langle g^{-1}n| \chi_{\mathbb{Z}}(g^{-1}n), \quad (\text{B.12})$$

where  $\chi_{\mathbb{Z}}(x)$  is the characteristic function on integers, namely  $\chi_{\mathbb{Z}}(x) = 1$  for  $x \in \mathbb{Z}$ ,  $\chi_{\mathbb{Z}}(x) = 0$  otherwise. It is easy to check that both Eq. (B.10) and (B.12) imply Eq. (B.9). In the following we will consider only the cases of spectra  $\mathbb{S}_{\hat{W}} = \mathbb{R}, \mathbb{R}^+, \mathbb{N}, \mathbb{Z}$ , as these are the only ones that are left invariant under amplification, i.e.  $g\mathbb{S}_{\hat{W}} \subset \mathbb{S}_{\hat{W}}$  (this will exclude, for example, the case of phase amplification). Moreover, for the sake of notation, if not explicitly written, we will assume  $\mathbb{S}_{\hat{W}} = \mathbb{R}$ .

Among all possible extensions of the amplification map (B.11) to all state vectors, the following ones are physically meaningful

$$\mathcal{A}_g^{\vee(\hat{W})}(|w\rangle\langle w'|) = g|gw\rangle\langle gw'|, \quad (\text{B.13})$$

$$\mathcal{A}_g^{\vee(\hat{W})}(|w\rangle\langle w'|) = g|gw\rangle\langle gw'| \delta(w - w'). \quad (\text{B.14})$$

In fact, both maps in Eqs. (B.13) and (B.14) are linear normal *completely positive* (CP) maps, and hence they can be realized through a unitary transformations on an extended Hilbert space [164]. The proof runs as follows. The map  $A$  is completely positive normal if and only if one has

$$\sum_{i,j=1}^n \langle \xi_i | A^\vee(|\eta_i\rangle\langle\eta_j|) | \xi_j \rangle \geq 0 \quad (\text{B.15})$$

for all finite sequence of vectors  $\{|\eta_i\rangle\}$  and  $\{|\xi_i\rangle\}$ . Upon expanding  $|\eta_i\rangle$  and  $|\xi_i\rangle$  on the orthonormal basis  $\{|w\rangle\}$ , for the map (B.13) one has

$$\begin{aligned} & \sum_{i,j=1}^n \langle \xi_i | A_g^{\vee(\hat{W})}(|\eta_i\rangle\langle\eta_j|) | \xi_j \rangle \\ &= g \int dw_1 dw_2 dw_3 dw_4 \langle w_1 | gw_2 \rangle \langle gw_3 | w_4 \rangle \sum_{i,j=1}^n \bar{\xi}_i(w_1) \eta_i(w_2) \bar{\eta}_j(w_3) \xi_j(w_4) \\ &= g \left| \sum_{i=1}^n \int dw dw' \langle w | gw' \rangle \bar{\xi}_i(w) \eta_i(w') \right|^2 \geq 0, \end{aligned} \quad (\text{B.16})$$

whereas for the map (B.14) one has

$$\begin{aligned} & \sum_{i,j=1}^n \langle \xi_i | A_g^{\vee(\hat{W})}(|\eta_i\rangle\langle\eta_j|) | \xi_j \rangle \\ &= g \int_{-\infty}^{+\infty} \frac{d\lambda}{2\pi} \left| \sum_{i=1}^n \int dw dw' \langle w | gw' \rangle \bar{\xi}_i(w) \eta_i(w') e^{i\lambda w'} \right|^2 \geq 0. \end{aligned} \quad (\text{B.17})$$

In the Schrödinger picture the two maps (B.13) and (B.14) are achieved by the following unitary transformations in an extended Hilbert space

$$\hat{U}_g |w\rangle \otimes |\psi\rangle = g^{\frac{1}{2}} |gw\rangle \otimes |\psi'\rangle \quad (\text{B.18})$$

$$\hat{U}_g |w\rangle \otimes |\psi\rangle = g^{\frac{1}{2}} |gw\rangle \otimes |\psi'(w)\rangle. \quad (\text{B.19})$$

with  $\langle \psi'(w_1) | \psi'(w_2) \rangle = \delta(w_1 - w_2)$ . Eqs. (B.13) and (B.14) are obtained by Eqs. (B.18) and (B.19) when the evolution is viewed as restricted to the signal mode only, namely

$$\mathcal{A}_g^{\vee(\hat{W})}(\hat{\rho}) = \langle \psi | \hat{U}_g \hat{\rho} \otimes 1 \hat{U}_g^\dagger | \psi \rangle. \quad (\text{B.20})$$

We name the device corresponding to Eq. (B.18) an *ideal coherence-preserving quantum amplifier* of  $\hat{W}$ , because it achieves the ideal amplification of  $\hat{W}$  without measuring  $\hat{W}$  ( $\psi'$  does not depend on  $w$ ; for  $\psi' = \psi$  the device is “passive”). On the other hand, the transformation (B.19) achieves the ideal amplification of  $\hat{W}$  by measuring  $\hat{W}$ , then performing the processing  $w \rightarrow gw$ , and finally preparing the state  $|gw\rangle$ . The measurement stage is the one which is responsible for the vanishing of all off-diagonal

elements in Eq. (B.14). (Eq. (B.20) together with Eq. (B.18) and (B.19) imply Eqs. (B.13) and (B.14) also for a nonorthogonal set  $\{|w\rangle\}$ , however, generally not when  $\langle\psi'_A(w_2)|\psi'_A(w_1)\rangle \neq 0$  for  $w_1 \neq w_2$ ). Since we want to exploit the ideal amplification of  $\hat{W}$  in order to achieve its ideal quantum measurement, we will consider only the coherence-preserving quantum amplification in Eq. (B.13) or (B.18), since the other kind of amplifier needs by itself the ideal measurement of  $\hat{W}$ .

## B.4 Approaching ideal quantum measurements by preamplified heterodyning

Let  $d\hat{H}_f(u)$  be the POM pertaining to the heterodyne measurement of the function  $f(\alpha, \bar{\alpha})$  of the field, and let consider a preamplified-heterodyne detection scheme corresponding to the following procedure:

1. the signal mode of the field is amplified by an ideal amplifier for  $\hat{W}$  with gain  $g$ ;
2. the field is heterodyne detected and the function  $f$  is evaluated;
3. the final result is rescaled by a factor  $g$ .

The above procedure corresponds to the following transformation

$$d\hat{H}_f(u) \longrightarrow \mathcal{A}_g^{(\hat{W})}[d\hat{H}_f(gu)] . \quad (\text{B.21})$$

We say that the preamplified heterodyne detection of the function  $f$  of the field approaches the ideal quantum measurement of the observable  $\hat{W}$  in the limit of infinite gain  $g$  if

$$\lim_{g \rightarrow \infty} \mathcal{A}_g^{(\hat{W})}[d\hat{H}_f(gu)] = du \delta(u - \hat{W}) , \quad (\text{B.22})$$

where the limit is to be regarded in the weak sense (i.e. for matrix elements) and the operator Dirac delta explicitly writes as follows

$$\delta(u - \hat{W}) = \int_{\mathbb{S}_{\hat{W}}} dw |w\rangle \langle w| \delta(u - w) , \quad (\text{B.23})$$

and the integral is to be understood as a sum for discrete spectrum  $\mathbb{S}_{\hat{W}}$ . A necessary and sufficient condition for validity of Eq. (B.22) is the following

$$\lim_{g \rightarrow \infty} \int \mathcal{A}_g^{(\hat{W})}[d\hat{H}_f(gu)] u^l = \hat{W}^l , \quad l = 0, 1, 2, \dots , \quad (\text{B.24})$$

where again the limit holds for expectations on any state. One can prove that condition (B.24) is necessary—i.e. Eq. (B.22) implies Eq. (B.24)—by simply substituting Eq.

(B.22) into Eq. (B.24), and exchanging the integral with the limit. On the other hand Eq. (B.24) implies

$$\lim_{g \rightarrow \infty} \int \mathcal{A}_g^{(\hat{W})} [d\hat{H}_f(gu)] \exp(iku) = \exp(ik\hat{W}), \quad (\text{B.25})$$

and taking the Fourier transform of both sides of the last identity one finds Eq. (B.22), proving that Eq. (B.24) is also a sufficient condition. Another sufficient condition in a form more convenient than Eq. (B.24) is the following

$$\int d\hat{H}_f(u) u^l = \hat{W}^l + o(\hat{W}^l), \quad (\text{B.26})$$

where  $o(g(x))$  is an asymptotic notation equivalent to the vanishing of the limit [165]

$$\lim_{x \rightarrow \infty} o(g(x))/g(x) = 0,$$

whereas, for an operator  $\hat{V}$ , by  $o(\hat{V})$  we mean

$$\lim_{\kappa \rightarrow \infty} \kappa^{-1} o(\kappa \hat{V}) = 0$$

in the weak sense. In fact, by amplifying both sides of Eq. (B.26) and rescaling the variable  $u$  by the gain  $g$  one obtains

$$\int \mathcal{A}_g^{(\hat{W})} [d\hat{H}_f(gu)] u^l = \hat{W}^l + g^{-l} o(g^l \hat{W}^l), \quad (\text{B.27})$$

which implies Eq. (B.24).

## B.5 Two examples

In this section we show that condition (B.24) holds for both the photon number  $\hat{W} = a^\dagger a$  and the quadrature  $W = \text{Re}(a e^{-i\phi})$ , corresponding to the functions of the field  $f(\alpha, \bar{\alpha}) = |\alpha|^2$  and  $f(\alpha, \bar{\alpha}) = \text{Re}(\alpha e^{-i\phi})$  respectively. This means that both the quadrature and the photon number operators can be ideally measured through the preamplified-heterodyne detection scheme in the limit of infinite gain. We also show that in both cases the detection scheme is robust to nonunit quantum efficiency of the heterodyne detector.

### B.5.1 Measurement of the quadrature

The POM  $d\hat{H}(x)$  that corresponds to the function  $f(\alpha, \bar{\alpha}) = \text{Re}(\alpha e^{-i\phi})$  of the field is given by

$$\begin{aligned} d\hat{H}_f(x) &= dx : \delta \left( x - \frac{1}{2} (a^\dagger e^{i\phi} + a e^{-i\phi}) \right) :_A = dx \int \frac{du}{2\pi} e^{iu(x - \hat{X}_\phi)} e^{-\frac{1}{8}u^2} \\ &= dx \sqrt{\frac{2}{\pi}} e^{-2(\hat{X}_\phi - x)^2}. \end{aligned} \quad (\text{B.28})$$

Nonunit quantum efficiency introduces additive Gaussian noise and replaces the POM (B.28) with the following one

$$d\hat{H}_f(x) = dx \sqrt{\frac{2\eta}{\pi(2-\eta)}} e^{-\frac{2\eta}{2-\eta}(\hat{X}_\phi - x)^2}. \quad (\text{B.29})$$

We can see that the POM in Eq. (B.29) satisfies the sufficient condition (B.26) for approaching the ideal quantum measurement of  $\hat{X}_\phi$ . In fact, the moments of the POM (B.29) are given by

$$\int d\hat{H}_f(x) x^l = \int_{-\infty}^{+\infty} dx \sqrt{\frac{2\eta}{\pi(2-\eta)}} e^{-\frac{2\eta}{2-\eta}x^2} (\hat{X}_\phi + x)^l = \hat{X}_\phi^l + O(\hat{X}_\phi^{l-2}), \quad (\text{B.30})$$

where  $O(g(x))$  is the customary asymptotic notation equivalent to the condition [165]

$$\lim_{x \rightarrow \infty} O(g(x))/g(x) < \infty,$$

implying that  $O(\hat{X}^{l-2}) \equiv o(\hat{X}^l)$ . On the other hand, one can directly verify the limit in Eq. (B.22) as follows

$$\mathcal{A}_g^{\hat{X}_\phi} [d\hat{H}_f(gx)] = dx \sqrt{\frac{2g^2\eta}{\pi(2-\eta)}} e^{-\frac{2g^2\eta}{2-\eta}(\hat{X}_\phi - gx)^2} \xrightarrow{g \rightarrow \infty} dx \delta(\hat{X}_\phi - x). \quad (\text{B.31})$$

The ideal amplification of the quadrature operator  $\hat{X}_\phi$  is achieved by means of a phase-sensitive amplifier [166] which rescales the couple of conjugated quadratures as follows

$$\hat{X}_\phi \rightarrow \frac{1}{g} \hat{X}_\phi, \quad \hat{X}_{\phi+\frac{\pi}{2}} \rightarrow g \hat{X}_{\phi+\frac{\pi}{2}}, \quad (\text{B.32})$$

$g$  being the gain at the amplifier. The Heisenberg transformations in Eq. (B.32) are achieved by the unitary operator

$$\hat{U}_g = \exp[-i \log g (\hat{X}_\phi \hat{X}_{\phi+\frac{\pi}{2}} - \hat{X}_{\phi+\frac{\pi}{2}} \hat{X}_\phi)]. \quad (\text{B.33})$$

### B.5.2 Measurement of the photon number

The case of the ideal measurement of the photon number  $a^\dagger a$  through preamplified-heterodyning is more interesting than the case of the quadrature  $\hat{X}_\phi$ , because here the amplification not only removes the excess noise due to the quantum measurement, but also changes the spectrum, from continuous to discrete. We consider the POM that corresponds to heterodyning the function  $f(\alpha, \bar{\alpha}) = |\alpha|^2$  of the field. This can be written as follows

$$d\hat{H}_f(h) = dh : \delta(h - a^\dagger a) :_A = dh \int \frac{du}{2\pi} e^{-iuh} \sum_{n=0}^{\infty} (iu)^n a^n a^{\dagger n}$$

$$\begin{aligned}
&= dh \int \frac{du}{2\pi} e^{-iuh} \sum_{n=0}^{\infty} (iu)^n \binom{a^\dagger a + n}{n} = dh \int \frac{du}{2\pi} e^{-iuh} (1 - iu)^{-a^\dagger a - 1} \\
&= dh e^{-h} \frac{h^{a^\dagger a}}{(a^\dagger a)!}.
\end{aligned} \tag{B.34}$$

The POM in Eq. (B.34) satisfies the sufficient condition (B.26). In fact, one has

$$\int dh e^{-h} \frac{h^{a^\dagger a + l}}{(a^\dagger a)!} = \frac{(a^\dagger a + l)!}{(a^\dagger a)!} = (-)^l \sum_{k=0}^l s_{l+1}^{(k+1)} (-a^\dagger a)^k = (a^\dagger a)^l + O[(a^\dagger a)^{l-1}], \tag{B.35}$$

where  $s_l^{(k)}$  denotes a Stirling number of the first kind. Hence, if the field is amplified through an ideal photon number amplifier [167, 168, 114] and then heterodyne detected, in the limit of infinite gain the scheme achieves ideal photon number detection. Indeed, using the ideal photon number amplification map [169, 51]

$$a^\dagger a \longrightarrow \hat{V}^\dagger a^\dagger a \hat{V} = g a^\dagger a, \tag{B.36}$$

with the isometry  $\hat{V}$  given by

$$\hat{V} = \sum_{n=0}^{\infty} |gn\rangle \langle n|, \tag{B.37}$$

one obtains the preamplified POM

$$\mathcal{A}_g^{a^\dagger a}[d\hat{H}_f(gh)] = \hat{V}^\dagger d\hat{H}_f(gh) \hat{V} = dh g e^{-gh} \sum_{n=0}^{\infty} \frac{(gh)^{gn}}{(gn)!} |n\rangle \langle n|. \tag{B.38}$$

In the limit of infinite gain  $g \rightarrow \infty$  the POM in Eq. (B.38) achieves the ideal POM for the photon-number operator measurement. This can be shown as follows. Upon writing the POM (B.38) in the form

$$\mathcal{A}_g^{a^\dagger a}[d\hat{H}_f(gh)] = dh \sum_{n=0}^{\infty} p_n^{(g)}(h) |n\rangle \langle n|, \tag{B.39}$$

we need to show that the function

$$p_n^{(g)}(h) = g e^{-gh} \frac{(gh)^{gn}}{(gn)!}, \tag{B.40}$$

approaches a Dirac delta-comb over integer values  $h \in \mathbb{N}$ . Using the Stirling's inequality

$$\sqrt{2\pi n} \left(\frac{n}{e}\right)^n < n! < \sqrt{2\pi n} \left(\frac{n}{e}\right)^n \left(1 + \frac{1}{12n-1}\right), \tag{B.41}$$

one obtains

$$\gamma_n^{(g)}(h) \left(1 + \frac{1}{12gn-1}\right)^{-1} < p_n^{(g)}(h) < \gamma_n^{(g)}(h), \tag{B.42}$$

where

$$\gamma_n^{(g)}(h) = \frac{1}{\sqrt{2\pi g^{-1}n}} \exp \left[ gn \left( 1 - \frac{h}{n} + \log \frac{h}{n} \right) \right]. \quad (\text{B.43})$$

From the inequality  $\log x \leq x - 1$  (with equality iff  $x = 1$ ) it follows that

$$\lim_{g \rightarrow \infty} \gamma_n^{(g)}(h) = \begin{cases} 0 & h \neq n \\ +\infty & h = n \end{cases}, \quad (\text{B.44})$$

and hence, from Eq. (B.42), one has

$$\lim_{g \rightarrow \infty} p_n^{(g)}(h) = \begin{cases} 0 & h \neq n \\ +\infty & h = n \end{cases}. \quad (\text{B.45})$$

Moreover, from the expansion for  $h$  near to  $n$

$$1 - \frac{h}{n} + \log \frac{h}{n} = -\frac{1}{2} \left( 1 - \frac{h}{n} \right)^2 + O \left( \left( 1 - \frac{h}{n} \right)^3 \right), \quad (\text{B.46})$$

one has the Gaussian asymptotic approximation for  $g \rightarrow \infty$

$$p_n^{(g)}(h) \simeq \frac{1}{\sqrt{2\pi g^{-1}n}} \exp \left[ -\frac{(h-n)^2}{2g^{-1}n} \right] \xrightarrow{g \rightarrow \infty} \delta(h-n), \quad (\text{B.47})$$

which proves the statement.

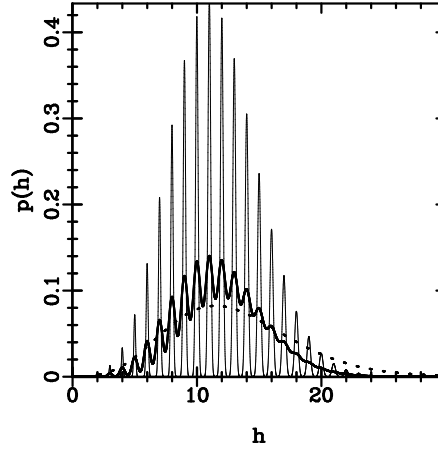


Figure B.1: Probability density  $p(h)$  for a coherent state with mean photon number  $\langle a^\dagger a \rangle = 12$  obtained through heterodyne detection of  $f(\alpha, \bar{\alpha}) = |\alpha|^2$ , preamplified by an ideal photon number amplifier. Different line-style denote different value of the gain  $g$  at the amplifier: the dashed line corresponds to  $g = 1$  (no amplification); the thick line corresponds to  $g = 10^2$ ; the thin line to  $g = 10^3$ .

In Fig. B.1 we show the probability distribution of the outcome  $h = |\alpha|^2$  from preamplified-heterodyne detection of a coherent state, for different values of the amplifier gain  $g$ . Notice the emergence of a discrete spectrum from a continuous one for increasingly large gains, in agreement with Eq. (B.47).

It is easy to show that the preamplified-heterodyne detection scheme is robust to nonunit quantum efficiency also in the present case of measuring  $a^\dagger a$ . In fact, the sufficient condition (B.26) is still satisfied for nonunit quantum efficiency, as one can check through Eqs. (B.8) and (B.35) as follows

$$\begin{aligned}
& \int \frac{d^2\beta}{\pi} \frac{\eta}{1-\eta} e^{-\frac{\eta}{1-\eta}|\beta|^2} \hat{D}(\beta) \left\{ (a^\dagger a)^l + O[(a^\dagger a)^{l-1}] \right\} \hat{D}^\dagger(\beta) \\
&= \int \frac{d^2\beta}{\pi} \frac{\eta}{1-\eta} e^{-\frac{\eta}{1-\eta}|\beta|^2} \left\{ [(a^\dagger - \bar{\beta})(a - \beta)]^l + O[(a^\dagger - \bar{\beta})(a - \beta)^{l-1}] \right\} \\
&= (a^\dagger a)^l + O[(a^\dagger a)^{l-1}].
\end{aligned} \tag{B.48}$$

## B.6 A counterexample

The necessary and sufficient condition (B.24) establishes when a self-adjoint operator  $\hat{W}$  is approximated by the classical observable  $f$  using a preamplified-heterodyne scheme. One could now address the inverse problem, namely: Given a self-adjoint operator  $\hat{W}$  is it possible to find a function of the field such that the preamplified-heterodyne measurement approximates the measurement of  $\hat{W}$ ? As we have shown in the previous section, this is certainly true for  $\hat{X}_\phi$  and  $a^\dagger a$ . For a generic observable  $\hat{W}$ , the problem becomes very difficult. However, on the basis of a counterexample, we will prove that the inverse problem has no solution for some operator  $\hat{W}$ , namely there are observables which cannot be measured through the preamplified-heterodyne detection scheme.

Consider the operator

$$\hat{K} \equiv -\frac{i}{2}(a^2 - a^{\dagger 2}) = \hat{X}\hat{Y} + \hat{Y}\hat{X}, \tag{B.49}$$

where  $\hat{X}$  and  $\hat{Y}$  are the conjugated quadratures  $\hat{X} \equiv \hat{X}_0$  and  $\hat{Y} = \hat{X}_{\pi/2}$ . We show that there is no polynomial function of the field that satisfies either the necessary condition (B.24).

In order to construct the CP amplification map for  $\hat{K}$ , one has to find the eigenstates of  $\hat{K}$ . These are given in Ref. [170], and here we report them. One has

$$\hat{K}|\psi_\pm^\mu\rangle = \mu|\psi_\pm^\mu\rangle, \tag{B.50}$$

with

$$\psi_\pm^\mu(x) \doteq \langle x|\psi_\pm^\mu\rangle = \frac{1}{\sqrt{2\pi}} |x|^{i\mu-\frac{1}{2}} \theta(\pm x), \tag{B.51}$$

where  $|x\rangle$  denotes the eigenvector of the quadrature  $\hat{X}$ , and  $\theta(x)$  is the customary step-function ( $\theta(x) = 1$  for  $x > 0$ ,  $\theta(x) = 1/2$  for  $x = 0$ ,  $\theta(x) = 0$  for  $x < 0$ ). The vectors  $|\psi_s^\mu\rangle$  form a complete orthonormal set

$$\langle \psi_r^\mu | \psi_s^\nu \rangle = \delta_{rs} \delta(\mu - \nu). \tag{B.52}$$

The amplification of  $\hat{K}$  is achieved by the unitary operator  $\hat{U}_g$  satisfying the relations

$$\hat{U}_g^\dagger \hat{K} \hat{U}_g = g\hat{K}, \quad \hat{U}_g |\psi_s^\mu\rangle = g^{\frac{1}{2}} |\psi_s^{g\mu}\rangle. \quad (\text{B.53})$$

In terms of the eigenvectors of  $\hat{K}$  the unitary operator  $\hat{U}_g$  has the form

$$\hat{U}_g = \sum_{s=\pm} \int_{-\infty}^{+\infty} d\mu g^{\frac{1}{2}} |\psi_s^{g\mu}\rangle \langle \psi_s^\mu| = g^{\frac{1}{2}} \int_{-\infty}^{+\infty} dx |x|^{\frac{1}{2}(g-1)} |x\rangle \langle x^{*g}|, \quad (\text{B.54})$$

where in the last identity in Eq. (B.54) we have written  $\hat{U}_g$  in terms of the eigenstates  $|x\rangle$  of the quadrature  $\hat{X}$ , upon introducing the notation

$$x^{*g} \equiv x|x|^{g-1} = \text{sgn}(x)|x|^g, \quad (\text{B.55})$$

where  $\text{sgn}(x)$  denotes the customary sign function. The analytic form (B.54) of  $\hat{U}_g$  is derived as follows

$$\begin{aligned} \hat{U}_g &= g^{\frac{1}{2}} \sum_{s=\pm} \int_{-\infty}^{+\infty} d\mu |\psi_s^{g\mu}\rangle \langle \psi_s^\mu| \\ &= g^{\frac{1}{2}} \int_{-\infty}^{+\infty} dx \int_{-\infty}^{+\infty} dx' |x'\rangle \langle x| \sum_{s=\pm} \int_{-\infty}^{+\infty} d\mu \psi_s^{g\mu}(x') \bar{\psi}_s^\mu(x) \\ &= g^{\frac{1}{2}} \int_{-\infty}^{+\infty} dx \int_{-\infty}^{+\infty} dx' |x'\rangle \langle x| |x'|^{\frac{1}{2}(g-1)} \sum_{s=\pm} \int_{-\infty}^{+\infty} d\mu \psi_s^\mu(x'^{*g}) \bar{\psi}_s^\mu(x) \\ &= g^{\frac{1}{2}} \int_{-\infty}^{+\infty} dx |x|^{\frac{1}{2}(g-1)} |x\rangle \langle x^{*g}|. \end{aligned} \quad (\text{B.56})$$

The Heisenberg evolution of the conjugated quadratures  $\hat{X}$  and  $\hat{Y}$  by the amplification  $\hat{U}_g$  can be evaluated through the following steps

$$\begin{aligned} \hat{U}_g^\dagger \hat{X} \hat{U}_g &= g \int_{-\infty}^{+\infty} dx \int_{-\infty}^{+\infty} dx' x |xx'|^{\frac{1}{2}(g-1)} |x^{*g}\rangle \langle x|x'\rangle \langle x'^{*g}| \\ &= g \int_{-\infty}^{+\infty} dx x^{*g} |x^{*g}\rangle \langle x^{*g}| = \hat{X}^{*\frac{1}{g}}; \end{aligned} \quad (\text{B.57})$$

$$\begin{aligned} \hat{U}_g^\dagger \hat{Y} \hat{U}_g &= \hat{U}_g^\dagger \int_{-\infty}^{+\infty} dx |x\rangle \left(-\frac{i}{2}\partial_x\right) \langle x| \hat{U}_g \\ &= g \int_{-\infty}^{+\infty} dx |x|^{\frac{1}{2}(g-1)} |x^{*g}\rangle \left(-\frac{i}{2}\partial_x\right) \langle x^{*g}||x|^{\frac{1}{2}(g-1)} \\ &= -\frac{i}{4}(g-1)\hat{X}^{*(-\frac{1}{g})} + \int_{-\infty}^{+\infty} du |u\rangle \left(-\frac{i}{2}|u|^{1-\frac{1}{g}}\partial_u\right) \langle u| \\ &= -\frac{i}{4}(g-1)\hat{X}^{*(-\frac{1}{g})} + g\hat{X}^{*(-\frac{1}{g})}\hat{X}\hat{Y} \\ &= \hat{X}^{*(-\frac{1}{g})} \left(\frac{1}{2}g\hat{K} + \frac{i}{4}\right) = \left(\frac{1}{2}g\hat{K} - \frac{i}{4}\right) \hat{X}^{*(-\frac{1}{g})}. \end{aligned} \quad (\text{B.58})$$

For what follows we also need to evaluate the Heisenberg evolution of the operator  $\hat{X}^2 + \hat{Y}^2 = a^\dagger a + \frac{1}{2}$ . From Eqs. (B.57-B.58) one has

$$\begin{aligned} \hat{U}_g^\dagger \left( a^\dagger a + \frac{1}{2} \right) \hat{U}_g &= |\hat{X}|^{\frac{2}{g}} + \frac{1}{4} \left( g\hat{K} - \frac{i}{2} \right) |\hat{X}|^{(-\frac{2}{g})} \left( g\hat{K} + \frac{i}{2} \right) \\ &= |\hat{X}|^{\frac{2}{g}} + \frac{1}{4} \hat{X}^{*(-\frac{1}{g})} \left( g^2 \hat{K}^2 + \frac{1}{4} \right) \hat{X}^{*(-\frac{1}{g})}. \end{aligned} \quad (\text{B.59})$$

Now, let us consider a quadratic function of the field  $f(\alpha, \bar{\alpha}) = -i(\alpha^2 - \bar{\alpha}^2 + ic|\alpha|^2)/2$ ,  $c$  an arbitrary constant, and let us evaluate the corresponding POM  $d\hat{H}_f(u)$  pertaining to heterodyne detection of the function  $f$  of the field. From Eq. (B.6) one has

$$\begin{aligned} d\hat{H}_f(u) &= du : \delta(u - f(a, a^\dagger)) :_A \\ &= du \int_{-\infty}^{+\infty} \frac{d\lambda}{2\pi} e^{-i\lambda u} e^{\lambda \frac{a^2}{2}} : e^{i\lambda \frac{c}{2} a^\dagger a} :_A e^{-\lambda \frac{a^{\dagger 2}}{2}} \\ &= du \int_{-\infty}^{+\infty} \frac{d\lambda}{2\pi} e^{-i\lambda u} e^{\lambda \frac{a^2}{2}} \left( 1 - i\lambda \frac{c}{2} \right)^{-(a^\dagger a + \frac{1}{2})} e^{-\lambda \frac{a^{\dagger 2}}{2}} \left( 1 - i\lambda \frac{c}{2} \right)^{-\frac{1}{2}}, \end{aligned} \quad (\text{B.60})$$

where we used the relation

$$: e^{za^\dagger a} :_A = \sum_{n=0}^{\infty} \frac{z^n}{n!} a^n a^{\dagger n} = \sum_{n=0}^{\infty} z^n \binom{a^\dagger a + n}{n} = (1 - z)^{-a^\dagger a - 1}. \quad (\text{B.61})$$

The product of operators in the last equality of Eq. (B.60) can be recast in the form of a single exponential function using the Baker-Campbell-Hausdorff (BCH) formula for the  $su(1,1)$  algebra [see the note at the end of the appendix]. According to the prescription in Eq. (B.21), we need to evaluate the preamplified POM

$$\mathcal{A}_g^{(\hat{K})}[d\hat{H}_f(gu)] \equiv g \hat{U}_g^\dagger (d\hat{H}_f(gu)) \hat{U}_g, \quad (\text{B.62})$$

in the limit of infinite gain  $g \rightarrow \infty$ . As shown in the Appendix, for the leading term in  $g$  one has

$$\begin{aligned} \mathcal{A}_g^{(\hat{K})}[d\hat{H}_f(gu)] &= du \int \frac{d\lambda}{2\pi} \exp \left( -i\lambda u + i\lambda \hat{K} + \frac{1}{8} i\lambda c g \hat{K}^2 \right) \\ &\times \exp \left[ -\frac{1}{8} \lambda^2 \left( 1 + \frac{c^2}{4} \right) \hat{K}^2 \right], \quad g \gg 1. \end{aligned} \quad (\text{B.63})$$

The preamplified POM in the limit of infinite gain writes as follows

$$\begin{aligned} &\mathcal{A}_g^{(\hat{K})}[d\hat{H}_f(gu)] \\ &\xrightarrow{g \rightarrow \infty} du \int \frac{d\lambda}{2\pi} \exp \left( -i\lambda u + i\lambda \hat{K} + \frac{i}{8} \lambda g c \hat{K}^2 \right) \exp \left( -\frac{1}{8} \lambda^2 \hat{K}^2 \right) \\ &= du \sqrt{\frac{2}{\pi \hat{K}^2}} \exp \left( -\frac{2(\hat{K} + \frac{1}{8} g c \hat{K}^2 - u)^2}{\hat{K}^2} \right). \end{aligned} \quad (\text{B.64})$$

The POM in Eq. (B.64) satisfies the necessary condition (B.24) for  $l = 0, 1$  upon choosing  $c = 0$ . However, the same condition for  $l = 2$  is not satisfied, because one has

$$\int du u^2 \sqrt{\frac{2}{\pi \hat{K}^2}} \exp\left(-\frac{2(\hat{K} - u)^2}{\hat{K}^2}\right) = \frac{5}{4} \hat{K}^2. \quad (\text{B.65})$$

Therefore, there is no quadratic function  $f(\alpha, \bar{\alpha})$  of the field that allows to approximate the ideal quantum measurement of the operator  $\hat{K} = -i(a^2 - a^{\dagger 2})/2$ . It is clear that also higher-degree polynomial functions of the field cannot satisfy condition (B.24), since in such case higher powers in  $a^\dagger$  and  $a$  will appear in Eq. (B.60) and the BCH formula will have no longer closed form. In conclusion of this section we notice that Eq. (B.64) for  $c = 0$  can also be easily obtained by the following formal asymptotic analysis

$$\begin{aligned} d\hat{H}_f(gu) &= du \int_{-\infty}^{+\infty} \frac{d\lambda}{2\pi} e^{-i\lambda u} e^{g^{-1}\lambda \frac{a^2}{2}} e^{g^{-1}-\lambda \frac{a^{\dagger 2}}{2}} \\ &= du \int_{-\infty}^{+\infty} e^{-i\lambda u} \exp\left\{ig^{-1}\lambda \frac{1}{2}(a^2 - a^{\dagger 2}) - \frac{1}{8}g^{-2}\lambda^2[a^2, a^{\dagger 2}] + O(g^{-3})\right\} \\ &= du \int_{-\infty}^{+\infty} e^{-i\lambda u} \exp\left\{ig^{-1}\lambda \hat{K} - \frac{1}{2}g^{-2}\lambda^2\left(a^\dagger a + \frac{1}{2}\right) + O(g^{-3})\right\}. \end{aligned} \quad (\text{B.66})$$

By amplifying the first and last members of Eq. (B.66) and using Eq. (B.59) one has

$$\begin{aligned} \mathcal{A}_g^{(\hat{K})}[d\hat{H}_f(gu)] &= du \int_{-\infty}^{+\infty} e^{-i\lambda u} \exp\left\{i\lambda \hat{K} - \frac{1}{8}\lambda^2 \hat{X}^{*(-\frac{1}{g})}\left(\hat{K}^2 + \frac{1}{4g^2}\right) \hat{X}^{*(-\frac{1}{g})} + O(g^{-3})\right\} \\ &= du \int_{-\infty}^{+\infty} e^{-i\lambda u} \exp\left\{i\lambda \hat{K} - \frac{1}{8}\lambda^2 \hat{K}^2 + O(g^{-1})\right\}, \end{aligned} \quad (\text{B.67})$$

namely Eq. (B.64).

## B.7 Conclusions

One may think that the heterodyne detector could be regarded as a universal detector, as it achieves the ideal measurement of the field operator  $a$ , and hence, in principle, it should achieve the measurement of any operator  $\hat{O} = \hat{O}(a, a^\dagger)$  of the field. However, due to the fact that the measurement of  $a$  corresponds to a joint measurement of two noncommuting conjugated observables, an intrinsic unavoidable 3dB noise is added to the measurement, even in the ideal case. We have considered the possibility of reducing such noise by means of a suitable ideal preamplification of  $\hat{O}$ , which we have shown to be feasible through a unitary transformation. We have shown that in the limit of infinite gain such preamplified-heterodyne detection scheme can achieve the ideal measurement of  $a^\dagger a$  and  $\hat{X}_\phi$ , even for nonunit quantum efficiency, also realizing

the transition from continuous to discrete spectrum in the case of the operator  $a^\dagger a$ . However, the scheme does not work for arbitrary operator, and, as a counterexample, we proved that the ideal measurement cannot be achieved even for the simple quadratic form  $\hat{K} = i(a^\dagger^2 - a^2)/2$ , apparently with no simple physical explanation other than the algebraic nature of the operator  $\hat{K}$  itself and its ideal amplification map. In the present study we have seen some of the problems which are faced in order to built a universal detecting machine, and we hope that this work will shed new light on the route for achieving such a challenging task.

### Note on the BCH formula

Upon defining  $k_+ = \frac{1}{2}a^\dagger^2$ ,  $k_- = \frac{1}{2}a^2$ , and  $k_3 = \frac{1}{2}(a^\dagger a + \frac{1}{2})$ , one recognizes the following commutation rules for the  $su(1,1)$  algebra

$$[\hat{k}_+, \hat{k}_-] = -2\hat{k}_3, \quad [\hat{k}_3, \hat{k}_\pm] = \pm\hat{k}_\pm. \quad (\text{B.68})$$

One needs the analytic form of the coefficients  $B_\pm, B_3$  and  $A_\pm, A_3$  in the following identity

$$\exp(A_- \hat{k}_-) \exp(2A_3 \hat{k}_3) \exp(A_+ \hat{k}_+) = \exp(2B_3 \hat{k}_3 + B_+ \hat{k}_+ + B_- \hat{k}_-). \quad (\text{B.69})$$

By using the faithful representation of the  $su(1,1)$  algebra in terms of the Pauli matrices with  $i\hat{\sigma}^\pm \equiv \hat{k}_\pm$ ,  $\hat{\sigma}^3 \equiv 2\hat{k}_3$ , Eq. (B.69) can be rewritten as follows

$$\begin{aligned} & \begin{pmatrix} 1 & 0 \\ iA_- & 1 \end{pmatrix} \begin{pmatrix} e^{A_3} & 0 \\ 0 & e^{-A_3} \end{pmatrix} \begin{pmatrix} 1 & iA_+ \\ 0 & 1 \end{pmatrix} = \\ & \cosh \Gamma \begin{pmatrix} 1 & 0 \\ 0 & 1 \end{pmatrix} + \frac{\sinh \Gamma}{\Gamma} \begin{pmatrix} B_3 & iB_+ \\ iB_- & -B_3 \end{pmatrix}, \end{aligned} \quad (\text{B.70})$$

where  $\Gamma = (B_3^2 - B_+ B_-)^{1/2}$ . From Eq. (B.70) one obtains the relation

$$B_3 = \frac{1}{2} \frac{\Gamma}{\sinh \Gamma} [(1 + A_+ A_-) e^{A_3} - e^{-A_3}], \quad (\text{B.71})$$

$$\sinh \Gamma = \left\{ \left[ \frac{(1 + A_+ A_-) e^{A_3} + e^{-A_3}}{2} \right]^2 - 1 \right\}^{\frac{1}{2}}, \quad (\text{B.72})$$

$$B_\pm = \frac{2A_\pm e^{\pm A_3}}{(1 - A_+ A_-) e^{A_3} - e^{-A_3}} B_3. \quad (\text{B.73})$$

For our purposes, we are just interested in the asymptotic expression of the POM  $\mathcal{A}_g^{(\hat{K})}[d\hat{H}_f(gu)]$  in Eq. (B.62) for  $g \rightarrow \infty$ . By comparing Eqs. (B.69) and (B.60) one has  $A_\pm = \mp g^{-1} \lambda$  and  $A_3 = -\ln(1 - ig^{-1} \lambda \frac{c}{2})$ . From Eqs. (B.71-B.73) one obtains the asymptotic values of  $B_\pm$  and  $B_3$  for  $g \rightarrow \infty$ , namely

$$B_\pm \simeq \mp g^{-1} \lambda, \quad B_3 \simeq \frac{1}{2} ig^{-1} \lambda c - \frac{1}{2} g^{-2} \lambda^2 \left( 1 + \frac{c^2}{4} \right). \quad (\text{B.74})$$

Hence, from Eq. (B.60) it follows

$$gd\hat{H}_f(gu) \xrightarrow{g \gg 1} du \int \frac{d\lambda}{2\pi} (1 + i\lambda g^{-1} \frac{c}{4}) e^{-i\lambda u} \quad (\text{B.75})$$

$$\times \exp \left\{ ig^{-1} \lambda \hat{K} + \frac{1}{2} \left[ i\lambda g^{-1} c - g^{-2} \lambda^2 \left( 1 + \frac{c^2}{4} \right) \right] \left( a^\dagger a + \frac{1}{2} \right) \right\} .$$

By applying the amplification map to the POM  $d\hat{H}_f(gu)$  through Eqs. (B.53) and (B.59), one obtains  $\mathcal{A}_g^{(\hat{K})}[d\hat{H}_f(gu)]$  in Eq. (B.63).

# Bibliography

- [1] J. A. Armstrong, N. Bloembergen, J. Ducuing and P. S. Pershan, *Phys. Rev.* **127**, 1918 (1962).
- [2] L. Mandel and E. Wolf, *Optical Coherence and Quantum Optics*, (Cambridge Univ. Press, 1995).
- [3] H. P. Yuen, *Phys. Rev. A* **13**, 2226 (1976).
- [4] Y. Yamamoto and H. A. Haus, *Rev. Mod. Phys.* **58**, 1001 (1986).
- [5] Special issues on Squeezed states: *J. Opt. Soc. Am. B* **4**, (H. J. Kimble and D. F. Walls Eds., 1987); *J. Mod. Opt.* **34** (R. Loudon and P. L. Knight Eds., 1987)
- [6] *Quantum Interferometry* F. De Martini, G. Denardo and Y. Shih, Eds. (VCH, Weinheim 1996).
- [7] B. R. Mollow and R. J. Glauber, *Phys. Rev.* **160**, 1076 (1967); **160**, 1097 (1967).
- [8] P. N. Butcher and D. Cotter, *The Elements of Nonlinear Optics* (Cambridge Univ. Press 1990).
- [9] R. L. Byer, *Nonlinear Optics*, Chap. 2, P. G. Harper and B. S. Wherrett Eds. (Academic Press, London, 1977).
- [10] G. M. D'Ariano, *Int. J. Mod. Phys. B* **6**, 1292 (1992).
- [11] D. R. Truax, *Phys. Rev. D* **31**, 1988 (1985).
- [12] M. Ban, *J. Opt. Soc. Am. B* **10**, 1347 (1993).
- [13] M. G. A. Paris, *Phys. Lett. A* **217**, 78 (1996).
- [14] M. Hillery and M. S. Zubairy, *Phys. Rev. A* **29**, 1275 (1984).
- [15] D. D. Crouch and S. L. Braunstein, *Phys. Rev. A* **38** 4696 (1988).
- [16] G. Scharf and D. F. Walls, *Opt. Comm.* **50**, 245 (1984).

- [17] D. F. Walls and R. Barakat, Phys. Rev. A **1**, 446 (1970).
- [18] D. F. Walls and C. T. Tindle, J. Phys. A **5**, 534 (1972).
- [19] B. Buck and C. V. Sukumar, Phys. Lett. A **81**, 132 (1981); C. V. Sukumar and B. Buck, J. Phys. A **17**, 885 (1984).
- [20] V. Bužek, Quant. Opt **1**, 53 (1989); J. Mod. Opt. **37**, 303 (1990).
- [21] J. Mostowski and K. Rzazewski, Phys. Lett. A **66**, 275 (1978).
- [22] R. Tanaś and Ts. Gantsog, Phys. Rev. A **45**, 5031 (1992).
- [23] V. Bužek and G. Drobný, Phys. Rev. A **47**, 1237 (1993).
- [24] M. Hillery, D. Yu and J. Bergou, Phys. Rev. A **49**, 1288 (1994).
- [25] G. Dattoli, J. C. Gallardo and A. Torre, Riv. Nuovo Cimento **11**, 1, (1988).
- [26] A. Bandilla, G. Drobný and I. Jex, Phys. Rev. Lett. **75**, 4019 (1995); Phys. Rev. A **53**, 507 (1996); Opt. Comm. **128**, 353 (1996).
- [27] G. M. D'Ariano, M. G. A. Paris and M. F. Sacchi, Nuovo Cimento B, 1998, in press.
- [28] G. Drobný and I Jex, Phys. Rev. A **46**, 499 (1992).
- [29] R. A. Campos, B. E. A. Saleh and M. C. Teich, Phys. Rev. A **40**, 1371 (1989).
- [30] H. P. Yuen and V. W. S. Chan, Opt. Lett. **8**, 177 (1983).
- [31] J. Janszky, C. Sibilía, M. Bertolotti and Y. Yushin, J. Mod. Opt. **35**, 1757 (1988); J. Janszky, P. Adam, M. Bertolotti and C. Sibilía, Quantum Opt. **4**, 163 (1992).
- [32] H. Fearn, Quantum Opt. **2**, 103 (1990); H. Fearn and R. Loudon, Opt. Comm. **64**, 485 (1987).
- [33] G. M. D'Ariano, Nuovo Cimento B **107**, 643 (1992).
- [34] G. M. D'Ariano, *Quantum estimation theory and optical detection*, in *Quantum Optics and the Spectroscopy of Solids*, T. Hakioglu and A. S. Shumovsky Eds. (Kluwer, Dordrecht 1997) pp. 139-174.
- [35] W. Schleich and J. A. Wheeler, Nature **326**, 574 (1987).
- [36] C. O. Alley and Y. H. Shih, Phys. Rev. Lett. **61**, 2921 (1988).
- [37] Z. Y. Ou and L. Mandel, Phys. Rev. Lett. **61**, 50 (1988).

- [38] J. G. Rarity and P. B. Tapster, *Phys. Rev. Lett.* **64**, 2495 (1990).
- [39] G. M. D'Ariano and M. F. Sacchi, *Phys. Rev. A* **52**, R4309 (1995).
- [40] G. M. D'Ariano and M. F. Sacchi, *Repeatable two-mode phase measurement* in Ref. [6], pp. 307-313.
- [41] D. Boschi, F. De Martini and G. Di Giuseppe, in Ref. [6], pp. 135-143.
- [42] D. N. Klyshko, *Phys. Lett. A* **132**, 299 (1988).
- [43] M. A. Horne, A. Shimony and A. Zeilinger, *Phys. Rev. Lett.* **62**, 2209 (1989).
- [44] C. M. Caves and B. L. Schumaker, *Phys. Rev. A* **31**, 3068 (1985).
- [45] G. M. D'Ariano and M. G. A. Paris, *Phys. Rev. A* **49**, 3022 (1994)
- [46] *Physica Scripta T48* (1993) (special issue on *Quantum Phase and Phase Dependent measurements*).
- [47] C. W. Helstrom, *Quantum Detection and Estimation Theory*, (Academic Press, New York, 1976).
- [48] J. H. Shapiro and S. R. Shepard, *Phys. Rev. A* **43**, 3795 (1991).
- [49] I. Bialynicki-Birula, M. Freyberger and W. P. Schleich, *Phys. Scripta T48* 113 (1993).
- [50] B. Daeubler, Ch. Miller, H. Risken and L. Schoendorff, *Phys. Scripta T48* 119 (1993).
- [51] G. M. D'Ariano, C. Macchiavello, N. Sterpi and H. P. Yuen, *Phys. Rev. A* **54**, 4712 (1996).
- [52] A. S. Holevo. *Probabilistic and statistical aspects of quantum theory*, (North-Holland, Amsterdam, 1982).
- [53] M. Ban, *Phys. Rev. A* **50**, 2785 (1994).
- [54] J. H. Shapiro, *Physica Scripta T 48*, 105 (1993).
- [55] A. Luis and L. L. Sánchez-Soto, *Phys. Rev. A* **48**, 4702 (1993).
- [56] G. M. D'Ariano, M. G. A. Paris and M. F. Sacchi, *Phys. Rev. A* **57**, 4894 (1998).
- [57] V. Buzek, C. H. Keitel and P. L. Knight, *Phys. Rev. A* **51**, 2575 (1995); *Phys. Rev. A* **51**, 2594 (1995).

- [58] K. Wodkiewicz, Phys. Rev. Lett. **52**, 1064 (1984); Phys. Lett. A **115**, 304 (1986); Phys. Lett. A **129**, 1 (1988).
- [59] M. G. A. Paris, A. V. Chizhov and O. Steuernagel, Opt. Comm. **134** 117 (1997).
- [60] G. M. D'Ariano and C. Macchiavello, Phys. Rev. A **48**, 3947 (1993).
- [61] G. M. D'Ariano, C. Macchiavello and M. G. A. Paris, in Second International Workshop on Squeezed States and Uncertainty Relations, D. Han et al. Eds. (NASA Conf. Public. 3219, Washington DC, 1992), p. 71.
- [62] J. Huang and P. Kumar, Phys. Rev. Lett. **68**, 2153 (1992).
- [63] P. Kumar, Opt. Lett. **15**, 1476 (1990).
- [64] J. H. Shapiro and S. S. Wagner, IEEE J. Quantum Electron. QE **20**, 803 (1984).
- [65] G. M. D'Ariano and M. F. Sacchi, Phys. Rev. A **52**, R4309 (1995).
- [66] H. P. Yuen and J. H. Shapiro, IEEE Trans. Inform. Theory IT **26**, 78 (1980).
- [67] H. Cramér, *Mathematical Methods of Statistics*, (Princeton Univ. Press, Princeton, NJ, 1951), pp. 489-506.
- [68] G. M. D'Ariano and M. F. Sacchi, in Ref. [6], pp. 307-313.
- [69] M. Ozawa, in Ref. [144], p. 263.
- [70] G. M. D'Ariano, M. Fortunato and P. Tombesi, Nuovo Cimento B **110**, 1127 (1995).
- [71] M. Ozawa, J. Math. Phys. **27**, 759 (1986).
- [72] M. Ban, J. Opt. Soc. Am. B **9**, 1189 (1992).
- [73] G. M. D'Ariano, C. Macchiavello and M. F. Sacchi, Phys. Lett. A **248**, 103 (1998).
- [74] W. van Dam, G. M. D'Ariano, A. Ekert, C. Macchiavello, and M. Mosca, unpublished.
- [75] G. M. D'Ariano and M. G. A. Paris, Phys. Rev. A **55**, 2267 (1997).
- [76] P. Carruthers and M. M. Nieto, Rev. Mod. Phys. **40**, 411 (1968).
- [77] R. Jackiw, J. Math. Phys. **9**, 339 (1968).
- [78] A. Bandilla, H. Paul, and H-H Ritze, Quantum Opt. **3**, 267 (1991).
- [79] C. M. Caves and P. D. Drummond, Rev. Mod. Phys. **66**, 481 (1994).

- [80] K. Yamazaki, O. Hirota and M. Nakagawa, *Trans. IEICE*, **E71**, 8, 775 (1988).
- [81] M. J. W. Hall, *Phys. Rev. A* **50**, 3295 (1994).
- [82] M. J. Holland, K. Burnett, *Phys. Rev. Lett.* **71**, 1355 (1993).
- [83] G. M. D'Ariano and M. F. Sacchi, in '5<sup>th</sup> Int. Conf. on Squeezed States and Uncertainty Relations' (NASA Conf. Publ., Washington DC, 1997), pp. 467-472.
- [84] G. M. D'Ariano and M. F. Sacchi, *Opt. Comm.* **149**, 152 (1998).
- [85] R. G. Gallager, *Information Theory and Reliable Communication* (Wiley, New York, 1968).
- [86] G. Lindblad, *Commun. Math. Phys.* **48**, 119 (1976).
- [87] M. J. W. Hall, *Phys. Rev. Lett.* **74**, 3307 (1995).
- [88] C. Kim and P. Kumar, *Phys. Rev. A* **5**, 5237 (1992).
- [89] C. Kim and P. Kumar, *Opt. Lett.* **16**, 755 (1991).
- [90] A. S. Holevo, *Probl. Inf. Trans.* **9**, 177 (1973).
- [91] H. P. Yuen and M. Ozawa, *Phys. Rev. Lett.* **70**, 363 (1993).
- [92] R. E. Blahut, *IEEE Trans. Inform. Theory*, **IT-18**, 460 (1972).
- [93] G. M. D'Ariano and M. F. Sacchi, *Mod. Phys. Lett. B.* **11**, 1263 (1997).
- [94] C. Kim and P. Kumar, in *OSA Annual Meeting, 1992 Technical Digest Series*, Vol. 23 (Optical Society of America, Washington, D.C. 1992), p. 193.
- [95] C. W. Gardiner, *Quantum noise*, (Springer-Verlag, Berlin, 1991).
- [96] M. G. A. Paris, *Phys. Lett. A* **225**, 28 (1997).
- [97] S. Y. Kilin and D. B. Horosko, *Phys. Rev. Lett.* **74**, 5206 (1995); W. Leonski, S. Dyrting, and R. Tanas, *J. Mod. Opt.* **44**, 2105 (1997); A. Vidiella-Barranco, and J. A. Roversi, *Phys. Rev. A* **58**, 3349 (1998).
- [98] M. G. A. Paris, *Int. J. Mod. Phys. B* **11**, 1913 (1997); M. Dakna, T. Hanput, T. Opatrny, L. Knoll, and D. G. Welsch, *Phys. Rev. A* **55**, 3184 (1997); M. Dakna, L. Knoll, and D. G. Welsch, *Opt. Comm.* **145**, 309 (1998).
- [99] K. Vogel, V. M. Akulin, and W. P. Scheich, *Phys. Rev. Lett.* **71**, 1816 (1993).

- [100] J. Krause, M. O. Scully, T. Walther, and H. Walther, Phys. Rev. A **39**, 1915 (1989); M. Kozirowski, and S. M. Chumakov, Phys. Rev. A **52**, 4194 (1995); P. Domokos, M. Brune, J. M. Raimond, and S. Haroche, Europ. Phys. J. D **1**, 1 (1998).
- [101] C. H. Bennett and B. P. Di Vincenzo, Nature **377**, 389 (1995).
- [102] G. M. D'Ariano and L. Maccone, Phys. Rev. Lett. **80**, 5465 (1998).
- [103] N. Imoto, H. A. Haus, and Y. Yamamoto, Phys. Rev. A **32**, 2287 (1985).
- [104] M. Ley and R. Loudon, J. Mod. Opt. **34**, 227 (1987).
- [105] S. M. Barnett, C. R. Gilson, B. Huttner, and N. Imoto, Phys. Rev. Lett. **77**, 1739 (1997).
- [106] J. von Neumann, *Mathematical Foundations of Quantum Mechanics* (Princeton Univ. Press, Princeton, NJ, 1955), pp. 442-445.
- [107] G. M. D'Ariano, M. F. Sacchi and R. Seno, 1998, submitted to Nuovo Cimento B.
- [108] G. M. D'Ariano and M. F. Sacchi, Phys. Lett. A **231**, 325 (1997).
- [109] J. H. Shapiro, Opt. Lett **20**, 1059 (1995).
- [110] A. La Porta, R. E. Slusher, and B. Yurke, Phys. Rev. Lett. **62**, 28 (1989).
- [111] Z. Y. Ou, S. F. Pereira, and H. J. Kimble, Phys. Rev. Lett. **70**, 3239 (1993).
- [112] S. F. Pereira, Z. Y. Ou, and H. J. Kimble, Phys. Rev. Lett. **72**, 214 (1994).
- [113] K. Bencheikh, J. A. Levenson, Ph. Grangier, and O. Lopez, Phys. Rev. Lett. **75**, 3422 (1995).
- [114] H. P. Yuen, Phys. Lett. A **113**, 405 (1986); Opt. Lett. **12**, 789 (1987).
- [115] F. De Martini, L. De Dominicis, E. Del Re, and F. Truc, in Ref. [6], p.210.
- [116] C. Bennett, G. Brassard, C. Crépeau, R. Josza, A. Peres, and W. K. Wootters, Phys. Rev. Lett. **70**, 1895 (1993); D. Bouwmeester, J.-V. Pan, K. Mattle, M. Eibl, H. Weinfurter, and A. Zeilinger, Nature **390**, 575 (1997); D. Boschi, S. Branca, F. De Martini, L. Hardy, and S. Popescu, Phys. Rev. Lett. **80**, 1121 (1998); S. L. Braunstein and H. J. Kimble, Phys. Rev. Lett. **80**, 869 (1998); A. Furusawa, J. L. Sørensen, S. L. Braunstein, C. A. Fuchs, H. J. Kimble, and E. S. Polzik, Science **282**, 706 (1998).

- [117] M. Brune, E. Hagley, J. Dreyer, X. Maitre, A. Maali, C. Wunderlich, J. M. Raimond, and S. Haroche, *Phys. Rev. Lett.* **77**, 4887 (1996).
- [118] C. Monroe, D. M. Meekhof, B. E. King, and W. J. Wineland, *Science* **272**, 1131 (1996).
- [119] D. P. DiVincenzo, *Science* **270**, 255 (1995).
- [120] A. K. Ekert, *Phys. Rev. Lett.* **67**, 661 (1991).
- [121] P. G. Kwiat, K. Mattle, H. Weinfurter, A. Zeilinger, A. V. Sergienko, and Y. H. Shih, *Phys. Rev. Lett.* **75**, 4337 (1995).
- [122] G. M. D'Ariano, M. Vasilyev, and P. Kumar, *Phys. Rev. A* **58**, 636 (1998).
- [123] B. Yurke and D. Stoler, *Phys. Rev. Lett.* **57**, 13 (1986).
- [124] F. De Martini, *Phys. Rev. Lett.* **67**, 661 (1998); *Phys. Lett. A* **250**, 15 (1998).
- [125] F. De Martini, M. Fortunato, P. Tombesi, and D. Vitali, 1999, submitted to *Phys. Rev. A*.
- [126] D. M. Greenberger, M. A. Horne, and A. Zeilinger, in Ref. [6], p. 119.
- [127] A. Einstein, B. Podolsky and N. Rosen, *Phys. Rev.* **47**, 777 (1935).
- [128] N. Bohr, *Phys. Rev.* **48**, 696 (1935).
- [129] J. S. Bell, *Physics* **1**, 195 (1965).
- [130] J. F. Clauser, *Phys. Rev. Lett.* **36**, 1223 (1976); A. Aspect, J. Dalibard, and G. Roger, *Phys. Rev. Lett.* **47**, 460 (1981); A. J. Duncan, W. Perrie, H. J. Beyer and H. Kleinpoppen, in *Fundamental Processes in Atomic Collision Physics*, Plenum, New York, 1985, p. 555; Z. Y. Ou and L. Mandel, *Phys. Rev. Lett.* **61**, 50 (1988); C. O. Alley and Y. H. Shih, *Phys. Rev. Lett.* **61**, 2921 (1988); J. D. Franson, *Phys. Rev. Lett.* **62**, 2200 (1989); K. Mattle, H. Weinfurter, P. G. Kwiat and A. Zeilinger, *Phys. Rev. Lett.* **76**, 4656 (1996).
- [131] J. F. Clauser, M. A. Horne, A. Shimony, and R. A. Holt, *Phys. Rev. Lett.* **23**, 880 (1969); J. F. Clauser and M. A. Horne, *Phys. Rev. D* **10**, 256 (1974); A. Garuccio and V. A. Rapisarda, *Nuovo Cimento A* **65**, 269 (1981).
- [132] L. De Caro and A. Garuccio, *Phys. Rev. A* **54**, 174 (1996).
- [133] D. T. Smithey, M. Beck, M. G. Raymer and A. Faridani, *Phys. Rev. Lett.* **70**, 1244 (1993).

- [134] G. Breitenbach, S. Schiller and J. Mlynek, *Nature* **387**, 471 (1997).
- [135] G. M. D'Ariano, *Measuring quantum states*, in *Quantum Optics and the Spectroscopy of Solids*, T. Hakioglu and A. S. Shumovsky Eds. (Kluwer, Dordrecht 1997) p. 175.
- [136] G. M. D'Ariano, L. Maccone, M. F. Sacchi and A. Garuccio, "Homodyning Bell's inequality", in '4<sup>th</sup> Int. Conf. on Quantum Communication, Measurement, and Computing' (Plenum, 1998), in press.
- [137] G. M. D'Ariano, L. Maccone, M. F. Sacchi and A. Garuccio, 1998, submitted to *Europ. Phys. J. D*.
- [138] C. Kim and P. Kumar, *Phys. Rev. Lett.* **73**, 1605 (1994).
- [139] G. M. D'Ariano, in *Quantum Communication, Computing, and Measurement*, O. Hirota, A. S. Holevo and C. M. Caves Eds., (Plenum Publishing, New York and London, 1997), p. 253.
- [140] G. M. D'Ariano, U. Leonhardt and H. Paul, *Phys. Rev. A* **52**, R1801 (1995).
- [141] L. Mandel, *Proc. Phys. Soc.* **72**, 1037 (1958).
- [142] C. K. Hong and L. Mandel, *Phys. Rev. Lett.* **54**, 323 (1985); *Phys. Rev. A* **32**, 974 (1985).
- [143] M. Hillery, *Phys. Rev. A* **36**, 3796 (1987).
- [144] *Squeezed and Nonclassical Light*, P. Tombesi and E. R. Pike, Eds., (Plenum Publishing, New York 1989).
- [145] G. S. Agarwal and K. Tara, *Phys. Rev. A* **46**, 485 (1992).
- [146] C. T. Lee, *Phys. Rev. A* **44**, R2775 (1991); *Phys. Rev. A* **52**, 3374 (1995).
- [147] D. N. Klyshko, *Phys. Usp.* **37**, 1097 (1994); *Phys. Usp.* **39**, 573 (1996); *Phys. Lett. A* **213**, 7 (1996).
- [148] Arvind, N. Mukunda, and R. Simon, *J. Phys. A* **31**, 565 (1998).
- [149] G. M. D'Ariano, P. Kumar and M. F. Sacchi, *Phys. Rev. A* **59**, 826 (1999).
- [150] K. Vogel and H. Risken, *Phys. Rev. A* **40**, 2847 (1989).
- [151] J. Huang, Ph.D. thesis, Northwestern University, 1991 (unpublished).
- [152] G. M. D'Ariano and C. Macchiavello, *Phys. Rev. A* **57**, 3131 (1998).

- [153] Th. Richter, *Phys. Rev. A* **53**, 1197 (1996).
- [154] G. M. D'Ariano and M. F. Sacchi, *Nuovo Cimento B* **112**, 881 (1997).
- [155] E. P. Wigner, *Phys. Rev.* **40**, 749 (1932).
- [156] *The Physics of Phase Space*, Y. S. Kim and W. W. Zachary Eds., (Springer, Berlin, 1986).
- [157] H. Weyl, *The Theory of Groups and Quantum Mechanics* (Dover, New York, 1950).
- [158] K. E. Cahill and R. J. Glauber, *Phys. Rev.* **177**, 1857 (1969).
- [159] K. E. Cahill, *Phys. Rev.* **138**, B1566 (1965).
- [160] K. E. Cahill and R. J. Glauber, *Phys. Rev.* **177**, 1882 (1969).
- [161] A. Orłowski and A. Wünsche, *Phys. Rev. A*, **48**, 4697 (1993).
- [162] G. M. D'Ariano, C. Macchiavello, and S. Moroni, *Mod. Phys. Lett. B* **8**, 239 (1994).
- [163] E. B. Davies and J. T. Lewis, *Commun. Math. Phys.* **17**, 239 (1970).
- [164] M. Ozawa, *J. Math. Phys.* **25**, 79 (1984).
- [165] R. Estrada and R. P. Kanwal, *Asymptotic Analysis: A Distributional Approach* (BirkhHauser Boston, Basel, Berlin 1994).
- [166] H. P. Yuen, in *Quantum Optics, Experimental gravitation, and Measurement Theory*, P. Meystre and M. O. Scully Eds. (Plenum, New York 1983), pp. 249-268.
- [167] H. P. Yuen, *Phys. Rev. Lett.* **56**, 2176 (1986).
- [168] H. P. Yuen, in *Photons and Quantum Fluctuations*, E. R. Pike and H. Walther Eds. (Hilger, London, 1988), pp. 1-9.
- [169] G. M. D'Ariano, *Phys. Rev. A* **45**, 3224 (1992).
- [170] C. G. Bollini and L. E. Oxman, *Phys. Rev. A* **47**, 2339 (1993).